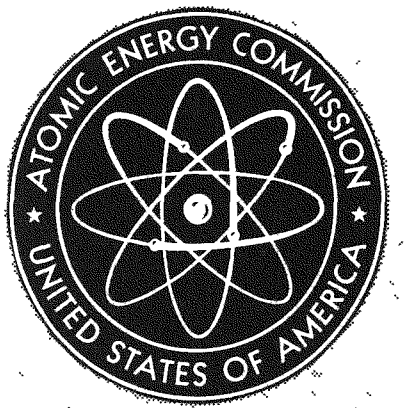

MND-P-3010
PHYSICS AND MATHEMATICS

SNAP PROGRAMS

Quarterly Progress Report No. 2, Tasks 2, 3, 5 and 6 [for] January to March 31, 1960

December 1960
[OTI Issuance Date]

Nuclear Division
Martin Company
Baltimore, Maryland

UNITED STATES ATOMIC ENERGY COMMISSION • OFFICE OF TECHNICAL INFORMATION

DISCLAIMER

LEGAL NOTICE

USAEC Office of Technical Information Extension
Oak Ridge, Tennessee

MND-P-3010

SNAP PROGRAMS

Quarterly Progress Report No. 2

Tasks 2, 3, 5 and 6

January to March 31, 1960

Approved By:

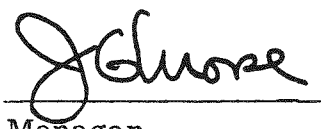

Manager
Isotopic Power Department

Nuclear Division
Martin Company
Baltimore, Maryland

FOREWORD

This is the second unclassified SNAP quarterly progress report prepared by The Martin Company. It covers the work performed during January 31 through March 31, 1960 under Contract AT(30-3)217 for the U.S. Atomic Energy Commission.

CONTENTS

CONTENTS (continued)

CONTENTS (continued)

CONTENTS (continued)

SUMMARY

A. TASK 2.0

1. Subtask 2.1--System Design

Several improvements have been incorporated into the design of the environmental and ground test generators. These include a chem-milled outer skin, an improved thermoelectric element adjustment and access plug, a flexible stainless steel-aluminum joint welded via ultrasonic techniques, a flexible hot shoe assembly which would permit prebonding of the elements and a thermal hydraulic heat dump system.

Design of the isotope-loaded ground test generator was completed along with all the ground handling equipment. An operating procedures manual for loading, shipping, assembly and testing of the ground handling equipment was prepared and submitted as a separate document.

The design of the remote welder was reviewed with ORNL and detail design was completed.

2. Subtask 2.2--Materials Analysis

Burnup studies on fuel forms were continued with cerous fluoride and ceric oxide. Additions of metal carbides and nitrides to the oxide form were made, sintered and tested. Of these, silicon carbide proved most promising. A cerium density of 4.0 gm/cc was obtained for the oxide form (versus cerous fluoride with a density of 3.74 gm/cc) with an addition of 10% silicon carbide and 1/2% calcium oxide as a sintering aid. The burnup properties of this mixture were found to be superior to those of cerous fluoride.

An evaluation of particle size distribution on fuel form materials ablated in a plasma flame is underway.

Particles which are carried by the gas stream are collected on greased slides. Larger particles which drop from the gas stream are not evaluated. Data from these tests are still being reduced.

Compatibility tests of Allegheny Ludlum S-816 alloy were completed. Results show that the alloy is resistant to attack by ceric oxide and cerous fluoride, but is attacked by cerium metal. Mercury corrosion, atmospheric oxidation and sea water corrosion tests gave satisfactory results. The alloy appears promising for use as a container material.

Coordination with ORNL generally resolved the hot cell fuel loading techniques. Further refinements must await hardware checkout.

3. Subtask 2.3--Hazards Analysis

Analysis of launch abort impact zones for the open core continued. Refinement of assumptions in the input data to more credible conditions are expected to significantly reduce the size of the impact zone.

An analysis of aerodynamic burnup for near orbital injection on two types of molybdenum fuel cores was completed. Results indicated that one design, a bonded cluster of tubes, would melt completely at 118,000 feet, and the other design, a 4-inch diameter block, would undergo partial burnup before impacting on the earth.

The summary report on aerodynamic re-entry analysis for the Task 2 generator was completed and distributed. An interim report on handling and safety procedures for the generator was prepared for distribution.

A final hazards summary report and a summary film report are in preparation. The latter will include pictures of the latest high velocity impact tests, explosion tests, high temperature fire test, LOX immersion test, plasma flame tests and materials corrosion and compatibility tests.

Presentations pertaining to the hazards aspects of ground handling and launch abort of the Task 2 generator were made at several west coast installations.

4. Subtask 2.4--Manufacturing

Test hardware and equipment were fabricated in support of the hazards testing program, the fuel form and fuel container development and the materials compatibility tests.

Work on the ground handling equipment was suspended. The isotope cask and the gimbal fixture were almost complete when the stop order was issued. Items for the collar shield tank were partially complete.

Fabrication and assembly of the first electrically heated generator was completed. Progress was slow because of the extreme care that had to be taken when working the fragile Min-K insulation. Dusting of the insulation, leaks in hermetic seal areas and some thermoelement breakage contributed to the delay. Following installation of the thermal shutter mechanism, a continuity checkout was made on the overall circuit and the generator was submitted for testing.

Fabrication of the second electrically heated generator was started.

The inner truss assembly was welded, and instrumented with strain gauges, and the conical heat reflecting shield installed. Other parts are in detail manufacturing.

The environmental test fixture for vibration testing is in fabrication. Procurement of materials for the remote welder was suspended.

5. Subtask 2.5--System and Component Test

The final report by the subcontractor on the radiation study program was reviewed. Initial results indicated that lead telluride couples used as control samples increased in resistivity after heating to 1000° F and masked resistivity changes due to radiation. Heat treatment prior to testing stabilized the elements. Resistivity increases after irradiation at both 1000 and 300° F occurred in all samples. Because of the extreme fragility of the test samples after irradiation to a dose of 4.6×10^{16} electrons/cm^2, power output measurements were made on N-type elements only. The results were not conclusive. It was concluded that variations in the data measurements were the result of nonuniformity in the sample elements themselves.

A second set of high velocity impact tests was completed. Six full-scale Inconel X cores were heated to approximately 1500° F and impacted on either granite or water targets. All of the cerium metal loaded cores ruptured. Cores loaded with lavite pellets were recovered intact with no apparent release of the simulated fuel. Data are still being evaluated.

One-third scale fuel cores were evaluated in a shock wave test in which 2000 pounds of TNT were detonated to simulate a launch pad booster failure. Of the eight original test specimens, only five were recovered, all apparently in excellent condition. Test data and films are still being processed.

Plans for the high temperature fire tests are complete, and final preparations for the test are being made. Hypergolic fuels will be mixed and poured over electrically heated specimens located at various positions in a 25-foot tower. Simultaneously, a cerium metal alloy will be burned and the resulting fallout measured via prepositioned fallout trays and air samplers. Cameras will monitor the test proceedings. The test awaits suitable weather conditions.

Heat transfer mockup tests were completed with a revised two-layer stainless steel heat shield. Under vacuum conditions, an equilibrium shutter heat dump of 3200 watts at 1100° F hot skin temperature was obtained. Because of a better thermal radiation view factor in the gen-

erator design, it was concluded that the shutter heat dump requirements for the ground test generator, in an air environment, will be satisfied.

Bonding tests aimed at lowering the lead telluride element to hot shoe interface resistance were continued. Conditioning of the iron shoes, either by sandblasting or lead tinning prior to bonding produced only fair results. More promising results were indicated by tests in which germanium telluride and doped lead telluride were predeposited and melted onto the iron shoes prior to assembly and bonding.

The first electrically heated generator was tested. Difficulties, in the form of electrical shorts or discontinuities, plagued the test and necessitated frequent shutdowns. A power output of 78 watts was obtained successfully at average hot and cold skin temperatures of 1043 and 297° F, respectively.

B. TASK 3.0

During the month of January, the 3M1G3 thermoelectric generator, which had failed last year during the parametric tests, was repaired and parametric testing of this generator was resumed. Performance of the repaired unit was only approximately 60% of the performance originally reported by the Minnesota Mining and Manufacturing Company when the unit was delivered to The Martin Company in May 1959. It was decided to continue parametric testing of this unit, however, since the output appeared stable. As of the end of this period, four tests have been completed, two with the generator operating with an internal vacuum condition and two with an internal gas of 85% nitrogen and 15% hydrogen at 2 atmospheres pressure.

The thermoelectric generator life test, using the 3M1G10 generator purchased for this purpose, has been operating continuously since January 26, 1960, with a constant power input and a fixed load. The results of this test have shown a continual decrease in the power output of the generator due to a decrease in Seebeck voltage and increasing internal resistance. The most rapid decrease in performance occurred at the start of the life test and, as of the end of this period, the unit appears to be leveling off at a constant power output level.

The second SNAP-III generator to be fueled with a radioisotope (Polonium-210) has been returned to The Martin Company to be refueled. The power output of this unit has been measured and, although very low due to the natural decay of the isotope, proof of thermoelectric generator operation for at least a period of a year has been demonstrated.

C. TASK 5.0

1. Subtask 5.1--Advanced Thermoelectric Power System

The SNAP-IIIA thermoelectric generator, which had been returned to Westinghouse for repair, was delivered to The Martin Company, complete with drawings and operating manual on January 28, 1960. After comparison of the test data supplied by Westinghouse on the SNAP-IIIA generator, with other SNAP-III generators, it became apparent that SNAP-IIIA is substandard. Westinghouse decided to design and fabricate an entirely new generator for this application. This second generator was completed and delivered to The Martin Company on March 10, 1960. Although this second generator is a completely new design, the performance characteristics are only marginally better than the original SNAP-IIIA thermoelectric generator. It was recommended by The Martin Company, to the Atomic Energy Commission, that all further technical evaluation of the generators be cancelled. A final report will be prepared covering the entire SNAP-IIIA program.

2. Subtask 5.2--Basic Thermionic Development

Work under this subtask consists of effort in three areas:

(1) Study and tests of cesium diode.

(2) Related tests and research.

(3) Development of improved collectors in a vacuum diode environment.

a. Cesium diodes

During the past quarter, tests were performed on metal encased and ribbon emitter types of tubes. The metal-encased diode employs an electron bombardment heater and a metal envelope. Tests have been conducted on the principal components. Detailed designs have been completed on the tube and test apparatus and fabrication has been initiated. The ribbon emitter tube fabricated during the last quarter was tested. The tube broke during a subsequent run and a second tube was fabricated and tested. Twelve I/V curves were taken at different emitter temperatures and different oil bath temperatures. The results obtained are a valuable aid in correlating experimental and theoretical results.

b. Related tests and research

The efforts in this area were devoted to work on three types of

heaters and determining the effects of cesium and rubidium on metals. The three types of heaters are:

(1) Wire wound ceramic.

(2) Tungsten wire radiation.

(3) Metallized ceramic.

Tests on the wire wound ceramic heater were satisfactory, but it is considered too fragile for use in a prototype. A tungsten wire radiation heater was also fabricated and tested. The test results were very encouraging and the heater appears to be very rugged. It will be incorporated in a test device as a part of Subtask 5.3. A metallized ceramic heater was assembled and tested. However, hot spots developed on the metallized portion of the heater. At 1500° K the metallizing burned out. It is hoped that hot spots can be eliminated by machining the metallizing so the helix is wider.

A cesium corrosion test device was designed and fabricated. Several sample materials and brazes were tested. These cesium corrosion tests indicate that tantalum, molybdenum, copper, nickel, titanium, platinum, Driver-Harris alloy and Type 304 stainless steel can be used as the structural metals. Copper, copper-silver, nickel and Incusil are suitable braze materials in high temperature cesium devices.

c. Development of improved collectors

This is a continuation of the Work Function Tests described in the last quarterly report. The work concentrated on the molybdenum collector used in conjunction with a Type B impregnated tungsten emitter. A series of tests were run which have shown that:

(1) Results with the first tube are reproducible.

(2) Certain modifications to the activation procedure resulted in even a lower collector work function.

(3) An activated pair of electrodes can be exposed to air for a period of hours without destroying the surface properties.

(4) The collector firing temperature is the factor of prime importance in determining the value of the collector work function.

Work was also initiated on a diode with a nickel collector and a

barium impregnated emitter. An apparatus was designed and partially constructed to determine the relationship between collector temperature and collector work function in a continuously pumping vacuum system.

3. Subtask 5.3--Development of Low Power Thermionic Generator

Thermionic Generators 1A and 1B were completed and the dynamic testing of Unit 1B was accomplished. The design of the more advanced generator, based on a Curium-242 heat source, was initiated.

Work on improved heat transfer between the emitter holder and the heat source revealed that placing a layer of molybdenum powder between the two surfaces is preferred to other methods tested since it gives not only a lower film drop, but also more consistent results. It has been shown that attempts to braze the emitter to the emitter holder to reduce this film drop have resulted in adverse effects on the emission characteristics of the emitter. This effort will continue.

A vacuum shell identical to that used in Generator 1A was tested prior to fabricating Unit 1A. Tests on electrical leadthroughs have shown that the reactive metal leadthroughs are much superior to other types considered.

Creep tests on sapphire spacers (Al_2O_3) have shown that some creep takes place above 1200° C, and above 1300° C, the strength of the sapphire falls off rapidly. Tests to determine surface distortion of the emitter and collector and the differential thermal expansion of the sapphire rods were initiated.

The parametric study initiated last quarter was completed. The results show the relationship existing between the power density of the heat source and the efficiency and geometry of the thermionic converter. It has been shown that the lower power, inherently less efficient devices require higher power density isotopes for operation near their maximum efficiency point than do the high power units. The higher power units require an isotope power density of only 6 to 10 watts/cm^3 to achieve 95% of the maximum attainable efficiency, whereas a practical 5-watt unit requires a power density of approximately 50 watts/cm^3 to operate at 95% of its peak efficiency. The dimensions of the isotope, and hence the dimensions of the generator, become impractical at high values of isotope power density and influence the choice of isotope to be used in a thermionic generator.

A device for measuring the thermal expansion of ceric oxide fuel pellets while in a hot cell was fabricated. However, attempts to accurately

calibrate it failed. The Bureau of Standards has been contacted concerning this problem.

Experiments aimed at determining the interaction of oxygen with ceric oxide and molybdenum have shown that a quite complex interaction takes place. It was determined that it is not safe to assume that the oxygen liberated in the decay of ceric oxide (Ce-144) will be gettered by the molybdenum fuel capsule, and a pressure buildup will not occur. Work will be continued in an attempt to better understand the interaction that occurs.

A device to sample the gas generated in a ceric oxide fueled molybdenum capsule at the end of a half life has been successfully tested.

4. Subtask 5.5--Operational Thermoelectric 2- to 5-Watt Generator For Space Use

a. Generator operational tests

Altitude chamber tests were completed successfully. The sublimation test was halted after 300 hours of operation since extensive deterioration occurred in all but the spray-coated couple. Components are being prepared for a second test run using an improved method. The power flattening life test indicated the feasibility of a gas-leak method.

A shock wave test proved the capsule can survive missile propellant detonation. Two additional runs on the high velocity test track resulted in successful impacts of capsule specimens. Salt water and salt spray tests demonstrated that Haynes-25 material has a high corrosion resistance. A horizontal range of 270 feet was achieved using the redesigned thruster for ejection. Plasma jet tests at the General Electric Aeroscience Laboratory were initiated and completed during this period with some differences apparent between the predicted and actual behavior. Test data are currently being correlated to vehicle trajectories. Pressures of 30,000 psi at 1700° F and 74,000 psi at room temperature have been reached with insignificant capsule deformation. Several successful penetrations of isotope capsules contained in generator specimens were achieved with shaped charges weighing 34 grams.

b. System conceptual design

Power output versus time plots were developed for both the cerium- and polonium-fueled systems using altitude chamber test data. A mounting arrangement has been designed and analyzed. An empirical equation has been developed to predict generator output at any time for variable resistance loads.

5. Subtask 5.6--1-Watt (e) Power Supply

This second quarterly report covers the status of the work completed on the 1-watt (e) power supply, the integration of the generator into a satellite system, the design of the Mod I generator and thermoelectric radiator breadboard test device, the design and test of a converter, and a resume of the work thus far completed in the hazards and shielding evaluation. A separate hazards and shielding evaluation report will be released at the end of this fiscal year.

Accomplishments thus far in the program have been on schedule and in accordance with the contract schedule requirements. The following list, by percentage complete as of March 31, 1960, defines the status of work.

	(%)
System integration in satellite	70
Generator design and analysis	85
Thermoelectric-breadboard test device	70
Converter design and analysis	100
Hazards and shielding evaluation	25
Total contract dollar expenditures	80

6. Subtask 5.7--100-Watt Thermoelectric Generator

The objective of this Subtask was to prepare a conceptual design of a 100-watt thermoelectric generator, fueled with Cu-242 and suitable for operation for six months in a space environment.

The work was completed during the quarter, and the final report, MND-P-2342, is being printed.

7. Subtask 5.8--Conceptual Design of a 13-Watt Thermoelectric Generator

The conceptual design of the 13-watt(e) Curium-242 fueled thermoelectric generator for a six-month space probe mission was essentially completed, except for details relating to power flattening and the heat source. Thermal and electrical characteristics of the final conceptual design were calculated. Heat transfer in the ground handling container was investigated.

The objective of the program was altered to conform to a hard lunar impact mission, with an operational life of two months. Development of a configuration for the new requirement was initiated. Hazards associated with the launch-to-target sequence were evaluated.

I. INTRODUCTION

This is the second of three quarterly progress reports required by Contract AT(30-3)-217 between The Martin Company and the AEC for Fiscal 1960.

The SNAP program has been extensively reorganized under the current contract. The present organization is as follows.

Task 1--Inactive

Task 2--125-Watt Thermoelectric Generator Development

Task 3--Nuclear Thermoelectric Generator Development (Formerly SNAP III)

Task 4--Classified

Task 5--Advanced Technology Program

- Subtask 5.1 Advanced Thermoelectric Power System
- 5.2 Basic Thermionic Development
- 5.3 Development of Low Power Thermionic Generator
- 5.4 (Inactive)
- 5.5 Thermoelectric 2 to 5 Watt Generator for Space Use
- 5.6 Nuclear 1.0 Watt Power Supply
- 5.7 100-Watt Thermoelectric Generator Conceptual Design
- 5.8 13-Watt Thermoelectric Generator Conceptual Design

Task 6--Fuel Technology Development

- Subtask 6.1 General Development and Material Requirement
- 6.2 Americium and Curium Radioisotope Preparation Processes

6.3 Fuel Form

6.4 Hazards Criteria and Shielding

6.5 Radiation Damage Testing

Each task is separately administered. Tasks 2, 3, 5 and 6 are now unclassified. This report is the second unclassified technical progress document published since the inception of the radioisotope power program. It covers work done on the unclassified tasks during January through March 1960.

II. TASK 2

The Task 2 program is directed toward the completion and ground test demonstration of a radioisotope-fueled, 125-watt, thermoelectric generator for space application. During this quarterly reporting period, hardware fabrication of the third generator, fueled with Cerium-144, and all associated ground handling equipment was terminated in accordance with directions from the USAEC. It is planned to resume this work in Fiscal Year 1961 to correspond with the delivery of the radioisotope fuel from ORNL.

Fuel core development and hazards studies were continued to obtain complete fuel containment in all cases of vehicle failure at the launch pad or during launch ascent, and to obtain fuel core burnup upon re-entry from orbit. Testing in the areas of fuel core containment, materials compatibility and plasma flame burnup has shown that these objectives can be obtained.

A. SUBTASK 2.1--SYSTEM DESIGN

During this quarterly reporting period, the planned objectives for Subtask 2.1 were:

(1) Design support and engineering analysis associated with the fabrication, assembly and test of two prototype, electrically heated, 125-watt thermoelectric generators, related test equipment and testing programs.

(2) Design of one generator for fueling with 8.8×10^5 curies of Cerium-144 in the pelletized ceric oxide form.

(3) Completion of ground handling equipment designs and procedures required for shipment of the radioisotope-fueled block, loading of the ground test generator and hot cell generator testing.

(4) Completion of a remote welding mechanism and fuel block cooling rig design to facilitate loading and sealing of the radioisotope fuel core at ORNL.

1. Design Support and Engineering Analysis

Design support*. During this quarter, several design improvements have been incorporated for use in the electrically heated environmental test generator and the isotope-fueled ground test generator. These changes include:

* P. J. Dick, B. Callender

(1) Use of chem-milled outer aluminum skins to provide integral bosses for thermoelectric accessibility, and to improve welding characteristics at the skin joints.

(2) Making the cold junction heat transfer cup an integral part of the thermoelectric access plug.

(3) Establishing the flexible dissimilar metal joints required at six places between the inner stainless steel skin and the outer aluminum skin to provide structurally sound, gas-tight seals. An ultrasonic welding technique has been developed to obtain a metallurgical bond between the dissimilar metals.

(4) Obtaining minimum electrical contact resistance at the hot junction of each thermoelectric assembly by prebonding to individual iron hot shoes. The boron nitride electrical insulating shoe will be replaced with a flame spray coating of aluminum oxide (Al_2O_3) on the iron hot shoes.

(5) Obtaining electrical continuity between individual iron hot shoes of a P and N couple by a flexible copper jumper lug. Details of the thermoelectric assembly and outer chem-milled skin configuration are shown in Fig. II-1.

(6) Dividing the electrical circuit for the thermoelectric system into eight sections with eight external test points to facilitate electrical test measurements. Conax connectors are used at the electrical test points.

(7) Completing the detail design of the thermal-hydraulic heat dump shutter control system. Actuating bellows for the mercury vapor system will have an effective piston area of one square inch and a spring rate of 50 pounds per inch.

Engineering analysis*. A force analysis was made to determine the operating characteristics of the bellows in the thermal-hydraulic shutter control system to be used with the environmental test and isotope ground test generators. This analysis indicated that the systems would operate from fully closed to fully open over an inner skin temperature range of 1040 to 1115° F. This temperature range is satisfactory for adequate temperature control.

---

* W. Lyon

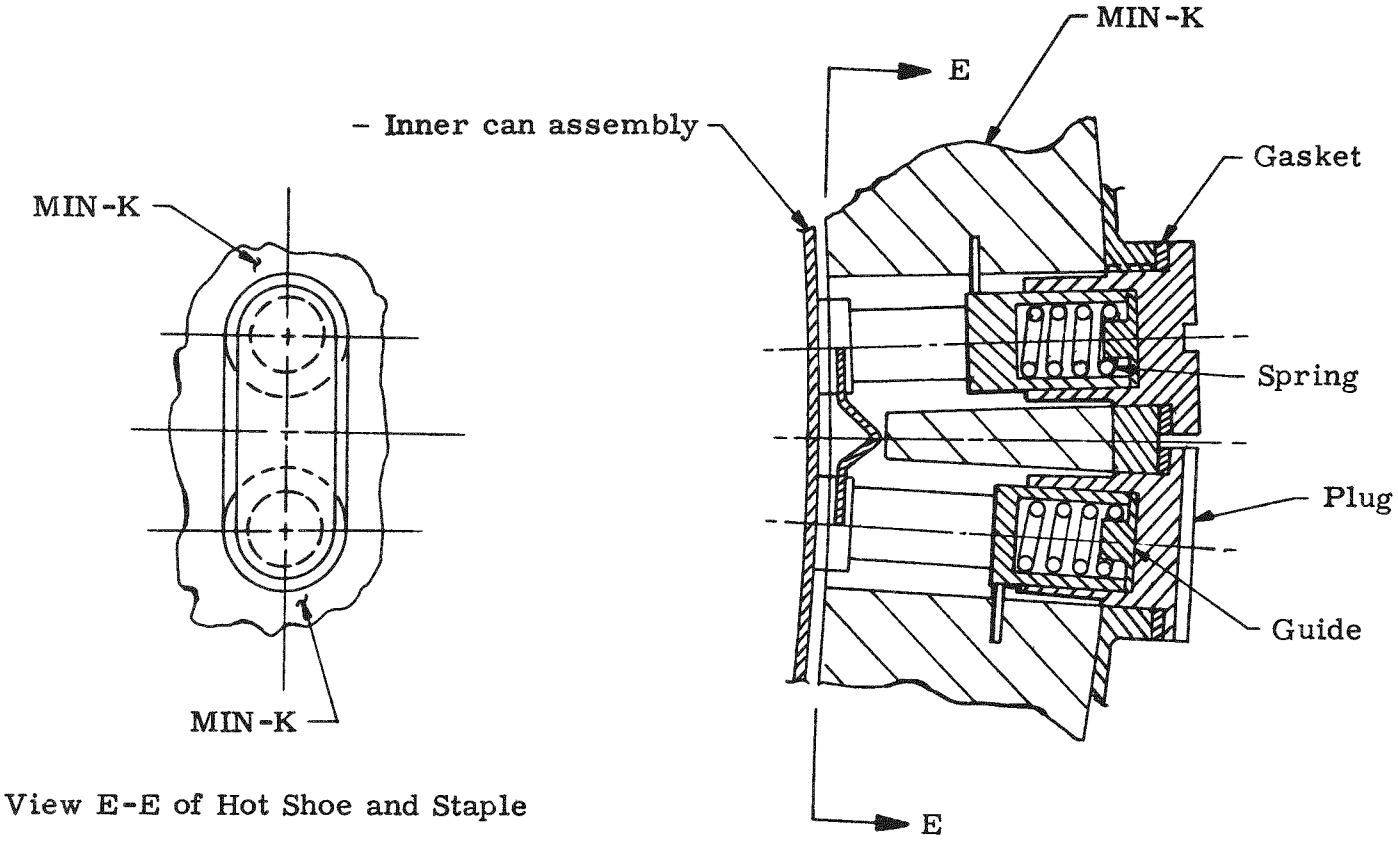

Fig. II-1. Typical View of Thermoelectric Element Assembly

An investigation of the thermoelectric hot junction contact resistance for the initial electrically heated prototype generator was made using single couple experimental data obtained in the laboratory. Using the average values obtained in 14 test runs, the thermoelectric couple hot junction contact resistance was found to be approximately 8 milliohms, or 46% of the thermoelectric material resistance at 1100° F hot junction temperature. Generator power output was then extrapolated by calculation to be 86 watts at 25 volts. These data indicated the need for improved hot junction bonding techniques to achieve the design power output of 125 watts. A prebonding technique has been established to minimize this contact resistance for the environmental test generator.

2. Isotope Ground Test Generator Design*

The isotope ground test generator design was completed during this quarterly reporting period. This generator is identical in design to the environmental test unit with the exception of the fuel block, fuel block support and block locking mechanism. The isotope fuel block is shown in Fig. II-2. An artist's drawing of the isotope ground test generator is shown in Fig. II-3.

3. Ground Handling Equipment Design**

Design studies, procurement specifications and drawings for all ground handling equipment to be used for hot cell generator tests were completed during this quarterly reporting period. The engineering drawings completed are:

(1) Test dolly cold plates.

(2) Test dolly plumbing system.

(3) Shipping cask dolly.

(4) Collar shield assembly.

(5) Cask assembly.

(6) Shipping cask loading stand.

(7) Collar shield, generator and loading stand hoisting slings.

---

* T. Sullivan
** M. J. Reilly

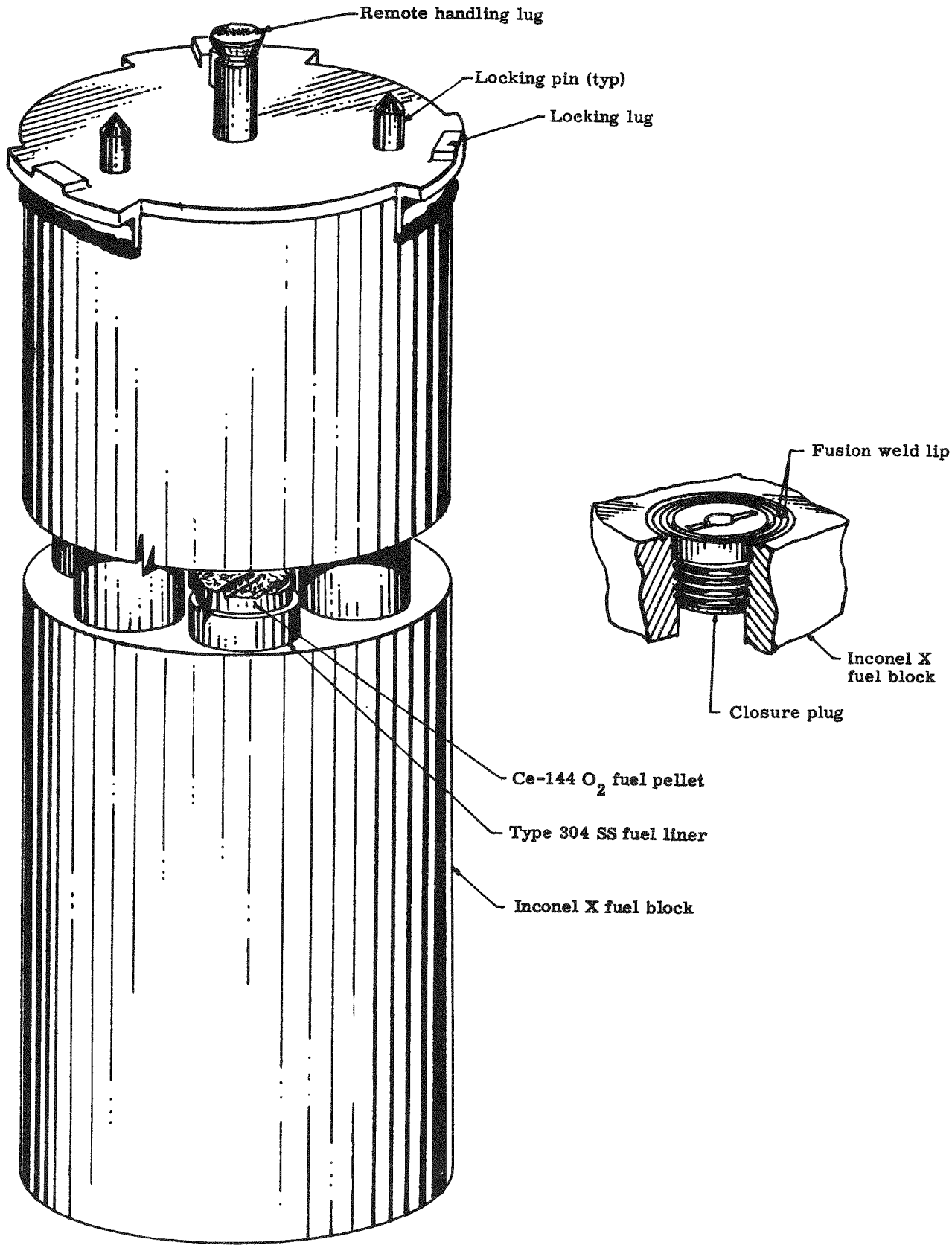

Fig. II-2. Task 2 Isotope Ground Test Generator Fuel Core

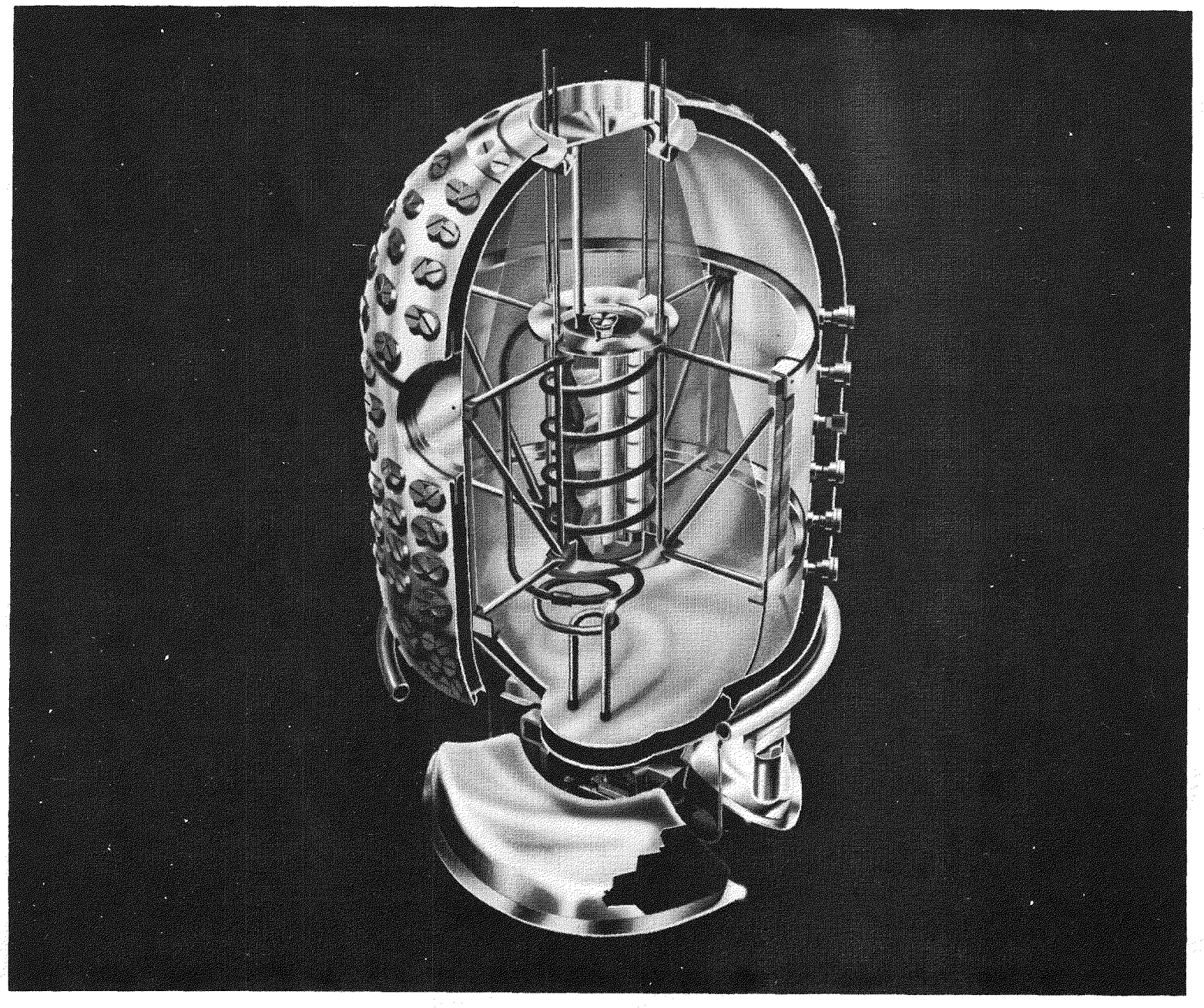

Fig. II-3. Isotope Ground Test Generator

The operating procedures manual for the Task 2 Ground Handling System was completed. This report, MND-P-2316, is entitled "Preliminary Technical Manual, Loading, Shipping and Testing Procedures for Task 2 Isotopic Powered Thermoelectric Generator." It includes preparation and procedures for shipping, assembly and loading at Oak Ridge. Also included are pertinent drawings and photographs for the transfer and test operations to be performed at the Martin Nuclear hot cell facility.

Shipping Permit No. 898 has been received from the Bureau of Explosives to allow transportation of the Task 2 radioisotope fuel block in the shipping cask (Fig. II-4). Conditions of approval were:

(1) The installation of a protective enclosure around the cask to preclude inadvertent physical contact with the cask surface. (This design work has been accomplished.)

(2) Prior notification to the Bureau of Explosives concerning date of shipment, origin, destination, type of transportation and curie level of the radioactive material being shipped.

4. Remote Welder and Fuel Core Cooling Rig Design*

Proposed configurations for the remote welder and fuel block cooling rig have been reviewed with ORNL personnel. The configuration on Fig. II-5 was selected and the detail design has been completed.

B. SUBTASK 2.2--MATERIALS ANALYSIS

During this quarterly reporting period, the planned objectives were to:

(1) Continue the development of cerium fuel forms having appropriate burnup characteristics during post orbit re-entry.

(2) Continue the testing and evaluation of fuel container materials having appropriate environmental compatibility and postorbit re-entry burnup characteristics.

(3) Coordinate with ORNL on a radioactive ceric oxide fuel form and fuel delivery schedule for one Task 2, 125-watt, thermoelectric ground test generator.

---

* T. Sullivan

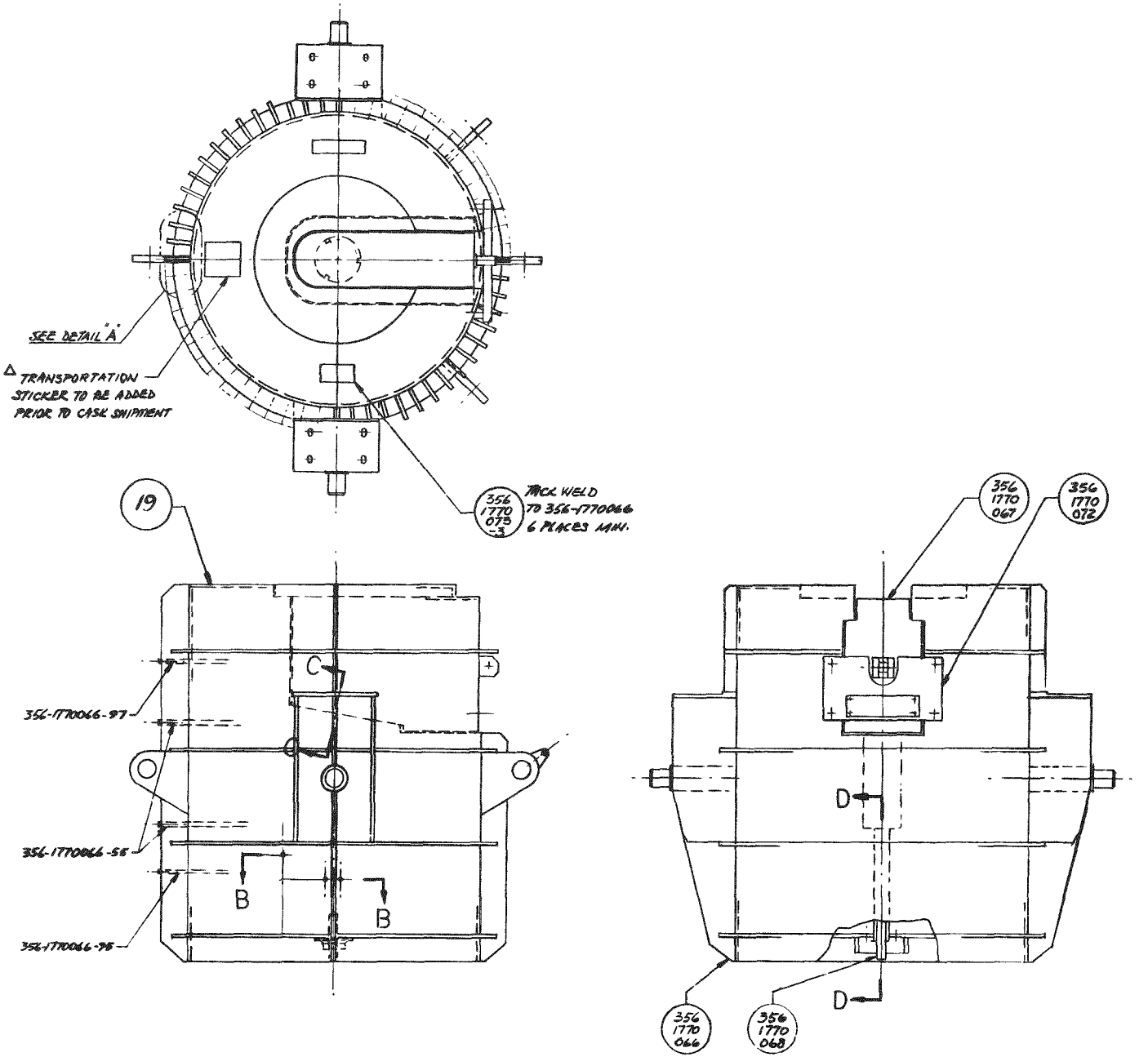

Fig. II-4. Shipping Casks

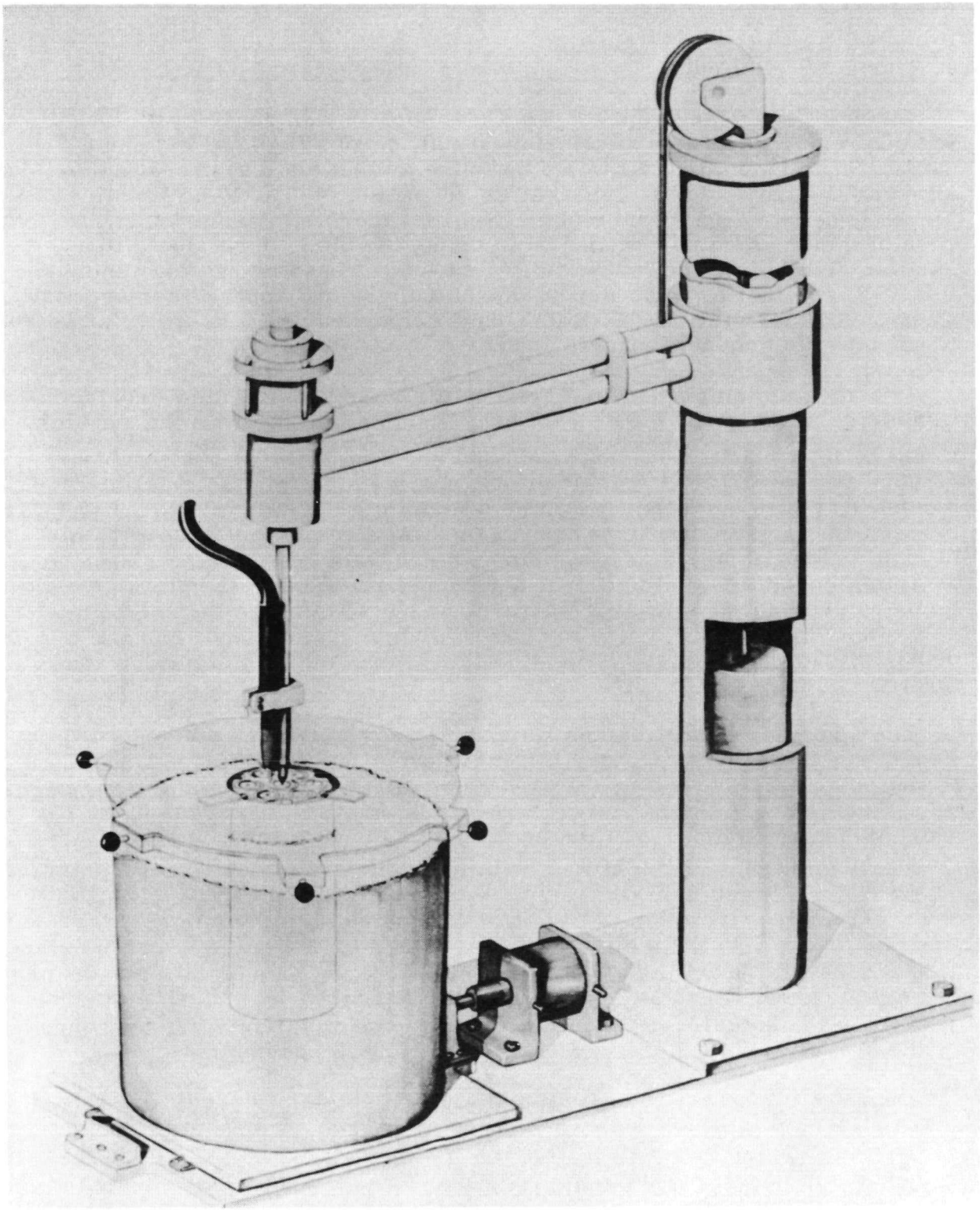

Fig. II-5. Task 2 Remote Welder

1. Cerium Fuel Study*

Material screening studies. Fuel materials under consideration for the Task 2 generator are cerium metal, cerous fluoride and ceric oxide. Since cerium metal would be in the molten state at operating temperature, it would be dispersed as droplets as soon as the container block burned through to the molten metal upon orbital re-entry. In the case of the cerous fluoride and ceric oxide, the block must ablate to a smaller size before the fuel is fully exposed to re-entry heating conditions. These fuel form burnup studies are therefore confined to cerous fluoride and ceric oxide. Additions have been used with the ceric oxide to improve the burnup characteristics.

Previous tests using an oxyacetylene flame have shown that iron additions to ceric oxide (15% Fe-85% CeO_2--cerium density--4.5 gm/cc) would melt at a much lower temperature than the straight ceric oxide (1800° C versus 2700° C). However, plasma tests on this material indicated that the "burn-through" time was quite long and it appeared that much of the iron "sweated out" during heating, leaving a porous ceramic of high melting temperature. Attempts were made to add metals such as aluminum which would produce a thermite reaction at the elevated temperatures encountered during re-entry. However, the thermite reaction usually went to completion during sintering operations and the densities of the specimens made with this type of addition were, therefore, very low.

The additions of metal carbides and nitrides were then studied as it was known that these materials decompose at elevated temperatures. It was postulated that the metal carbide or nitride, at elevated temperature, would reduce the ceric oxide to cerous oxide. The cerous oxide, which has a much lower melting point than the ceric oxide, is pyrophoric and the decomposition products would aid in shattering the pellet. Additions of tantalum carbide, titanium carbide, silicon carbide and silicon nitride were made. Specimens containing tantalum carbide and titanium carbide after sintering were pitted on the surface and had very low density. Density of the specimen containing silicon nitride was only slightly lower than that of the fluoride (10% Si_3N_4-90% CeO_2--cerium density, 3.63 gm/cc). No further work was done on the nitride, however, as the silicon carbide appeared most promising in burnup tests.

Sintering of ceric oxide with metal carbide and nitride additions was accomplished initially in both a hydrogen and argon atmosphere. Argon was used for the subsequent work, as argon sintering produced higher density specimens. The original density of the CeO_2 + 10% SiC specimens was quite low. Use of particle sizes coarser than the 600 mesh

* H. Barr

powder originally used was of no benefit. Therefore, the sintering times and temperatures were varied from 1300 to 1550° C and from 1/2 to 8 hours. Although the density was improved slightly by adjusting the sintering schedule, the cerium densities were not as high as the cerous fluoride (3.74 gm/cc). It was noted after several of the tests that the CeO_2 + 10% SiC had reacted with the zirconia setter tile on which it was sintered. Tests with granular SiC and alumina setter plates revealed that no reaction took place on these materials and the density was much improved. The density was further improved by the addition of 1/2% CaO (as $CaCO_3$), a sintering aid. A cerium density of 4.0 gm/cc was obtained by sintering a mixture of CeO_2 + 10% SiC + 1/2% CaO at 1550° C for 4 hours on alumina setter tile.

Additions of 5 and 7-1/2% SiC were also made to the CeO_2 to determine the effect on density and burnup rates. Preliminary burnup tests with the plasma flame indicated the 5% SiC showed little improvement over pure CeO_2. While the 7.5% SiC addition improved burnup, it was not quite as good as the material containing 10% SiC.

The increase in burnup properties of ceric oxide by the addition of SiC is due to the reduction of CeO_2 to Ce_2O_3. A test therefore was run to determine the stability of the compacts at the temperature maintained by Cerium-144. Heating the specimens to 1000° F in air for 15 minutes produced oxidation of the Ce_2O_3 back to CeO_2, with a subsequent growth and spalling of material from the surface of the pellet. This test indicated that compacts which will be thermally hot due to the radioactive Ce-144 must be handled and stored in an inert atmosphere to prevent immediate oxidation.

Plasma flame testing. The plasma flame generator produces a high temperature gas plasma by confining an electric arc to a restricted area. The arc is stabilized by gas flowing through a nozzle in which the arc is produced. This gas also conducts the heat to the specimens being tested. The primary gas used in these tests to obtain the plasma was nitrogen with oxygen added to the plasma as a secondary gas.

In the initial work with the plasma flame, an attempt was made to obtain the ablation rate at various temperatures. A number of tests were performed, but it was very difficult to obtain a higher temperature after the melting point of the test material had been reached. Calibration of the plasma at various electrical inputs and gas flows was then initiated. In all tests, a mixture of nitrogen and oxygen in a ratio to simulate air was used.

Two calibration techniques were used to determine the plasma flame heat flux. The test facility is shown in Fig. II-6. The first method used the temperature rise with time of a 1/4-inch diameter by 1/4-inch long copper cylinder as a measure of the heat flux. The cylinder is encased in a phenolic nylon holder, 3/4 inch in diameter and about 3 inches long. Because of the widely differing diffusivities of the two materials mentioned, it has been assumed that the heat loss from the copper to the holder is negligible compared to the heat absorbed by the copper from the plasma flame. The second method uses the time to initiate melting of an assumed infinitely long cylinder as a measure of the incident heat flux. A 1/2-inch diameter by 3-inches long pure aluminum cylinder encased in a 3/4-inch diameter phenolic nylon holder was used. Test specimens are shown in Fig. II-7.

Eighteen calibration runs were used to obtain heat fluxes at five machine settings. The two calibration methods were used at each machine setting together with some additional runs to determine reproducibility using the short copper cylinders. The agreement in some cases was excellent. A preliminary summary of the available calibration results is tabulated in Table II-1.

TABLE II-1

Calibration Results

Current (amp)	Air Flow (ft^3/hr)	Heat Flux in Cylinder ($Btu/ft^2/sec$)	
		Copper	Aluminum
700	100	*	324
450	100	165	178
		200	
450	150	169	169
		183	
350	100	152	152
350	50	*	*

*Data not yet available.

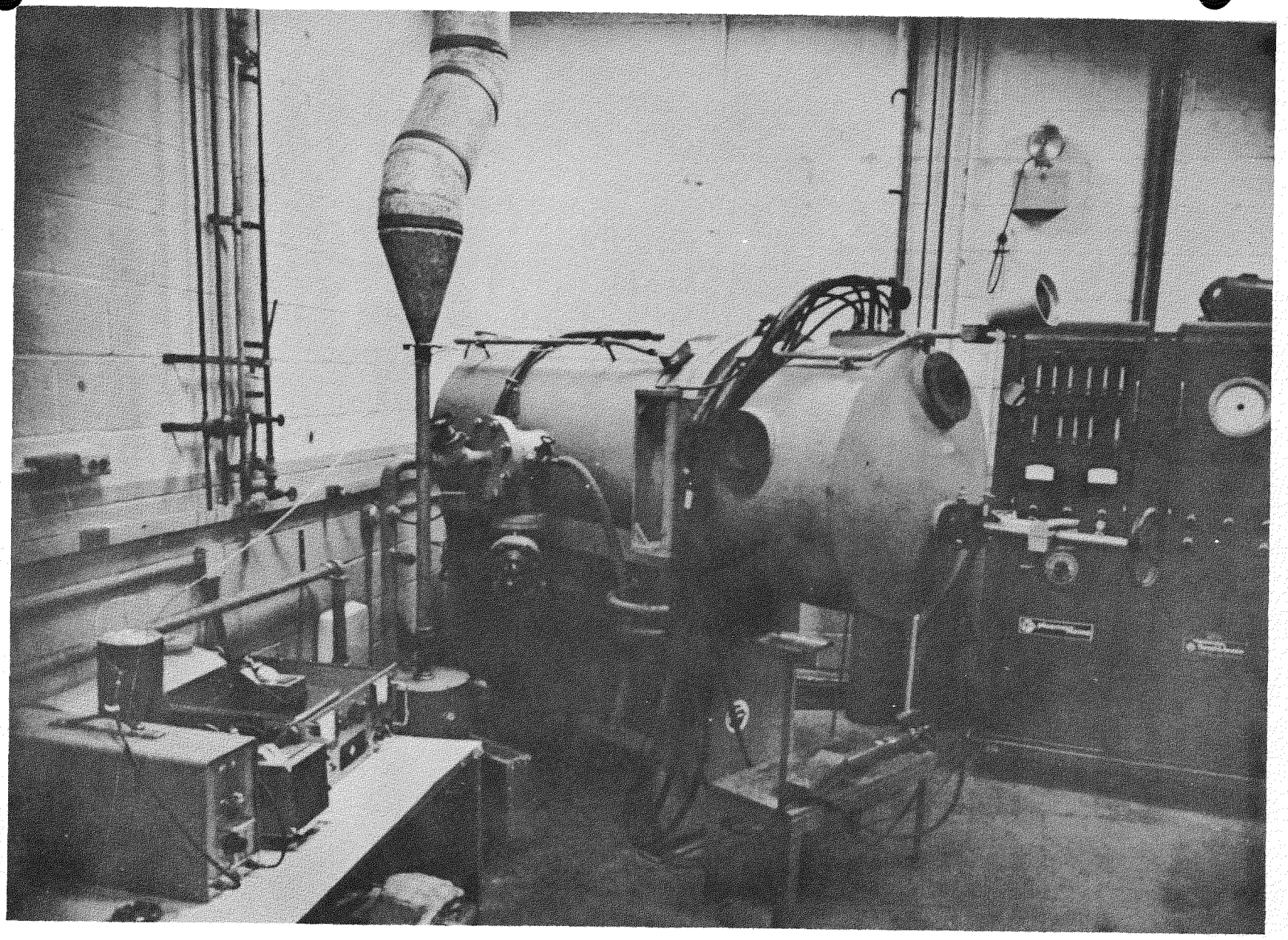

Fig. II-6. Arc Heated Wind Tunnel Facility

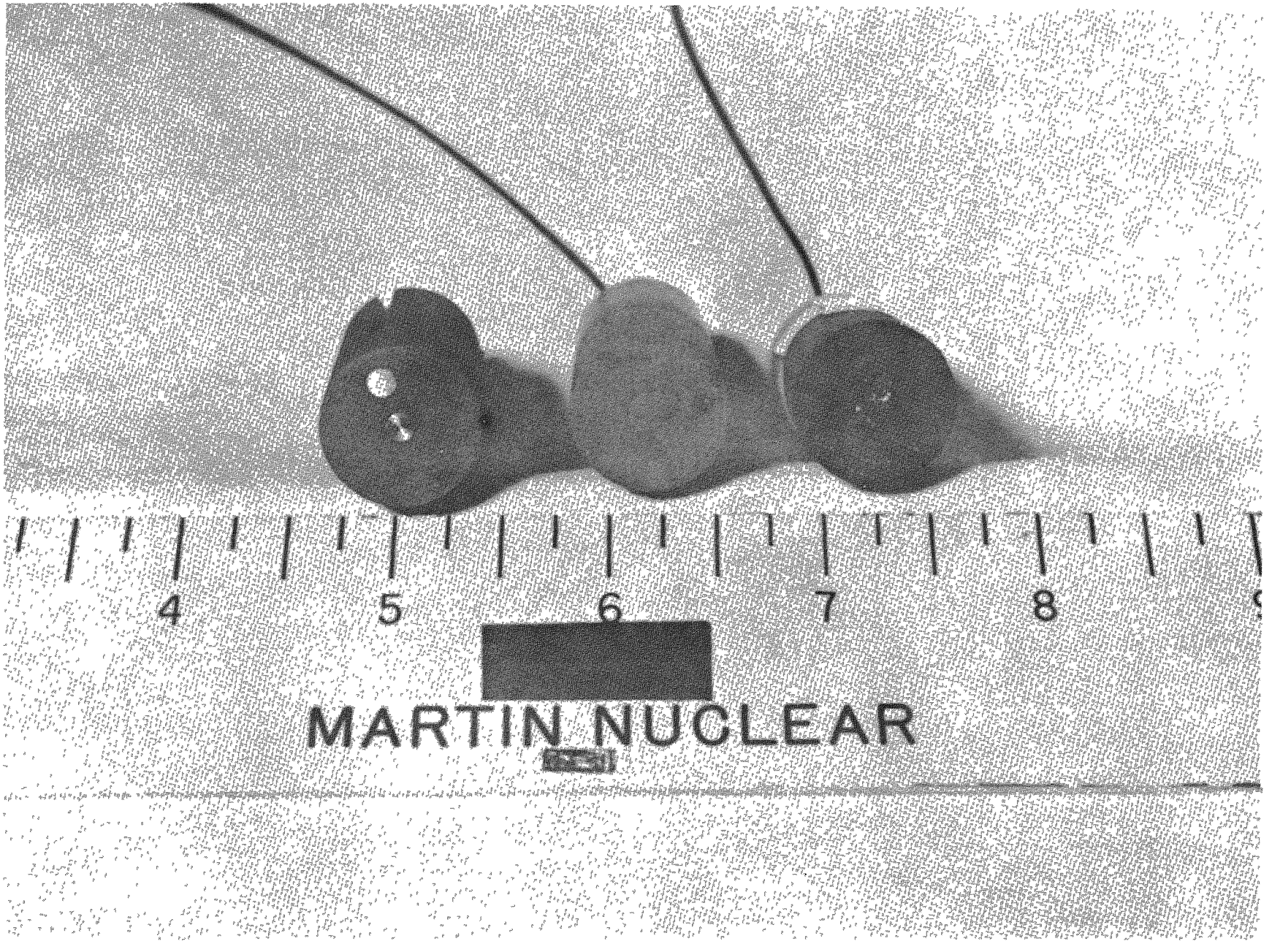

Fig. II-7. Front View of Calibration Specimens

Figure II-8 shows a typical calibration sample test setup.

The ablation rate was determined by subjecting specimens of 1/2-inch diameter and varying thickness to heat inputs between 150 and 325 $Btu/ft^2/sec$. The specimens were mounted in a 3/4-inch diameter graphite holder. The burnup or ablation time was determined to 1/10th second by recording the elapsed time period between placing the model in the plasma and the abrupt temperature rise of a thermocouple placed in the holder behind the specimen to indicate burn-through. Specimens of phenolic nylon, stainless steel, zirconia and graphite were tested in an attempt to find a holder which would minimize the heat losses. However, it was found that there was very little difference in ablation or burn-through time with any of the holders tested. Graphite holders were chosen as they were more durable and were more readily fabricated. Figure II-9 shows a specimen of ceric oxide plus 10% SiC being ablated in the plasma flame.

The results of the burn-through tests for determining the effect of various holders is shown in Table II-2. These tests were run with a power setting of 600 amperes at 45 volts, and a gas flow of 165 cfh (130 cfh N_2 and 35 cfh oxygen).

TABLE II-2

Effect of Holder Material on Burn-Through Time

Material	Thickness (in.)	Holder	Burn-Through Time (sec)	Ablation Time (sec/in.)
CeF_3	0.113	Phenolic nylon	9.2	81.4
CeF_3	0.113	Stainless steel	9.5	84.0
CeF_3	0.113	Zirconia	9.1	80.5
CeF_3	0.113	Graphite	9.3	82.3

The diffusivity of the holder materials shown in Table II-2 was considerably different, and should be reflected in the burn-through rates. However, for the duration of the test and the model configuration, no apparent radial heat losses were evident and unidimensional heating was considered.

The burn-through and ablation time for cerous fluoride, ceric oxide + 10% SiC and ceric oxide + 7.5% SiC, are given in Table II-3.

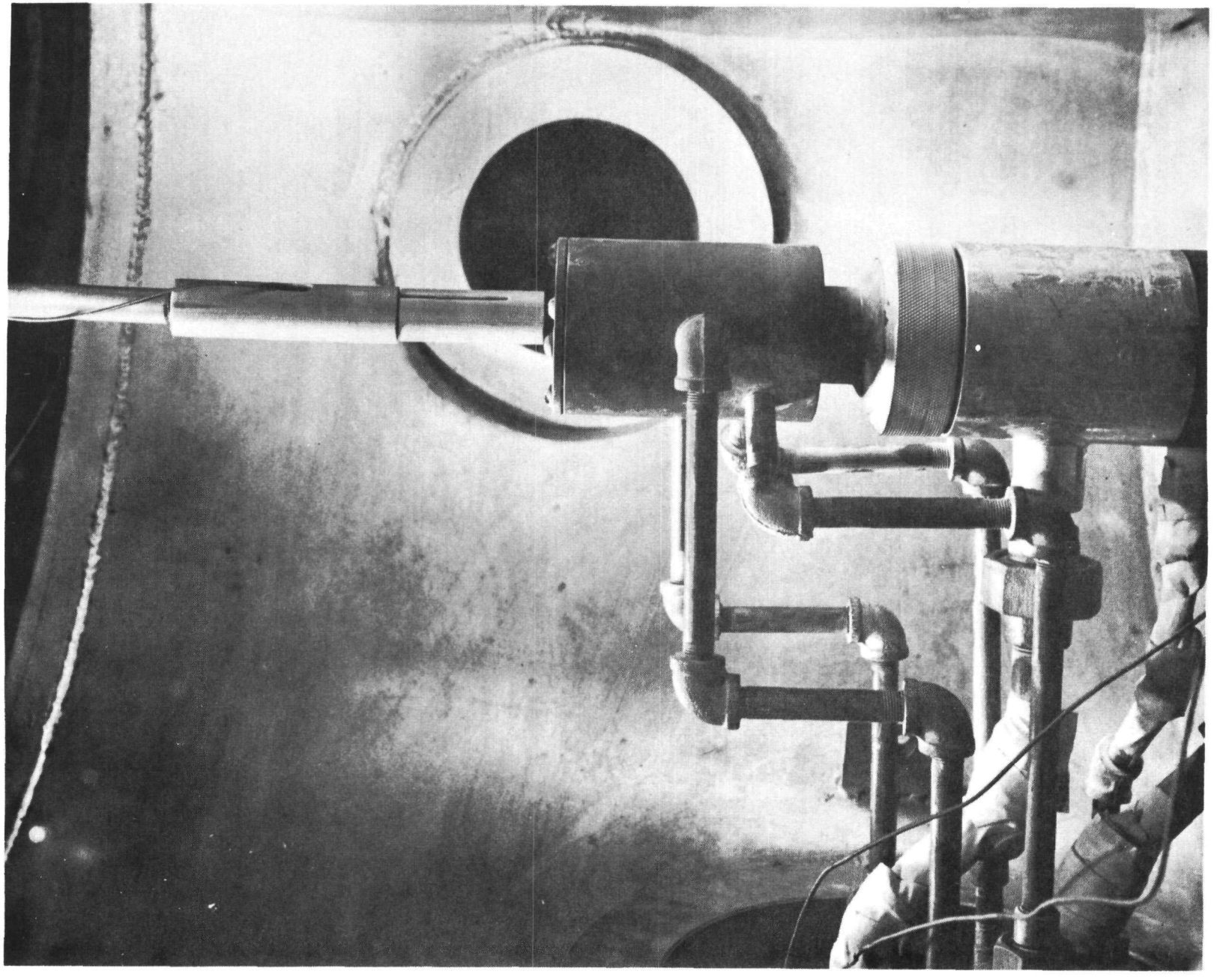

Fig. II-8. Plasma Nozzle with Calibration Model in Place

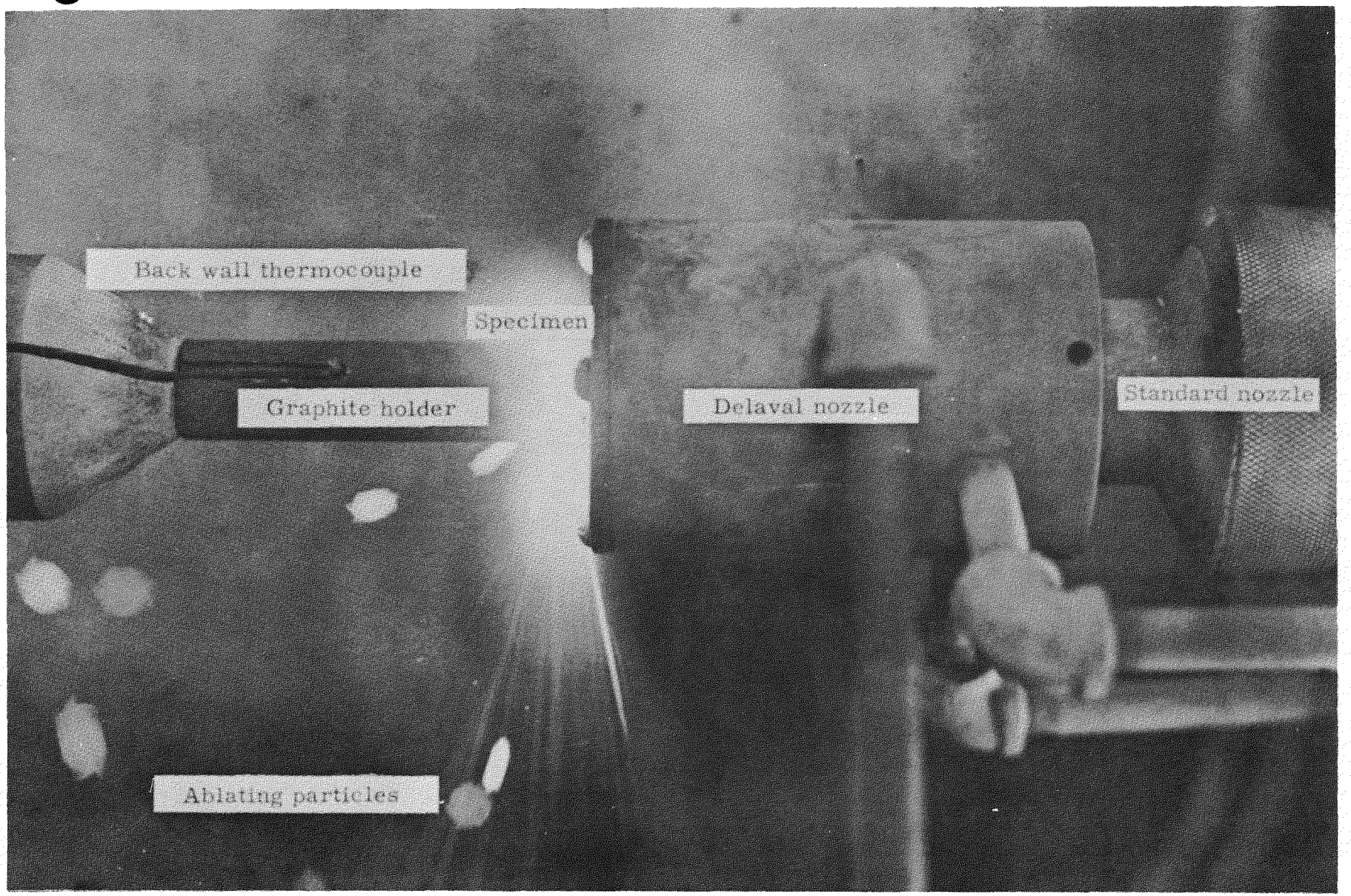

Fig. II-9. Ablation Test of Materials

TABLE II-3

Ablation Rate of Fuel Material

Material	Thickness (in.)	Heat Flux (Btu/ft^2/sec)	Gas Flow (cfh)	Burn-Through Time (sec)	Ablation Rate (sec/in.)
CeF_3	0.098	152	100	21.7	221.5
	0.150	152	100	33.5	216.5
	0.200	152	100	41.1	205.5
					Avg 214.5
CeF_3	0.098	174	150	12.8	130.7
	0.150	174	150	21.3	142.0
	0.200	174	150	25.5	127.5
					Avg 133.4
CeF_3	0.098	181	100	11.4	116.3
	0.150	181	100	17.3	115.3
	0.200	181	100	22.8	114.0
					Avg 115.2
CeF_3	0.098	325	100	4.72	48.2
	0.150	325	100	7.56	50.4
	0.200	325	100	9.46	47.5
					Avg 48.6
CeO_2 + 10% SiC	0.100	152	100	13.5	135.0
	0.150	152	100	18.1	121.0
	0.200	152	100	26.6	133.0
					Avg 129.6
CeO_2 + 10% SiC	0.100	174	150	10.2	102.5
	0.150	174	150	12.7	84.7
	0.200	174	150	17.0	98.0
					Avg*
CeO_2 + 10% SiC	0.100	181	100	5.0	50.0
	0.150	181	100	7.9	52.6
	0.200	181	100	11.6	58.0
					Avg 53.5
CeO_2 + 10% SiC	0.100	325	100	3.6	36.0
	0.150	325	100	5.2	34.7
	0.200	325	100	5.8	29.8
					Avg 33.5
CeO_2 + 7.5 SiC	0.100	152	100	45.3	453.0
	0.150	152	100	44.3	295.0
	0.200	152	100	38.1	191.0
					Avg*
CeO_2 + 7.5 SiC	0.100	174	150	10.0	100.0
	0.150	174	150	17.0	113.2
	0.200	174	150	21.0	105.0
					Avg 105.5
CeO_2 + 7.5 SiC	0.100	181	100	8.3	83.0
	0.150	181	100	11.0	73.1
	0.200	181	100	13.4	67.2
					Avg 74.4
CeO_2 + 7.5 SiC	0.100	325	100	3.5	35.0
	0.150	325	100	5.57	37.1
	0.200	325	100	7.08	35.4
					Avg 35.8

* Retests are being made.

In Table II-3, the ablation rate is reported in seconds per inch. It can be seen that within the experimental error, the ablation rate is a constant for the various thicknesses tested. The ablation rate is reported in this manner since the fuel pellets will be approximately one inch in diameter when they are released from the boiler. As shown in Fig. II-10, upon re-entry 175 seconds are available for burnup of the last pellets to be released from the fuel block, and an available heat input of 188 Btu/ ft^2/sec on initial release. Referring to Table II-3, with a heat input of 174 Btu/ft^2/sec, an ablation rate of 133 sec/in. was obtained with cerous fluoride, 100 sec/in. for ceric oxide + 10% SiC and 106 sec/in. was obtained with ceric oxide + 7.5% SiC. Under actual re-entry conditions, the ablation rate of the pellets would be considerably higher than the ablation rate found for this heat input because:

(1) The fuel pellets would be at an elevated temperature (approximately 1500° C) whereas the specimens in the plasma flame test were at room temperature at the start of the test.

(2) The heat flux would increase by aerodynamic heating as the fuel pellet is ablating and reducing in size.

(3) The heat flux would increase by aerodynamic heating as the fuel pellet encounters the more dense atmosphere of the lower altitudes.

Also, no correction has been made as yet for altering the incident flux during the heating cycle. As the melting points of the fuel materials are around 3000° F, and the calibration was done at approximately 500° F, a correction factor must be applied.

Evaluation of particles from plasma flame tests. Since the fuel form is to be burned up to a particle size of 10 microns or less, a study of the particle size of material ablated from specimens subjected to the plasma flame is being undertaken. In the plasma flame test, only the particles which can be carried by the gas stream are evaluated. The very large particles which drop from the gas stream are not evaluated. Figure II-11 shows the apparatus used for collecting particles, and the position of the glass slides which are used to collect the particles. The slides are coated with a fine film of vacuum grease providing an adhesive surface on which the particles can adhere. Tests are being run at 450 amperes and at gas flows of 50, 100 and 150 cfh. Figure II-12 shows an example of the particles obtained during a trial test of the operating procedure.

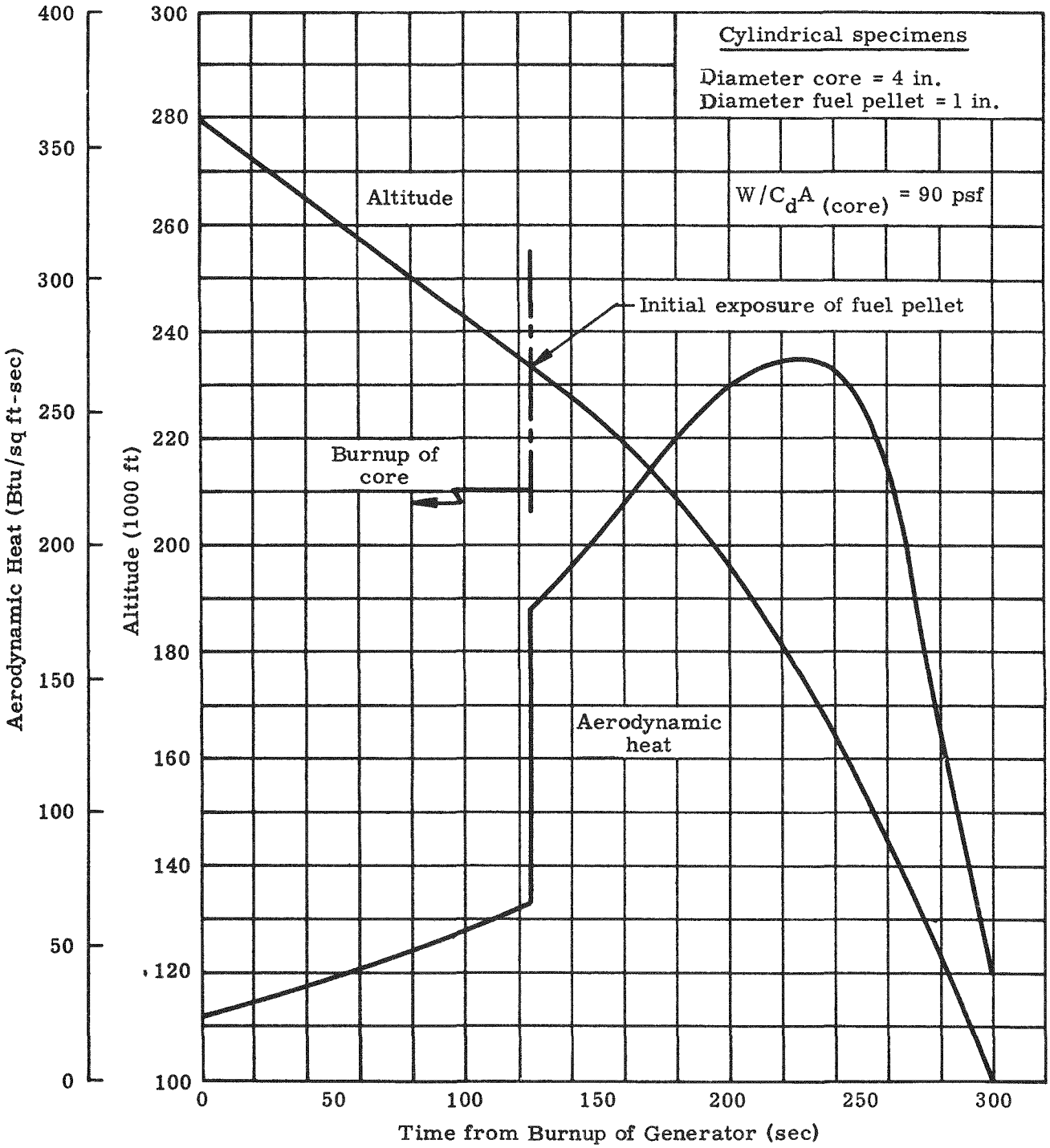

Fig. II-10. Aerodynamic Data for Core and Fuel Pellet Post-Orbital Re-entry

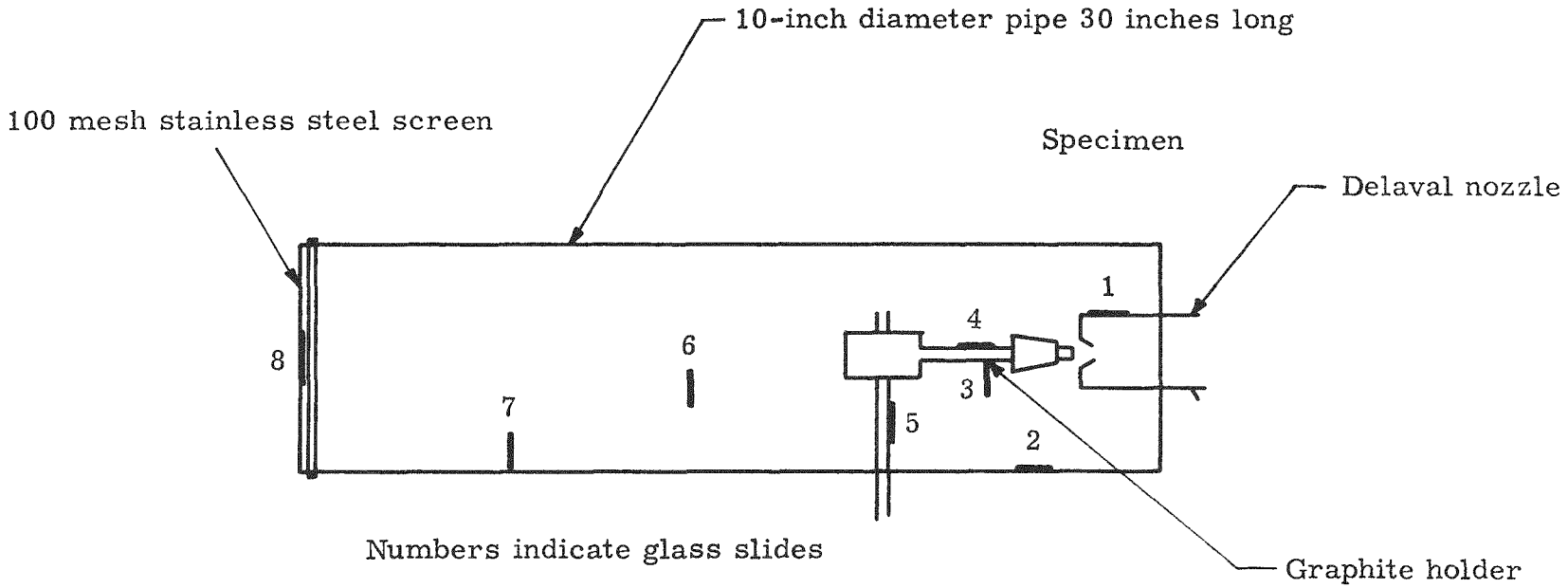

Entire apparatus in wind tunnel

Fig. II-11. Apparatus for Collecting Particles

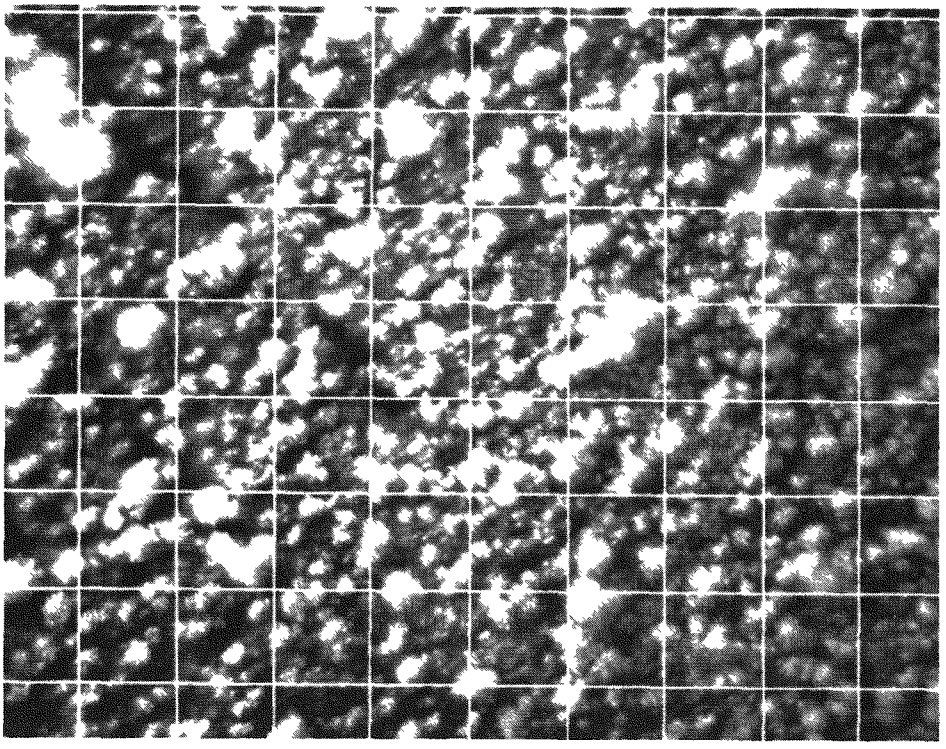

Fig. II-12. Particles Ablated from CeF_3 with Slide Horizontal 2.5 Inches Behind Sample (magn 500X)

Evaporation rate of cerium fuel forms. The evaporation rate study of cerium fuel forms was conducted in an induction furnace evacuated to pressures of less than 0.1 μ. Sample materials were placed within a molybdenum container, and the temperature was raised rapidly from room temperature to the desired temperature in less than five minutes. All samples tested were cylindrical in shape, with approximate dimensions of 1/2-inch diameter and 1/2-inch height.

Initially, cerous fluoride samples were tested at temperatures above their melting point. The method used, however, proved unsatisfactory as the sample spattered when the melting point was reached. Consequently, results were inaccurate. Another method involved rapidly raising the temperature to a point just below melting, and then very gradually heating to the melting point. This, too, proved ineffective as spattering still resulted, although to a lesser degree. In addition to the spattering effect, the samples had a tendency to bubble out of the molybdenum container. This was probably due to the higher temperature attained at the base of the sample where direct contact with the container metal occurred. A consequent buildup of pressure at this point caused the overflow.

Further testing at temperatures above sample melting points has been discontinued until a suitable technique can be developed.

Testing of cerous fluoride samples was continued at temperatures below their melting point. Each test was run for 10 minutes duration at the desired temperature. Temperatures were measured with an optical pyrometer and recorded for every two minutes of the test run, and then an average temperature was determined. To this average temperature, a correction factor of 60° C was added. This correction factor results from earlier test runs using CeF_3 where it was observed that melting occurred at optical readings of 1400° C. The actual melting point of cerous fluoride is given as 1460° C.

Three samples of cerous fluoride tested in this manner gave the following evaporation rates:

(1) At 1280° C--4.35×10^{-5} gm/cm^2/sec.

(2) At 1180° C--8.75×10^{-6} gm/cm^2/sec.

(3) At 1305° C--2.10×10^{-5} gm/cm^2/sec.

These values are plotted in Fig. II-13 and are compared to the theoretical evaporation rate curve for cerous fluoride. In each case, the experimental value is higher than the theoretical value at the given temperature.

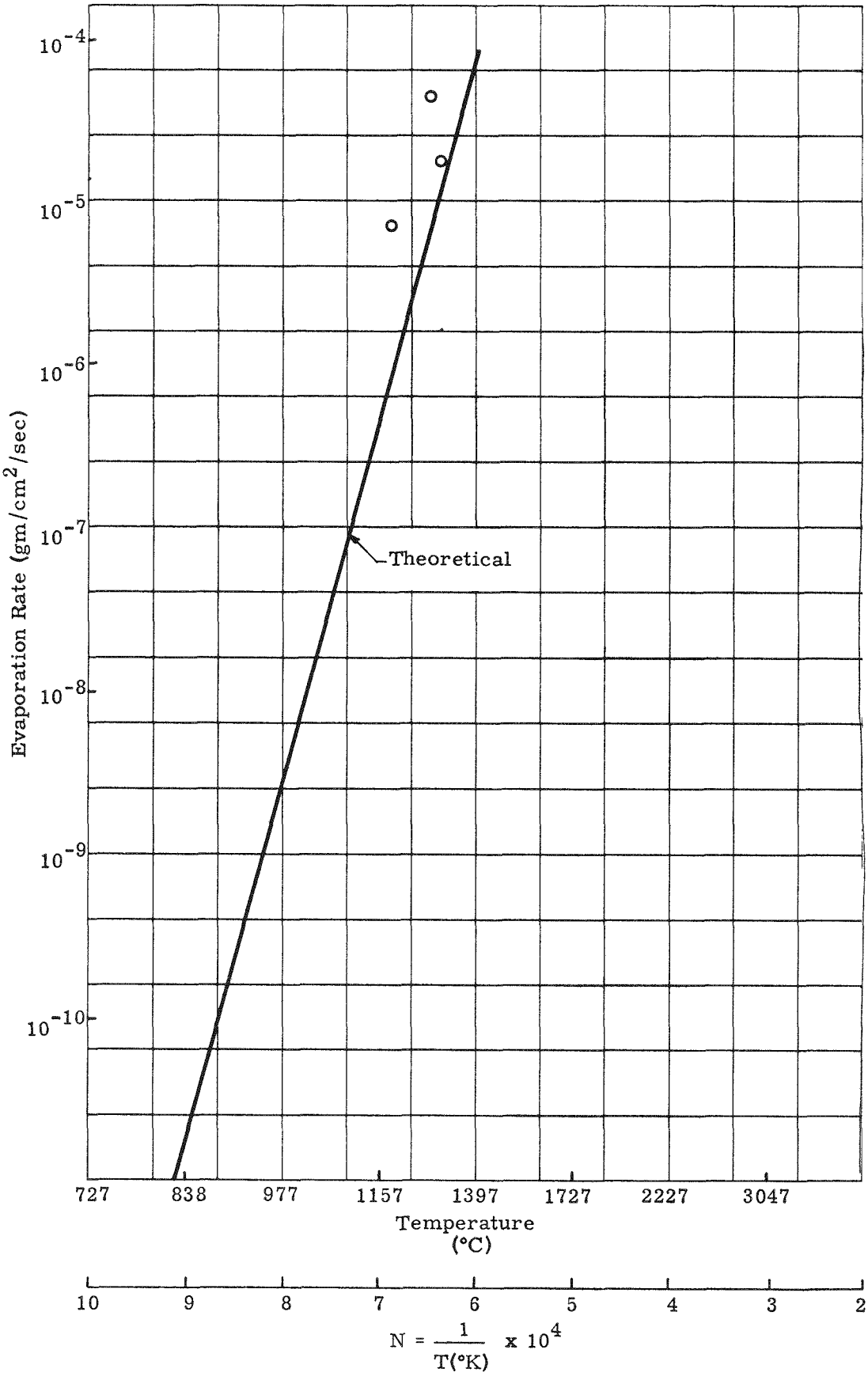

Fig. II-13. Evaporation Rate of CeF_3

2. Fuel Container Material Compatibility Studies*

Allegheny Ludlum S-816 corrosion tests were completed during this reporting period. This alloy contains 18.5 to 20.5% Cr; 19 to 21% Ni; 42 to 44% Co; 3.5 to 4.0% Mo; 3.5 to 4.0% W; 3.5 to 4.0% Cb; 0.35 to 0.45% C; 1.0% Mn maximum; 1.0% Si maximum and the remainder iron.

a. Fuel compatibility tests

Compatibility with ceric oxide. S-816 appeared in good condition after the 120-hour tests in ceric oxide at 1700° F. The photomicrograph, Fig. II-14, does not show evidence of attack. A corrosion rate of 54.35 milligrams per square decimeter per day was observed.

Compatibility with cerous fluoride. S-816 did not show evidence of attack, as shown in Fig. II-15. The corrosion rate was 14.63 milligrams per square decimeter per day.

Compatibility with cerium metal. S-816 is unsuitable containment material for cerium metal. One of the alloy constituents, nickel, is soluble in liquid cerium at 1700° F.

b. Mercury corrosion tests.

S-816 alloy remained unchanged during the 600° F, 30-day mercury tests.

c. Atmospheric oxidation tests

A uniform gray-gold oxide film formed on all of the specimens. The photomicrograph, Fig. II-16 shows no changes in the specimens resulting from the 1700° F tests. For comparison, S-816 had a corrosion rate of 581.4 milligrams per square decimeter per day, Hastelloy B had a corrosion rate of 2821 milligrams per square decimeter per day, and Inconel X had a corrosion rate of 255 milligrams per square decimeter per day. S-816 would be satisfactory for use at 1700° F.

d. Sea water corrosion tests

S-816 corrosion test specimens maintained at 180° F were resistant to attack by 70° F sea water. Low corrosion rates of 0.5 and 0.4 milligrams per square decimeter per day resulted.

This work completes all the corrosion screening tests, and Tables II-4 and II-5 are included to summarize the results.

---

* J. McGrew

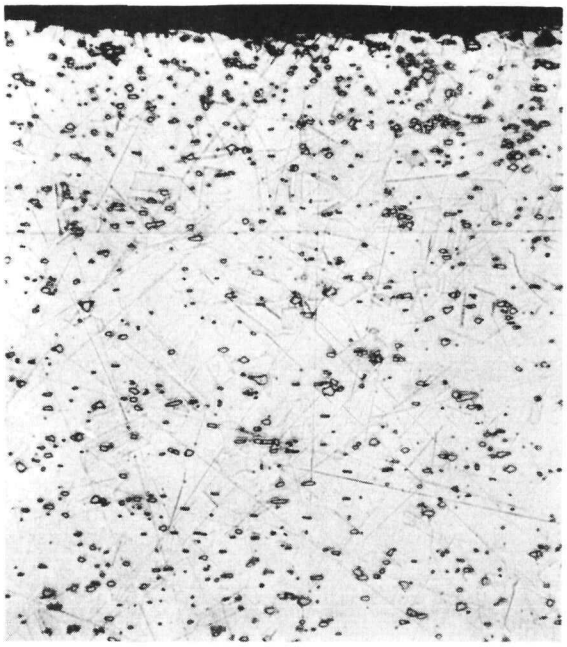

In contact with cerium oxide

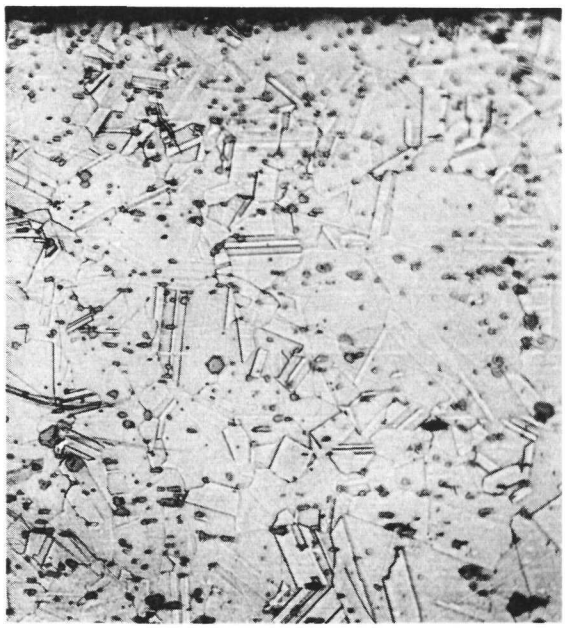

Control sample

Fig. II-14. Allegheny Ludlum Alloy S-816 Heated to 1700° F for 120 Hours in Vacuum (magn 250X)

In contact with cerous fluoride

Control sample

Fig. II-15. Allegheny Ludlum Alloy S-816 Heated to 1700° F for 120 Hours in Vacuum (magn 250X)

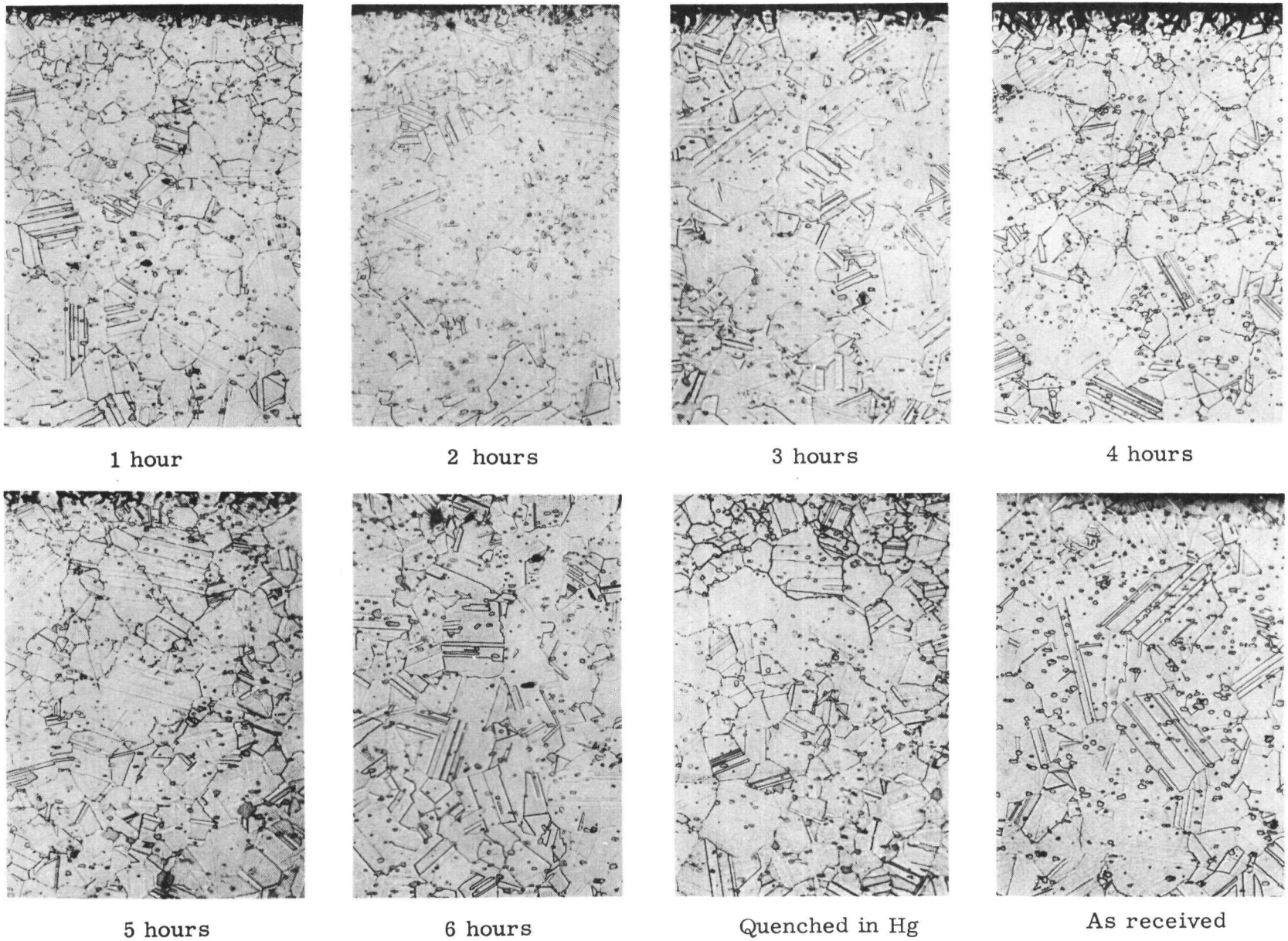

Fig. II-16. Allegheny Ludlum Alloy S-816 Heated to 1700° F for Various Times in Air (magn 250X)

TABLE II-4

Test Results

Test	Test Time	Material	Corrosion Rate (mdd)	Penetration Rate (mpy)	Control Corrosion Rate (mdd)	Control Penetration Rate (mpy)
Air oxidation	6 hr	Hastelloy B	2821			
1700° F	6 hr	Inconel X	255			
	6 hr	S-816	581.4			
Fuel tests						
1700° F						
(a) CeO_2	72 hr	Inconel X	Formed lightly adherent oxide film	--	nil	nil
	96 hr	Hastelloy B	107	16.7	nil	nil
	120 hr	S-816	54.35	9.11	5.92	0.09
(b) CeF_3	96 hr	Inconel X	nil	nil	nil	nil
	96 hr	Hastelloy B	1.3	0.2	nil	nil
	120 hr	S-816	14.63	2.4	6.62	1.1
Sea water	30 d	Hastelloy B	4.4	0.7	0.7	0.1
ΔT 110° F	41 d	Inconel X	0.7	0.1	nil	nil
	30 d	Vanadium	3.9	0.9	nil	nil
	41 d	316 SS	79.0	16	nil	nil
	30 d	S-816	0.5 0.4	0.08 0.06	0.06 + 0.06 +	0.01 0.01
Mercury	30 d	Hastelloy B	nil	nil		
tests	30 d	Inconel X	nil	nil		
600° F	30 d	Vanadium	nil	nil		
	30 d	316 SS	0.56	0.1		
	30 d	S-816	nil	nil		

TABLE II-5

Evaluation of Results

Material	Air Oxidation 1700° F	Mercury 600° F	Cerium 1700° F	Ceric Oxide 1700° F	Cerous Fluoride 1700° F	Sea Water Δ T 110° F
Inconel X	Good*	Good	Not good	Good	Limited*	Limited because of crevice corrosion and pitting
Hastelloy B	Poor*	Good	Not good	Poor	Limited*	Limited because of crevice corrosion and pitting
S-816	Good*	Good	Not good	Limited	Limited	Good
316 SS	Poor*	Good	---	---	---	Poor

The evaluation of results in Table II-5 is based on corrosion rate standards as follow:

Rating	Rate of Attack (mpy)
Good	> 1
Limited	1 to 10
Poor	10
Not good	Complete incompatibility

The tests marked with an asterisk were evaluated by metallographic examination. Tantalum is a good material for containing cerium, but must be welded and stored in an inert atmosphere to prevent oxidation at elevated temperature.

3. ORNL Coordination for Radioisotope-Fueled Ground Test Generator*

Fuel block loading. Coordination of hot cell fuel core loading plans for the Task 2 ground test generator was continued. Agreements were reached concerning all major aspects of the fuel loading procedure and remote welder-chill block design studies. Oak Ridge National Laboratory (ORNL) personnel will assist in preliminary checkout of the remote fuel block welder and chill block at The Martin Company.

Additional agreements reached in discussions with ORNL personnel were:

(1) Martin will furnish 560 grams of powdered tantalum, which will be loaded into the fuel tubes along with the ceric oxide. This material, 80 grams in each of seven fuel tubes, will act as a getter for free oxygen release during approximately two half-lives of radioisotope decay (570 days).

(2) Manipulators and tongs will be provided by ORNL to insert fuel tubes into the fuel container, to insert threaded closure caps, to remove the loaded fuel core from the chill block and to install the loaded fuel core into the shipping cask.

(3) Hot cell manipulators will be used to rotate the fuel container in the chill block assembly after each closure plug is welded. Convenient handling knobs and indexing detents will be provided on the chill block.

(4) An air motor will be added to the shipping cask assembly by Martin to actuate the sliding plug screw jack.

(5) A shipping cask support platform will be provided by ORNL to prevent damage to the tracked dolly rails on the floor of the hot cell.

(6) Martin will add provisions to the shipping cask to engage the fuel core ram rod from the sliding plug side using the hot cell manipulators.

Fuel delivery schedule. A chemical explosion which occurred during decontamination of the plutonium fission product separation plant at ORNL will delay the fueling operation of the Task 2 ground test generator fuel core until about November 1960. The fuel core delivery date is now estimated to be December 1960. Hot cell testing, therefore, has been rescheduled for January 1961.

---

* P. J. Dick

C. SUBTASK 2.3--HAZARDS ANALYSIS

During this quarterly reporting period, the planned objectives were:

(1) To continue the refinement of analytical studies associated with the behavior of the Task 2 generator upon re-entry from orbit or near orbital injection.

(2) To prepare an aerodynamic heating summary report for the Task 2 generator.

(3) To prepare a preliminary operational hazards report for the Task 2 generator.

(4) To initiate the preparation of a final summary hazards report and summary film report for the Task 2 generator.

(5) To continue active participation in SNAP Hazards Committee activities.

1. Re-entry Burnup Studies*

Analysis was continued on the refinement of data to predict the zone of open core impact resulting from final stage failure of the satellite vehicle. The original study, outlined in MND-P-2184, "Preliminary Hazards Report for the Task 2 Generator," was conducted to determine the zone limits of open core impact using the worst possible theoretical final stage malfunctions. The new data will be based upon the maximum credible vehicle deviation due to final stage malfunction. As an example, one of the original assumptions considered perfect final stage operation within 4000 fps of burnout velocity. At this point, the vehicle instantaneously yawed 90 degrees to the velocity vector while maintaining full thrust. A refinement of this type of failure to a credible condition and other data improvements should provide a significant reduction in the size of the impact zone. This information will be utilized in the preparation of a final summary hazards report.

An analysis of the aerodynamic burnup characteristics for two molybdenum fuel core design concepts was completed. One design employed a cluster of four 1-7/8-inch diameter fuel capsules, which were banded together with stainless steel straps. The second design was a conventional four-inch diameter block containing seven, 1-inch diameter, drilled holes for fuel. A final stage propulsion failure was considered, wherein a velocity 400 fps short of orbital velocity was reached. The results of this analysis are shown in Fig. II-17, and may be summarized as follows:

---

* R. Oehrli

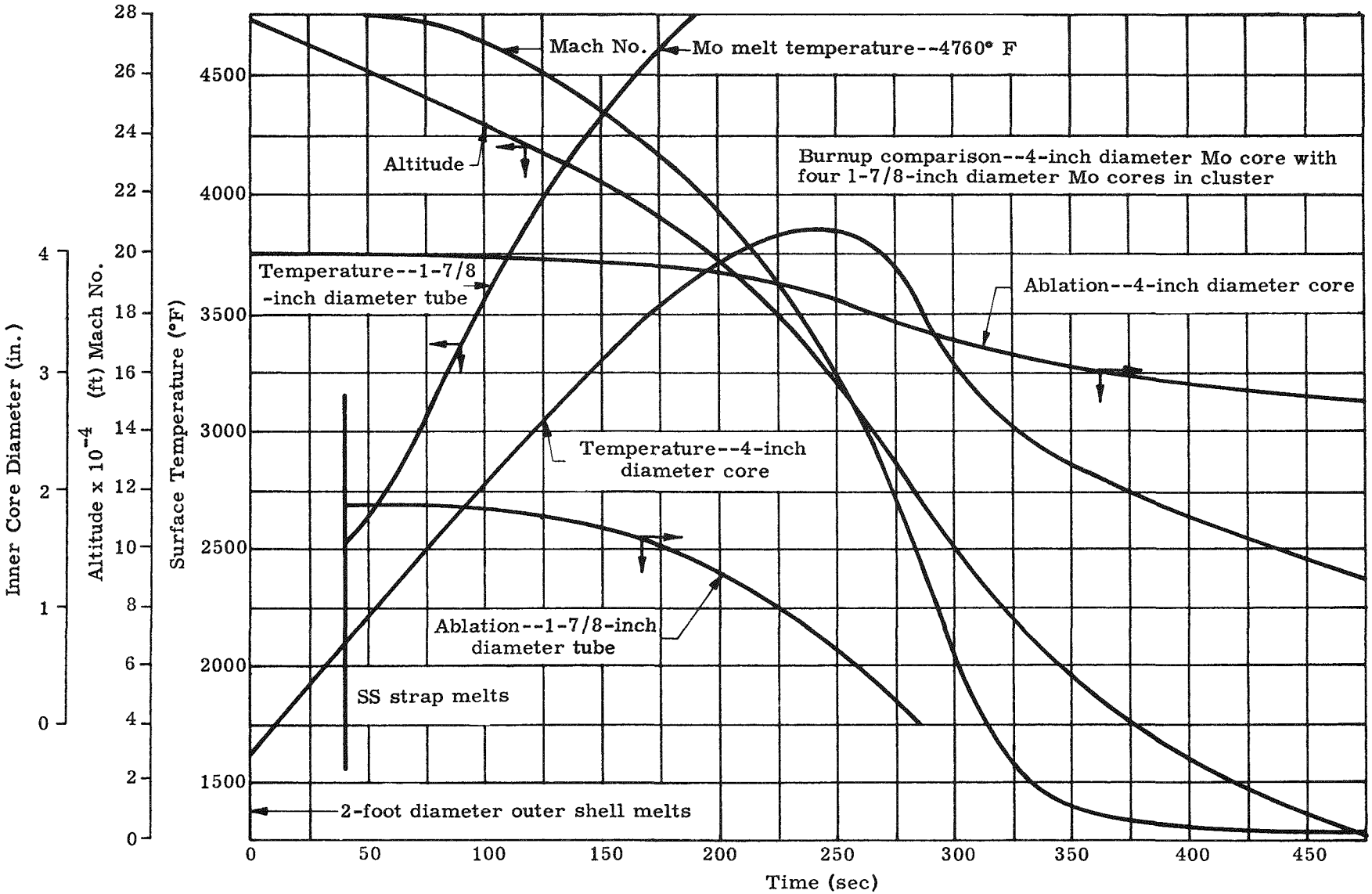

Fig. II-17. Thermoelectric Generator Hazard Study--Condition 5A

(1) The banded cluster of fuel tubes oxidized and melted completely in 285 seconds at an altitude of 118,000 feet.

(2) The 4-inch diameter block was oxidized to a depth of 5/8 inch at earth impact.

It was therefore concluded that, from a re-entry standpoint, a molybdenum fuel tube cluster could be considered in the design of a burnup-type fuel core.

2. Aerodynamic Heating*

Report MND-P-2291 entitled "Summary Report Aerodynamic Re-entry Analysis, Task 2 Thermoelectric Generator," was completed and distributed.

In this report, an analytical trajectory and aerothermodynamic analysis of a satellite containing a Task 2 thermoelectric generator was made. A 300-statute mile circular polar orbit was used for this analysis, and the launch was assumed to be from Vandenberg Air Force Base.

Results of this study show that, upon normal re-entry from a successful mission, the radio-cerium fuel will burn up in space at high altitude. Thus, only a very minor amount of radio cerium will be released to the stratosphere.

A complete analysis of the fate of the radio-cerium fuel following various aborted launching attempts also has been carried out. Charts summarizing the various assumed failures and locations of the fuel following failure are shown.

A technical discussion of the methods used in performing the analysis is included in the report.

3. Preliminary Operational Hazards Report **

Report number MND-P-2335 entitled "Interim Report on Safety Procedures for the Task 2 Thermoelectric Generator," was prepared for publication and will be distributed in May 1960.

---

* R. Oehrli, W. Hagis
** L. Klein

This report describes the operational hazards associated with the use of a radioisotope-fueled auxiliary power unit for a satellite mission. Two Task 2 generators will be utilized to power certain electrical equipment in a satellite system. Procedures have been established for the safe handling and operation of the Task 2, 125-watt thermoelectric generator throughout its factory to flight sequence. Included are suggested special procedures to be followed in the event of a launch pad abort, or an aborted flight ending in the impact of the generator within the limits of the launching area.

Chapter I outlines the factory to flight and/or retrieval and disposal sequences followed for the Task 2, 125-watt generator.

The generator design, fuel properties, fuel capsule characteristics and provisions for biological shielding that are relative to the operational hazards of the generator are given.

A discussion of the major equipment involved in loading and shipping the fuel core for the generator is provided, as well as an outline of the procedure for preshipping and loading operations. The general examination of the shipment itself, including the Bureau of Explosives Permit, special and routine shipping conditions and railroad accident statistics are discussed.

The sequence to be followed at the launch site from fueling of the generator through mating the generator to the satellite vehicle including the countdown period has been prepared. A description of the auxiliary equipment required at the launch site is included along with a discussion of the orientation of the generator within a satellite vehicle.

Procedures have been established to be used in retrieving and disposing of a unit that has impacted in the launching area or in the immediately adjacent ocean areas.

An evaluation of the radiation field present around a bare source, a shielded generator and around the ground handling equipment during the fuel transfer operation has been included.

4. Final Summary Hazards Report and Summary Film Report*

The final hazards summary report and summary film, which are being prepared, will summarize the current Task 2 hazards analysis and test programs conducted during Fiscal Year 1960. The information previously reported in MND-P-2184 will be refined and supplemented as a result of this effort.

---

* G. Dix

Films of the first series of fuel core high velocity impact tests have been edited and will be included in the Hazards Summary Film Report. This film will also include:

(1) The second series of fuel core high velocity impact tests.

(2) Fuel core integrity test resulting from a simulated booster vehicle explosion on the launch pad.

(3) Fuel core integrity test resulting from a simulated launch vehicle high temperature fire on the launch pad.

(4) Immersion of a Task 2 fuel core into liquid oxygen.

(5) Plasma flame burnup tests.

(6) Fuel container materials corrosion and compatibility tests.

(7) Launch flight trajectory and fate of the fuel core following launch failure.

5. SNAP Hazards Committee Activities

Presentations covering the current status of the Task 2 Program with respect to hazards, ground handling, fuel core development and thermoelectric development were given. These presentations were made at the following locations:

(1) Naval Radiological Defense Laboratory (NRDL), San Francisco, California.

(2) Pacific Missile Range (PMR), Point Mugu, California.

(3) Air Force Ballistic Missile Division (AFBMD), Inglewood, California.

The results of these presentations were as follows:

(1) The facilities of NRDL were made available to assist in the evaluation of the high temperature fire test results.

(2) The representatives of the PMR were receptive to the hazards concepts. Interest was shown in the application of the Task 2 generator for underwater use.

(3) US Air Force personnel at AFBMD reiterated their position with respect to the Task 2 system as a backup to solar systems and their desire to continue the system development through the hot cell ground test.

D. SUBTASK 2.4--MANUFACTURING

During this quarter the planned objectives were:

(1) To provide test hardware in support of the hazards testing and core development programs.

(2) To initiate fabrication of the ground handling system hardware.

(3) To fabricate and assemble one electrically heated generator for electrical testing.

(4) To fabricate and assemble one electrically heated generator complete with jigs and fixtures for environmental testing.

(5) To begin construction on a remote welding device for the isotope-loaded fuel block.

(6) To supply supporting effort for design changes or facilities modifications for the testing program.

As indicated previously, these objectives were changed at the direction of the New York Operations Office, and all fabrication related to Items 2 and 5 was terminated. The reported progress reflects these terminations.

1. Test Support Hardware*

Fuel block specimens and equipment were fabricated for the high velocity impact tests, the explosion tests and the high temperature fire testing portions of the hazards test program to be conducted at Aberdeen Proving Grounds. Full-scale Inconel X test specimens for the impact tests consisted of three cerium metal-fueled five-hole blocks, one five-hole block fueled with lavite pellets and two cerium metal-fueled, five-tube, separable assemblies. Examples of each type are shown in Fig. II-18. The samples are identified from left to right as the seven- and five-hole designs and the separable capsule design. A 4 x 4 x 12-foot plywood box to be used as a water impact target at Aberdeen was completed.

---

* E. J. Lemanski

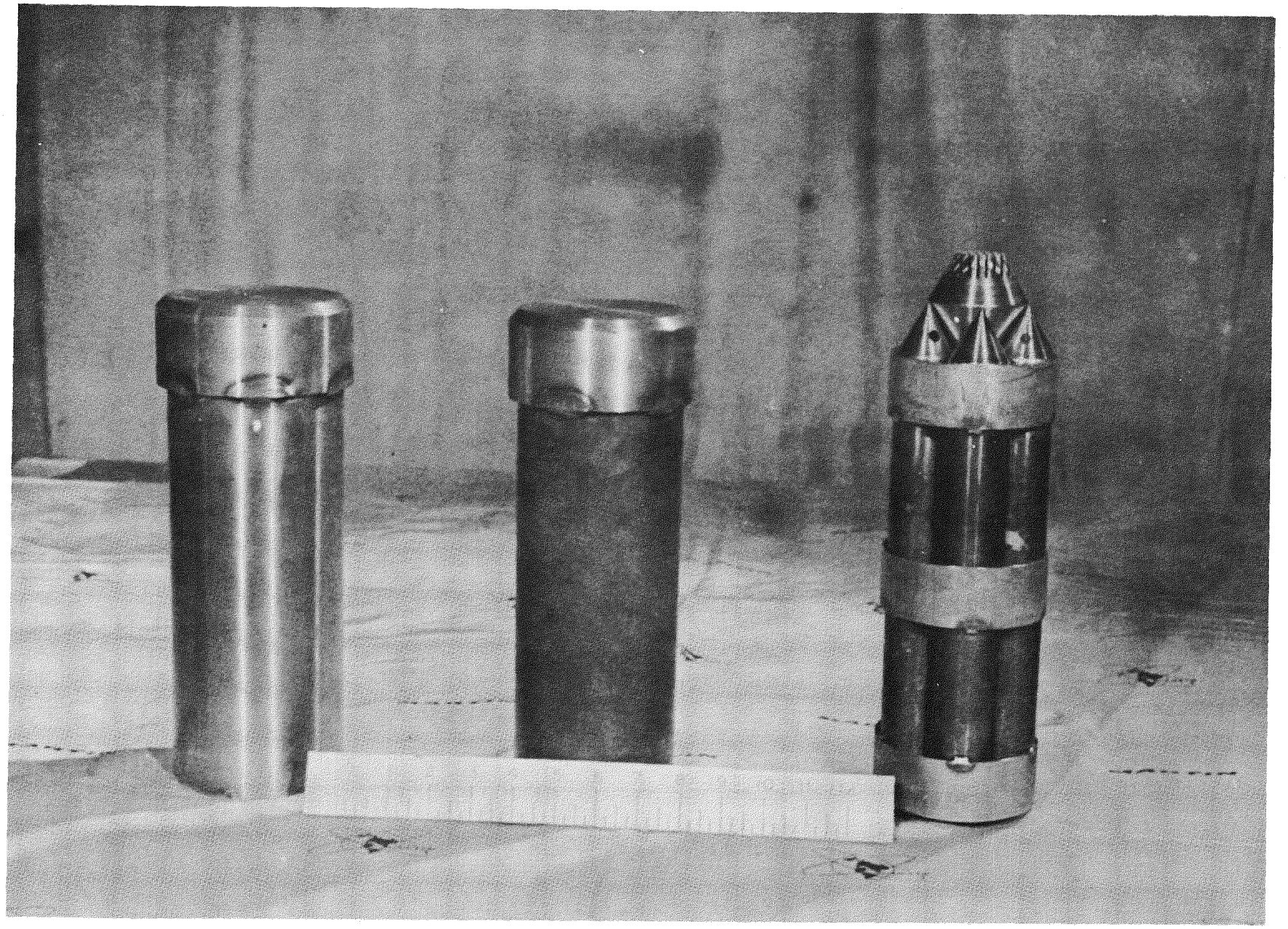

Fig. II-18. Inconel X Test Specimens for Impact Test

Fabrication was completed on specimens for the explosion tests. These included four 1/3-scale, electrically heated blocks; two of Hastelloy B, and two of Inconel X. In addition, four 1/3-scale blocks of aluminum, ranging in room temperature yield strength from 10,000 to 40,000 psi, were completed for testing. These will serve to bracket the failure level of specimens in the explosion.

Test specimens completed for the high-temperature fire test consisted of nine full-scale blocks. Of these, three were made of Hastelloy B, three of Inconel X and three of stainless steel. One of the Hastelloy B blocks was filled with cerium metal and the remaining with lavite pellets to simulate a cerium fuel form. Boxes of Marinite insulation were fabricated to house the cameras covering the fire test at close range.

The full-scale generator was completed in the previous quarter for use in the fire test. The unit is equipped with an electrically heated block to simulate the heat source. The thermoelectric conversion system has been omitted in this sample.

Miscellaneous items for the plasma flame tests such as calibration and test specimens, and ceramic specimen holders were prepared.

2. Ground Handling Equipment

Work on the ground handling equipment was stopped on March 30, 1960. Prior to this, the isotope shipping cask, (shown in Fig. II-19), fuel block ram assembly, the sliding plug, jack and lock assembly, and the gimbal fixture were approximately 97% complete. The dome detail for the collar shield tank was complete, and various details on the tank had been assembled and welded. When the stop order was issued the details in process were taken off the machines, tagged and returned to the stockroom.

3. Electrically Heated Generator

Assembly of the first electrically heated generator was completed in this quarter. The assembling procedure for installing the top and bottom Min-K domes was as follows. Cutouts were made in the top dome for clearing bellows seals, and the section was handworked and fitted to the inner skin to assure a close contact. All thermoelectric hot shoe grooves were routed out with a high speed air-driven tool. The dome was fired to burn off the reinforcing epoxy resin and placed into a supporting cradle where the hot shoes were installed; the generator was inverted, lowered into the dome and properly aligned. The supporting cradle and generator were clamped together and the assembly righted. When the supporting cradle was removed the interconnecting

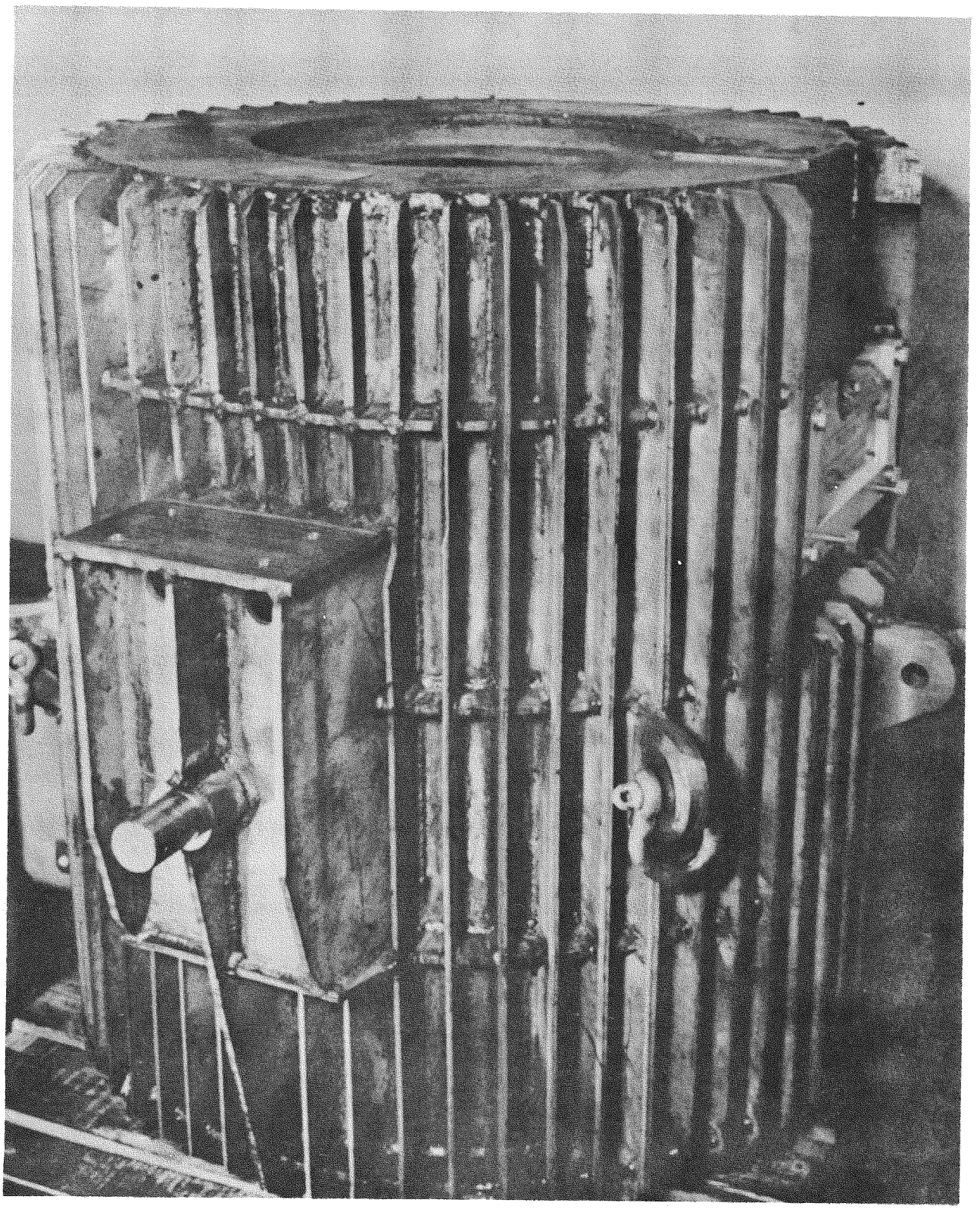

Fig. II-19. Isotope Shipping Cask

wiring slots were routed into the insulation. Min-K dust was then vacuumed from the holes and the thermoelement assemblies installed and wired together. After another vacuuming around the elements, a preliminary checkout to assure electrical continuity was made, and the outer skin was fitted and welded into place. Springs and cold shoe caps were fitted into the elements and the adjusting blocks were tack welded in place. A final electrical continuity checkout was made, and plugs were screwed into the adjusting blocks far enough to compress the springs approximately 1/16 inch.

The bottom insulation dome and skin were installed in a similar fashion. This procedure had to be closely followed because of the poor handling and structural properties of the insulation domes, and because only the insulation, closely fitted to the inner skin, held the hot shoe in place.

During the first continuity checkout, four broken elements were discovered and replaced. The aluminum adjustment blocks were tack welded to the aluminum outer skin to avoid possible deformation or shrinkage resulting from extensive welding. Following welding, the blocks were sealed with room temperature vulcanizing silicone rubber so the joints would be gas tight. Stainless steel-aluminum joints around the bellows, which looked like potential leak areas, were also sealed with silicone rubber.

Following sealing operations, the thermal shutters and the electromechanical shutter actuator were installed.

A complete continuity checkout was made on the overall circuit before the generator was turned over to the test group for installation in the test chamber. Figure II-20 shows the first completed generator mounted on the test stand. Details such as the adjustment blocks with adjusting screws, the lift points on the inner skin assembly, the thermal shutters and the shutter actuator assembly are readily seen.

4. Environmental Test Generator

A second electrically heated generator to be used for environmental testing was started in this quarter. Since the inner skin and truss assembly of the first generator proved satisfactory in thermal cycling and rapid heatup tests, their designs were essentially unchanged, and fabrication on the second unit was started from available parts. After the inner truss assembly was welded, truss members were instrumented with strain gauges. These will serve to convey information about internal vibration and resonance in the inner structure during the vibration tests. A conical heat shield was then installed.

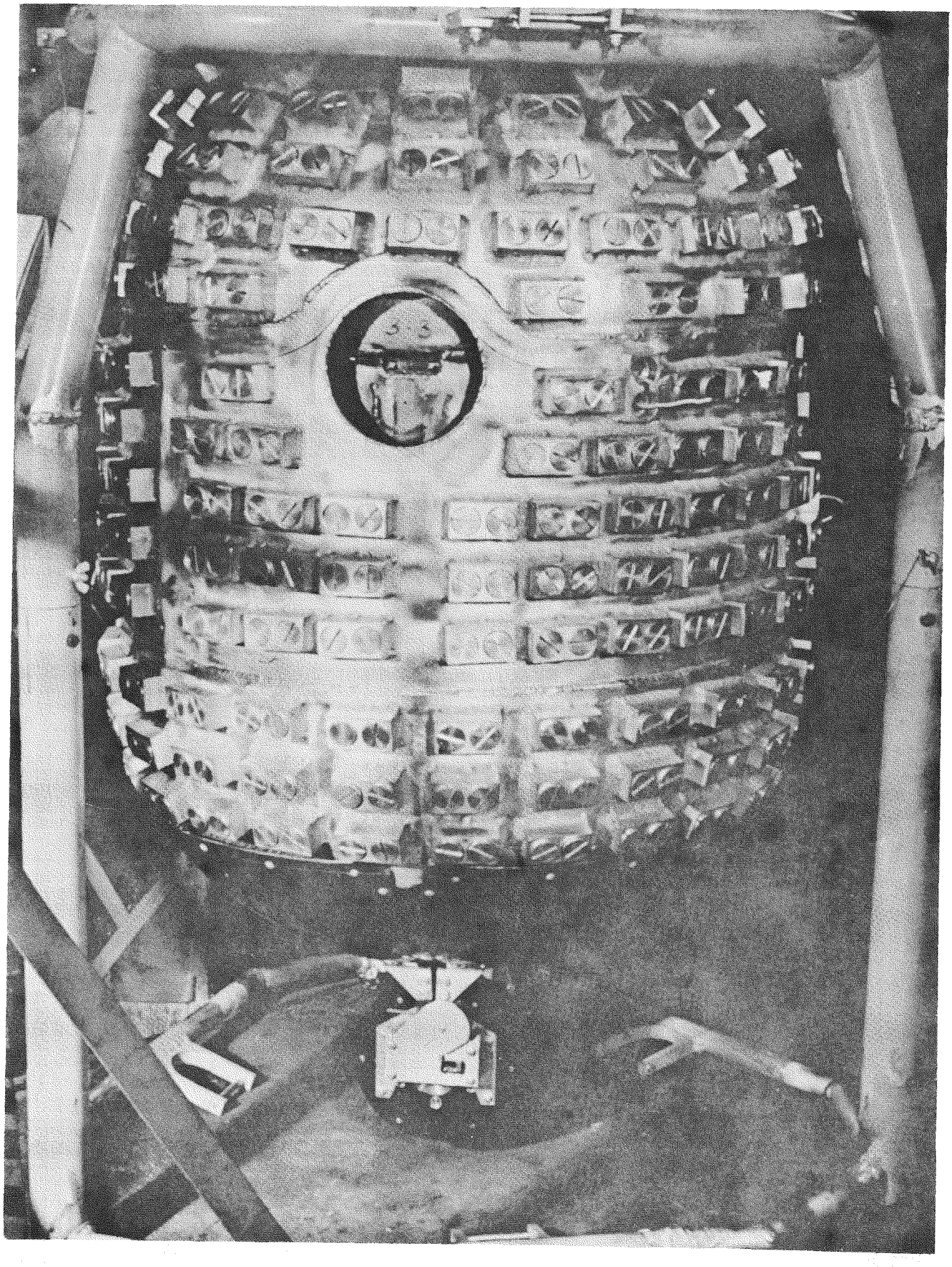

Fig. II-20. First Completed Generator

Material for the redesigned aluminum outer skins was received and the Marform operation was set up. Once these parts are formed, they will be chem-milled so that excess material adjacent to the adjusting plugs will be removed. The skins will then be trimmed, holes drilled and tapped and the bosses faced to provide a smooth gasketing surface.

The environmental test fixture for the vibration test is in fabrication. Magnesium weldments and plates are being assembled and machined to provide a lightweight, highly rigid fixture. Two granite slabs, which will serve as part of the vibration table test fixture, were delivered during this period.

5. Remote Welder

All work relating to the remote welding of the fuel blocks including the associated positioning, rotating and cooling equipment was stopped. Procurement of materials was terminated.

E. SUBTASK 2.5--SYSTEM AND COMPONENT TEST

During this quarter, the planned objectives were:

(1) To review the final report submitted by the subcontractor describing the radiation studies on the thermoelectric elements.

(2) To perform a second series of high velocity impact tests on a improved fuel block design and to conduct explosion tests and high temperature fire tests on the fuel block.

(3) To complete transient startup and equilibrium heat loss testing of the heat transfer mockup with its shutter heat dump system.

(4) To initiate testing of the first electrically heated thermoelectric generator for electrical power output, power flattening and for transient and equilibrium control characteristics.

1. Radiation Study Program

The radiation study program on lead telluride thermoelectrics, described in the previous quarterly, was concluded and the revised final report by the subcontractor received. The following discussion presents more of the detailed results submitted by the subcontractor.

In the high accumulated dose test, control samples were held at the temperature used during the radiation and for the same period of time

as the radiation exposure. Control samples held at 300° F showed no resistivity changes while those held at 1000° F showed resistivity changes. To determine the magnitude of these changes, samples used in the high temperature irradiation were first subjected to a prior heat treatment for three hours at 1000° F. The effect of this heat treatment is summarized in Table II-6. When the samples were subjected to heat treatment at even higher temperatures, they became stabilized and showed no further resistivity increases even after extended heat treatment at 1000° F.

A total accumulated dose of 4.6×10^{16} electrons/cm^2 did not measurably affect the weight and physical dimensions of the samples, although the strength of the material deteriorated. Attempts to measure the impact strength of the material with an Izod Tester before and after the radiation were unsuccessful. The tester apparently lacked the sensitivity necessary to detect changes.

Because of the extreme fragility of the test samples after irradiation, extensive power output measurements could not be made on the P-type elements. At least 12 samples broke during the irradiation or subsequent measurement. However, resistivity results were obtained from test samples or fragments of samples. These indicated an increase in resistivity ranging from 11% for Sample No. 61 to 22% for Sample No. 19. Typical results of samples irradiated at 1000° F are shown in Table II-7.

The fragility of the samples supplied led the subcontractor to supply samples of his own in an effort to complete the measurements. These samples were sintered and extruded from material essentially identical in composition with the material supplied. The original samples were cast specimens purchased from Minnesota Mining and Manufacturing. Transitron Electronics Company supplied the extruded samples. Samples listed in the tables are identified as to source.

Following irradiation at 1000° F to a total dose of 4.6×10^{16} electrons/cm^2, power output measurements were obtained on Sample No. 36, N-type material, listed in Table II-7. The test results are plotted in Fig. II-21. These results show that the large accumulated dose increased the power output of the specimen to about 11% at the low values of external load resistance. The peak power output and the power output at the higher values of external load resistance were apparently not significantly affected.

Typical results of the low temperature irradiation tests (300° F) are given in Table II-8. Increases in the electrical resistivity as a result of the radiation, occurred in all samples. These increases ranged from 11.8% for Sample No. 2, to 42% for Sample No. 50. Results of the power output measurements made on Sample No. 9, N-type material, are plotted

TABLE II-6

Effect of Heat Treatment at 1000° F for 3 Hours

Specimen No.	Type and Origin		Weight (gm)	Length (in.)	Width (mils)	Thickness (mils)	Resistivity (milliohm-in.)
45	N-3M	Before	2.2201	0.998	246	69	0.191
		After	2.2202	0.998	247	69	0.191
38	N-3M	Before	1.9400	0.988	218	69	0.148
		After	1.9405	0.988	216	69	0.142
22	N-TEC	Before	2.8020	0.858	373	67	0.297
		After	2.8018	0.857	372	67	0.301
68	P-3M	Before	2.1561	1.000	240	69	0.168
		After	2.1560	0.998	239	68	0.172
66	P-3M	Before	2.0612	0.983	247	67	0.151
		After	2.0609	0.982	245	68	0.143
69	P-TEC	Before	1.8211	1.0310	214	68	0.135
		After	1.8214	1.0311	213	68	0.139

TABLE II-7

Results of High Temperature Radiation

Specimen No.	Type and Origin		Weight (gm)	Length (in.)	Width (mils)	Thickness (mils)	Resistivity (milliohm-in.)
19	N-TEC	Before	2.7078	1.1436	294	68	0.139
		After	2.7075	1.1435	294	68	0.170
61	P-TEC	Before	3.0392	0.9962	376	70	0.236
		After	3.0387	0.9960	373	69	0.262
36	N-3M	Before	2.0730	1.0120	218	70	0.146
		After	2.0735	1.0121	218	71	0.173

Not included are the 12 samples which broke during irradiation or subsequent measurement.

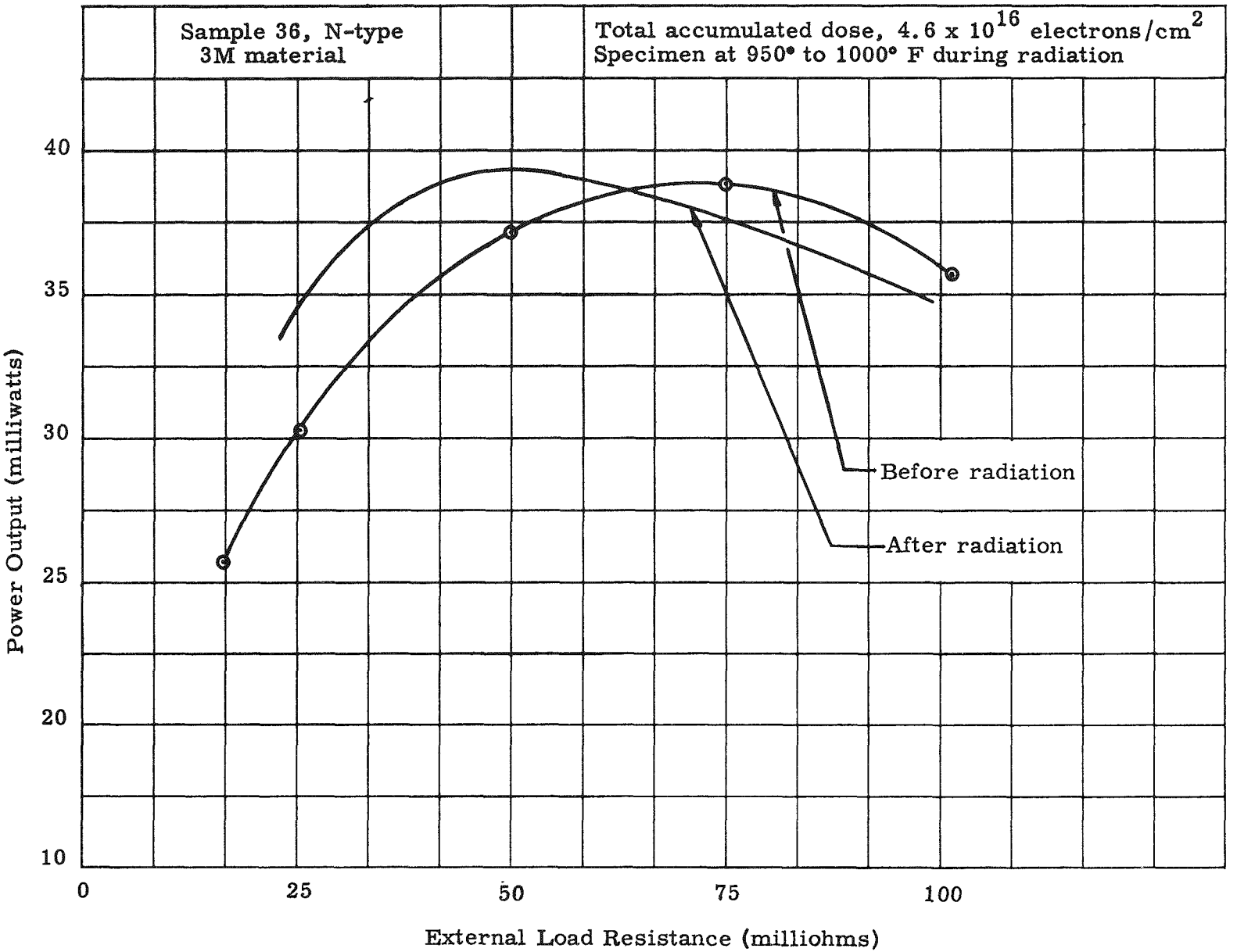

Fig. II-21. Power Output Versus External Load Resistance for Lead Telluride Thermoelectric

TABLE II-8

Results of Low Temperature Radiation

Specimen No.	Type and Origin		Weight (gm)	Length (in.)	Width (mils)	Thickness (mils)	Resistivity (milliohm-in.)
9	N-3M	Before	1.9821	0.9990	218	70	0.187
		After	1.9827	0.9990	218	70	0.214
21	N-TEC	Before	1.6890	0.9540	205	67	0.142
		After	1.6863	0.9540	205	67	0.163
23	N-TEC	Before	1.7843	0.7274	280	67	0.128
		After	1.7850	0.7272	281	68	0.169
50	N-TEC	Before	3.0685	1.4710	381	65	0.148
		After	3.0680	1.4700	380	65	0.210
2	P-3M	Before	2.2265	0.998	247	69	0.435 -0.118
		After	2.2270	0.998	247	69	0.472 -0.131

on Fig. II-22. A decreased power output over the full range of external load resistances was noted. At the peak output, a decrease of 16% was noted.

In view of the conflicting results obtained, namely a power output increase after radiation at 1000° F, and a power output decrease after radiation at 300° F, no specific statement can be made as to the actual effect of irradiation on power output. Since the power output measurement was difficult to make because of the extreme fragility of the test bars after irradiation, a large number of samples could not be successfully tested. Thus, no sampling or averaging techniques can be applied.

The subcontractor carried out some experiments independently to obtain information on the effects of radiation on resistivity and thermoelectric power (Seebeck coefficient, α) as a function of temperature using round bars. A sintered and extruded lead telluride bar was radiated in segments around the circumference until the whole bar had been exposed and the bar had received a dose of 4.6×10^{16} electrons/cm^2 over its length. Results are shown in Figs. II-23 and II-24. Figure II-23 is a plot of thermoelectric power (Seebeck coefficient) versus temperature. The curves shown indicate that the radiation exposure results in a decrease in thermoelectric power. The magnitude at this effect is most noticeable at temperatures of 800 to 950° F.

Figure II-24 is a plot of resistivity for the same bar versus temperature. It should be noted that the resistivity increased after radiation, the increase being more pronounced at lower temperatures. These results, in part, support the resistivity increase effects noted earlier, in that the resistivity increase is greater at lower temperatures. For example, resistivity increases for the thin slab samples irradiated at 1000° F ranged from 11 to 22%; resistivity increases for the thin slab samples irradiated at 300° F ranged from 11.8 to 42%. This would indicate that an annealing effect takes place at the higher temperature. Quantitatively, however, the magnitude of this annealing effect is not supported by the results obtained on the bar samples. These results, plotted in Fig. II-24, show no resistivity change at 900 to 950° F.

Subsequent to the receipt of these results, a comparison of the subcontractor's resistivity and Seebeck coefficient measurement data at room temperature with Martin data was made. It was concluded that, within the limits of experimental error, the accuracy of the subcontractor's measurements was satisfactory. Any variation in the data measurements was apparently the result of a lack of uniformity within the sample elements. This inherent nonuniformity tends to mask any small changes which might take place and, in addition, makes it difficult to obtain consistent results. If a large number of samples were tested,

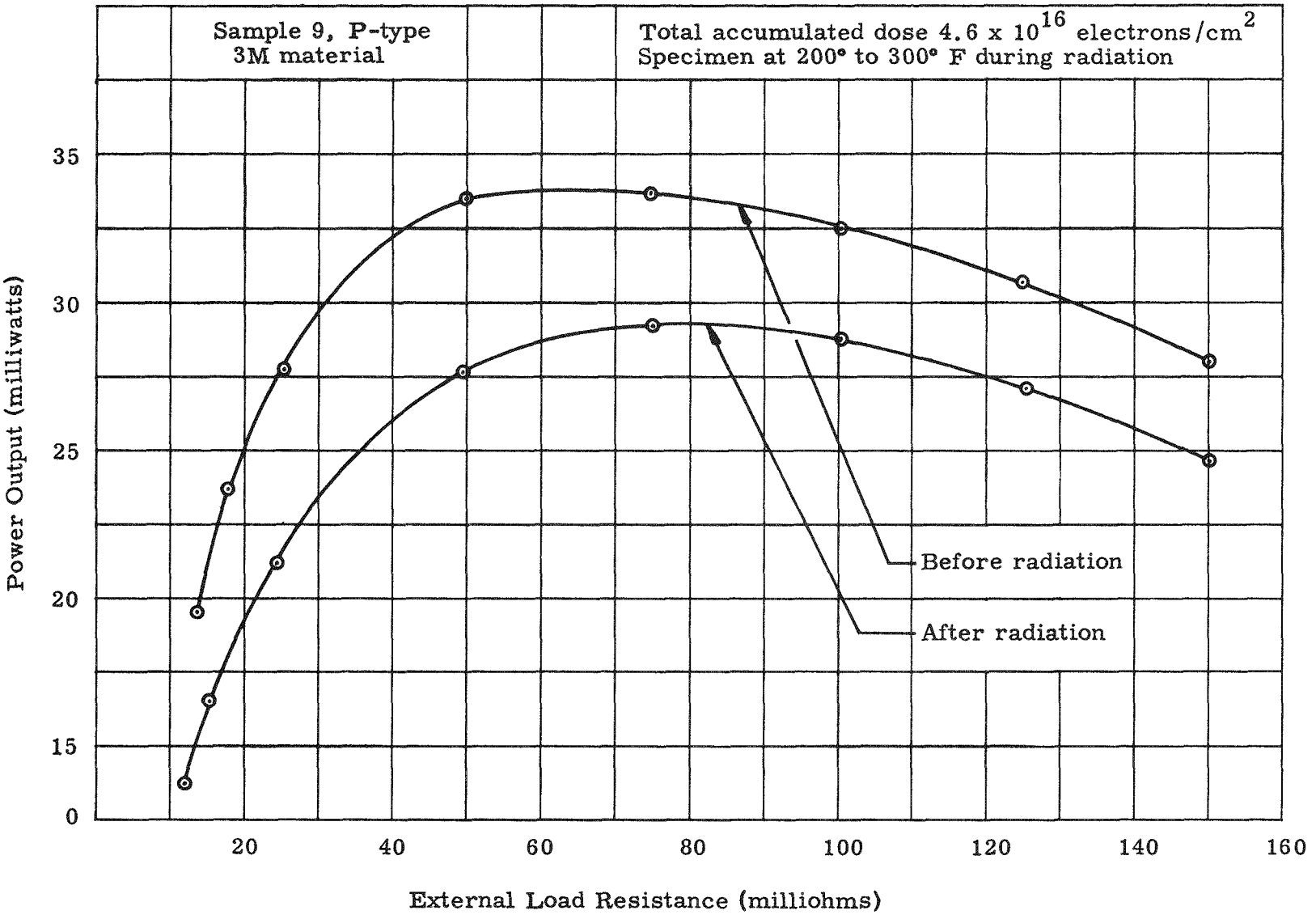

Fig. II-22. Power Output Versus External Load Resistance for Lead Telluride Thermoelectric

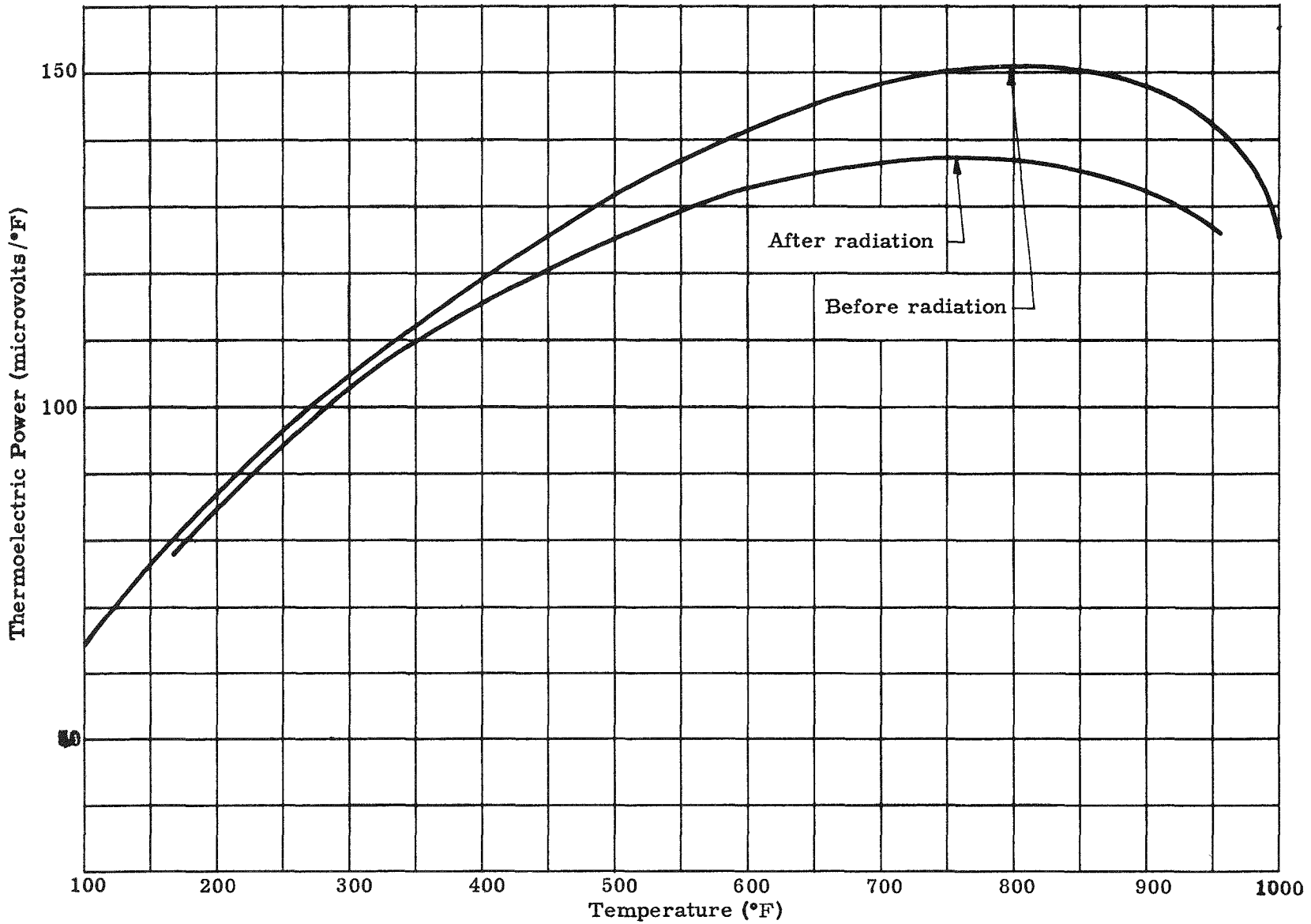

Fig. II-23. Thermoelectric Power (Seebeck Coefficient) Versus Temperature--Lead Telluride N-Type, Sintered

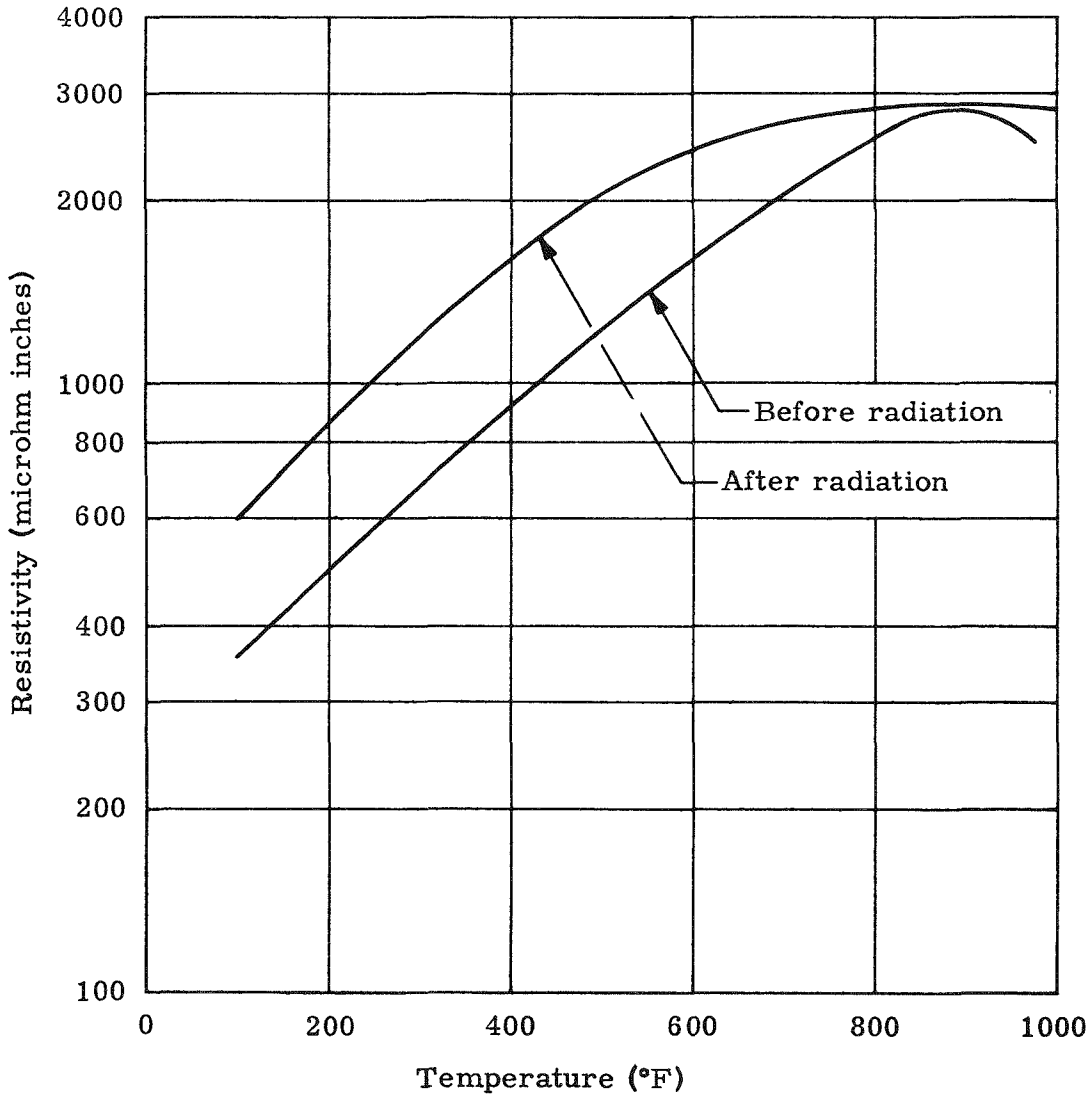

Fig. II-24. Resistivity Versus Temperature--Lead Telluride N-Type Sintered

statistical methods could be used and erratic results could be rejected. It may be concluded from the tests that operating lead telluride elements undergo no detectable changes in physical or thermoelectric properties (electrical power output) over periods of up to 30 minutes at dose levels to 1.33×10^{14} electrons/cm^2/hour.

Irradiation of the lead telluride elements to a total dose of 4.6×10^{16} electrons/cm^2 causes an increase in element resistivity and a marked decrease in the physical strength of the elements. No measurable effect on weight and physical dimension of the sample was noted as a result of the total dose mentioned.

2. Simulated Abort Tests*

High Velocity Impact Tests. The second set of high velocity impact tests was completed in March. A total of six full-scale cores of Inconel X were heated to approximately 1500° F and impacted on either granite or water targets. Only the preliminary test results, given in Table II-9, are available at this time. The data will be contained in an APG report which has not been received. The documentary and high speed Fastax film records are being processed.

TABLE II-9

Preliminary Results of Impact Test

Specimen	Planned Impact Velocity (fps)	Planned Impact Temperature (°F)	Target	Remarks
Cerium metal loaded 5-hole impact cap design	500	1500	Granite	Rupture of specimen. Cerium released. "Blooming"-type failure.
Lavite pellet loaded 7-hole impact cap design	500	1500	Granite	Specimen recovered intact. Crackout of welded filling plug found with no apparent release of lavite.

* T. Dobry

TABLE II-9 (continued)

Specimen	Planned Impact Velocity (fps)	Planned Impact Temperature (°F)	Target	Remarks
Cerium metal loaded 5 separable capsule design	500	1500	Granite	Rupture of specimen. Cerium released.
Cerium metal loaded 5 separable capsule design	500	1500	Granite	Identical with above.
Lavite pellet loaded 7-hole impact cap design	500	1700	Granite	Specimen recovered intact. No release of lavite, no cracks or fissures in specimen.
Lavite pellet loaded 7-hole impact cap design	500	1700	Water	Specimen recovered intact. No visible damage.

A photograph of three 7-hole impact cap design specimens loaded with lavite pellets (simulated CeO_2) is shown in Fig. II-25. The specimen on the right was impacted against granite. When the impact cap was chiseled off, a welded filling plug was found to have broken loose at the edge of the weld area. None of the contained lavite was spilled.

The specimen shown on the left of Fig. II-25 was also impacted against granite. Except for plastic deformation, the specimen was intact. The center specimen was impacted against a water target consisting of a totally enclosed, filled plywood box, 12 feet by 5 feet by 4 feet. No deformation or cracking of the specimen was evident.

Figure II-26 shows the cerium metal loaded five-hole impact cap design after impacting against granite. The blooming-type of failure shown was typical of that experienced with all of the cerium metal loaded specimens. Marked corrosion of the specimen is also evident. A metallographic evaluation of the specimen is in process. More complete information will be included in the next quarterly.

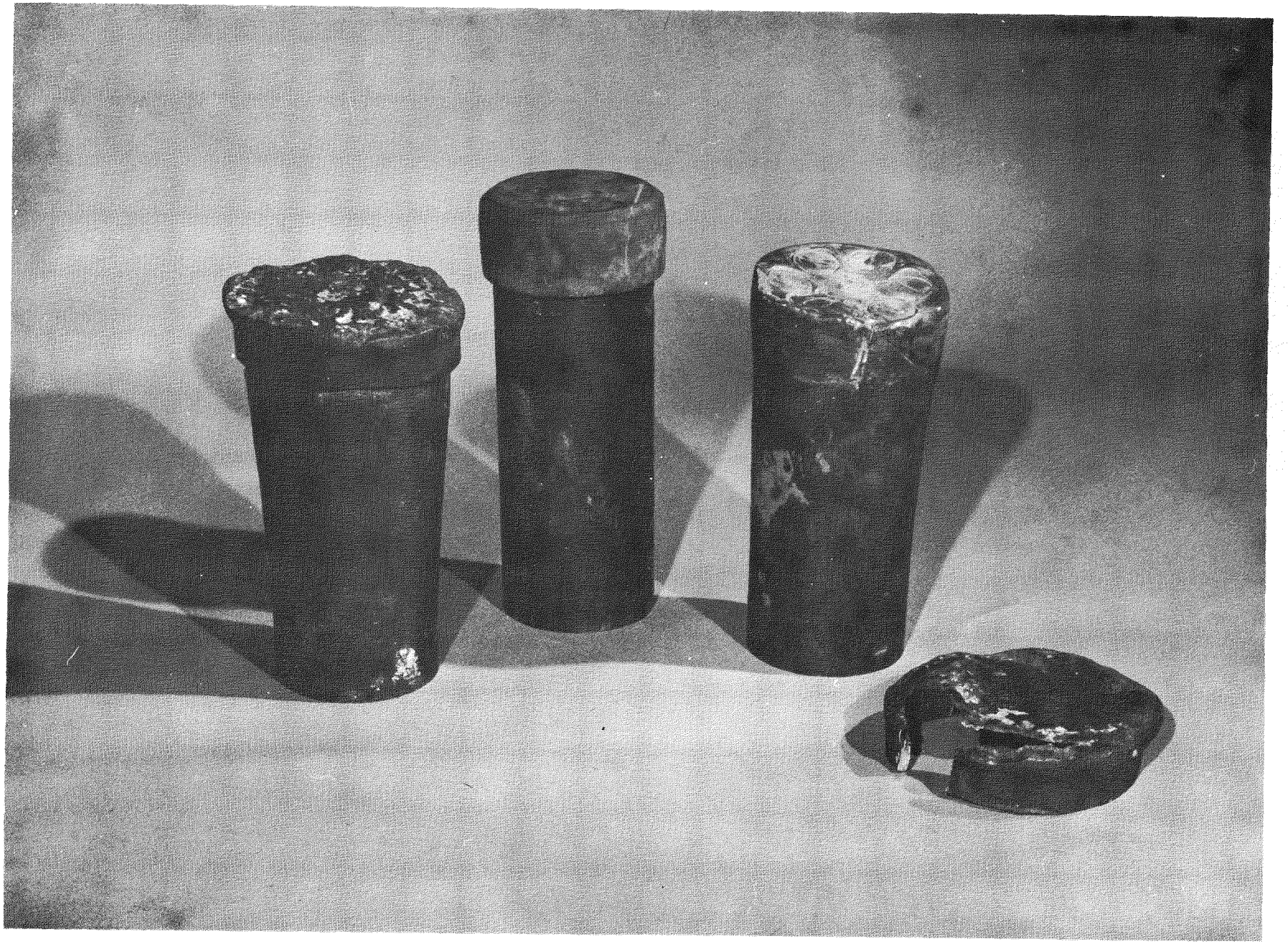

Fig. II-25. Seven-Hole Impact Cap Specimens

Fig. II-26. Cerium Metal Loaded Five-Hole Impact Cap Design

Shock Wave Test. One-third-scale fuel blocks were evaluated in the shock wave test conducted at Aberdeen Proving Grounds in March. The test was designed to simulate the shock loading imposed on the fuel block in a launch pad booster failure. Shock waves were generated by detonating 2000 pounds of TNT, an amount scaled down from the estimated TNT yield of the liquid fuel of the vehicle. Samples were positioned 12 feet from the center of the charge and were tied to a 100-foot length of nylon rope which aided the sample recovery. Scaling down of the explosion made it necessary to scale down the test samples, with the result that 1/3-scale fuel blocks were used.

A total of eight samples was tested. These included:

(1) Two 7-hole Inconel X specimens.

(2) One single-hole Hastelloy B specimen.

(3) One 7-hole Hastelloy B specimen.

(4) Four graded-strength aluminum specimens.

The Inconel X and Hastelloy B specimens were equipped with electrical heaters so they would be heated to their approximate operating temperatures during the test. An electrical disconnect cut off power to the heaters immediately before the test. Unheated, graded-strength aluminum specimens ranging in yield strength from 10,000 to 40,000 psi were included in the blast area to measure the level of failure.

At this writing, the test data and films are still being processed. Only five of the original eight specimens were recovered:

(1) One 7-hole Inconel X specimen.

(2) One single-hole Hastelloy B specimen.

(3) Three graded-strength aluminum specimens.

All the recovered specimens appeared to be in excellent condition. Pitting on the surface of one of the graded-strength aluminum specimens, apparently the result of impacting debris, was the only noticeable damage. Quantitative results on the peak pressures developed as a result of the explosion will be included in the next quarterly report.

High Temperature Fire Tests. Because of weather conditions, high temperature fire tests tentatively scheduled for the latter part of March 1960 will be delayed until April 1960. At the same time, a simulated

radioactive fuel release test will be conducted in which the fallout will be measured. A single test setup will be used to simulate a high temperature environment that might be expected when a missile fails on a launch pad. The missile structure will be simulated by 20,000 pounds of scrap metal composed of aluminum, magnesium and steel. These metals will be separated into five zones along the length of a 25-foot tower. A total of 18 capsule specimens will be positioned throughout this structure. The specimens will be electrically heated to simulate the operating temperatures of the isotopic generator.

Temperatures of the order of 6000° F will be generated by mixing hypergolic fuels, i.e., red fuming nitric acid and aniline, over the simulated missile structure. Containers of the propellants will be positioned at the top of the tower and split open remotely by activating shaped charges designed to penetrate the cask.

Two hundred pounds of mischmetal containing about 100 pounds of cerium will be encapsulated in lead foil containers and positioned in the top zone of the fire tower. This pyrophoric metal will be used as fuel for the fallout cloud. The lead foil is used to check the release of the cloud for a few seconds after the fire is started. This will enable the cameras covering the test to distinguish between the propellant cloud and the cerium cloud. A total of 11 cameras will be used to observe the cloud rise, size and path downwind.

The fallout field is designed for a northwest wind as shown in the accompanying layout (Fig. II-27). The test will be run only when optimum meteorological conditions exist for this particular setup. Fallout trays and air samplers will be used to collect air concentration and fallout data from the cerium cloud. They will be positioned as shown on the layout in a 60 degree quadrant on 13 different radii from 50 to 1600 meters. The fall field will cover an area of 1.34×10^6 square meters or 1.44×10^7 square feet. The air samplers are of the Staplex high volume type developed in the laboratories of the New York Office of the United States Atomic Energy Commission. Ashless filter paper of the type TFA No. 41 will be used to measure cerium air concentrations in the fallout area. Fallout trays will be gummed polyethylene of the type used by the AEC for their fallot studies.

A list of specimens to be used in the fire test is given in Table II-10.

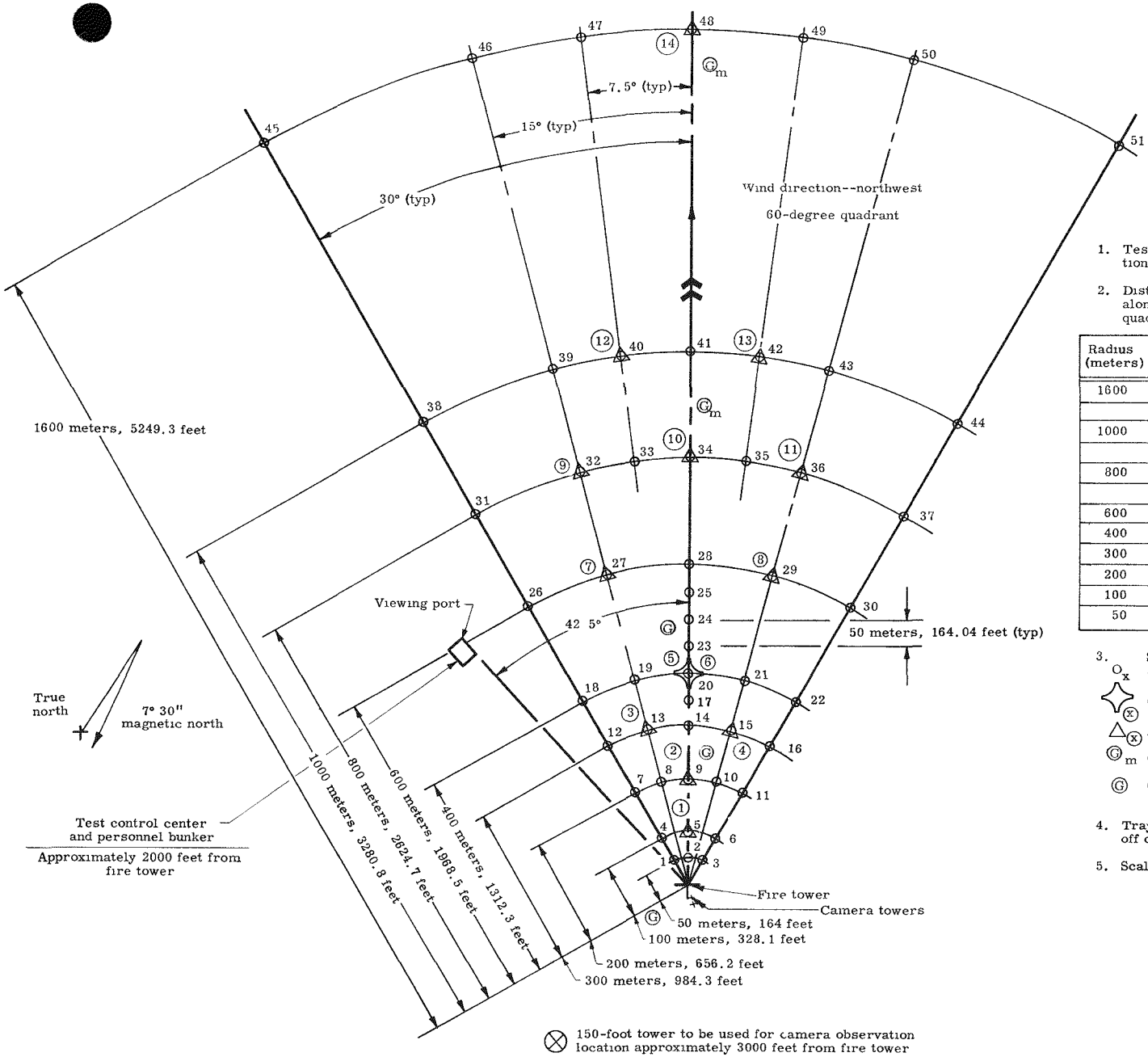

NOTES.

1. Test to be run when wind direction is from the northwest.
2. Distance between fallout trays along the circumference of the quadrant.

Radius (meters)	Angle (degrees)	Distance Between Trays (ft)
1600	7.5	687.14
	15	1374.28
1000	7.5	429.46
	15	858.9
800	7.5	343.58
	15	687.15
600	15	515.36
400	15	343.58
300	15	257.68
200	15	171.79
100	30	171.8
50	30	85.9

3. Symbol Code
   - Fallout trays--quantity 51
   - Two air samplers-- elevation 80 feet and 30 feet
   - Air samplers--elevation 0 to 30 feet
   - Generator--manually controlled
   - Generator--controlled from TCC
4. Trays 17, 23, 24 and 25 may be staggered off of the northwest direction line.
5. Scale--1 foot = 500 ft

Fig. II-27. Layout for Cerium Fallout Test--60-Degree Quadrant

TABLE II-10

High Temperature Fire Test Specimens

Specimen No.	Specimen Type	Shape	Material	Remarks
1	10	Cylinder, ends hemispherical	Cylinder-Inconel X Shell-Aluminum	
2	4	Cylinder	Hastelloy B	One-hole design
3	3	Cylinder	Hastelloy B	Seven-hole design
4	3	Cylinder	Hastelloy B	Seven-hole design
5	1	Cylinder	Inconel X	Seven-hole design
6	1	Cylinder	Inconel X	Seven-hole design
7	1	Cylinder	Inconel X	Seven-hole design
8	2	Cylinder	Stainless steel--316	Seven-hole design
9	2	Cylinder	Stainless steel--316	Seven-hole design
10	2	Cylinder	Stainless steel--316	Seven-hole design

After the test, the fallout tray depositions and air sampler filters will be collected and stored in individually marked metal cans, for delivery to the Martin Chemical Laboratory for analysis. Measurements will be made either by spectrographic or activation analysis.

Test specimens will be removed from the tower and visually inspected for damage. Photographs of each specimen will be taken and damage to each recorded. A more complete analysis will be made on the specimens in the Martin Laboratory.

Final preparations for the test are being made. To date, over three miles of wire have been laid to service a portion of the 62 air samplers and nine cascade impactors that have been procured for the test.

3. Heat Transfer Mockup Tests*

Testing of the heat transfer mockup was continued. The heat source was relocated in the geometrical center of the unit, and a revised thermal shield was located between the heat source and the inner hot skin surface. The shield consisted of two thicknesses of 0.01 inch stainless steel sheet, separated by a fine mesh stainless steel screen and formed into two truncated conical sections as follows:

		(in.)
Lower cone section	Large diameter	20
	Small diameter	12
	Vertical height	15
Upper cone section	Large diameter	12
	Small diameter	5
	Vertical height	4

With the inner skin surface at 1000° F, an equilibrium heat dump of 2550 watts was obtained. This represents approximately 100 watts less heat dump than in the case of the lowered block with a single thermal shield. It was estimated that with a single thermal shield, lowering of the block resulted in the dumping of 400 watts more heat. Returning the block to the geometrical center of the unit should have resulted in 400 watts less heat dump. Therefore, the dual shield was worth 300 watts of additional heat dump when compared to the single shield. Results of the test are given in Table II-11. It is noted that with the shutters open, a center block temperature of 1875° F was reached for a temperature of 1000° F at the inner skin. This is the same block temperature obtained with a lowered block and a single thermal shield. It was expected that a higher block temperature would have resulted. This indicates that a further improvement in the thermal shield arrangement can be made for increasing the heat dump before the block temperature becomes excessive.

A plot of power input versus inner skin temperature is given in Fig. II-28. Also plotted is the shutter heat dump. An equilibrium shutter heat dump of 3200 watts at 1100° F in vacuum conditions is noted. Based upon previous results, a total shutter heat dump in air of 3750 watts can be expected. The shutter heat dump requirement of 4000 watts for the

* J. Vogt, J. Dinwoodie

TABLE II-11

Data Summary

Heat Transfer Mockup with Double Thermal Shield

Vacuum Environment

Power Input (watts)	Temperatures: Block Center (°F)	Hot Skin (°F)	Hot Skin (°F)	Hot Skin (°F)	Hot Skin (°F)	Shutter (°F)	Shield Inside (°F)	Shield Outside (°F)	Cold Skin (°F)	Tank (°F)
				Shutters Closed						
2240	1599	1001	1000	1048	1104	1189	1195	1090	340	56
2000	1535	949	946	997	1053	1138	1144	1040	321	55
1800	1475	897	894	945	1000	1085	1092	992	301	55
1610	1410	845	840	891	945	1036	1036	939	293	54
890	1125	640	633	625	720	809	815	735	205	51
				Shutters Open						
2000	1387	688	670	661	674	642	873	776	226	53
3000	1610	833	815	801	814	756	1018	914	276	55
4040	1789	945	930	911	920	845	1138	1024	319	58
4400	1851	985	974	950	956	874	1181	1061	338	59
4600	1875	1002	991	965	970	884	1200	1078	344	58

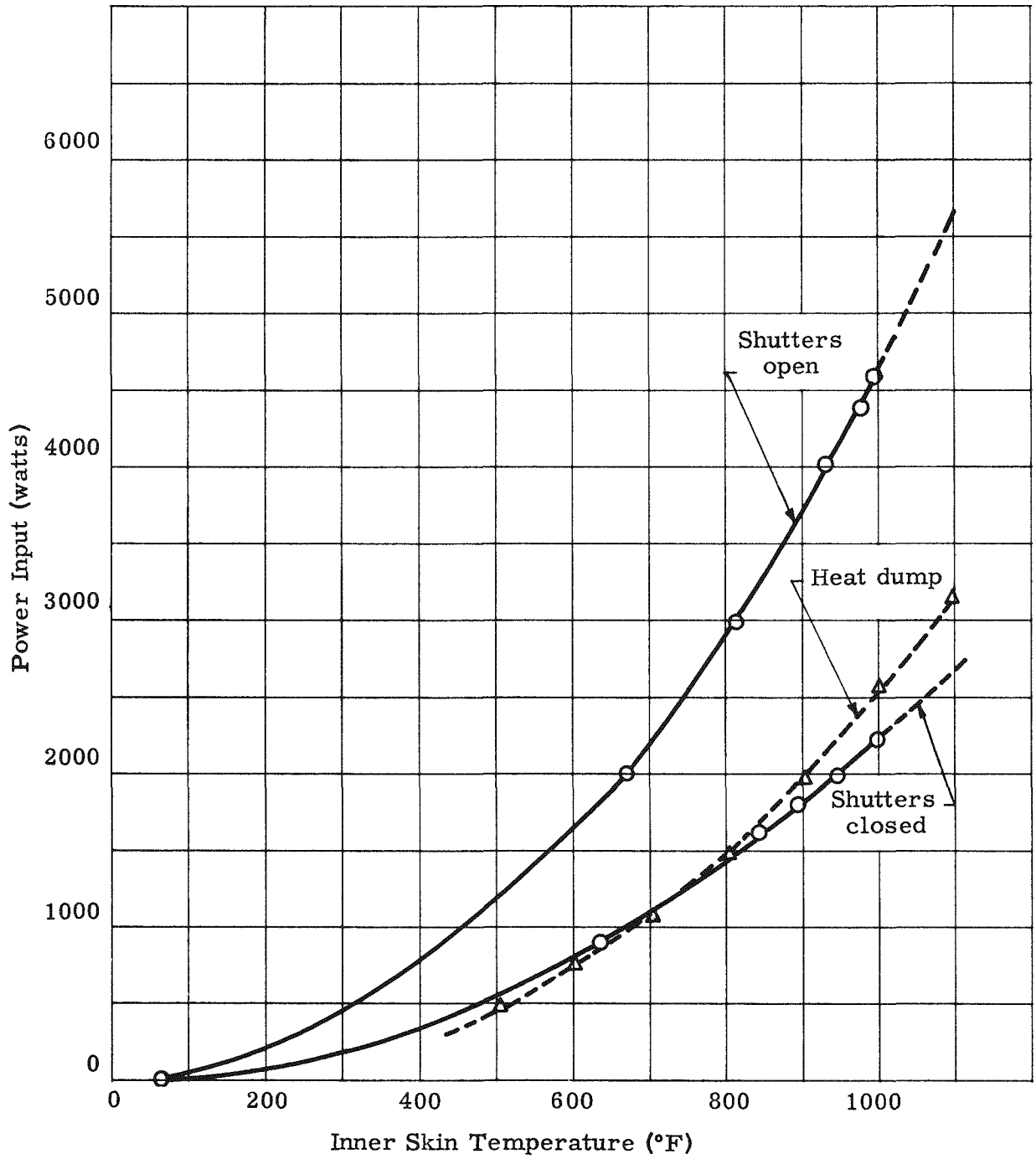

Fig. II-28. Power Input Versus Inner Skin Temperature--Heat Transfer Mockup in Vacuum, Double Thermal Shield, Heater Block Located at Center of Unit

isotope ground test unit will therefore be satisfied because of the increased view factor inherent in the generator design when compared to the heat transfer mockup configuration.

Tests were made to determine the temperature of the block and the inner skin during a startup transient. This test simulated time after draining of the biological shield and the cutoff of coolants to the unit. The results are shown on a time-temperature plot in Fig. II-29. Temperatures of the block center, side and inner skin are shown. Results indicate that an average block temperature of 1500° F would be reached 20 minutes after the biological shield was drained and circulation of cooling water stopped. Since the aerodynamic analysis indicates that surface impact of the intact fuel core due to vehicle failure through Vernier burnout will take place within 12-1/2 minutes after launch, the maximum temperature of the block at impact for the high velocity tests at Aberdeen was fixed at 1500° F.

4. Bonding Tests on Thermoelectrics*

Bonding tests described in the previous quarterly report were continued to obtain information on lowering the element to hot shoe interface resistance. In one test, the iron shoe was tinned with lead prior to element assembly. Precautions were taken to degrease all contacting surfaces with toluene. Following assembly, the couple was placed in a Bell jar, the jar evacuated and then purged continuously with a 75% N_2-25% H_2 gas mixture. An N and P element couple was operated at approximate hot and cold junction temperatures of 1000 and 350° F for extended periods of time. The hot shoe temperature was raised to 1350° F, maintained for one hour and then lowered to 1000° F for data taking. The cold junction temperature was 328° F. Total overall resistances of 22.3 and 10.7 milliohms were recorded for the P and N elements, respectively.

In a second test, the iron shoe was sandblasted, the element faces roughened with emery cloth and all contacting surfaces cleaned with acetone. The same conditioning procedure was followed and at operating temperatures total overall resistances of 16.5 and 12.0 milliohms were recorded for the P and N elements, respectively.

The tests were continued using thermoelectric element materials as the bonding agents. The materials were crushed, placed on the shoes and melted in a hydrogen furnace. After cooling, the resulting deposits were filed flat and sanded smooth. A listing of the materials used in the tests follows.

* J. Ascenzi

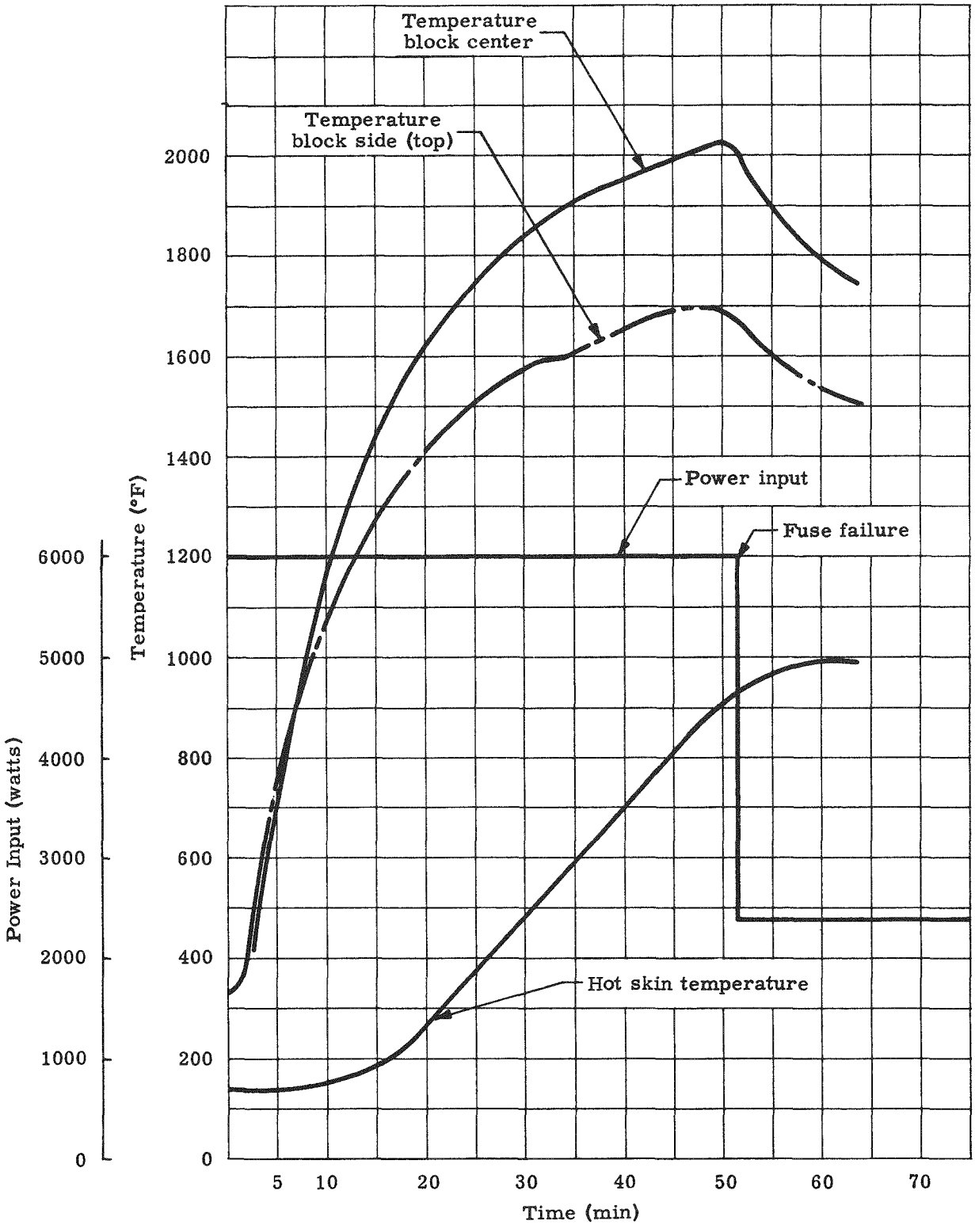

Fig. II-29. Temperature Versus Time--Transient Startup Time for Heat Transfer Mockup in Air, Double Thermal Shield, Heater Block Located at Center of Unit

Test Run No.	Material at P Element End	Material at N Element End
3	P-type PbTe, 1% Na doping	N-type PbTe, 0.03% PbI_2 doping
4	Undoped PbTe	N-type PbTe, 0.03% PbI_2 doping
5	Undoped germanium telluride	N-type PbTe, 0.03% PbI_2 doping

Results are given in Table II-12.

The test results of Run No. 3 showed fairly low values of resistance for both P and N elements, indicating fair metallurgical bonding. Disassembly and subsequent inspection, however, revealed that the N elements had indeed bonded well as shown in the top photo of Fig. II-30. The P element, however, had bonded to the deposit, but the deposit had detached itself from the iron shoe.

In Test Run No. 4, the iron shoes were drilled out slightly before furnace conditioning in an attempt to increase the mechanical strength of the bonds. Inspection after the test revealed that the N element had not bonded well. This was apparently due to some misalignment in the testing assembly. The P element was found to have bonded metallurgically to the deposit but the deposit was only mechanically attached to the iron shoe.

The data of Test Run No. 5 did not indicate any high degree of bonding. Inspection of the assembly after test, however, showed that the solder caps at the cold junction were loose and were probably contributing to the high resistances recorded. Possible overheating at the cold junction may have melted the solder. A good metallurgical bond had been achieved at both N and P element hot junctions, even though less than half of the individual element surfaces had bonded. It was surprising to note that the open circuit voltage at the end of of the test had increased substantially over that at the start--apparently the result of the intrinsic thermoelectric property of the germanium telluride used as the bonding material.

These results were very promising and showed that prebonding of thermoelectric materials to the hot shoes in the hydrogen furnace merits further investigation.

TABLE II-12

Results of Bonding Test on Prebonded Iron Shoes

Test Run No.	Junction Temperature Hot (°F)	Junction Temperature Cold (°F)	Total Open Circuit Voltage (volts)	Total Resistance P Element (milliohms)	Total Resistance N Element (milliohms)	Remarks
3	1007	254	0.2176	14.2	11.2	Start of test
3	1009	253	0.2196	12.6	10.8	After conditioning at 1350°F for 1 hr and some 16 hr of operation. See text.
4	1002	349	0.2009	73.5	31.3	Start of test
4	1000	359	0.1910	62.9	17.8	After conditioning at 1350°F for 1 hr. See text.
5	1006	345	0.2168	33.6	27.8	Start of test
5	999	335	0.2220	39.7	14.5	After conditioning at 1350°F for 1 hr. See text.

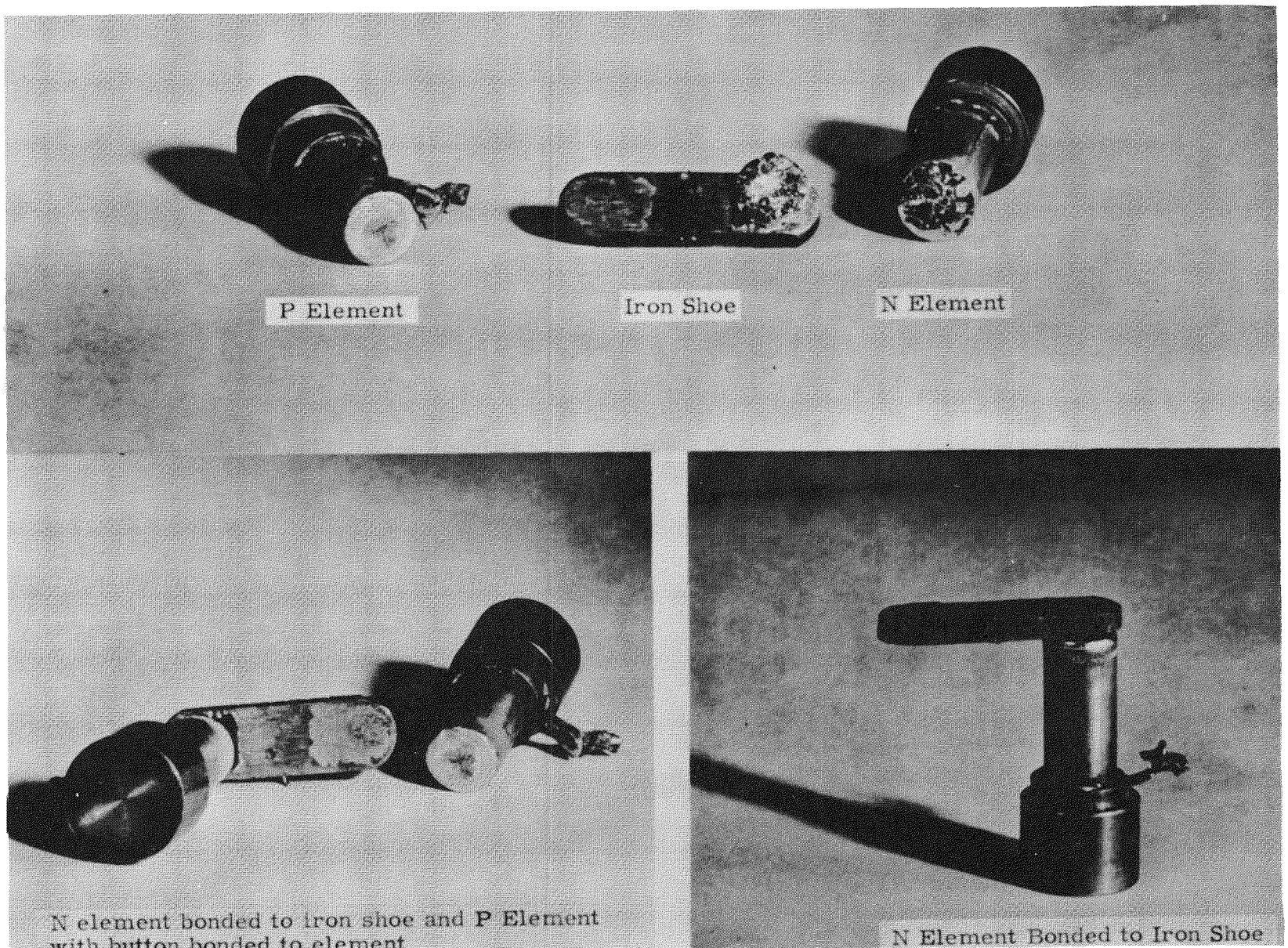

Fig. II-30. Bonded PbTe Thermoelectric Pair (Test Run No. 3)

5. Electrical Tests

The first electrically heated generator was delivered for testing in early March 1960 and was installed in the test chamber. Prior to initial heatup, the chamber and the insulated hermetic seal area of the generator were evacuated for 60 hours in an effort to degas the Min-K insulation. Nitrogen was then admitted to the chamber while the hermetic seal was filled with hydrogen. Numerous leaks in the generator, especially around the aluminum adjusting bosses, made it necessary to maintain a slightly positive pressure on the generator seal area and to burn off the exhaust gases from both the seal area and test chamber.

While the unit was being purged in this manner, the heaters were activated and the inner hot skin raised to approximately 500°F. As a result of the heatup, the largest section of thermoelectrics lost continuity and had to be bypassed. Results on the remaining 40% of the elements in the circuit were as follows:

Power input	1360 watts
Power output	0.4 watt
Open circuit voltage	4.66 volts
Load voltage	1.70 volts
Load current	0.019 ampere
Hot skin temperature (avg)	494°F
Cold skin temperature (avg)	178°F

Following this checkout, the heaters were shut off and the generator was purged with argon and the test chamber with nitrogen. After all the hydrogen had been purged, the chamber was opened and the generator removed. The majority of the leaks were located and repaired and electrical continuity in the generator restored. To allow for thermal expansion of the inner skin relative to the outer skin, the adjusting plugs were backed out approximately 1/16 inch. This resulted in a continuity loss, but testing was resumed, since it was felt that heating and subsequent expansion would restore continuity. With 80% of the elements in the circuit, the following results were obtained:

Power input	3600 watts
Power output	33 watts
Open circuit voltage	22.9 volts
Load voltage	11.3 volts
Load current	2.9 amperes
Hot skin temperature (avg)	1006°F
Cold skin temperature (avg)	311°F

During the test, several short circuits to the ground developed. This necessitated another shutdown and removal of one pair of elements. Further test results on the generator are summarized as follows:

Power input	2900 watts
Power output	63.6 watts
Open circuit voltage	48 volts
Load voltage	24.7 volts
Load current	2.54 amperes
Hot skin temperature (avg)	962°F
Cold skin temperature (avg)	293°F

It was planned to continue testing to determine equilibrium data for hot skin temperatures up to 1150°F. However, thermocouples monitoring the outer skin temperature in the vicinity of the shutter area indicated that local overheating of the cold junction would occur before the hot skin reached 1050°F. A water cooling tube was added below the lowest row of elements in an attempt to reduce outer skin temperatures in this localized area.

This modification proved successful, and a power output of 78.2 watts was obtained. The pertinent data for this run are:

Power input	3320 watts
Power output	78.2 watts
Open circuit voltage	57.5 volts
Load voltage	28.6 volts
Load current	2.7 amperes
Hot skin temperature (avg)	1043°F
Cold skin temperature (avg)	297°F

The element pair removed from the unit showed bonding at the N element hot junction but none at the P element junction. This result supports that obtained earlier in bonding single element pairs in the Bell jar setup.

Testing will continue to determine equilibrium data for hot skin temperatures up to 1150°F with the cold skin not exceeding 350°F maximum.

III. TASK 3--SNAP-III THERMOELECTRIC GENERATOR*

The purpose of this task is to determine, through a test program, the operating characteristics of a SNAP-III-type thermoelectric generator.

The specific objectives during this report period were:

(1) To continue parametric testing of the 3M1G3 generator under various internal and external pressure conditions.

(2) To determine the long term operating characteristics of SNAP-III generators, by operating a new generator continuously at a fixed input power and load condition, while making periodic readings of generator performance.

(3) To refuel the second isotope-fueled thermoelectric generator.

A. PARAMETRIC TESTS

The reassembly of the 3M1G3 thermoelectric generator used in the parametric testing program was completed in January. Before reassembly, the ends of the elements were squared for optimum contact with the face of the iron hot shoes, the two broken P-type elements were replaced with 3M standard 1/4-inch diameter elements machined to the proper diameter, new isomica sleeves were installed and the heat source spider ring was coated with Rockite and stone honed for maximum surface contact with the hot shoes. The ends of the hot shoes were also coated to prevent electrical shorting between elements. This latter procedure was a simplification of the original procedure used by 3M in the assembly of the generator wherein each individual hot shoe was coated with Rockite.

During the assembly and preliminary heat run, two other P-type elements shattered. These were replaced with standard 1/4-inch diameter elements after several attempts to machine elements to the smaller diameter had failed. The laminated isomica sleeves had to be split and spread to accommodate the 1/4-inch elements. The splits in the layers were oriented to provide maximum protection to the element. The generator, as finally assembled, contained the original thermoelectric elements except for the four P-type elements.

---

* G. H. Storrs

The repaired generator was delivered to the Engineering Laboratory on January 25, 1960. The generator internal conditions were 85% N_2 and 15% H_2 at one atmosphere pressure. The generator was stabilized at 68.8 watts input power at a load of 2.98 ohms. This was done to compare the reassembled generator with vendor-furnished data on the original generator.

The following is the comparison as of February 1, 1960.

	Power				Effi-	Inter- nal Re- sist-	Junction Temperatures	
	In (watts)	Out (watts)	Load (volts)	Seebeck (volts)	ciency (%)	ance (ohms)	Hot (°F)	Cold (°F)
Original	68.6	4.4	3.5	6.8	6.4	2.62	1087	218
2/1/60	68.8	2.4	2.68	5.38	3.5	3.13	947	226

All parametric tests were run with the unit inside a large copper tube which was painted black on the inside. A water cooling coil maintained the tube at a relatively uniform temperature. Figure III-1 is a photo of the test setup with the test generator installed.

To prevent variation of external generator conditions, the Bell jar was left in place for both the one atmosphere external pressure and the vacuum conditions. With the natural convection of the air in the Bell jar, the average generator temperatures were slightly lower than with a vacuum inside the Bell jar.

After the generator was installed in the test system, it was operated in an open circuit condition to determine the input power required for a 900° F hot junction temperature with internal and external vacuums. This power input was 46.7 watts and is approximately the power input at which all succeeding tests were run. This procedure was used to assure that the maximum allowable hot junctions temperatures would not be exceeded.

Short circuit and 10 other loads were used to determine generator performance. The generator was considered stabilized after three readings, spaced 10 minutes apart, showed no variation. The maximum power load was determined from this equilibrium data. With the generator stabilized at maximum power, six other points were obtained in rapid succession to determine transient loading performance.

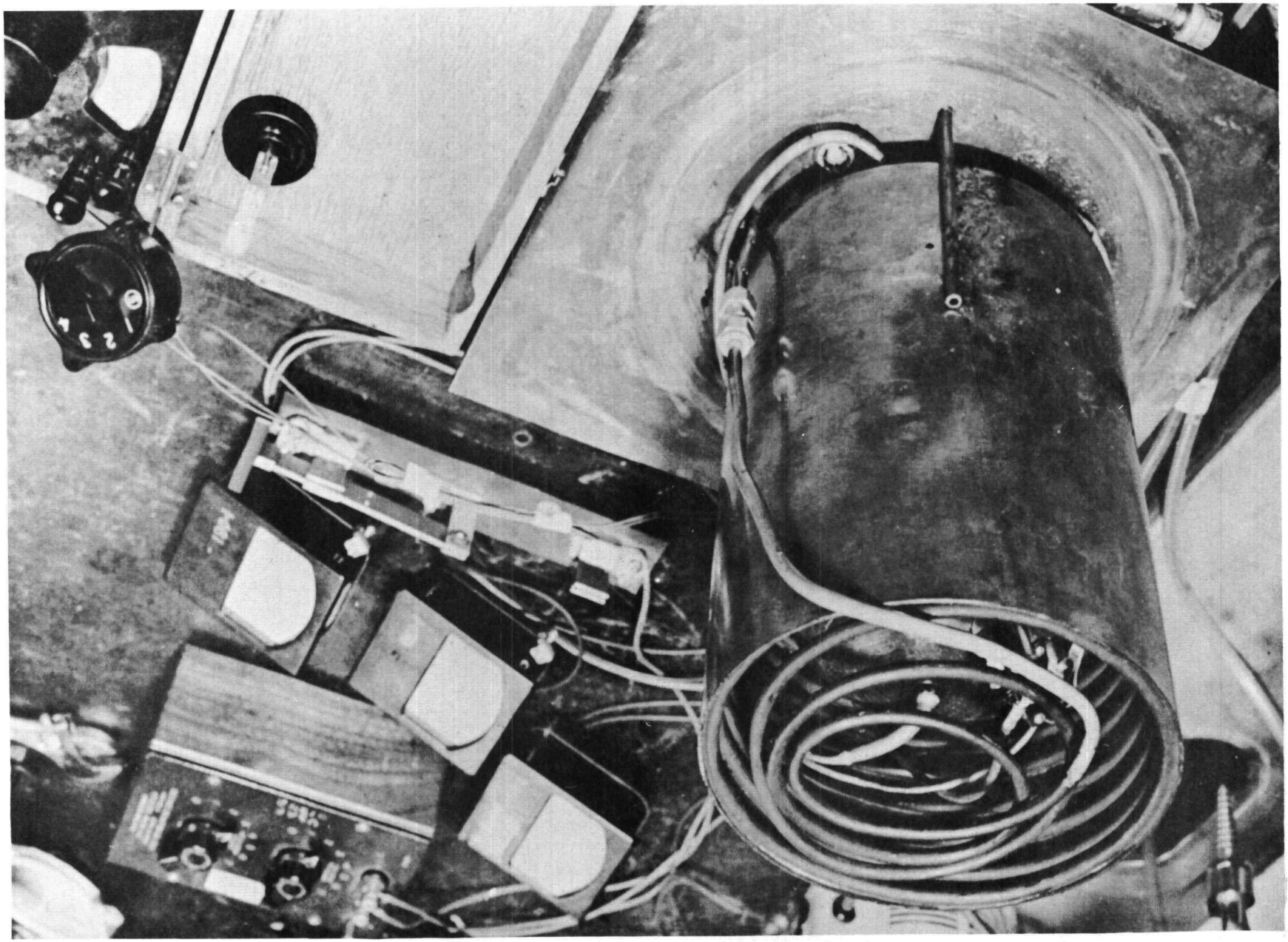

Fig. III-1. Test Setup with Generator Installed

At the end of this report period, the generator has been tested under four parametric conditions. Two tests were run with a vacuum inside the generator, and two tests were run with two atmospheres of 85% nitrogen and 15% hydrogen inside the generator. For each internal generator condition, a test was run with a vacuum inside the Bell jar and with ambient pressure of one atmosphere.

Figures III-2 and III-3 show the results of tests with an internal and external vacuum. Figures III-4 and III-5 show results with an internal vacuum and an external ambient (1 atmosphere) air pressure.

The characteristics obtained with two atmospheres (abs) of 85% nitrogen and 15% hydrogen internal and with one atmosphere of air external to the generator are shown in Figs. III-6 and III-7. This test was repeated with the same internal atmosphere conditions but with a vacuum external to the generator. When these conditions were established, the generator developed a leak in the main shell soldered seam. Two unsuccessful attempts were made to repair the leak using 50-50 solder. It is believed the combination of elevated shell temperatures (250° F) at external vacuum conditions plus the two-atmosphere differential pressure caused a solder expansion and leakage. The generator was resealed employing a 90-10 solder (90% Pb, melting point approximately 600° F). This joint held pressure for about three days before developing another leak. The generator operated for a sufficient period to obtain an equilibrium generator performance curve but the failure occurred prior to the collection of transient data. The data obtained are shown in Figs. III-8 and III-9. The transient data will be completed at the end of the test series now in progress. It is anticipated that these tests, which involve lower internal pressures, will not cause leaks.

A comparison of several parameters for the four tests completed to date is shown in Table III-1. The maximum in the table applies to values at the maximum power output point.

B. GENERATOR LIFE TEST

The 3M1G10 generator, as received from the vendor, contained an internal fill of 95% argon and 5% hydrogen at an internal pressure of one atmosphere. No attempt will be made to change this atmosphere throughout the life test.

The first test run with this generator was to determine the operating parameters to be used in the life test. The power input selected was 66.7 ± 0.3 watts, which was the power level that produced a hot junction temperature of 1100° F with no external load connected to the generator.

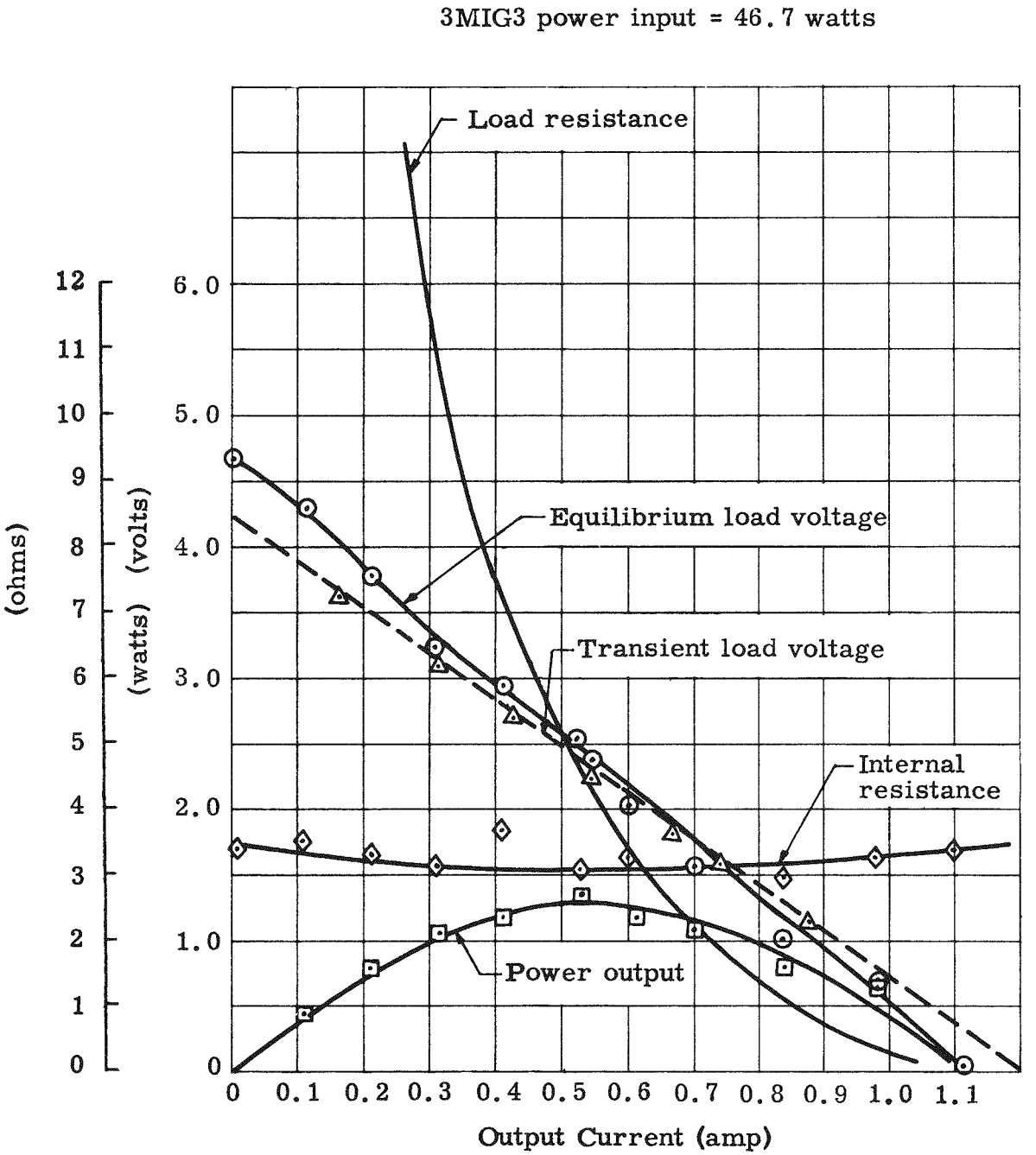

Fig. III-2. Generator Characteristics--Vacuum Internal and External

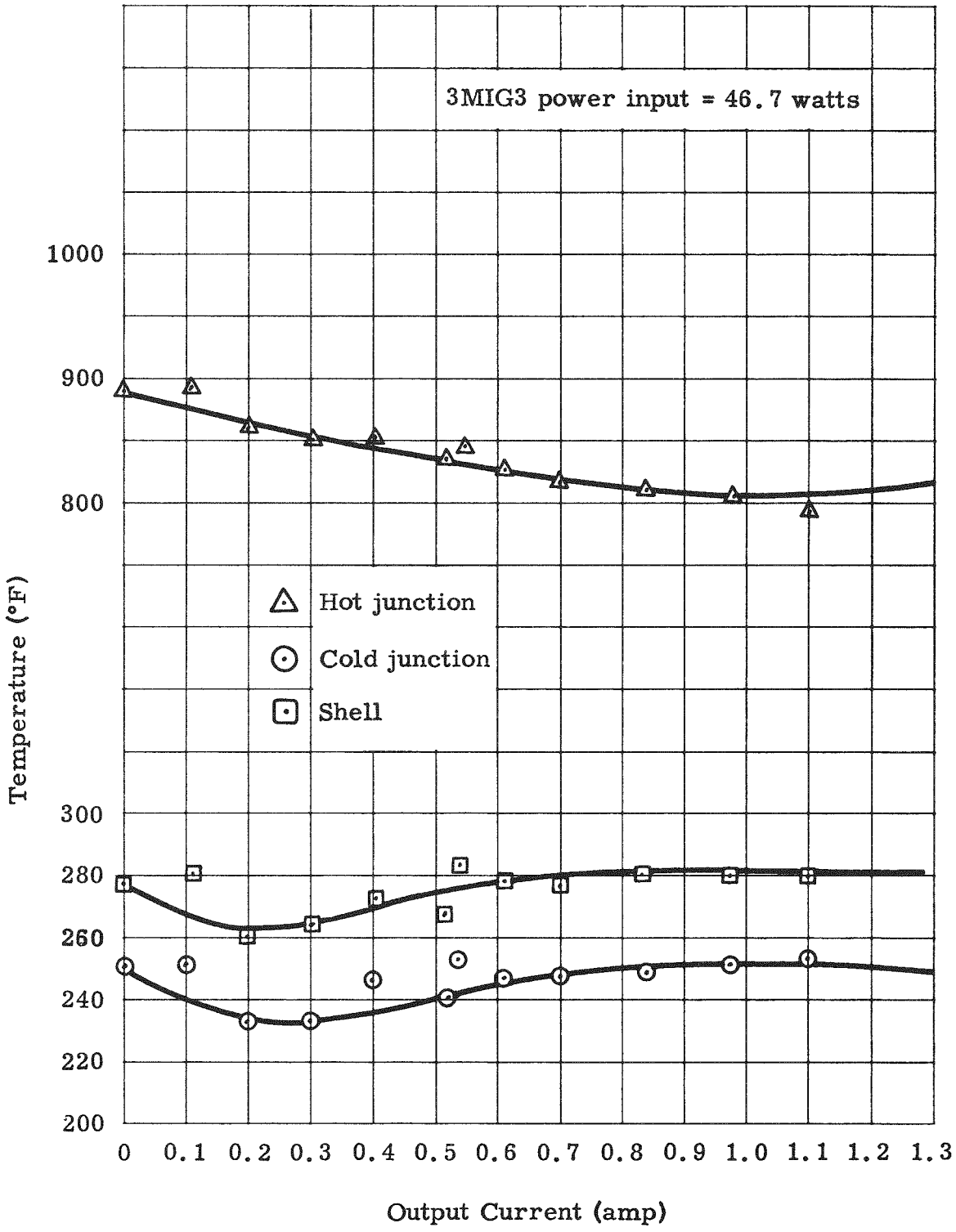

Fig. III-3. Generator Junction Temperatures--Vacuum Internal and External

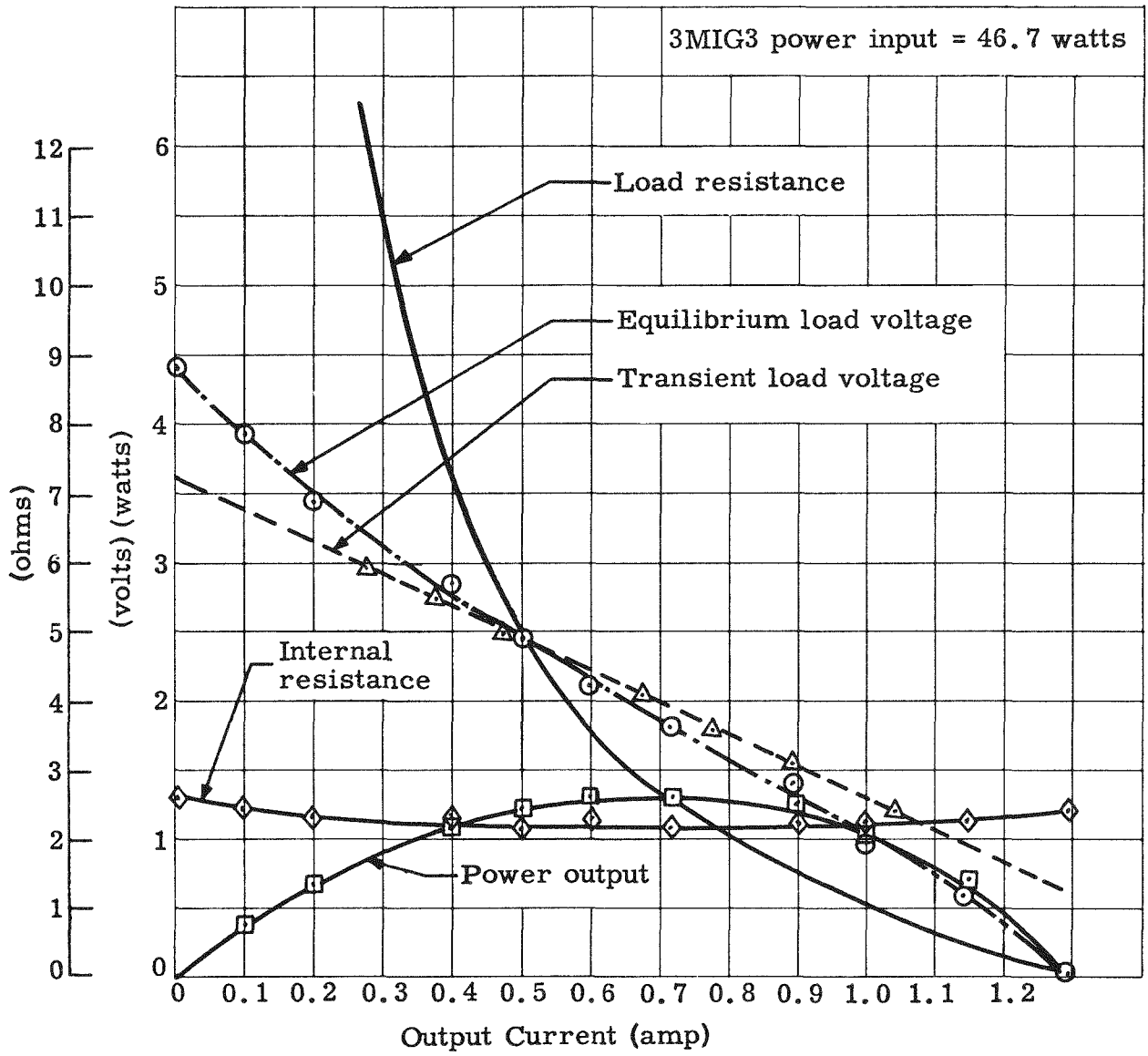

Fig. III-4. Generator Characteristics--Vacuum Internal, One Atmosphere Air External

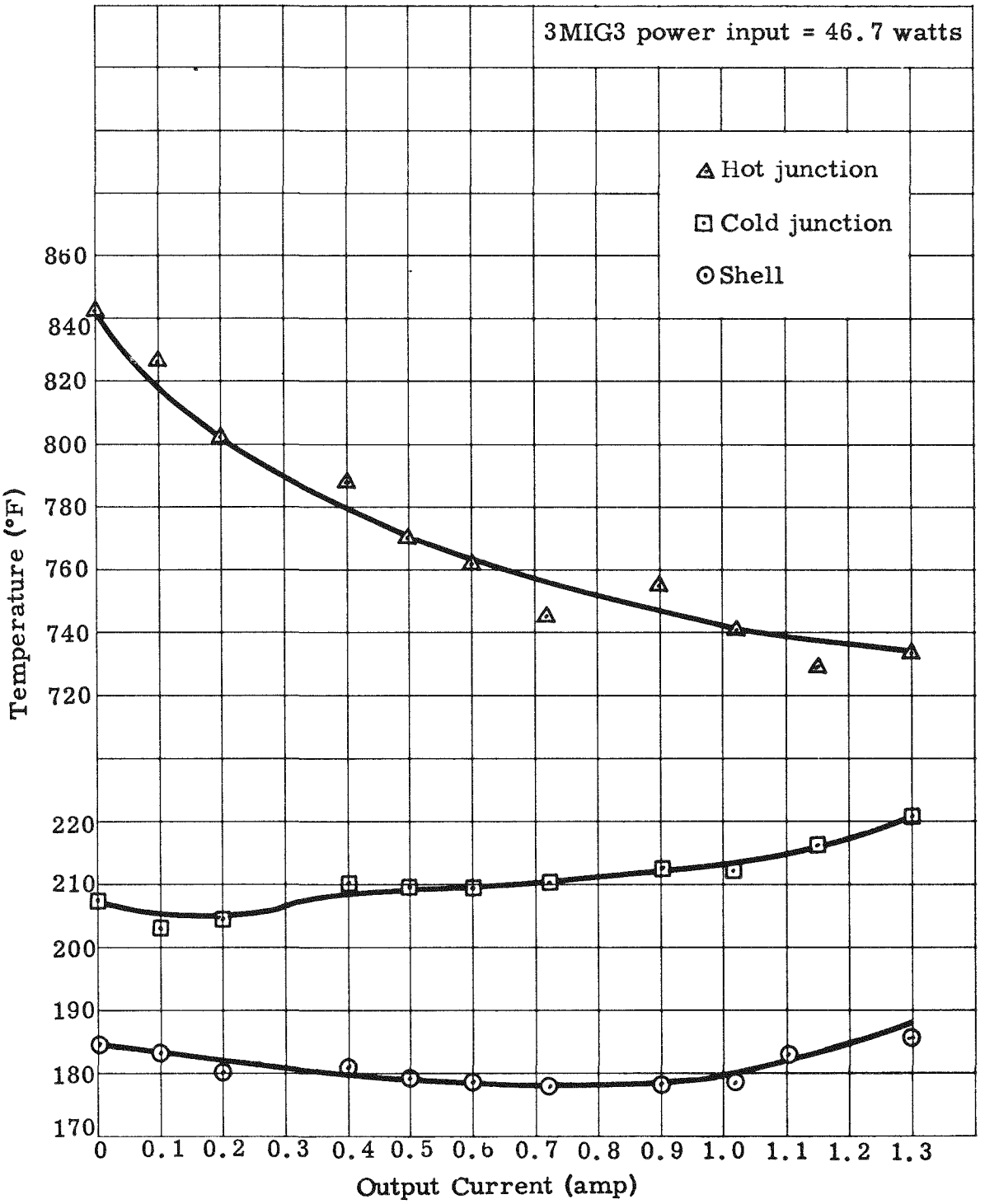

Fig. III-5. Generator Junction Temperatures Vacuum Internal, One Atmosphere Air External

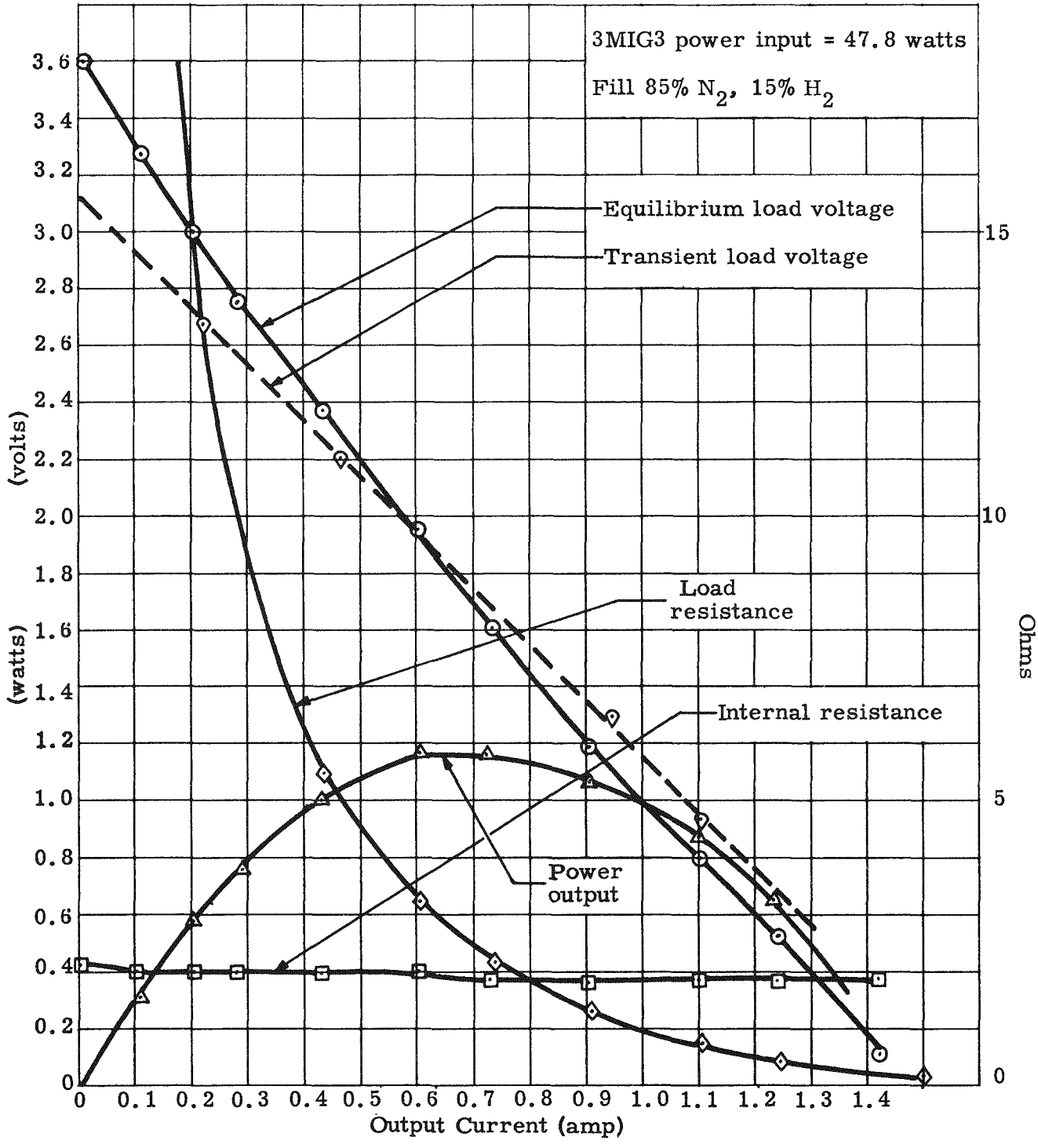

Fig. III-6. Generator Characteristics--Two Atmospheres Internal, One Atmosphere External

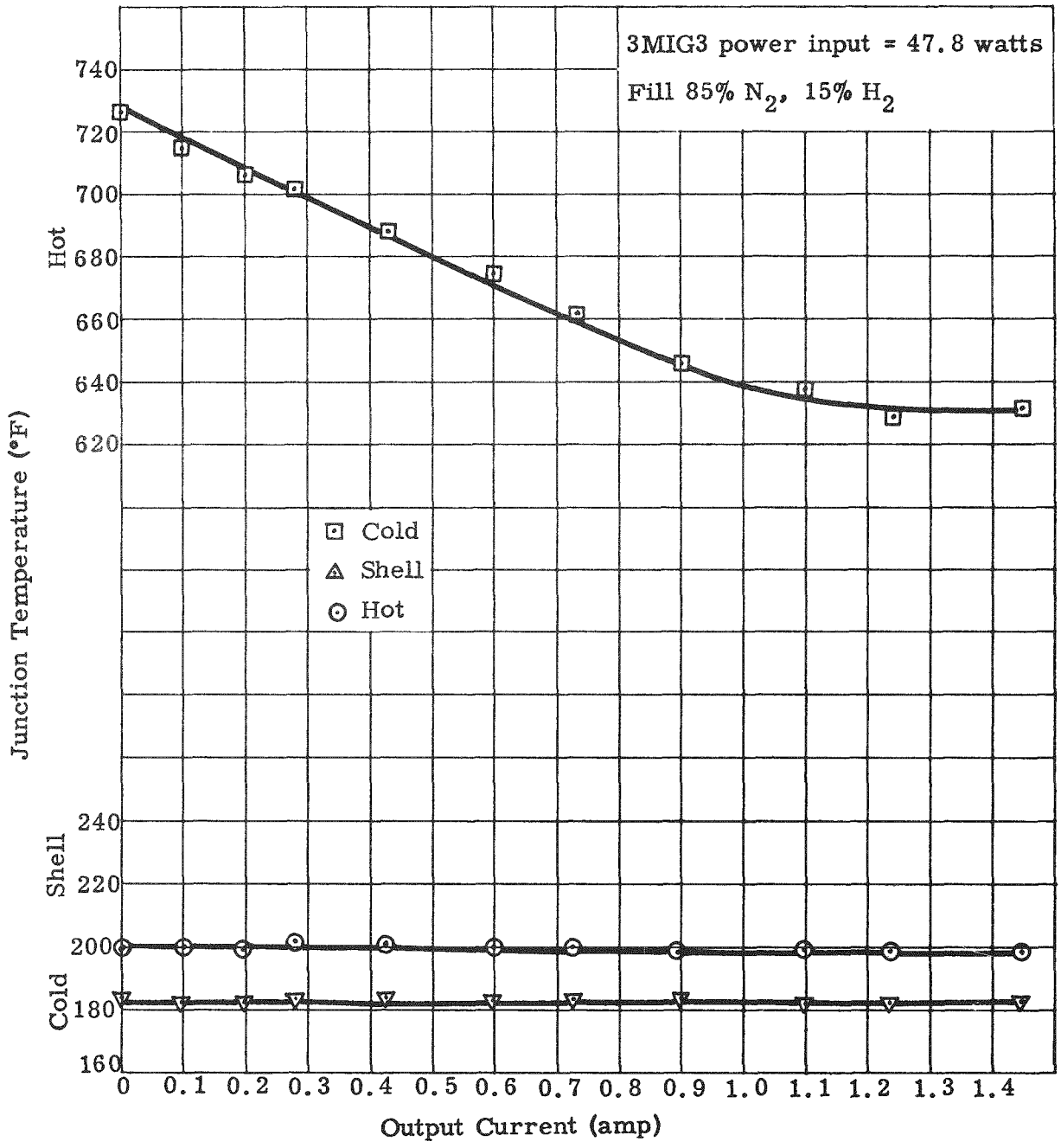

Fig. III-7. Generator Junction Temperatures--Two Atmospheres Internal, One Atmosphere External

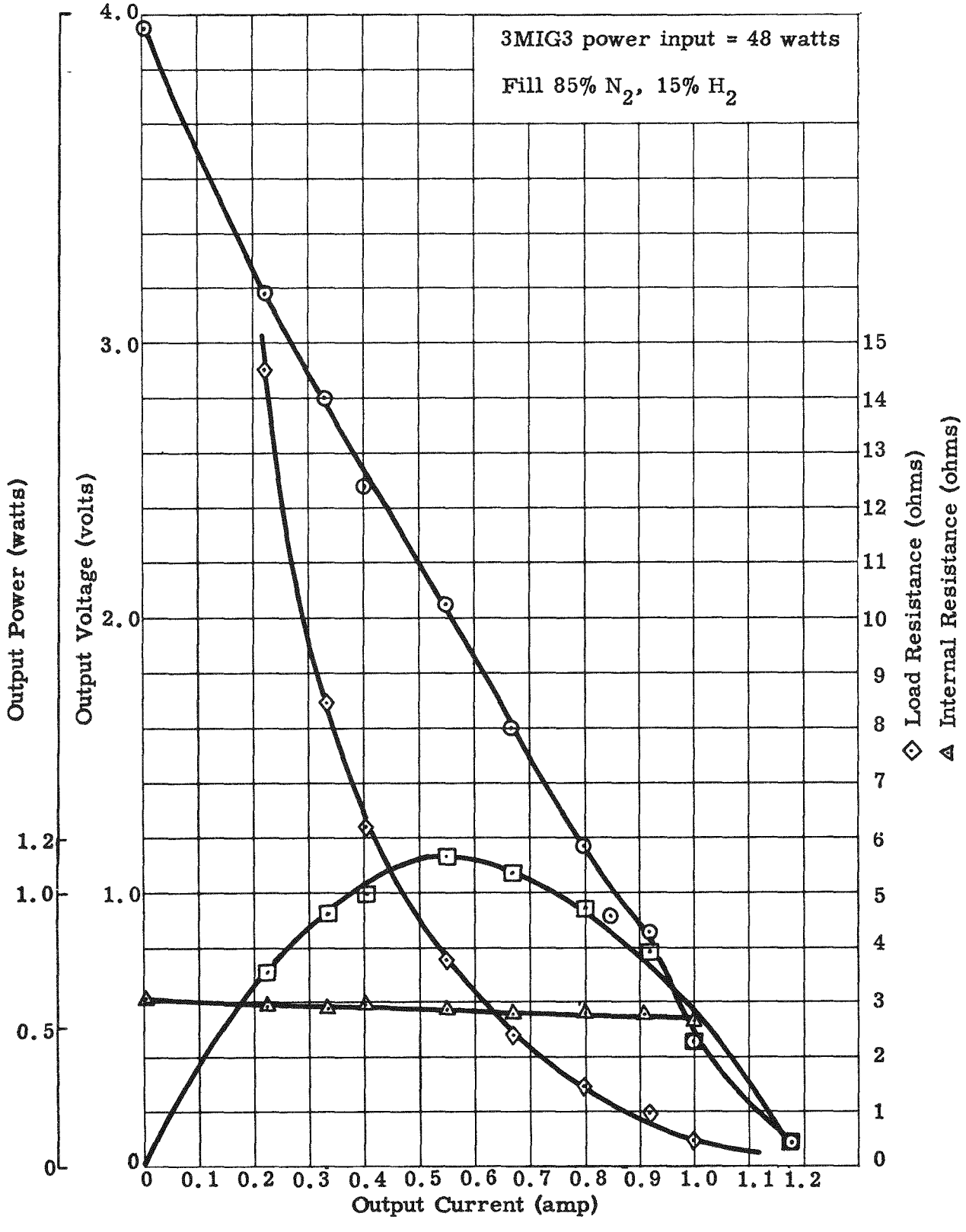

Fig. III-8. Generator Characteristics--Two Atmospheres Internal, Vacuum External

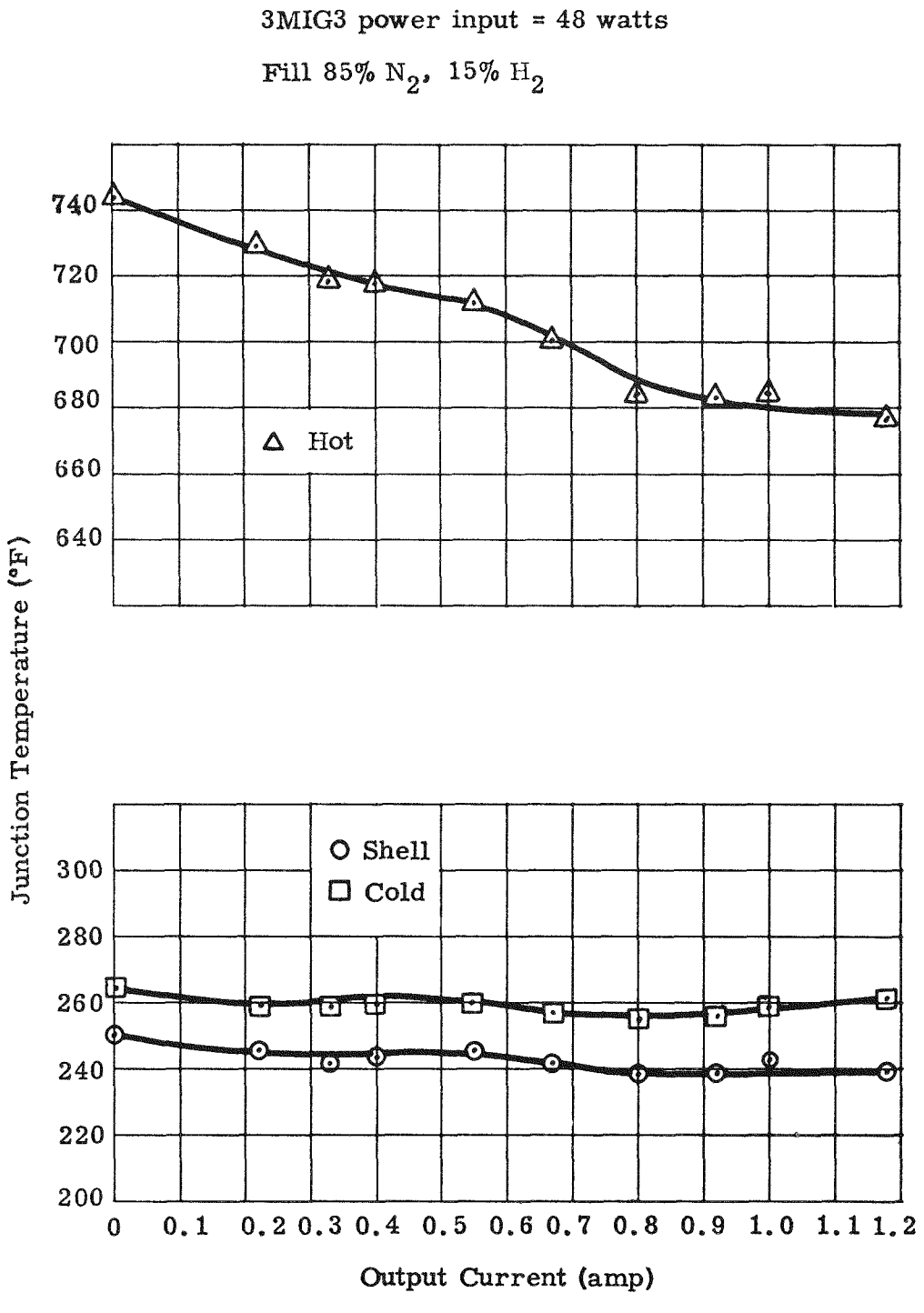

Fig. III-9. Generator Junction Temperatures--Two Atmospheres Internal, Vacuum External

TABLE III-1

T/E Generator Performance vs Operating Parameters

Environment Internal	Vacuum	Vacuum	2 atmospheres 85% N_2	2 atmospheres 85% N_2
Environment External	Vacuum	1 atmosphere air	1 atmosphere air	Vacuum
Power output (max)--watts	1.3	1.3	1.16	1.12
Resistance load (max)--ohms	4.18	3.09	2.51	3.40
Open circuit voltage--volts	4.75	4.4	3.6	4.1
Short circuit current--amperes	1.1	1.3	1.5	1.2
Load current (max)--amperes	0.52	0.70	0.68	0.52
Internal resistance (max)--ohms	3.2	2.2	1.9	2.8
Temperature (max)--°F				
Hot shoe	831	758	665	712
Cold shoe	277	212	200	260
Generator efficiency--%	2.78	2.78	2.42	2.34

At this input power level, an output voltage versus current characteristics at equilibrium conditions was obtained. From this curve, the maximum power output load was determined to be approximately 4.5 ohms.

The generator is located in a freely vented box to shelter it from the effects of air drafts within the laboratory. A photograph of the test setup is shown in Fig. III-10.

The generator has been operating at the predetermined power input level of approximately 67 watts and optimum load of 4.5 ohms since the start of the life test on January 26, 1960. The load has remained essentially constant between 4.4 and 4.6 ohms. The load is a fixed wirewound resistor and variations probably are due to output meter reading errors. As can be seen in Fig. III-11 (a time history of this generator), there now appears to be a slight leveling off tendency of the output values and internal resistance. Performance has continued to decrease but the rate of decrease has continually lessened. This leveling off tendency appears most prevalent in the internal resistance curves and to a lesser extent in the other curves, except for open circuit voltage. The mean cold junction temperature has remained nearly constant but the source and hot junction temperatures have decreased about 15° F during the period. This could signify a thermal conductivity change between the source and the sink.

C. ISOTOPE-HEATED THERMOELECTRIC GENERATOR, 3M1G1

The second SNAP-III Po-210 fueled generator was returned to The Martin Company on March 15, 1960. This unit was originally fueled with 1738 curies on March 27, 1959. As of the end of March 1960, the curie strength is reduced to 270 curies. A power output characteristic was run on this generator which showed the maximum power output of the generator to be 0.097 watt with a Seebeck voltage of 0.48 volts. The original output of this unit was approximately 2.5 watts with a Seebeck voltage of 3.5 volts.

The power curves for this generator (equilibrium and transient conditions) are shown in Fig. III-12. The internal atmosphere composition and pressure are unknown since it was sealed and the external environment was at normal room conditions. No thermocouples are available on this generator to determine junction temperatures.

The dry box and its accessories have been readied for removing the heat source from the generator. A manometer has been installed for monitoring dry box pressure. Unloading of the polonium heat source is planned on the assumption that the heavy walled capsule has ruptured and opening of the generator case would release the radioisotope. A practice defueling operation will be observed by Health Physics personnel to allow evaluation of the techniques involved.

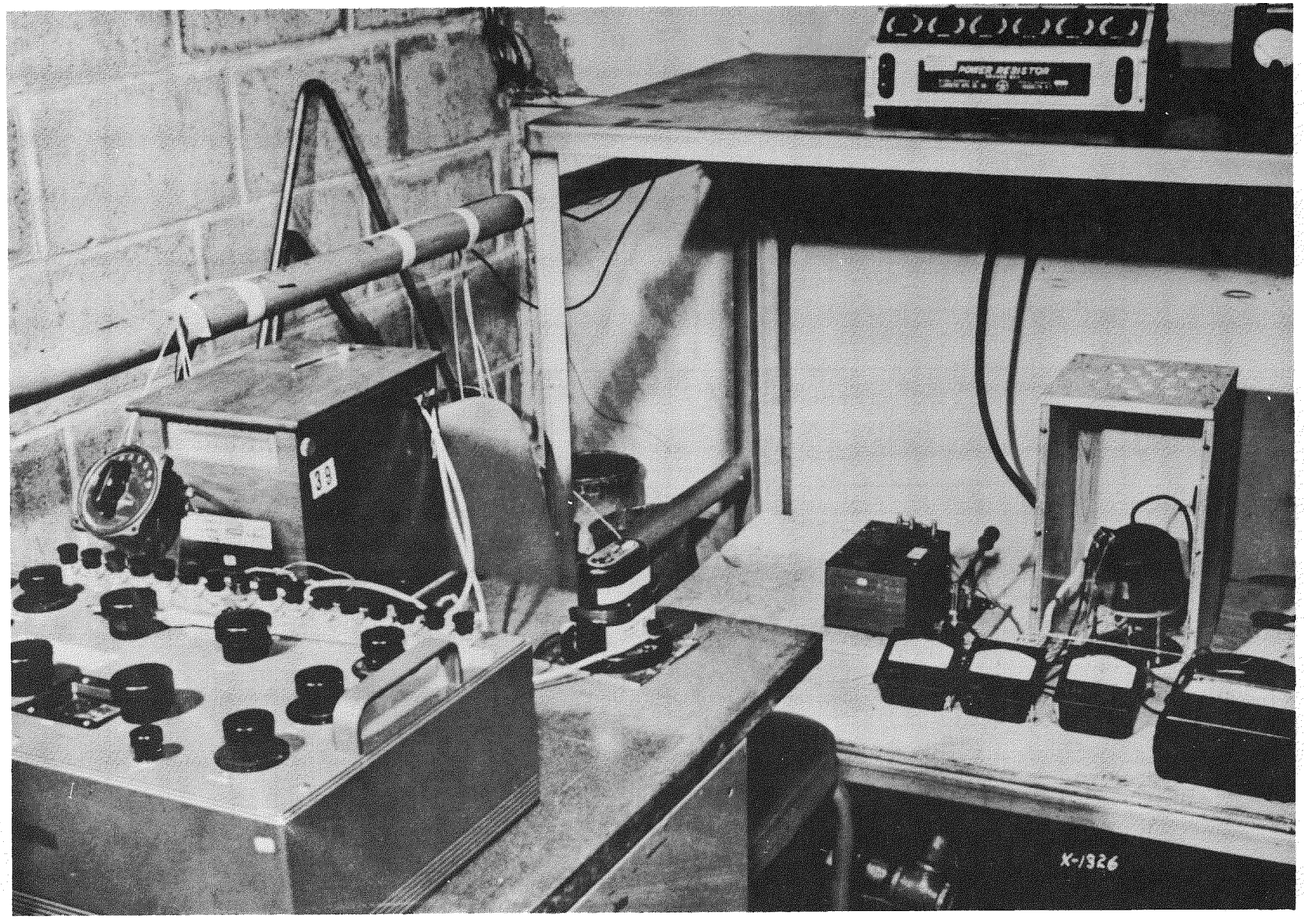

Fig. III-10. Life Test Setup

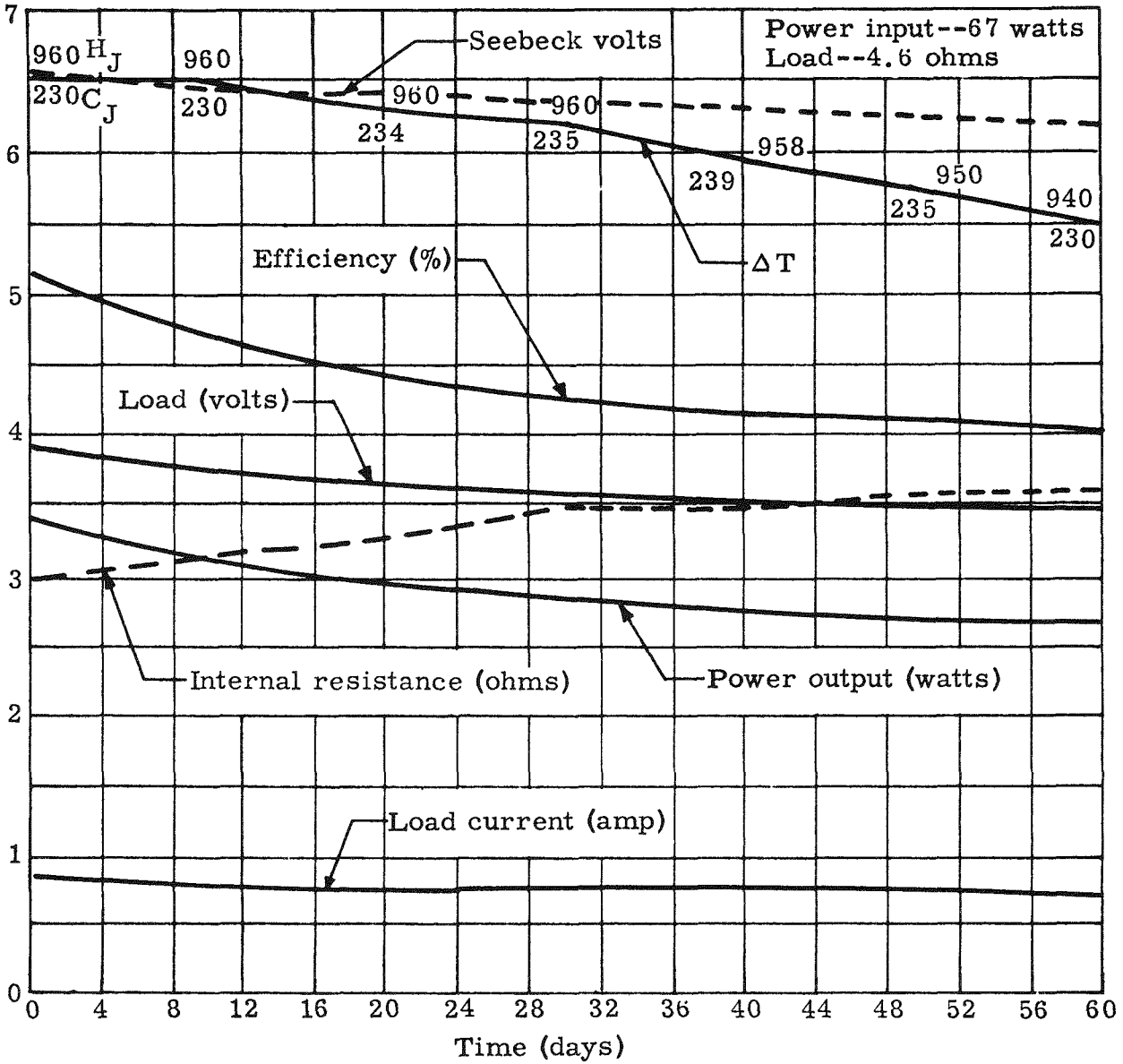

Fig. III-11. Life Test of 3MIG10 Generator

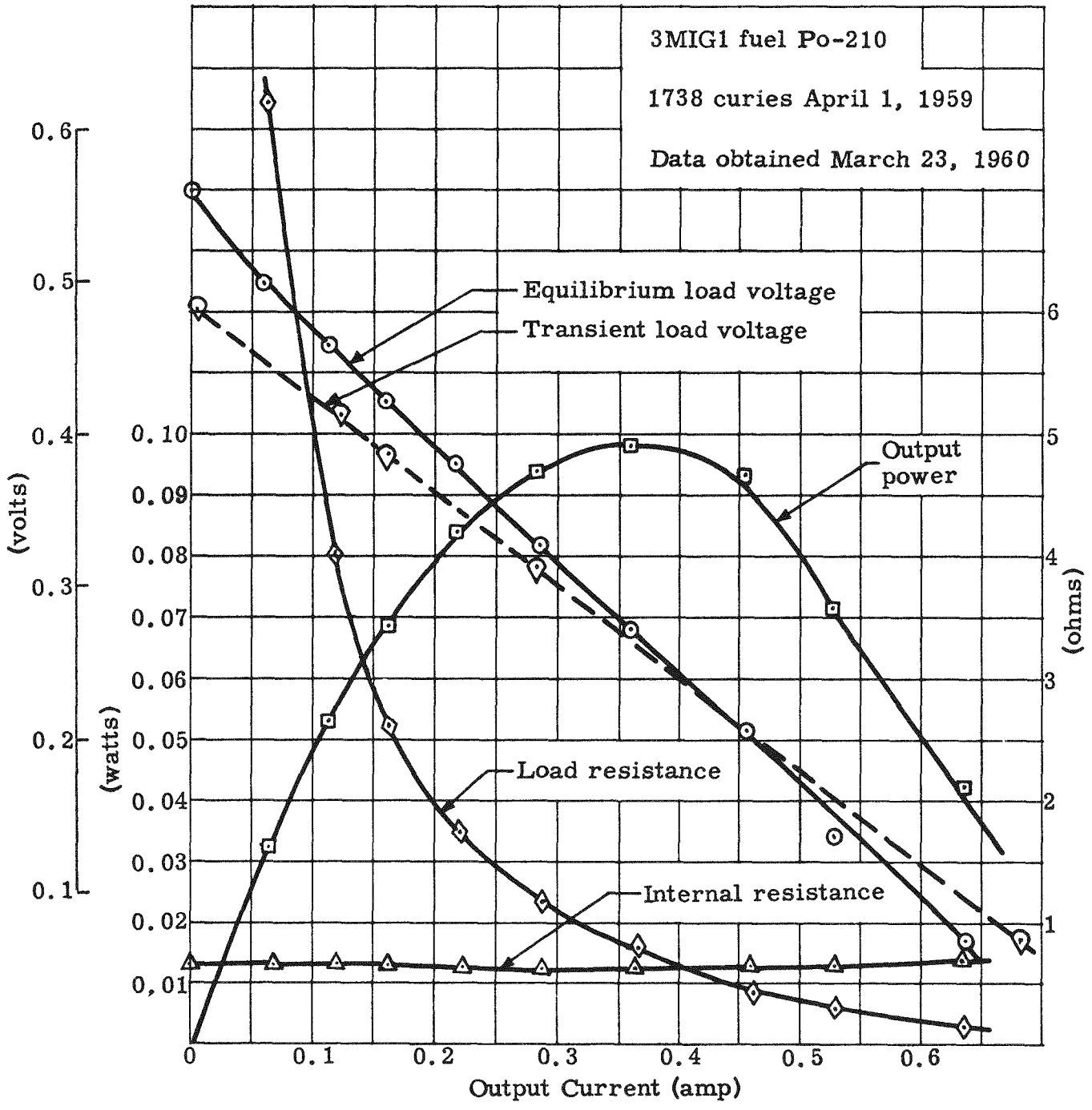

Fig. III-12. Po-210-Fueled Thermoelectric Generator Characteristics

IV. TASK 5

A. SUBTASK 5.1--ADVANCED THERMOELECTRIC POWER SYSTEM*

The objective of this subtask is to evaluate and determine the performance characteristics of the electrically heated, 3-watt thermoelectric generator (SNAP-IIIA) fabricated by the New Products Engineering Department of Westinghouse. This generator includes a variable heat dump mechanism for thermal power flattening.

1. Status of the Westinghouse Generator

The SNAP-IIIA thermoelectric generator which had been returned to Westinghouse for repair, was sent back to The Martin Company, complete with drawings and operating manual, on January 28, 1960. Westinghouse undertook the design and fabrication of an entirely new generator for this application because the first generator did not meet the objective specifications. The second generator (designated SNAP-IIIA-2) was completed and delivered to The Martin Company on March 10, 1960. Although SNAP-IIIA-2 is a completely new design, the performance characteristics were only marginally better than the original SNAP-IIIA generator. The Martin Company recommended to the Commission that all further technical evaluation of the generators be cancelled. This recommendation was made because:

(1) Both generators exhibited electrical power-to-weight ratios substantially less than what is considered to be reasonable or optimum for the state of thermoelectric conversion technology at this time (0.14 watt/lb, 0.22 watt/lb as compared to 0.6 to 0.7 watt/lb).

(2) Overall thermal-to-electrical conversion efficiencies are substantially less than that attainable with other generators of similar size and power range, based on data reported to Martin by Westinghouse (see Tables IV-1 and IV-2).

(3) In tests conducted by Westinghouse, the power flattening mechanism of the SNAP-IIIA generator failed to operate properly. (Data on the power flattening characteristics of SNAP-IIIA-2 are not available at this time.)

(4) Neither of the generators employ advanced thermoelectric materials capable of operating at hot junction temperatures in excess of 600° C, one of the design specifications.

---

* R. Harvey

TABLE IV-1

Westinghouse SNAP-IIIA-1 Performance Data

Item \ Run Number	1	2	3	4	5	6
Argon pressure (mm Hg)	760	760	760	7.5	0.5	0.07
Bell Jar pressure (mm Hg)	10	0.06	0.018	0.015	0.013	0.013
Heater temperature* (°C)	577	537	541	537	539	544
Cold junction temperature* (°C)	224	229	227	216	202	172
Heat dump temperature* (°C)	234	229	230	219	198	175
Internal resistance (mΩ)	482	468	467	434	400	385
Power input (w)	169	157	163	144	98	91.5
Power output (w)	1.78	1.45	1.41	1.13	0.795	0.83
Voltage, open circuit (v)	1.85	1.65	1.62	1.4	1.13	1.13
Voltage, load (v)	0.54	0.53	0.52	0.47	0.41	0.41
Efficiency (%)	1.05	0.925	0.865	0.785	0.81	0.908

Data taken on December 11, 1959

* Since there is only one thermocouple in the generator which is on the electrical heater, there is no way of knowing what the actual hot junction temperature is. Similarly with the cold junction, the temperatures recorded are those on the outside of the generator and not the actual cold junction temperature.

TABLE IV-2

Westinghouse SNAP-IIIA Performance Data

Item \ Run	Number						
	1	2	3	4	5	6	7
Argon pressure (mm Hg)	760	100	50	25	5	1	0.07
Bell jar pressure (mm Hg)	0.035	0.012	0.013	0.013	0.013	0.013	0.013
Heater temperature (°C)	537	542	539	537	533	536	547
Cold junction temperature (°C)	225	223	220	214	200	184	170
Heat dump temperature (°C)	226	226	222	219	204	186	176
Internal resistance (mΩ)	480	473	467	454	429	398	389
Power input (w)	151	149.5	144	139.5	120	106	95
Power output (w)	1.42	1.36	1.27	1.22	1.02	0.86	0.805
Voltage, open circuit (v)	1.65	1.60	1.54	1.49	1.32	1.17	1.16
Voltage, load (v)	0.52	0.51	0.50	0.49	0.45	0.42	0.42
Efficiency (%)	0.94	0.91	0.88	0.875	0.85	0.81	0.85

Data taken on December 14 and 15, 1959

2. SNAP-IIIA-1 Performance

The SNAP-IIIA-1 thermoelectric generator, which was described in the last quarterly progress report, was tested by the New Products Department of Westinghouse prior to delivery to Martin Nuclear. The results of these tests were made available to Martin when the generator was delivered and are the basis for the Tables IV-1 and IV-2. Martin Nuclear has not tested the generator.

Two sets of performance data are shown in Tables IV-1 and IV-2. A one-hour time interval was allowed between readings to ensure that a steady-state equilibrium condition existed.

These data are indicative of the performance of the generator. Because a complete set of operational data is not available, it is difficult to make many specific observations concerning the generator.

Notice that for every case reported, the temperature of the radiator of the heat dump mechanism is several degrees higher than the temperature of the radiator in the vicinity of the cold junction. This means that for all cases reported, whether they be for high argon pressures or low pressures, the heat flux through the heat dump mechanism is greater than that through the thermoelectric portion of the generator. Not only is this a high loss that reduces the efficiency of the generator, but it creates a secondary effect that raises the cold junction temperature because of the flow of heat from the heat dump areas to the cold junction area. This in turn reduces the ΔT of the thermoelectric elements and hence reduces the efficiency even more. This is a very serious design limitation and definitely should have been corrected in the early design stages. This is probably the most significant reason for the extremely low efficiency of the generator.

The purpose of the power flattening device is to maintain a relatively constant power output over the life of the generator. This means that when the internal gas pressure is one atmosphere (760 mm) the power input required to produce a given power output should be approximately twice that at an internal gas pressure of 0.07 mm. By referring to Tables IV-1 and IV-2, it is evident that the power flattening mechanism has not accomplished this. The power output does not remain constant over the pressure range of 760 to 0.07 mm but drops as much as 0.61 watt; the output voltage, instead of remaining constant over this pressure range, has decreased by 19.2 to 22.3%; the efficiency, which should increase by a factor of two over this pressure range, remains almost constant. In short, the power flattening device is not capable of accomplishing the purpose for which it was designed.

As was reported in the previous quarterly report, the weight of the generator, including the heater or heat source, is 10.18 pounds. The maximum power output, with the heater temperature in the vicinity of 540° C is 1.45 watts. This yields a specific power of 0.142 watt per pound.

3. Comparison with Other SNAP-III Generators

The preceding section described the performance of the Westinghouse SNAP-IIIA-1 generator. In this section, the performance of a typical Minnesota Mining and Manufacturing Company SNAP-III thermoelectric generator is presented as a basis of comparison. It should be remembered that the 3M generator does not include a power flattening mechanism as does the Westinghouse SNAP-IIIA.

TABLE IV-3*

Minnesota Mining and Manufacturing Company SNAP-III

Thermoelectric Generator Performance Data

Hot junction temperature	594° C (1100° F)
Cold junction temperature	110° C (230° F)
Power in	77.6 watts
Power out	4.6 watts
Voltage optimum load	4.0 volts (dc)
Efficiency	5.9%

* Data taken from TE Generator No. 3M1G10.

A comparison of the data in Table IV-3 with the data contained in Tables IV-1 and IV-2 immediately reveals the relative difference in performance. The SNAP-IIIA-1 was designed to use more advanced thermoelectric materials capable of higher hot junction temperature operation. The device, however, does not operate at as high a hot junction temperature as the 3M SNAP-III. The difference in performance characteristics is apparent. The approximate specific power of an isotopic-fueled SNAP-III generator is 0.67 watt per pound, whereas the specific power of the electrically heated SNAP-IIIA-1 generator is 0.142 watt per pound.

The most significant design feature of the SNAP IIIA-1 generator is the bonding of the thermoelectric elements to a plate at the hot junction, thereby reducing or eliminating the electrical contact resistance at the hot junction. This is the most serious drawback in other SNAP-III thermoelectric generators.

4. Description of the SNAP-IIIA-2 Generator

The SNAP-IIIA-2 generator is shown in Fig. IV-1. The configuration of this second generator is substantially different than the original SNAP-IIIA. The generator employs a disc-shaped heat source with 17 thermoelectric couples applied against one of the flat faces of the disc (see Fig. IV-2) and the heat dump mechanism operating from the other face. This thermal isolation of the heat dump from the thermoelectric converter eliminates the most serious disadvantage of SNAP-IIIA-1. The details of the heat dump mechanism and the thermoelectric elements themselves are similar to those used in the previous SNAP-IIIA generator, which is described in the last quarterly progress report. The arrangement of thermoelectric couples at the hot junction is shown in Fig. IV-3. The valve, which controls the gas pressure, and hence the quantity of heat being dumped, is mounted on the top of the generator. This arrangement facilitates adjustment and calibration of the valve--another definite improvement over the original SNAP-IIIA. Also located on top of the generator section are the power output terminals, the leads for internal instrumentation and the electrical heater, and a gas-charging valve for filling the thermoelectric section with a reducing atmosphere. There is a separate charging line for filling the heat dump with an inert gas.

This generator was not tested at The Martin Company. However, Westinghouse has reported that the generator produces 1.6 watts with an output voltage of 1.44 volts at the maximum power point. The hot junction temperature is 480° C and the cold junction temperature is 190° C. The efficiency at the start of life (one atmosphere of argon in heat dump) is 0.88% and the projected efficiency at the end of a half life is 1.20%.

In spite of the fact that this second generator has eliminated many of the objectionable features of the original generator, the performance is still far below the objective specificatons.

B. SUBTASK 5.2--BASIC THERMIONIC DEVELOPMENT

The objective of this Subtask is to advance the technology of thermionic converters; specifically, to increase the efficiency of thermionic generators by developing better emitter and collector materials and by reducing heat losses. This work is being performed by Thermo Electron Engineering Corporation.

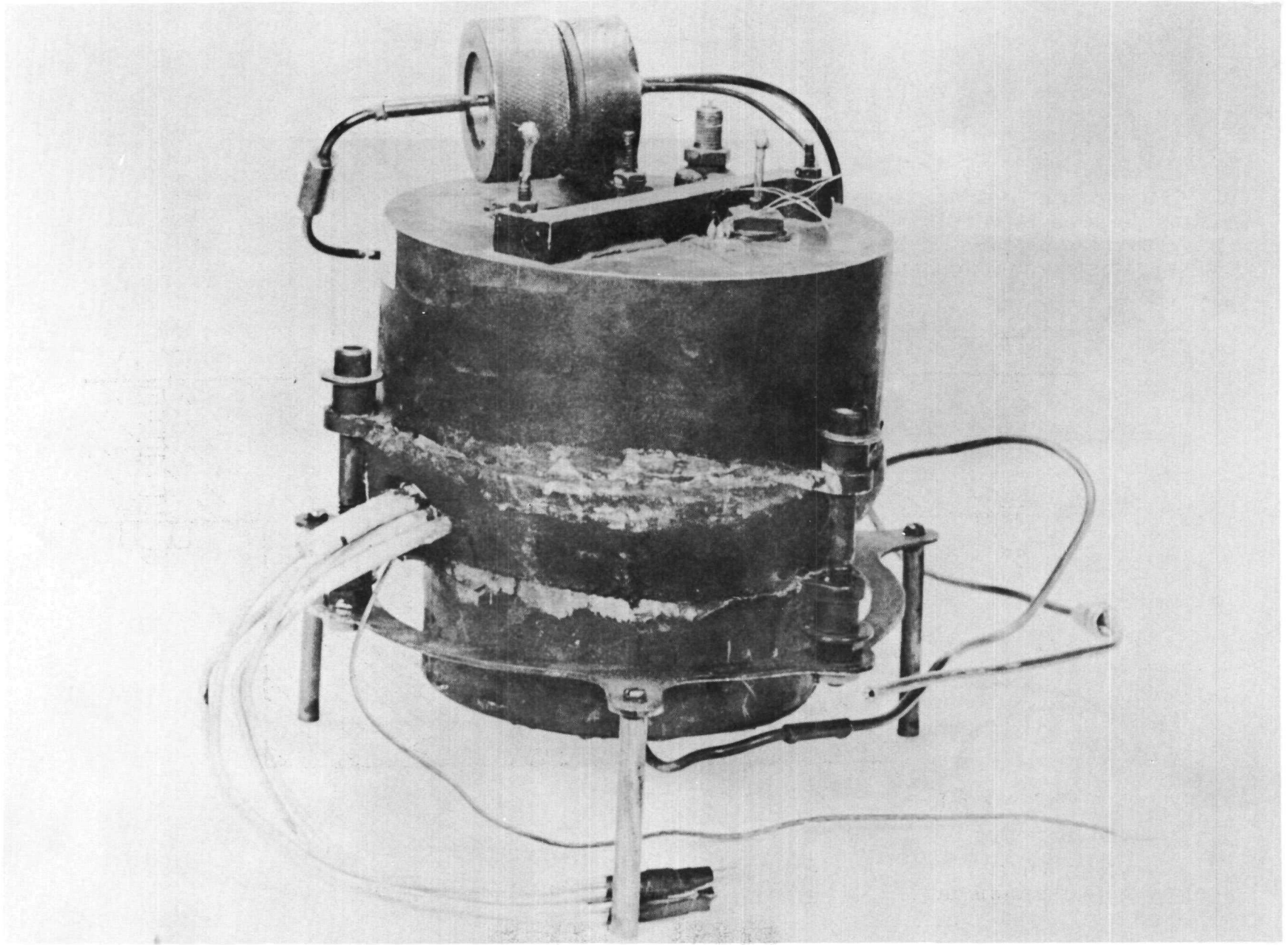

Fig. IV-1. SNAP-III A2 Thermoelectric Generator

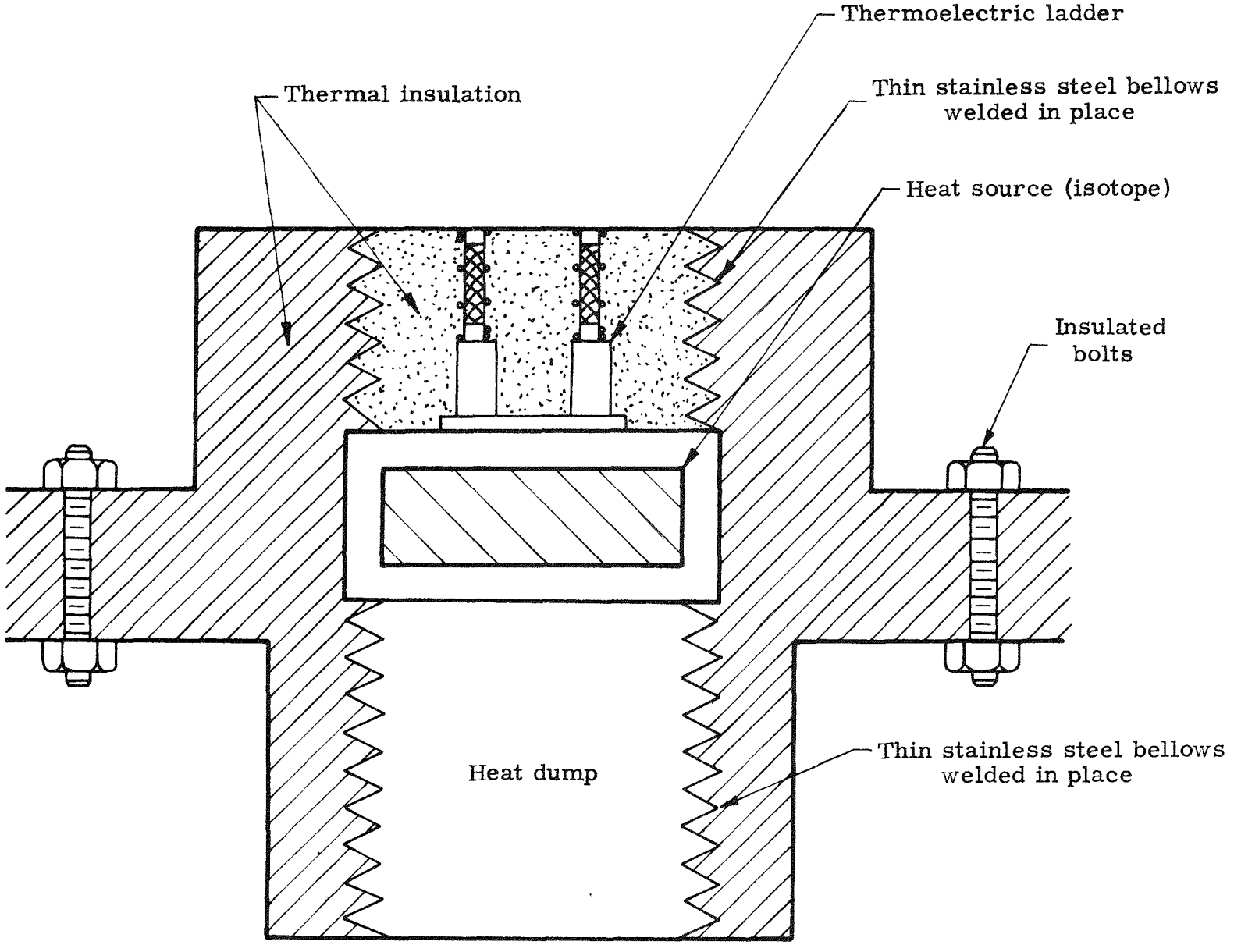

Fig. IV-2. Cross Section of SNAP-III-B

Fig. IV-3. Thermoelectric Ladder for SNAP-IIIB

The work under this Subtask consists of effort in three areas:

(1) Study and tests of cesium diodes.

(2) Related tests and research.

(3) Development of improved collectors in a vacuum diode environment.

1. Cesium Diodes

The purpose of the cesium diode tests is to provide experimental data to be used in conjunction with the analysis of the cesium phenomena to develop a thorough understanding of this type of thermionic device. The immediate objective of the work this quarter was to develop standard test articles in which reproducible data can be obtained and verified. The following types of tubes were tested:

(1) Metal encased.

(2) Ribbon emitter.

The metal-encased diode employs an electron bombardment heater and a metal envelope (Fig. IV-4). This tube can achieve higher cesium pressure than the glass envelope tubes. During this quarter, materials were selected for the major components of the diode. The principal components of the tube, such as the gasket seal test device shown in Fig. IV-5, were tested. The design of the circuit for the power supply and magnetic amplifier (Fig. IV-6) was completed and fabrication initiated.

The ribbon emitter tube fabricated during the last quarter was tested this period. Experimental results obtained with this tube checked within 10% of the theoretically determined performance. The ribbon emitter broke during testing. The tube design was revised and a second tube fabricated (Fig. IV-7). The test setup employed was such that the a-c component, as well as the average d-c component, of the output could be observed. The circuit diagram is shown in Fig. IV-8. Twelve complete current/voltage curves were taken at different emitter temperatures and different oil bath temperatures (varying cesium pressures). Nine of these are shown in Figs. IV-9 and IV-10. During a run, the glass press cracked at the point where it was joined to the envelope. The results obtained are a valuable aid in correlating experimental and theoretical results.

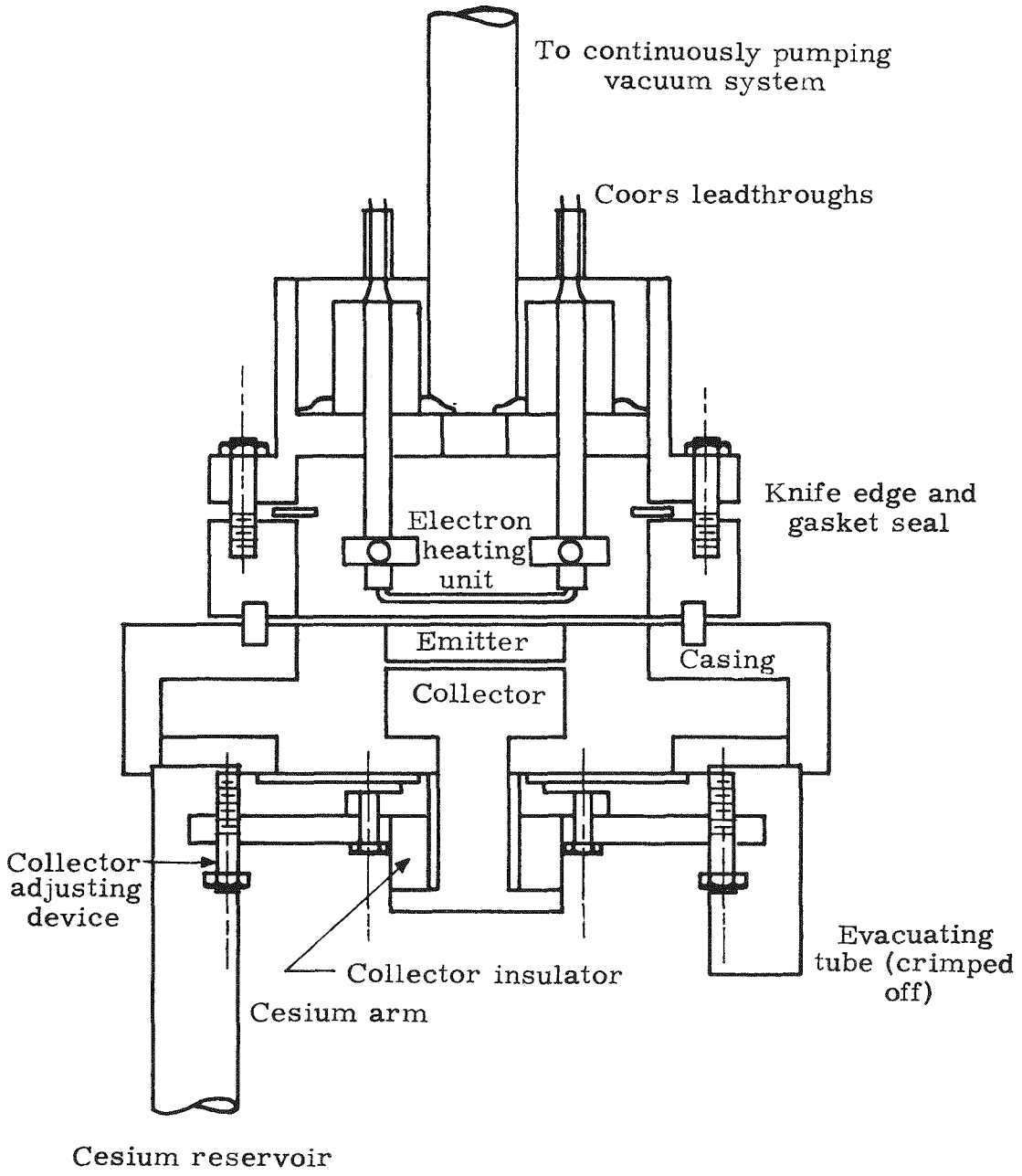

Fig. IV-4. Metal-Encased Electron-Heated Cesium Diode

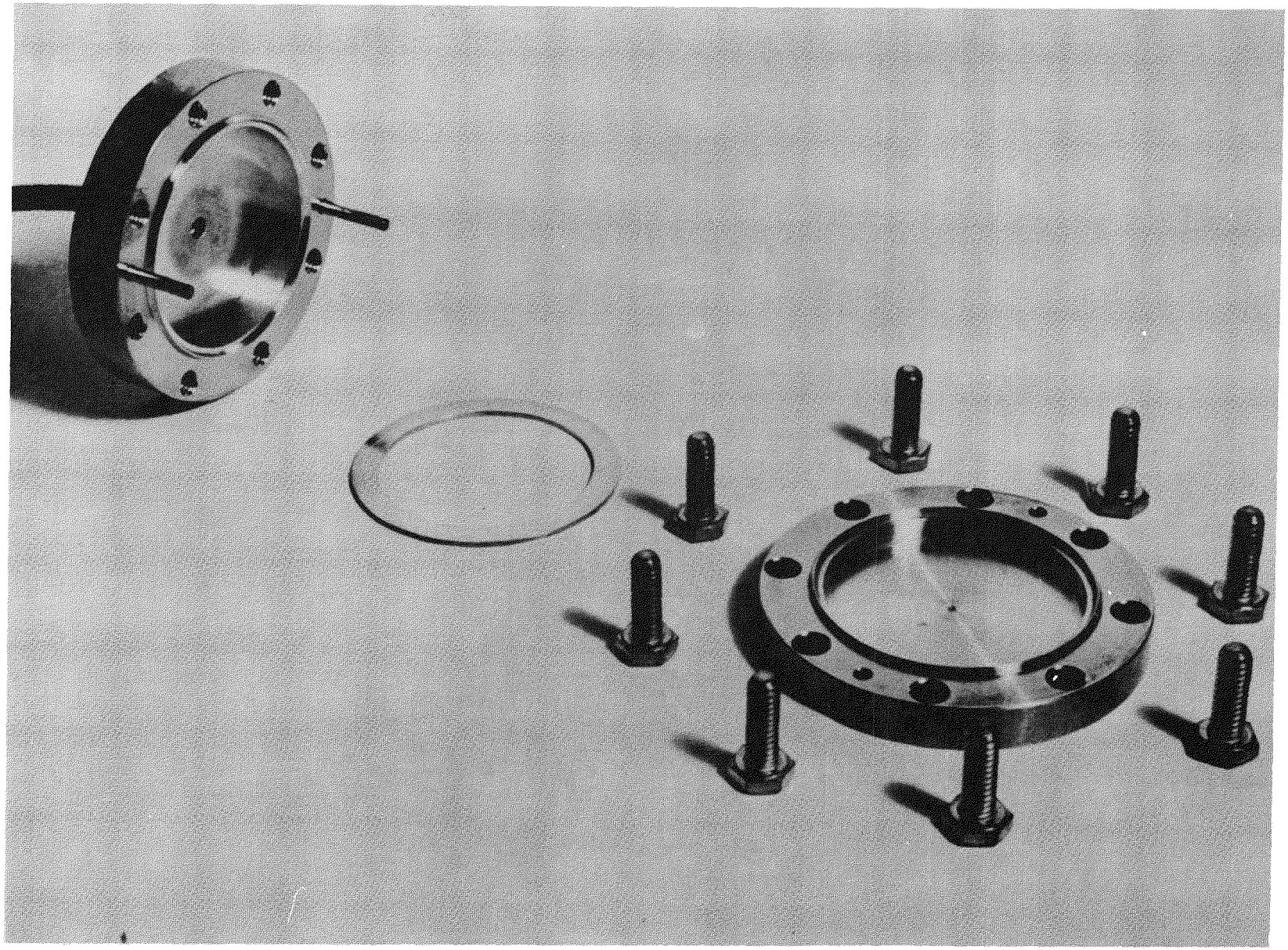

Fig. IV-5. Gasket Seal Test Device Showing Stainless Steel Knife Edge Flanges and Bolts and Nickel Gasket

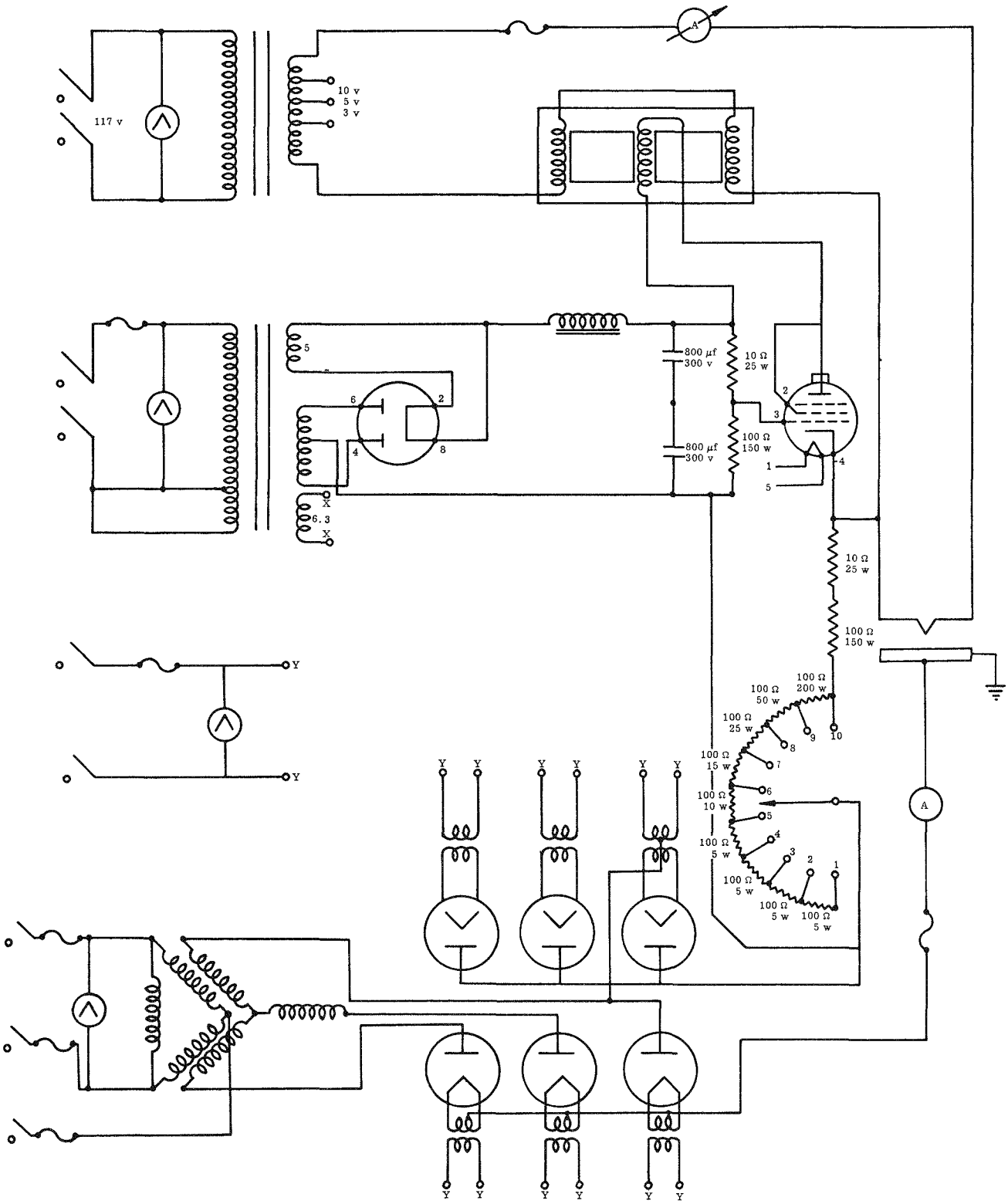

Fig. IV-6. Circuit Diagram for Electron Heating Magnetic Amplifier and Power Supply

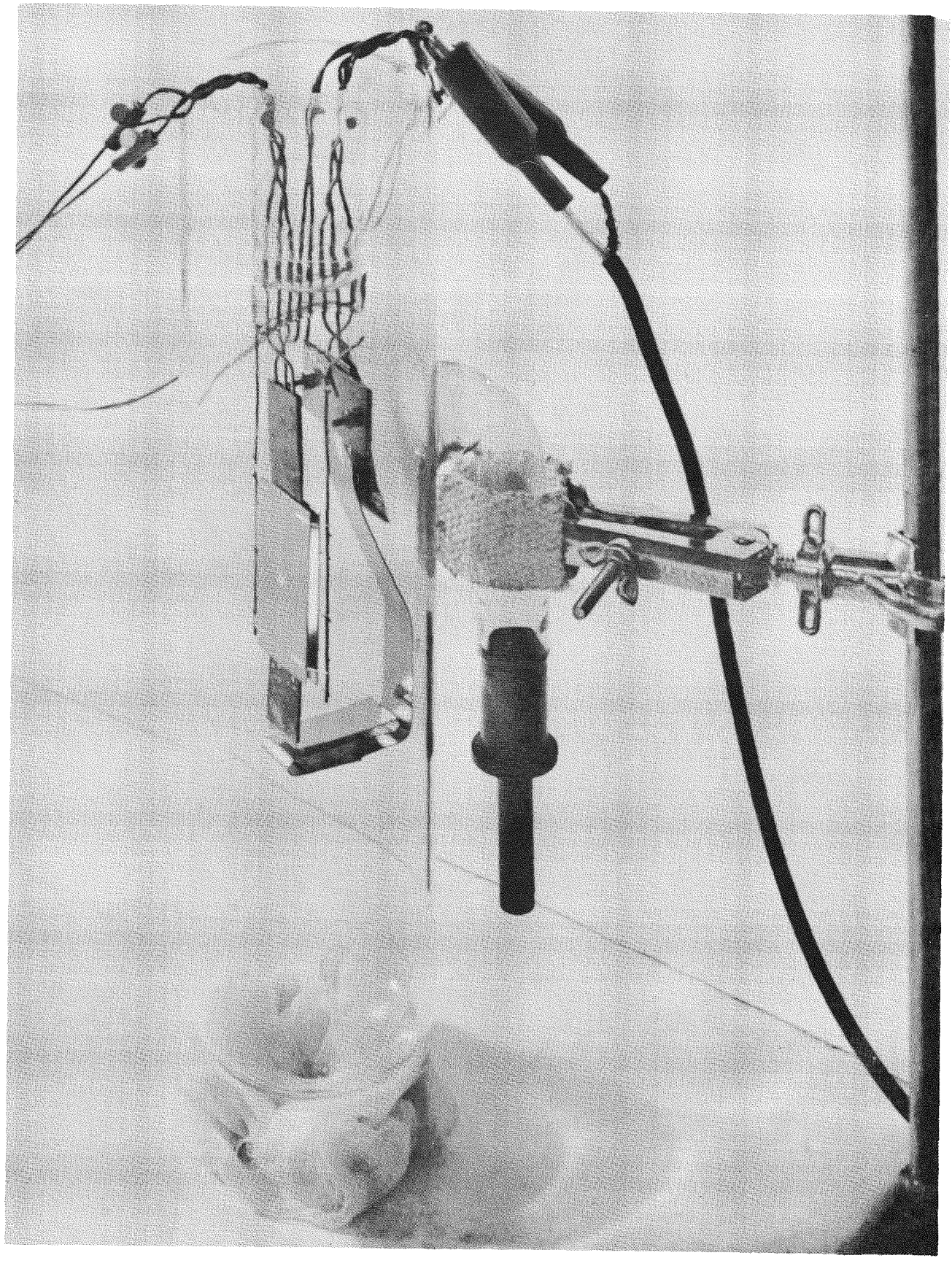

Fig. IV-7. I^2R-Heated Tungsten Ribbon Emitter Cesium Diode

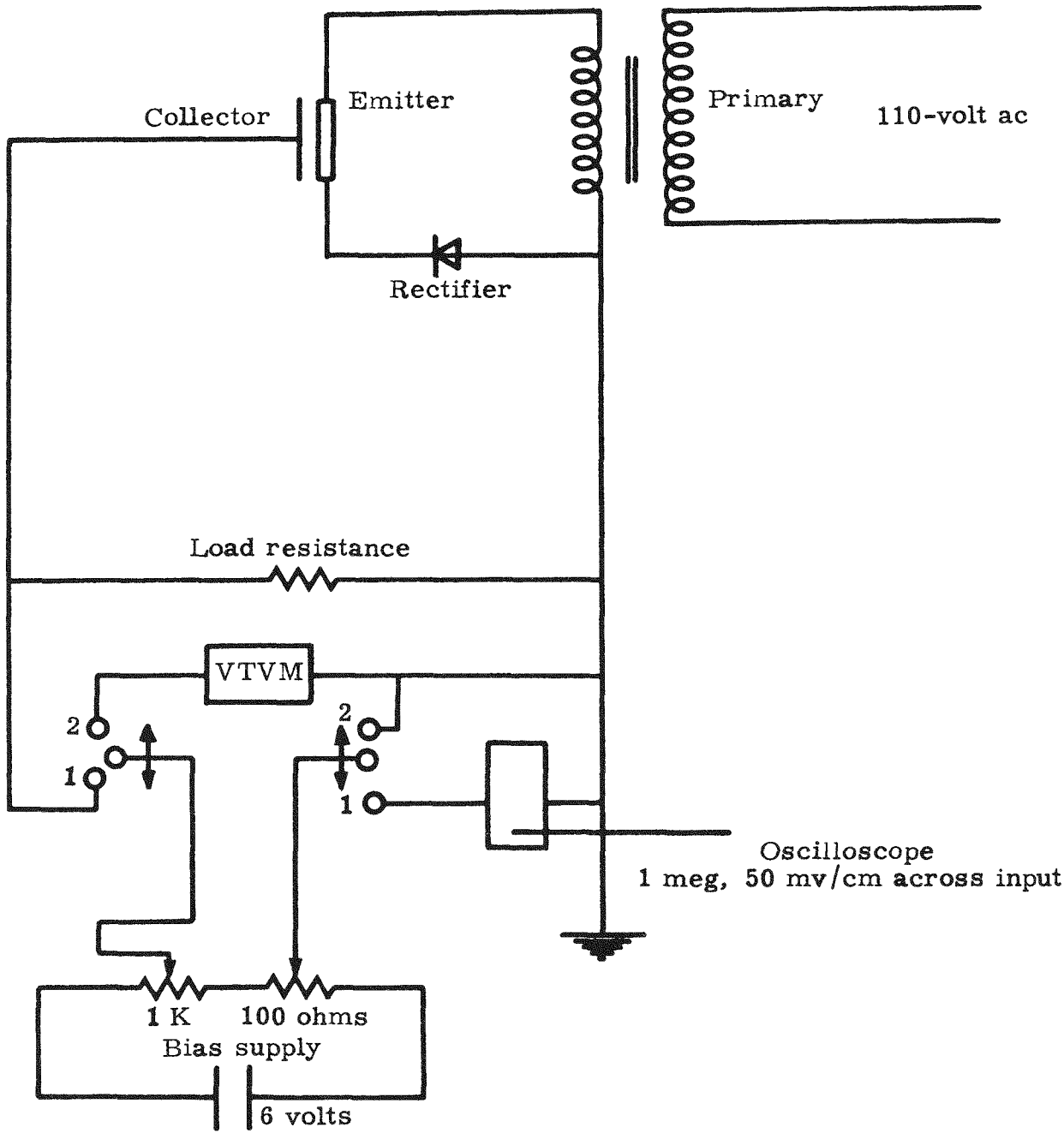

Fig. IV-8. Circuit Diagram Used for the Test of I^2R-Heated Ribbon Emitter Cesium Diode

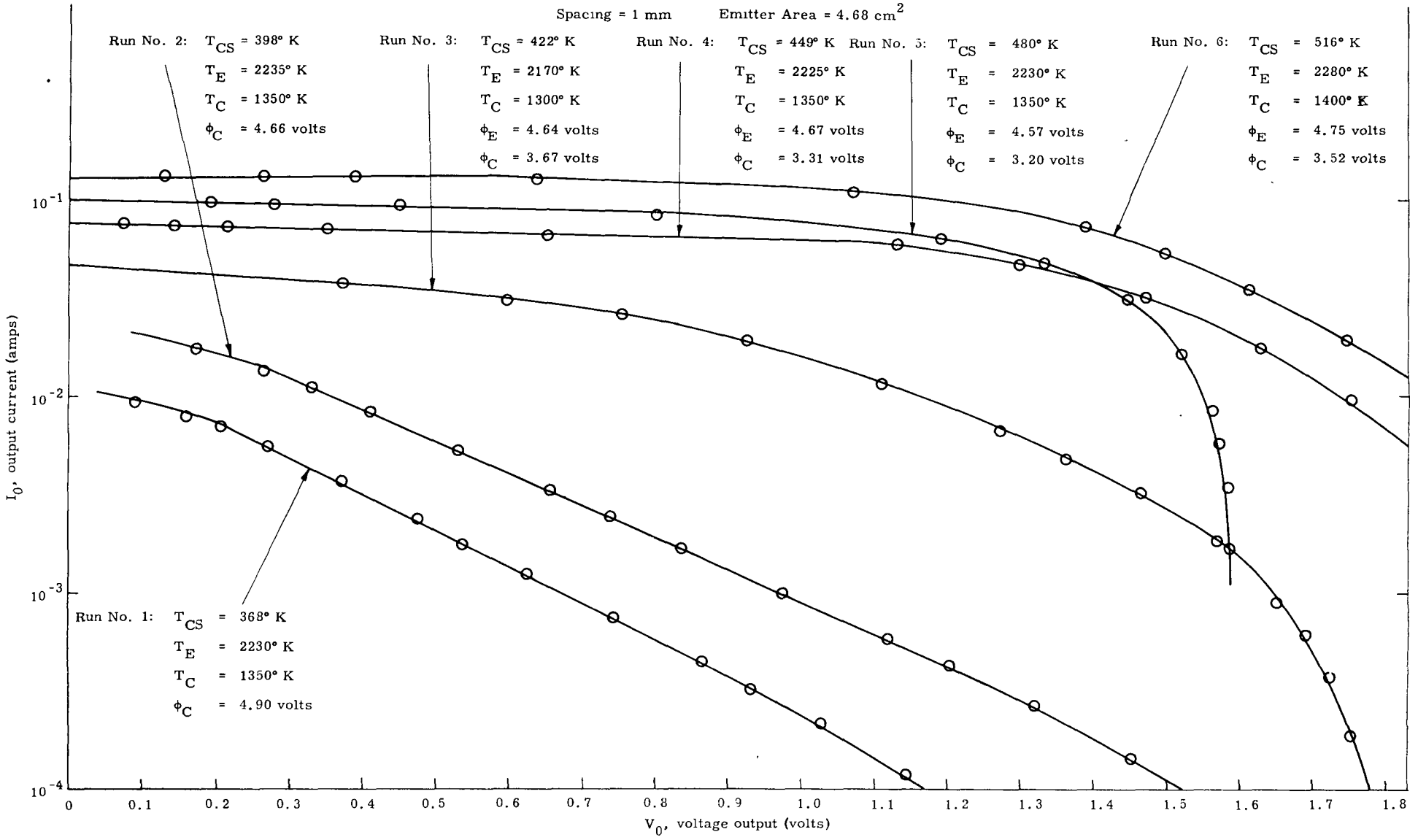

Fig. IV-9. I^2R-Heated Tungsten Ribbon Emitter Cesium Diode Test Results

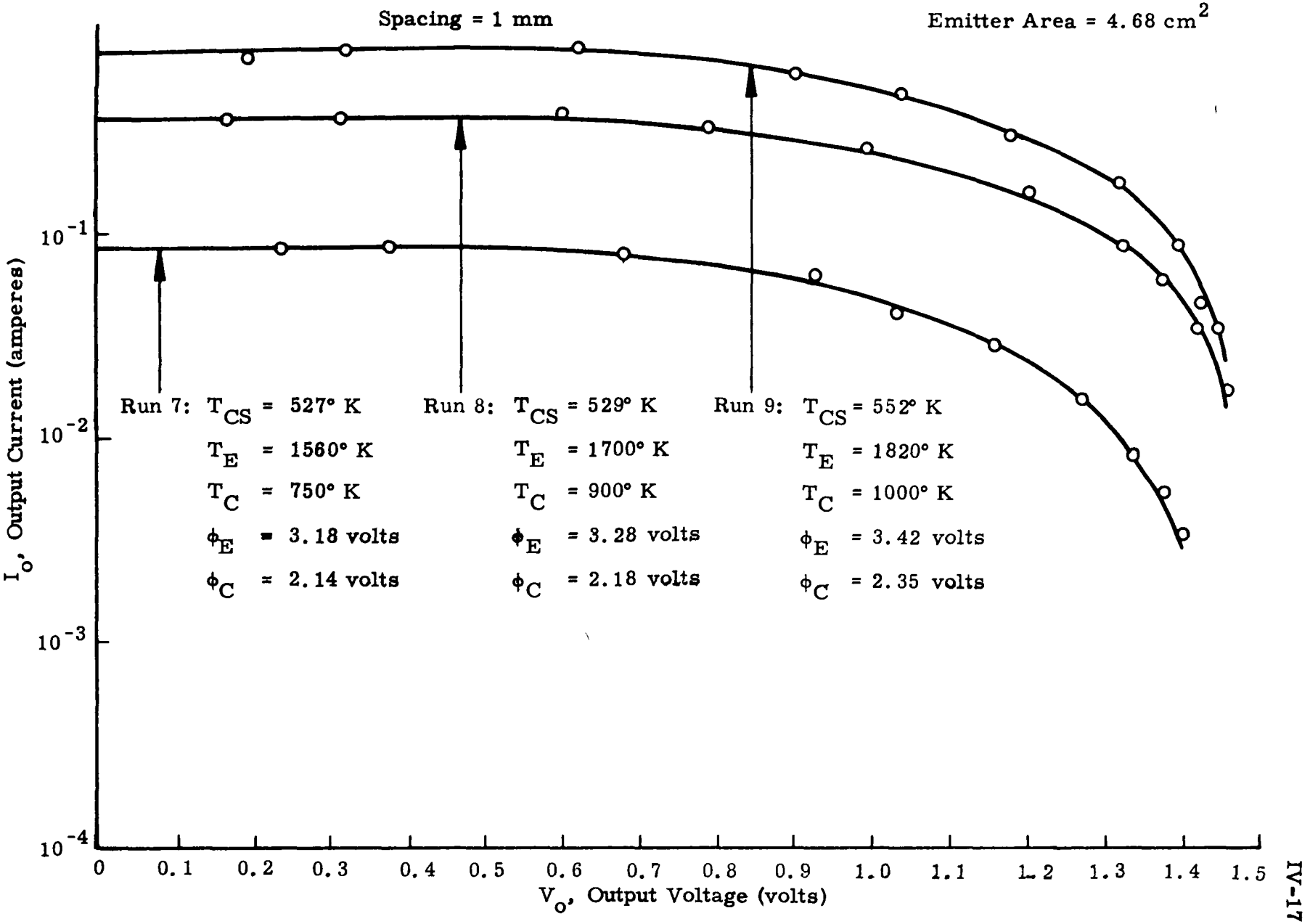

Fig. IV-10. I^2R-Heated Tungsten Ribbon Emitter Cesium Diode Test Results

2. Related Tests and Research

The efforts in this area were devoted to work on three different types of heaters and determining the effects of cesium and rubidium on metals. The three types of heaters are:

(1) Wire-wound ceramic.

(2) Tungsten wire radiation.

(3) Metallized ceramic.

The wire-wound ceramic heater, as shown in Fig. 12 of the last quarterly report, was fabricated and tested. The tests were successful; however, the heater is considered too fragile for use in a prototype. A tungsten wire radiation heater was also fabricated, and thoroughly tested. The heater consists of 0.002-inch tungsten wire, 6 inches long, coiled with a diameter of 3/4 inch. The heater in its test setup is as shown in Fig. IV-11. The test results were very encouraging and the heater appears to be very rugged. The next step is to incorporate it into a test device as a part of Subtask 5.3. A metalized ceramic heater, as shown on page 28 of the last quarterly report, was assembled and tested. However, hot spots developed on the metalized portion of the heater. As the voltage across the heater was increased further, the metalizing burned out at the hot spots. The metalizing temperature was at 1500° K when it burned out.

The metalized ceramic heater promises to be the most rugged type of heater when it is perfected. Therefore, effort will continue on the metalized ceramic heater. It is hoped that the hot spots can be eliminated by machining the metalizing so that the helix is wider, enabling higher temperatures to be achieved.

The cesium experiments completed this period consisted of sample materials in glass envelopes to determine the corrosive effects of the cesium. During the experiments it was established that there is a severe reaction of cesium with glass, and therefore, future tubes are to have metallic envelopes. A sample capsule of cesium was analyzed to determine the impurities present in the cesium and the quantity of each.

A cesium corrosion test device was designed and fabricated. Four sample materials were placed in the test device, and exposed to a cesium atmosphere (400° C) for almost 100 hours. These four materials were:

(1) Nickel.

(2) Driver-Harris alloy.

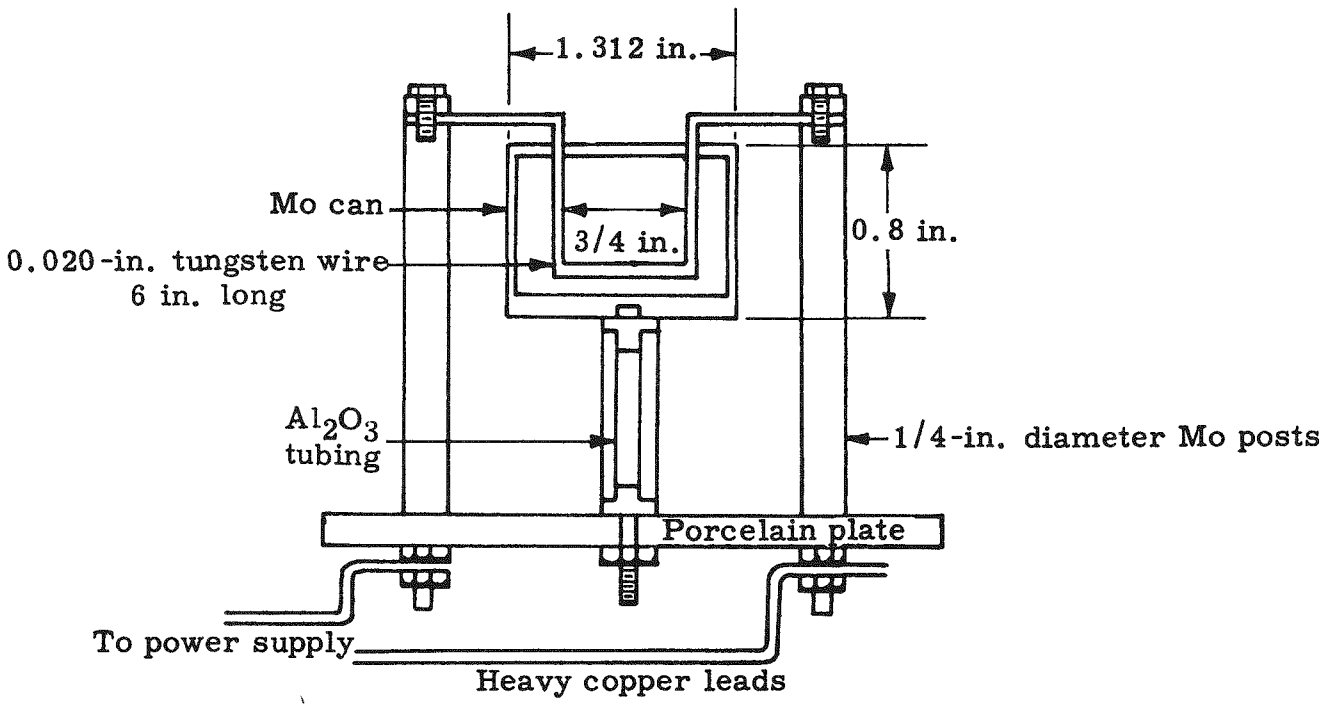

Fig. IV-11. Tungsten Wire Radiation Heater Test Setup

(3) Type 304 stainless steel.

(4) Molybdenum.

Cesium had no apparent effect on the nickel sample. The Driver-Harris (iron-nickel) alloy was slightly darkened, but there was no apparent corrosion. The stainless steel and molybdenum were darkened and the surfaces were slightly corroded. Past experience with molybdenum in the presence of high temperature cesium indicated good cesium corrosion properties. Therefore, additional molybdenum testing will be required. The amount of corrosion on any of these samples was not sufficient to preclude its use in a cesium device.

The effects of cesium on brazed assemblies were also investigated. Two specimens were tested by brazing a titanium cylinder to a foil. The one used a platinum foil with an Incusil braze and the second used a tantalum foil and a gold-nickel braze. After the 100-hour exposure, the first specimen showed no ill effects. The tantalum foil and the titanium cylinder were unaffected by the cesium. However, the gold-nickel braze flaked off the titanium cylinder.

These cesium corrosion tests indicate that tantalum, molybdenum, copper, nickel, titanium, platinum, Driver-Harris alloy and Type 304 stainless steel can be used as the structural metals in a cesium device, and that copper, copper-silver, nickel and Incusil are suitable braze materials in devices containing cesium at high temperatures.

3. Development of Improved Collectors

The work this quarter was concentrated on the molybdenum collector used in conjunction with a Type B impregnated tungsten emitter because of the success with this diode last quarter.

The first step was to reproduce the results obtained with the first tube, and verify the activation prcedure required to achieve the low collector work function. The secondary aim was to achieve these same results only at a much higher power density.

The design of this second tube was identical to that of the first tube except for a much smaller spacing between electrodes (0.0003 inch as compared to 0.0006 inch at room temperature). The tube was fabricated and tested. The current/voltage curve (Fig. IV-12) indicates an emitter temperature of 1510°K, collector work function of 1.91 volts, interelectrode spacing at operating temperature of 0.0006 inch with a power density of 0.254 watt/cm^2. Figure IV-13 shows the correlation of the experimental data with the universal curve. The collector work function re-

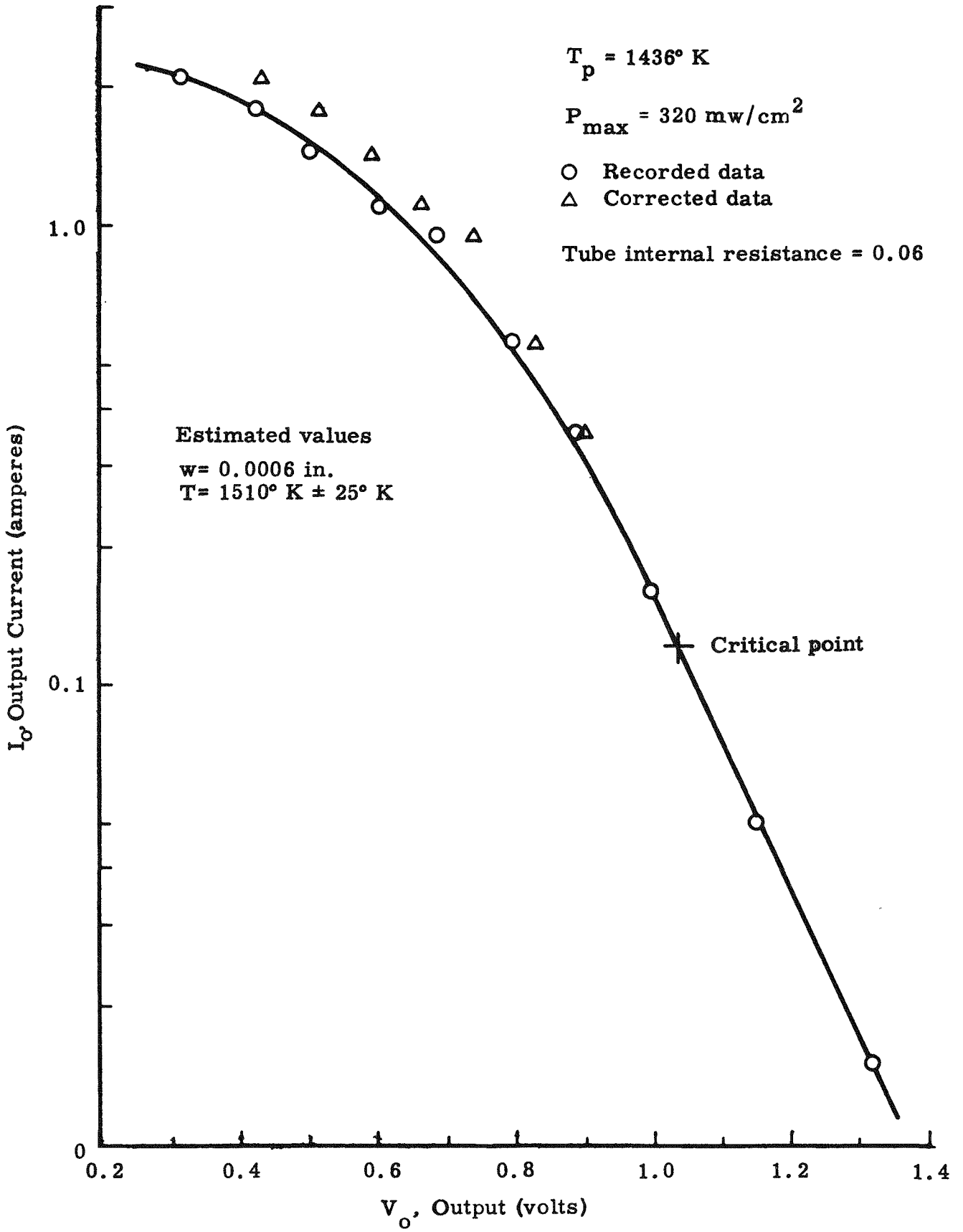

Fig. IV-12. Output Current Versus Output Voltage

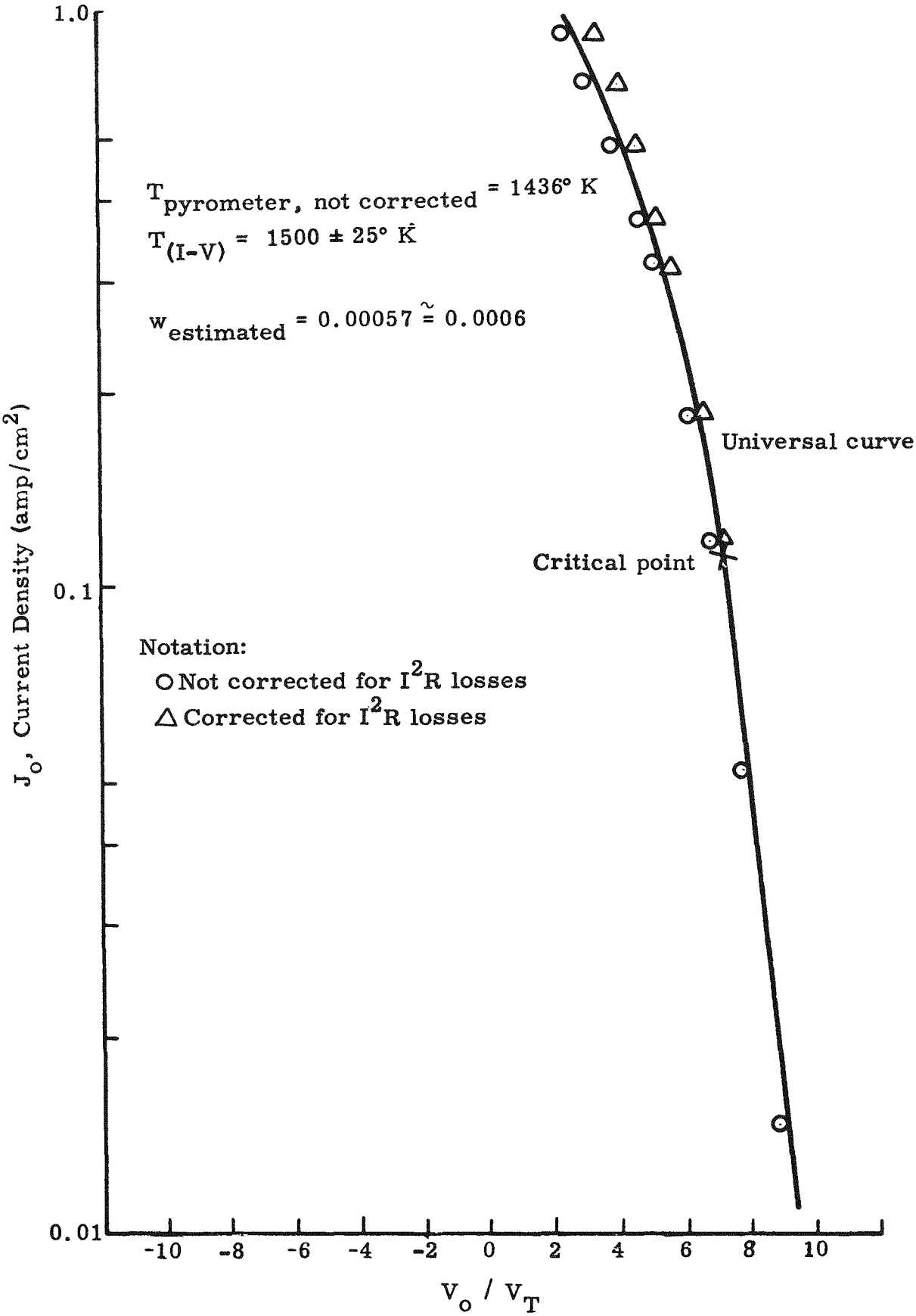

Fig. IV-13. Data Plotted with Universal Curve for Comparison

mained constant for more than 32 hours, indicating that the activation procedure could be reproduced. It also indicated that the same procedure is applicable even for this higher power density.

During the testing of this second tube, an occasional intermittent short developed which made further testing very difficult. Therefore, a third tube was fabricated. The purpose of this third tube was to determine if certain modifications to the activation procedure would result in even a lower collector work function than with the first two tubes. In addition, the secondary objective was to determine whether or not the activated pair of electrodes could be exposed to the atmosphere while at room temperature and still retain their surface properties when subsequently sealed off and brought up to operating temperatures. The design of the tube was essentially the same as the two previous tubes.

The revised activation procedure resulted in a collector work function of 1.67 volts at an emitter temperature of 1503° K. After 10 hours of operation, the heat input was shut off and the tube cooled to room temperature. Air was then allowed to enter the tube, and allowed to remain in the tube for 2-1/2 hours. The tube was then pumped down and baked out at 650 to 700° F for seven hours. When the emitter was brought up to temperature (see Fig. IV-14), the collector work function was exactly as before being exposed to air. This means that once the electrodes of a diode are properly activated, their physical characteristics are fairly insensitive to change. This is a very essential characteristic for multi-diode generators for practical applications. It also will facilitate mass production techniques.

As shown in Fig. IV-14, the tube was again exposed to air for 104 hours. After a three-hour recovery period, the collector work function again returned to its original value of 1.67 volts. A third exposure to air for 1-1/2 hours in the presence of a titanium shield produced no change in collector work function. The titanium shield was used to see if it would absorb the oxygen and therefore prevent the formation of barium oxide on the collector surface. No such effect took place in the tube.

Three more tubes were fabricated to investigate the effect of collector firing temperature during activation on the collector work function. In the first tube, three different firing temperatures were employed and each resulted in a significantly different work function, indicating the importance of this parameter. Quantitative data concerning the correct firing temperature were also obtained. The second tube was used to compare the effect of material initially discharged from the emitter during activation on the collector work function with the effect of discharging during normal operation. This comparison was made by using two different molybdenum collectors in the same tube. The experiment indicated that the collector firing temperature is the factor of prime im-

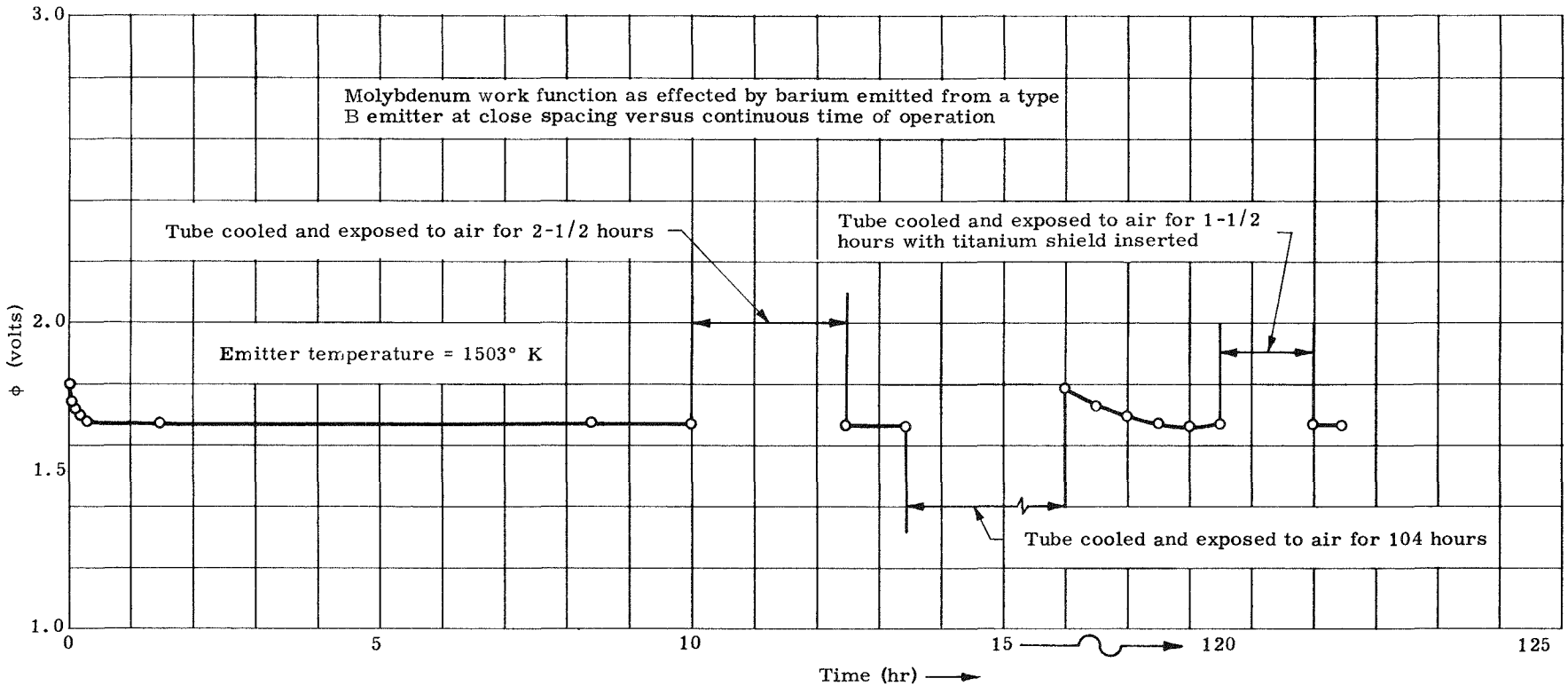

Fig. IV-14. Interpretation of Experimental Results of Collector Work Function

portance in determining the value of the collector work function, and that the prefiring of the emitter prior to assembly of the diode will only affect the collector work function at collector temperatures below 900° C. The third tube was designed and constructed to study the effect on the collector work function when the molybdenum radiation shield was replaced with a titanium shield. The change had no appreciable effect on the collector work function.

Work was also initiated on a diode with a nickel collector and a barium-impregnated emitter. Some difficulty was encountered in firing the collector at a high temperature because of the vapor pressure of nickel at these temperatures. Therefore, the design was revised so as to be capable of withstanding a higher firing temperature.

An apparatus was designed and partially constructed to determine the relationship between collector temperature and collector work function in a continuously pumping vacuum system. The device is designed so that various emitter and collector materials can be tested. The first tests will study the work function of a molybdenum collector when operating in conjunction with a barium-impregnated tungsten emitter.

C. SUBTASK 5.3--DEVELOPMENT OF LOW POWER THERMIONIC GENERATOR

The objective of this subtask is to develop, design, fabricate and test an operational power system coupling a thermionic conversion device to a radioisotope heat source. The thermionic development is being performed by Thermo Electron Engineering Corporation of Cambridge, Massachusetts, as a subcontractor to The Martin Company. The work on the isotopic heat source, environmental testing and all other related work is being done by the Martin Nuclear Division.

1. Thermo Electron Engineering Corporation (TEE CO) Efforts

The work performed by TEE CO can be conveniently broken down for reporting purposes as follows:

(1) Generator development.

(2) Heat transfer study and tests.

(3) Vacuum tests in prototype shells.

(4) Cathode and sapphire support creep tests.

(5) Parametric study.

Generator development. Work in this quarter was devoted to Generators 1A and 1B. Generator 1A is the first generator to include all of the features being developed as separate items of work. This includes the vacuum shell, the methods of improved heat transfer, interelectrode spacing, leadthroughs, crimp-off techniques, collector work function and all of the other related work that is being carried on simultaneously. This single-stage unit was to be the test bed to determine the feasibility and compatibility of these various design features.

Generator 1B was to use the same design features as Unit 1A, except it was to be a two-stage generator. Each of the individual stages would be similar to 1A. The purpose of this generator was to serve as an environmental test unit to determine the ability of the generator design features to withstand dynamic loads of vibration, shock and acceleration. Units 1A and 1B were not designed to be high performance generators, but were to supply information concerning the relative merits of the various design features in a reliable fashion.

The results obtained in the design, fabrication and testing of these two generators are to be incorporated into the design of Unit 2A, which is to be a high performance generator. The generator to be fueled will be a direct descendant of this generator.

Several design modifications were made on the design of Unit 1A. The modifications, in general, were concerned with minor changes in such things as the leadthroughs, evacuation pipe, cap braze, etc. These design modifications were made to simplify the assembly procedures. Essentially, the design does not differ from that presented in Fig. 24 of MND-P-3009-I. During the assembly of one of the units, the various design revisions were checked out. When the unit was completed and operating, however, the emission current was very low because of the dragged out assembly time. Finally the unit developed an intermittent short. Another generator was fabricated. This generator is shown in Fig. IV-15. The generator was tested and the experimental data checked precisely with the analytically determined performance. Figure IV-16 shows the experimental data plotted against the universal master curve, and as can be seen, the agreement is excellent. A summary of the performance data is given in Table IV-4, along with the performance if the spacing had been 10μ instead of 32μ and the collector work function 1.85 volts instead of 2.2 volts.

Upon completion of Unit 1A, Unit 1B was designed and fabricated using the information and experience acquired on Unit 1A. The design of this generator is shown in Fig. IV-17. The generator was fabricated and assembled with relative ease. Again the experimental data were in excellent agreement with the analytically determined performance. A summary of the test results is shown in Table IV-5.

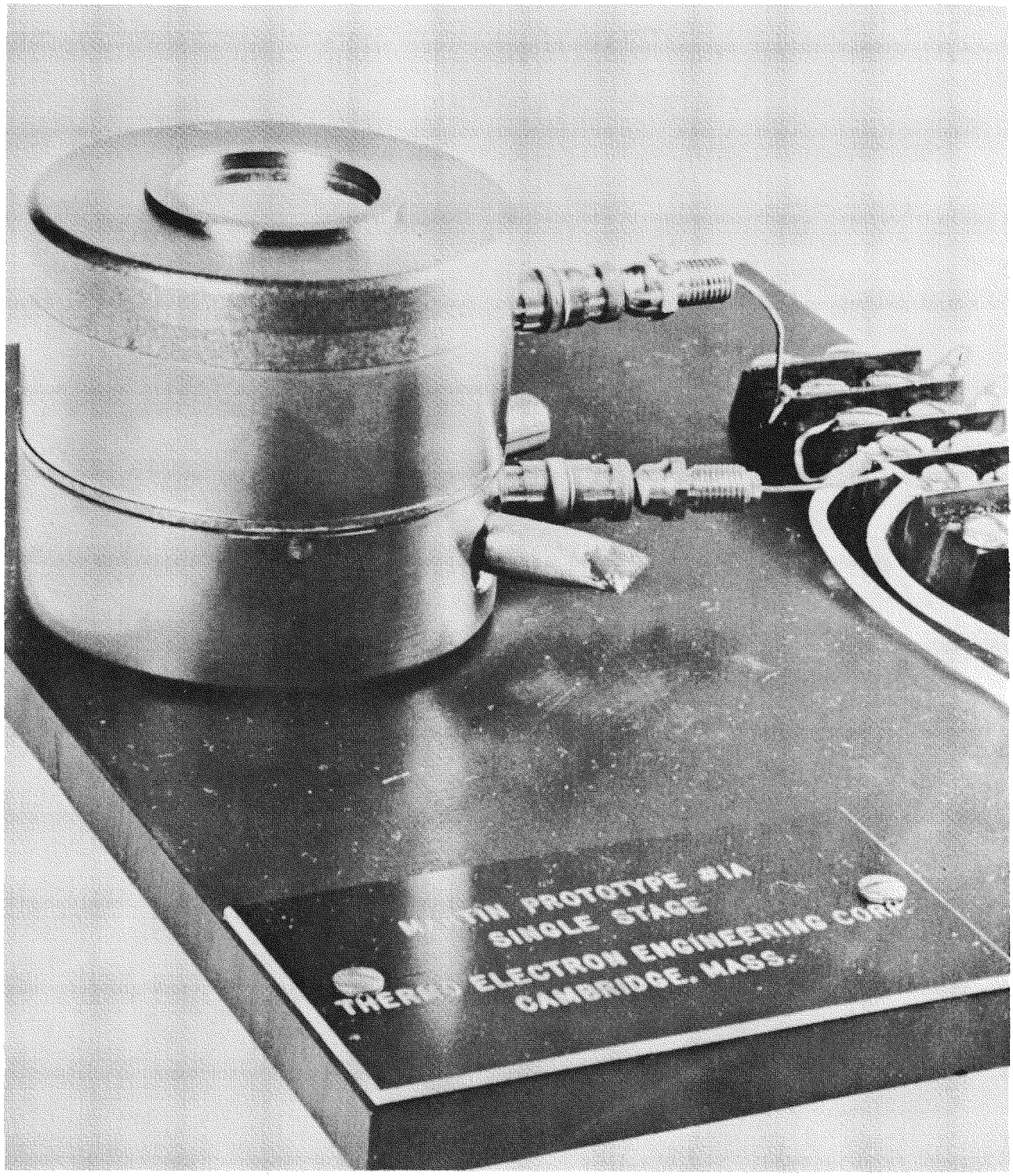

Fig. IV-15. Generator 1A

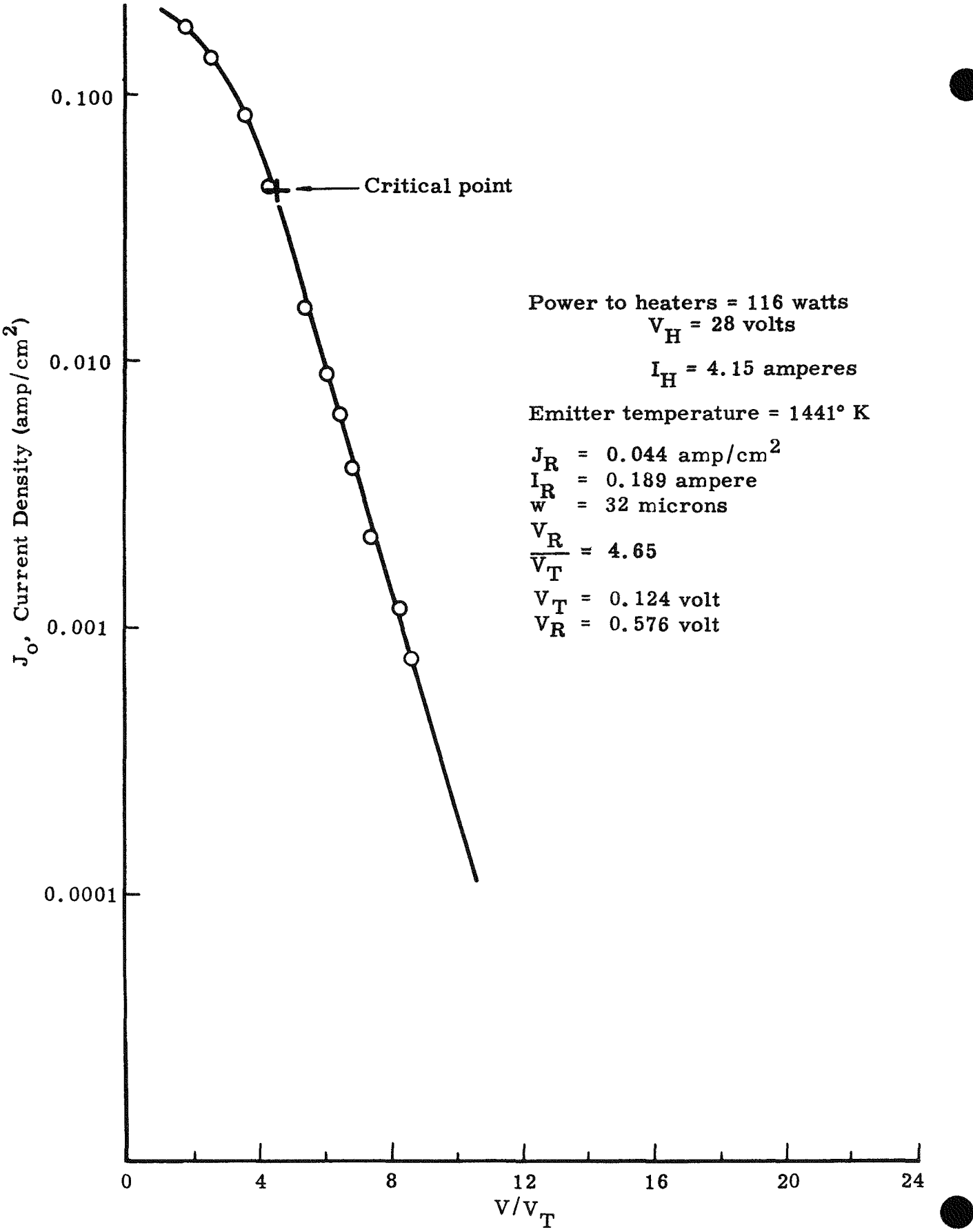

Fig. IV-16. Current Density Versus V/V_T Plotted Against Master Curve

TABLE IV-4

Summary of Test Data on Unit 1A

Description	Test Number	
	1	2
Total Heat Input--watts	116	104
Emitter Temperature--°K	1441	1411
Maximum Power Output--watts	0.199	0.148
Thermal Efficiency at Maximum Power--%	0.17	0.14
Collector Work Function, ϕ_2--volts	2.21	2.22
Spacing--microns	32	32
Calculated Maximum Power--watts	0.147	0.130
Adjusted Maximum Power for $w = 10\mu$--watts	1.46	1.33
Adjusted Thermal Efficiency for $w = 10\mu$--%	1.26	1.28
Adjusted Thermal Efficiency for Observed Power Output--%	1.67	1.39
Adjusted Maximum Power for $w = 10\mu$ and $\phi_2 = 1.85$ volts--watts	3.74	4.14
Adjusted Thermal Efficiency for $w = 10\mu$ and $\phi_2 = 1.85$ volts--%	3.22	3.97

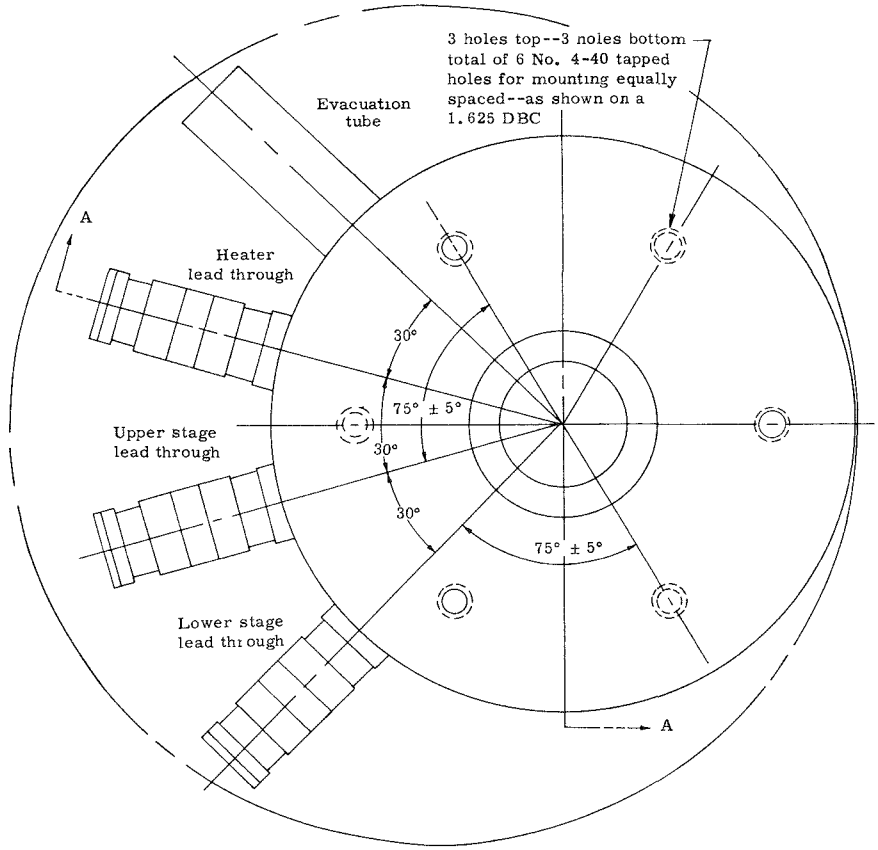

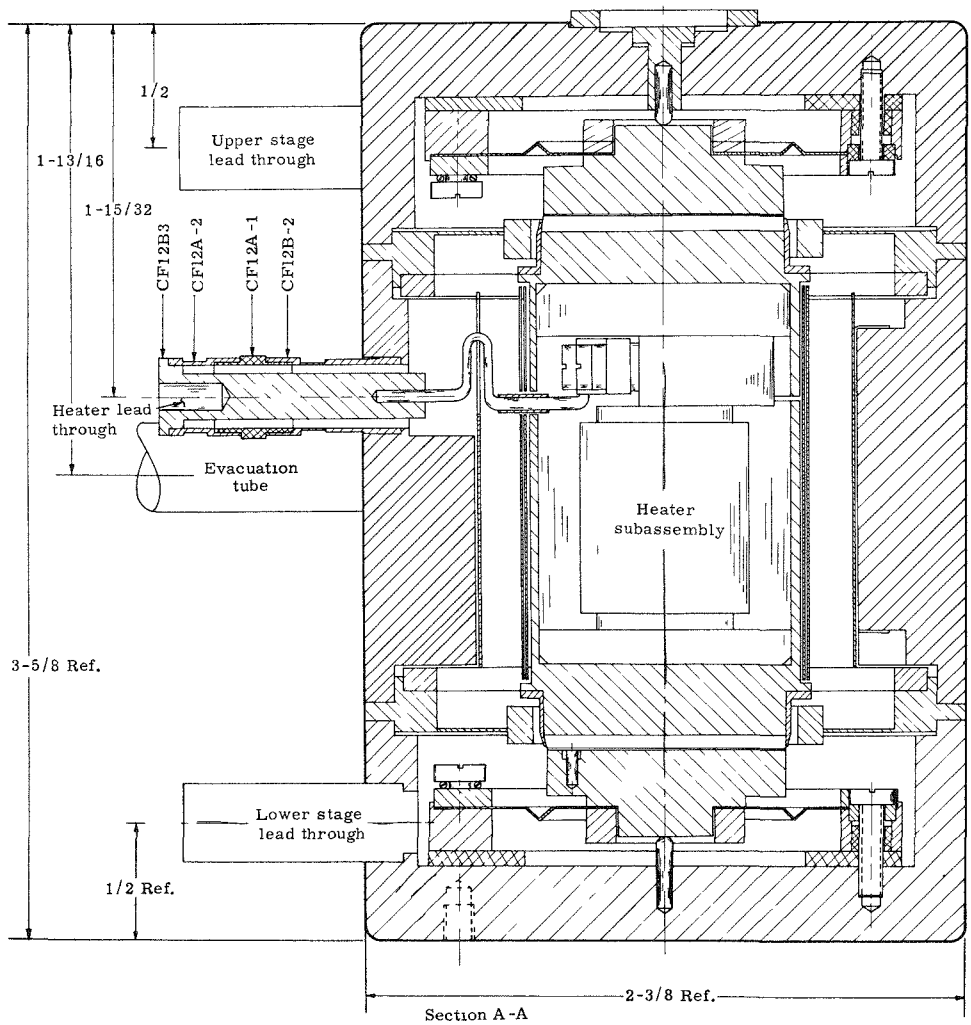

Fig. IV-17. Two-Stage Prototype 1B-1

TABLE IV-5

Summary of the Test Results of Generator 1B-1

Quantity	Test Number							
	1 Top	1 Bottom	2 Top	2 Bottom	3 Top	3 Bottom	4 Top	4 Bottom
Heater Volts, V_H--volts	35.2	---	34.5	---	33.0	---	30.0	---
Heater Current--amperes	4.70	---	4.60	---	4.58	---	4.30	---
Heat Input--watts	165	---	158	---	151	---	129	---
Emitter Temperature--°K	1525	1474	1500	1450	1472	1447	1442	1391
V_T--volts	0.1206	0.1269	0.1292	0.1249	0.1269	0.1247	0.1243	0.1199
V_R/V_T	2.6	4.3	2.6	4.2	2.4	4.0	2.25	4.0
Critical Volts--volts	0.314	0.546	0.337	0.525	0.305	0.499	0.280	0.480
Critical Amperes, J_R--amp/cm^2	0.050	0.070	0.045	0.055	0.042	0.070	0.028	0.070
Collector Work Function--volts	2.50	2.14	2.55	2.20	2.53	2.20	2.56	2.14
Spacing--microns	31	25	32	30	32	25	40	24
Calculated Maximum Power Output--watts	0.0568	0.270	0.0632	0.257	0.0525	0.224	0.0212	0.221
Observed Maximum Power Output--watts	0.0860	0.293	0.0731	0.256	0.0648	0.263	0.00933	0.240
Calculated Maximum Power Total--watts	0.327		0.319		0.276		0.241	
Observed Maximum Power Total--watts	0.379		0.329		0.328		0.249	
Observed Thermal Efficiency at Maximum Power--%	0.230		0.208		0.217		0.193	
Adjusted Maximum Power, w = 10, ϕ_2 = 1.85--watts	6.32	3.96	6.10	4.25	5.50	4.05	5.50	3.26
Total Adjusted Maximum Power, w = 10, ϕ_2 = 1.85--watts	9.86		10.35		9.56		9.29	
Adjusted Thermal Efficiency--%	5.98		6.55		6.33		7.12	

The completed generator was delivered to The Martin Company in the early part of March for dynamic environmental testing. The results of this testing are described under the Martin effort of this subtask. TEE CO provided the results of the electrical tests to Martin personnel and maintained liaison during the preparation for dynamic testing.

At the close of the quarter, work had been initiated on the design of Unit 2A. The fabrication of a test bed to check out several of the more recently developed techniques, such as new brazing techniques, higher outgassing temperatures, new type leadthroughs, and the features necessary to obtain a lower collector work function, was the first step. The design of the test bed was completed, and fabrication started during this quarter. The development of an electrical heater capable of simulating the power densities of the Curium-242 heat source (approximately 50 watts/cm^3) was also designed, and fabrication initiated. This was the status of the generator development at the close of the quarter--March 31, 1960.

Heat transfer study and tests. Unit 1A-1 was disassembled and examined after the unit failed in test. Examination of the thermal contact area between the emitter holder and heat source revealed that uniform contact had not been made. Figure IV-18 shows the distribution of molybdenum powder over the surface of the emitter holder. Further work on improving the heat transfer between the two surfaces is necessary and has been continued.

Two methods studied in part previously were:

(1) Grinding and lapping the surfaces in contact and measuring the temperature drop under different contact pressures at different temperature levels.

(2) Placing a layer of molybdenum powder between the two surfaces and again measuring the temperature drop under different contact pressures and at different temperature levels.

The test setup for conducting these tests is shown in Fig. IV-19. The purpose of the counterweight is to offset the force of atmospheric pressure on the bellows. Nine runs were made with emitter temperatures from 600° to 1100° C (heater voltages from 20 to 50 volts, respectively) and pressures from 0.35 to 10 lb/$in.^2$. These results are shown in Fig. IV-20. From this figure, it is apparent that all runs follow the same trend--the temperature drop across the film decreases with pressure in a more or less exponential manner. High temperature levels, therefore higher heat flux, result in high film drops; the film drop is

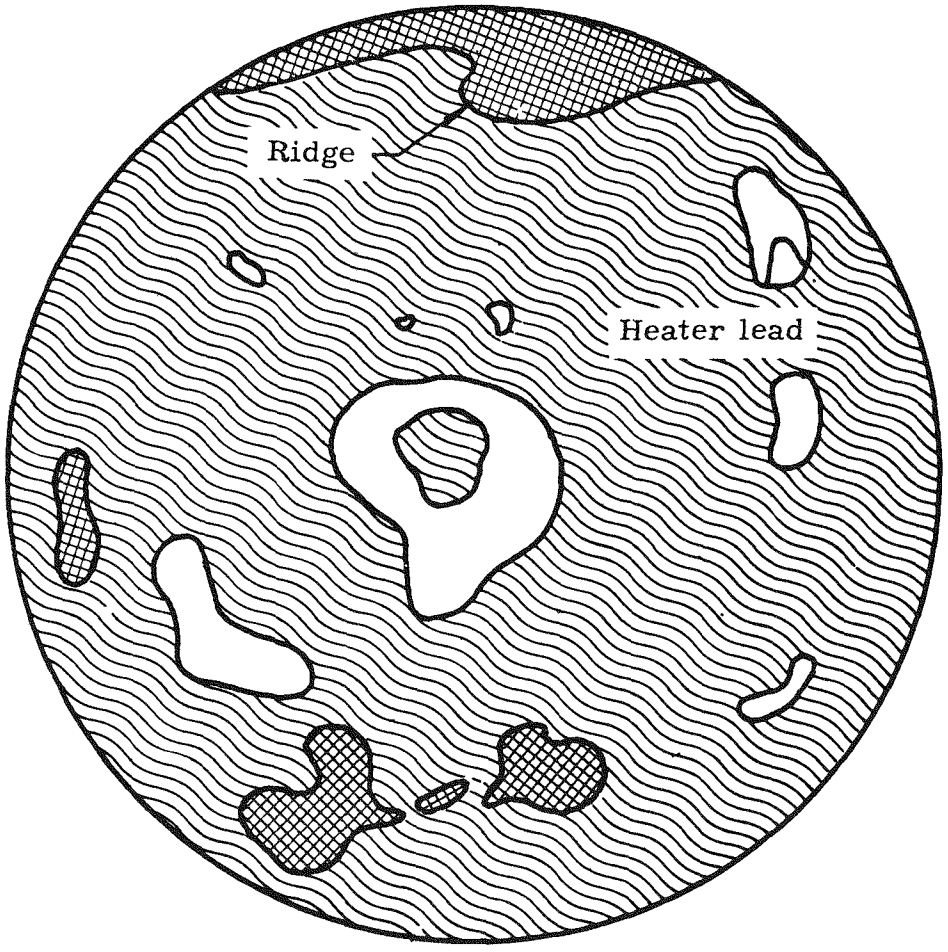

Average amount of molybdenum powder, no apparent contact with the emitter.

Very shiny layer of molybdenum powder, shiny surface also very thin.

Almost no molybdenum powder.

NOTE: The molybdenum under the molybdenum powder was flat to within 0.0001 inch.

Fig. IV-18. Molybdenum Powder in Emitter Holder After Disassembling Prototype 1A-1

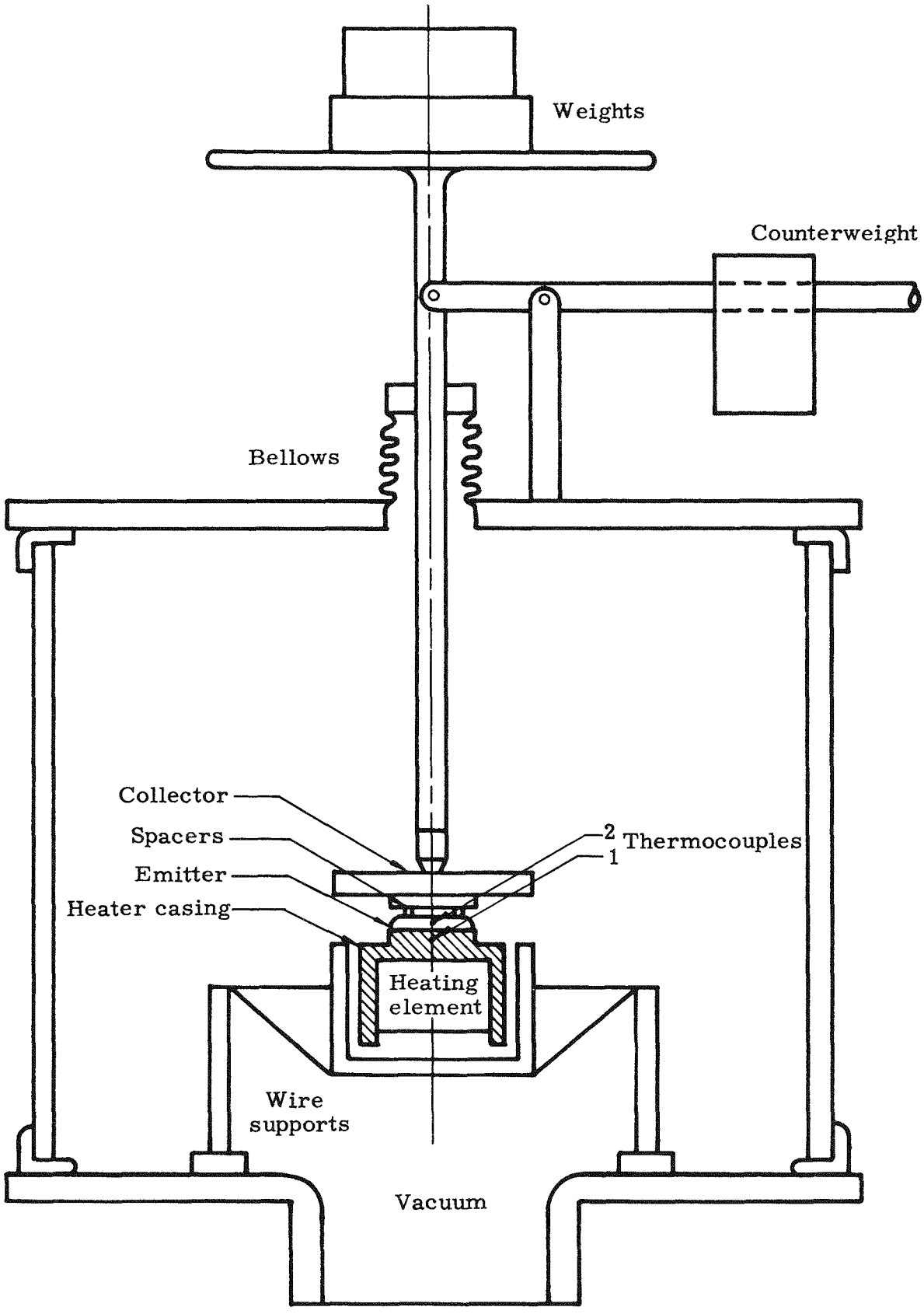

Fig. IV-19. Apparatus to Measure Heat Transfer Under Various Contact Pressures and Temperatures

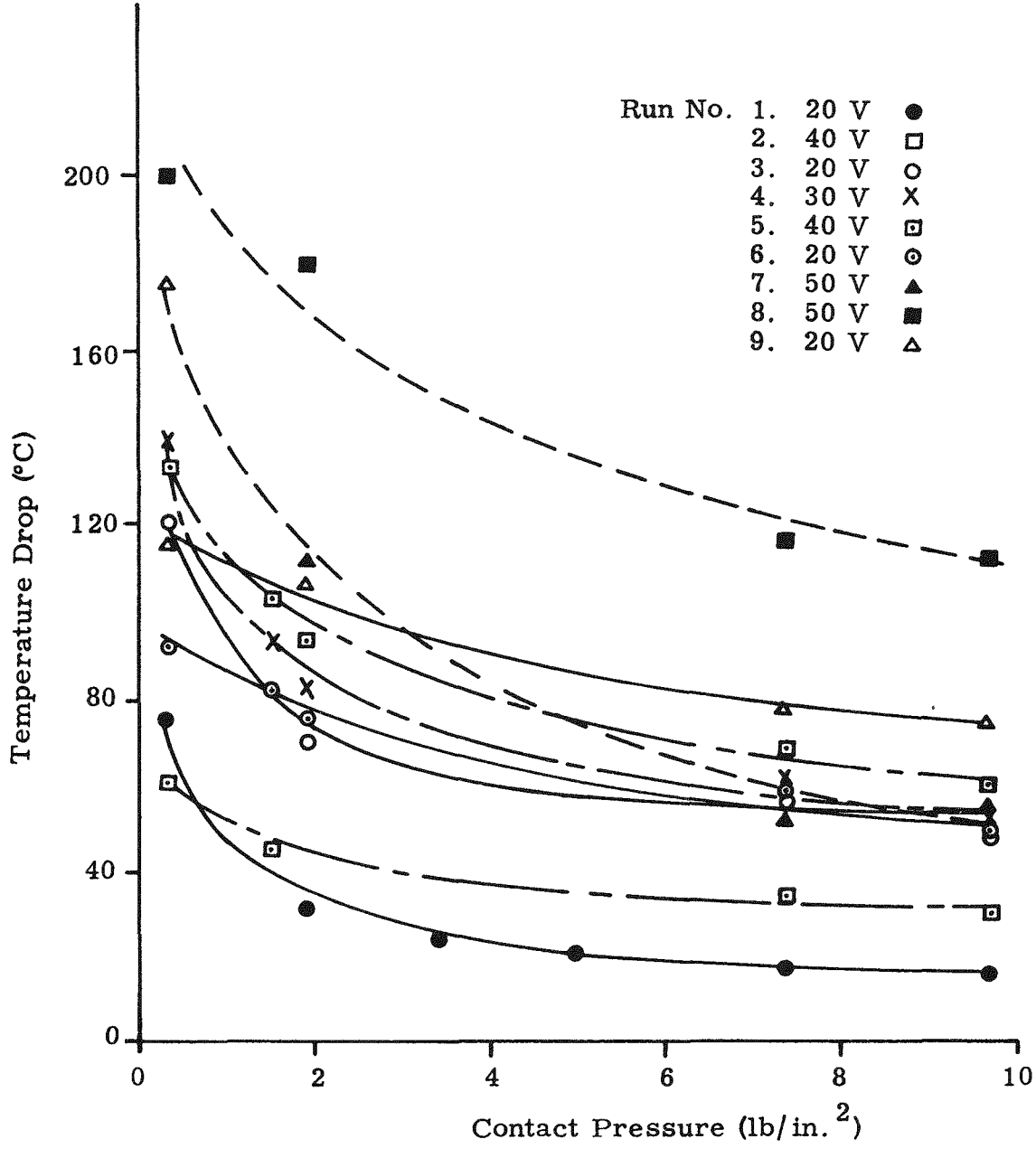

Fig. IV-20 Temperature Drop Versus Contact Pressure

not reproducible from run to run, and increases progressively with each run.

The unit was disassembled, and a coating of molybdenum powder (325 mesh) applied between the emitter and the heater casing. The coating was applied by painting with a suspension of molybdenum powder in acetone, and the emitter put in place before the acetone had dried to achieve a flat coating. The unit was reassembled, and runs taken as before. The results of these runs are shown in Fig. IV-21. It can be seen that increased pressure had less effect on the film drop, and that the film drops are generally lower than in the run with no powder. Again, higher temperature levels (higher heat flux) result in larger film drops. The reproducibility in this second test is much better than in the initial test.

Disassembly of the unit showed that the method of applying the molybdenum powder was only partially successful. The suspension of molybdenum powder in acetone had contracted upon drying into localized regions and was 0.003 inch thick, covering only 30% of the total contact area.

The fact that difficulty was encountered in measuring a consistent value of contact resistance in plain contact in a vacuum points out one of the principal problems--not only is it a poor heat transfer path, but more importantly, it is an unreliable heat transfer path. This means that it is not reasonable to use this approach in the design of practical generators. The use of molybdenum powder constitutes a better solution since the results showed both consistency and lower film drops, even though only 30% of the area was effective in transferring heat in this experiment. Further work in this area should result in better methods of achieving a more uniform covering with the molybdenum powder.

However, before proceeding with the work, there were several undesirable features of the test apparatus. Therefore, a new heat transfer apparatus was designed, constructed and tested. This apparatus is shown in Fig. IV-22. The principal advantage of this apparatus is that it is possible to determine the heat fluxes in addition to the film drop and other information obtained in the first apparatus. At the close of the quarter, this apparatus had just been calibrated.

The second heat transfer problem occurs between the emitter and the emitter holder. The best approach to this problem is to braze the emitter to the emitter holder. This would have several other advantages, such as ease of fabrication and the structural advantage. However, whatever braze material is chosen, it must be such as not to contaminate the emitter.

To determine the effects of brazing on the emission characteristics, it was decided to build several tubes, identical in every respect except that

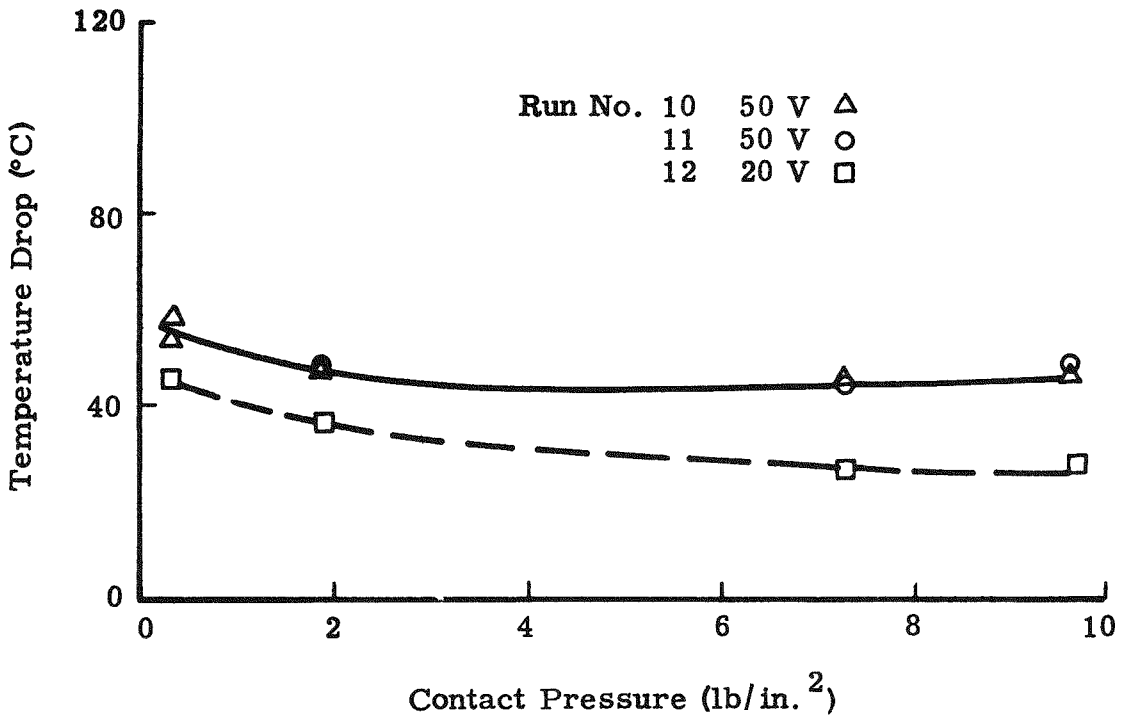

Fig. IV-21. Temperature Drop Versus Contact Pressure with Molybdenum Powder

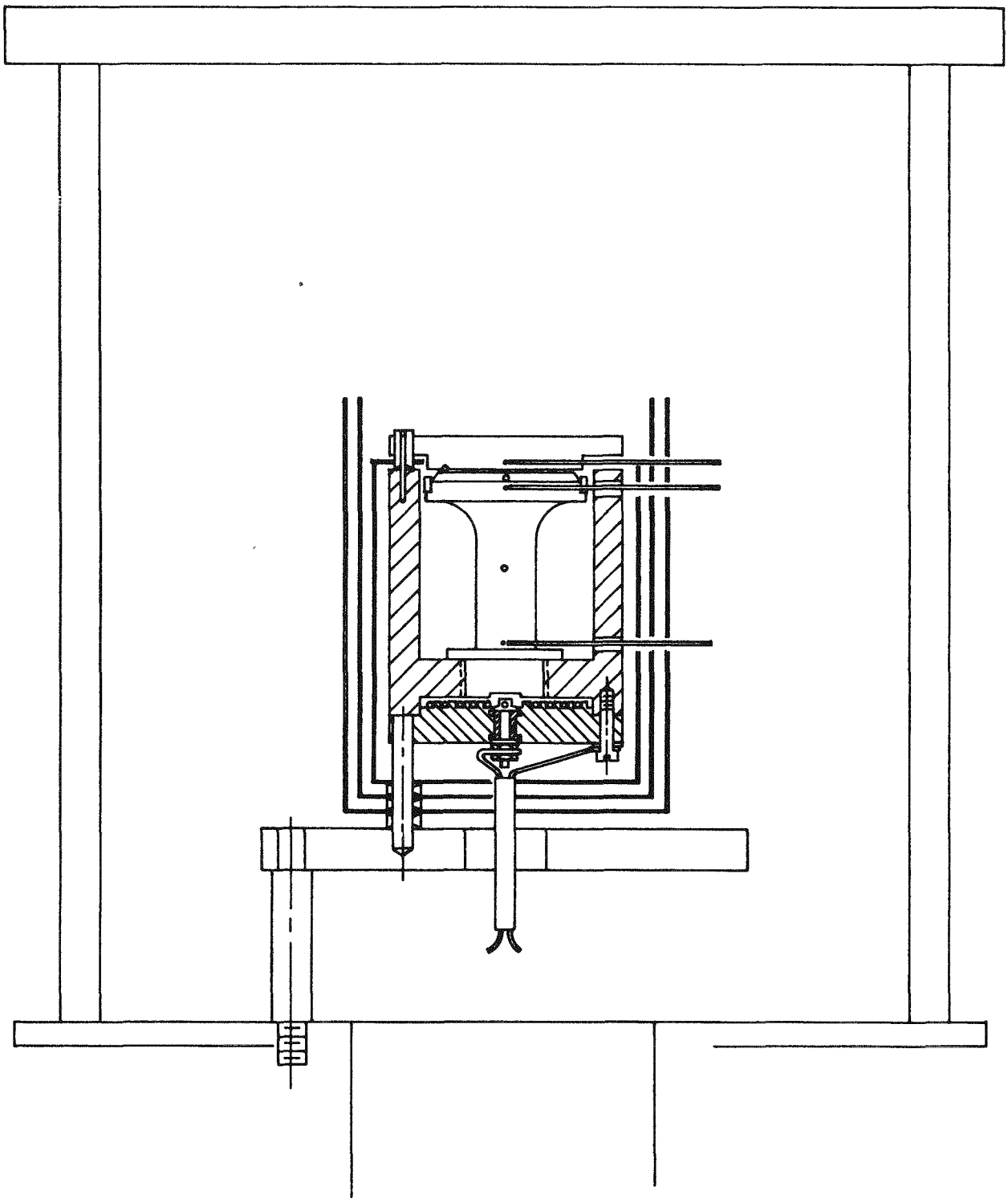

Fig. IV-22. Heat Transfer Measurements Apparatus

each would use a different braze material attaching the emitter to the emitter holder. One tube would use the standard pressure contact and would be a control tube to serve as a basis of comparison.

The control tube and a tube employing a nickel oxide braze were fabricated and tested. The emission from the control tube was five times greater than that from the brazed tube, indicating that the braze material did affect the emission characteristics. At least two more tubes will be tested; one with a platinum braze and the other with a nickel braze.

Vacuum tests in prototype shells. Four types of prototype shells were tested during the last quarter, to determine the lowest vacuums that could be achieved and the changes that occur in the level of vacuum with time. This work was continued in this quarter in addition to the continuation of work on electrical leadthroughs.

a. Prototype shells

A shell was constructed out of titanium and monel to determine the suitability of using this combination of materials for constructing prototype housings (Fig. IV-23). The unit was evacuated, the brazing performed and the vacuum measured. The ion gauge vacuum measurement indicated a leak in the unit. Cross sectioning of this assembly showed that, in spite of the copious formation of braze fillets at the interface of the monel and titanium, the monel did not alloy with the braze. A sharp hammer blow separated the monel from the titanium. Based on the results of this test, it can be concluded that the techniques employed in successfully brazing titanium to titanium cannot be directly applied to brazing monel to titanium. Two possible approaches are:

(1) Plate the monel with copper prior to brazing it to titanium (using the same brazing techniques as before).

(2) Investigate new brazing materials, compatible with both monel and titanium.

A second shell was fabricated and tested using the design features and procedures presently planned for use in Generator 1A. The unit, which is shown in Fig. IV-24, includes a CFI leadthrough and a copper evacuation tube mounted in the titanium housing. The copper tube was crimped off to simulate the prototype crimp off. The unit was evacuated and the brazing operation performed. Vacuum tests indicated that the unit was leaktight, and held a vacuum of 4×10^{-5} mm of Hg. Four days later, the vacuum was still 4×10^{-5} mm of Hg. This test verified the design features and procedures to be used in fabricating Generator 1A.

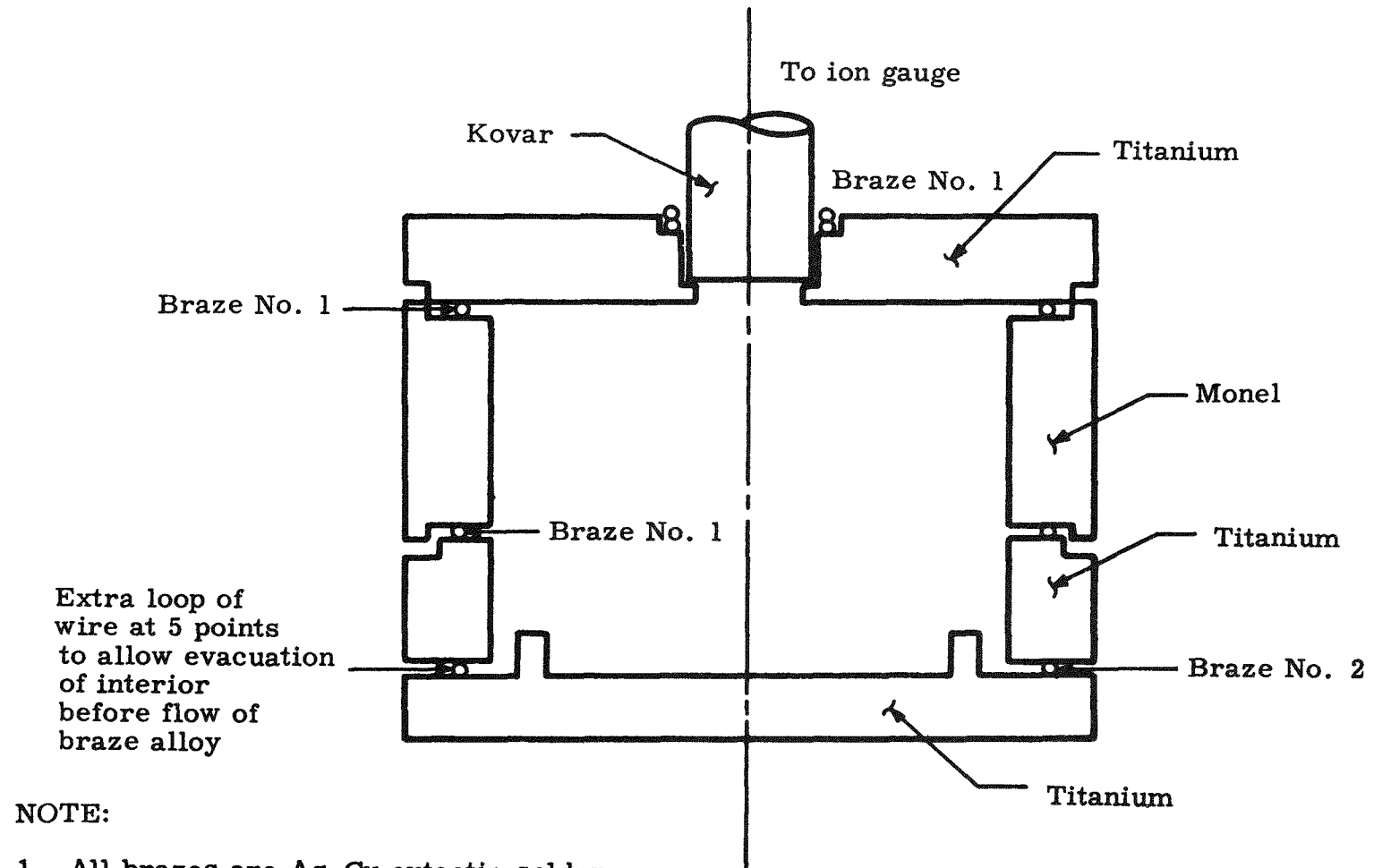

NOTE:

1. All brazes are Ag-Cu eutectic solder
2. Not to Scale
3. Entire unit mounted inside a Bell jar

Fig. IV-23. Titanium-Monel Vacuum Shell

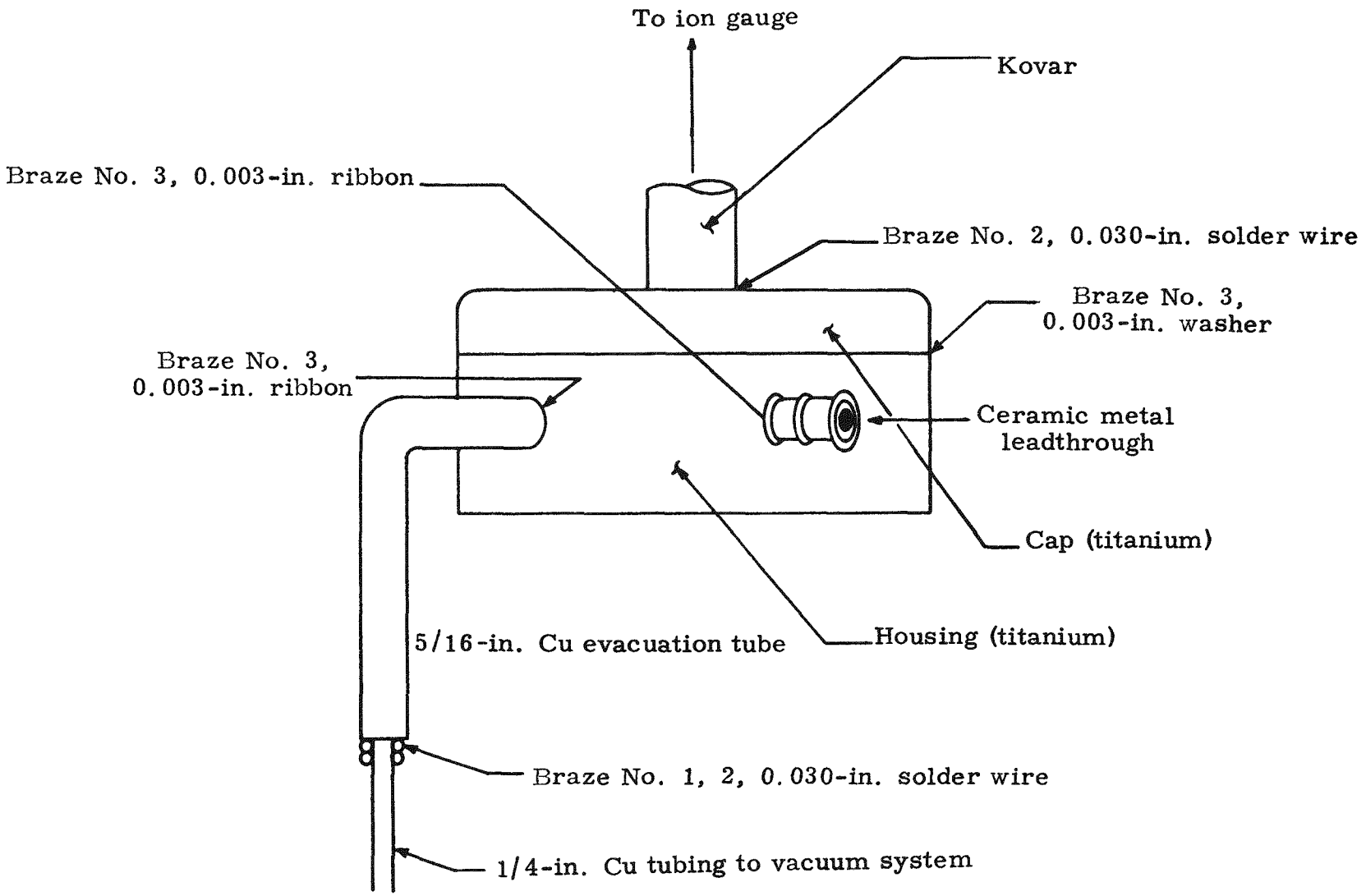

Fig. IV-24. Generator 1A Test Bed

b. Leadthroughs

In addition to the shell itself, the other problem area that arises in trying to maintain such high vacuums for indefinite periods of time is the electrical leadthroughs. Therefore, considerable effort was focused on developing a suitable leadthrough capable of withstanding bakeout temperatures of approximately 1000° C.

Oxidation tests were conducted on all three types of leadthroughs under development--the CFI, metalized ceramic and the reactive metal leadthroughs.

Two metalized ceramic leadthroughs were fabricated and tested. These leaked after 124 hours exposure at 400° C to relatively dry air. A CFI leadthrough, consisting of a metalized ceramic brazed with OFHC copper to thinwalled Kovar, leaked after 141 hours exposure at 400° C to relatively dry air. Two reactive metal leadthroughs were fabricated and tested. They consisted of titanium brazed to Al_2O_3 with a nickel shim which reacted with the titanium. This reaction formed a braze alloy which has an affinity for the Al_2O_3. The leadthroughs withstood over 500 hours exposure to air at 400° C without any trace of leakage or failure.

These tests indicate that leadthroughs of the CFI and metalized ceramic type will leak after approximately 125 to 150 hours exposure to air while at the expected operating temperature of 400° C. The reactive metal leadthroughs, however, showed no ill effects after 500 hours exposure to the same environment. Therefore, attention will be focused on the reactive metal leadthroughs.

Another related problem area is obtaining a satisfactory braze material and techniques for brazing the leadthrough and evacuation tube to the prototype housing. Several different types of brazes were tested during this period. This work will be continued into the next period.

Cathode and sapphire support creep tests. The interelectrode spacings required in a closed spaced thermionic diode are so small that all effects on the spacing, no matter how small they may appear, must be taken into account. This includes such effects as:

(1) The amount the sapphire rod creeps into the emitter and collector surfaces.

(2) Surface distortion of the emitter and collector due to bending stresses.

(3) The differential thermal expansion of the ceramic spacers (Al_2O_3).

a. Sapphire creep test

An apparatus was designed and fabricated for determining the creep rate of sapphire rods. The design of this apparatus is shown in Fig. IV-25. The creep rate is determined from the bending stress (15,000 psi) induced by supporting the 120-gram weight at the center of the sapphire beam. The temperature is controlled by the R-F coil. The tests were carried out for temperatures between 1000 and 1350° C. These tests indicate that no creep takes place at the operating temperature and pressure encountered in a practical generator. The tests conducted at temperatures greater than 1300° C indicate that the strength falls off very rapidly above 1300° C and the creep becomes appreciable. At 1200° C, some creep could still be observed, while at 1100° C no creep or plastic deformation occurred.

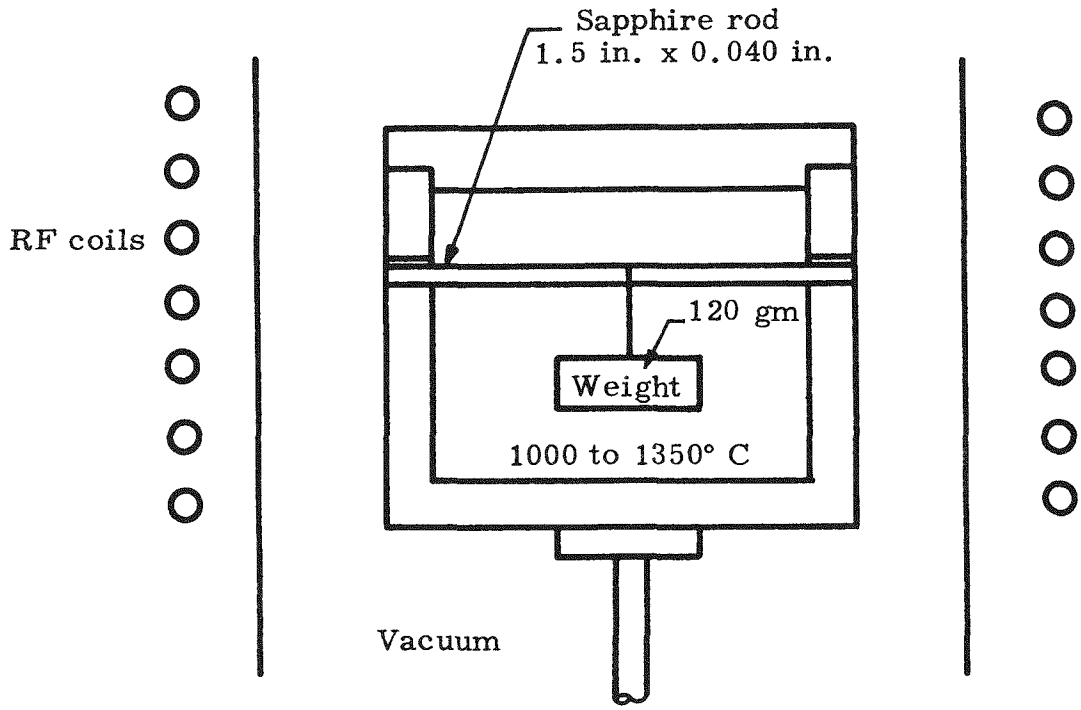

Fig. IV-25. Spacer Creep Test Apparatus

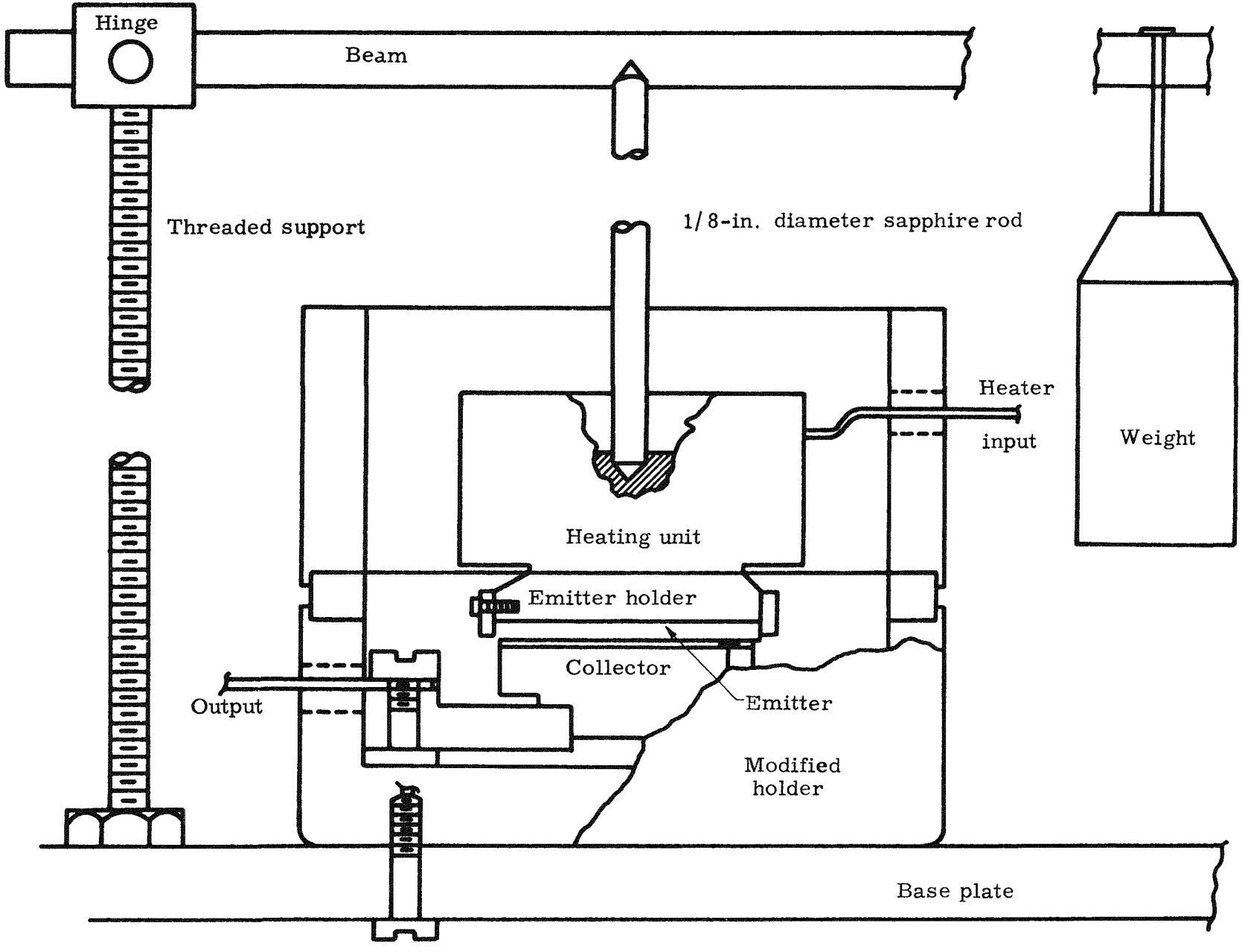

Fig. IV-26. Emitter Distortion Apparatus

b. Surface distortion

An apparatus was designed and fabricated to conduct several of the tests connected with creep (see Fig. IV-26). The first of these tests is to determine the distortion of the emitter. The flatness of an emitter was measured before the start of the test and the variation of the flatness from a specific reference was measured. Periodically, the emitter will be removed and tested for flatness, and the results will be compared to the initial condition. It is planned to run this test for 500 hours. Following this test, a similar test will be performed with a molybdenum collector.

c. Expansion test

An apparatus was designed and fabricated to determine the increased spacing due to the greater thermal expansion of the sapphire rods as compared to the expansion of the metallic parts of the generator (see Fig. IV-27).

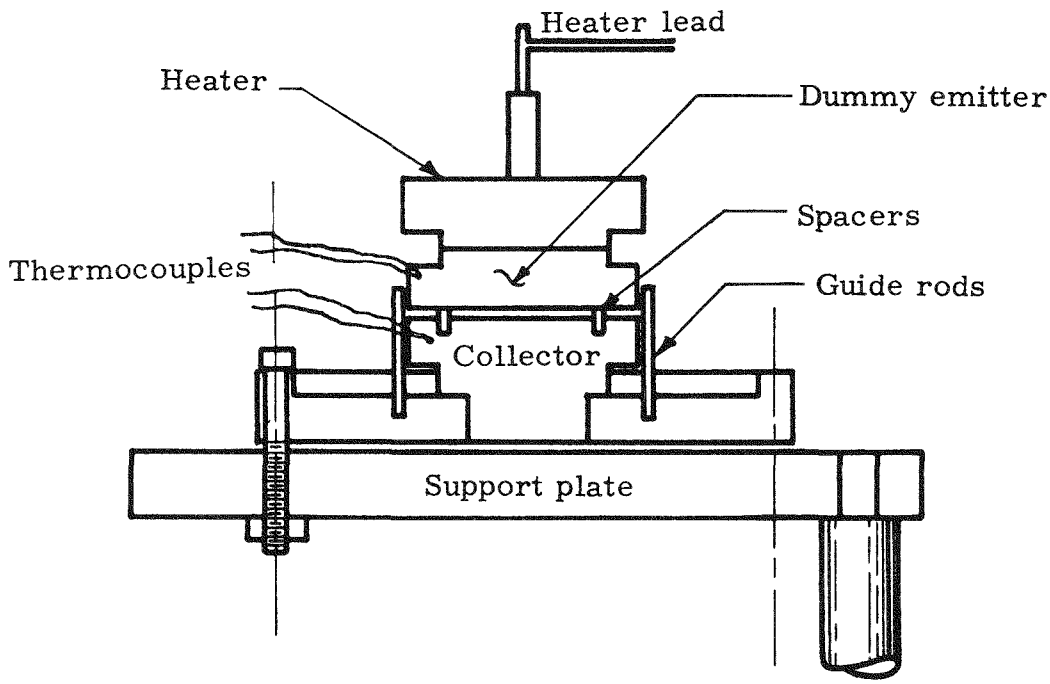

Fig. IV-27. Apparatus for Thermal Expansion Test

Parametric study. The parametric study that was initiated in the last quarter was completed. The objective of the study is to determine the relationship existing between the power density of the heat source and the efficiency and geometry of the thermionic converter, at varying electrical power outputs. The information is plotted in graphical form using the power density of the heat source as a common abscissa. In this way, the actual power density of a particular isotope can be lined in and the resulting performance and design parameters read directly. The efficiency and heat source dimensions were selected as the ordinates with the electrical power output as a common parameter.

The most efficient design of a thermionic generator would be one that covered the entire surface of the heat source with thermionic diodes. The power density and volume of the heat source would then be such that it produced the necessary heat flux to the emitter. In other words

$$\text{volume} \times \text{power density} = \text{heat flux} \times \text{area} = \frac{\text{power output}}{\text{efficiency}}$$

This would also guarantee the proper emitter temperature. However, practical considerations make it impossible to completely surround the heat source with emitting area. Therefore, two practical models were selected upon which to base the analysis. The first of these applies to the lower power devices (1 to 10 watts) and is similar to that used in the actual design of the two-stage generators. That is, it consists of two diodes on opposite ends of a cylindrical heat source. This model is shown in Fig. IV-28. The second model is also a cylindrical heat source with a polygonal cross section and is used at the higher power levels. Thermionic diodes are placed axially along the flat faces of the plygon. This model is shown in Fig. IV-29.

The results of the computations are shown in Fig. IV-30 through IV-32. Notice in Fig. IV-30 that, for higher power levels, the power density becomes of little importance as far as the efficiency is concerned, as long as it is above a threshold value for the particular electrical power level. However, at the lower power levels, the power density of the isotope is a critical factor. If the power density of the isotopic heat source is less than 10 watts/cm^3, one pays a severe penalty in efficiency. Notice also that the maximum attainable efficiency varies for the different power levels. This is due to the more or less fixed losses which must be amortized over the power output of the generator.

In Fig. IV-30, there are two families of curves shown for the 50- to 500-watt class generator. The upper set (f = 1) assumes that all of the cylindrical side area is covered with emitter area. The lower set (f = 0.95) is a more practical case which assumes only a 95% coverage.

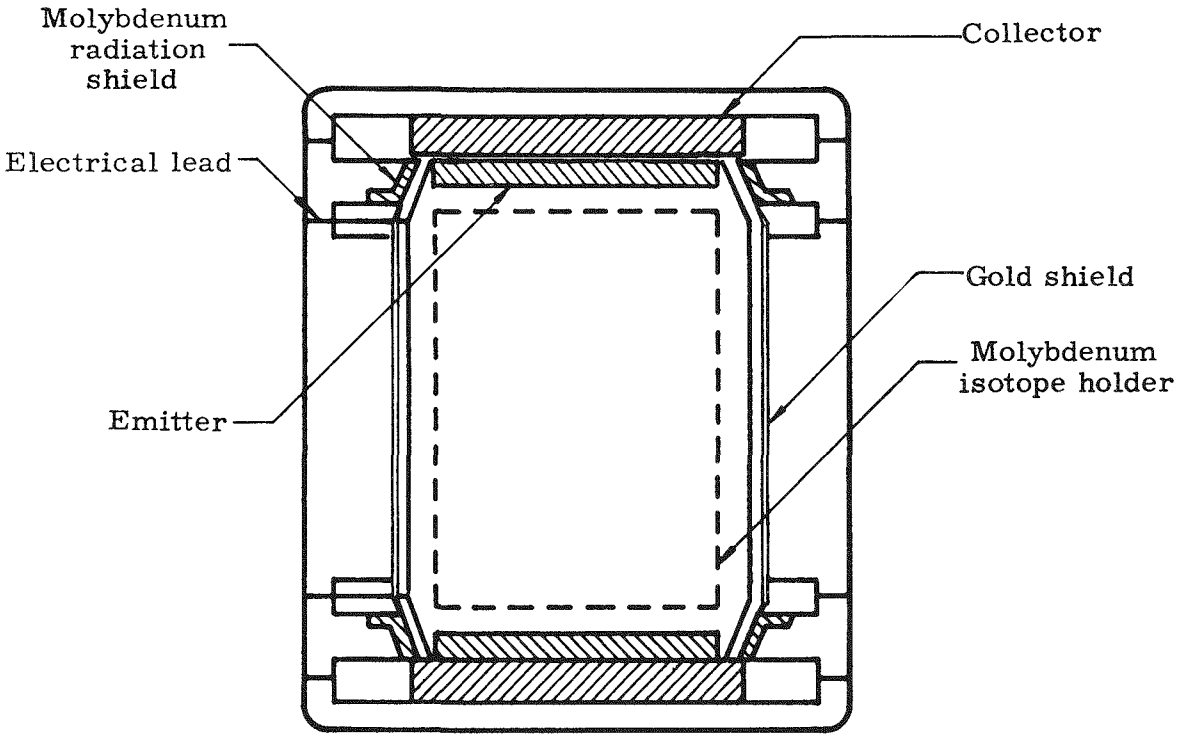

Fig. IV-28. Two-Stage Practical Thermoelectron Engine

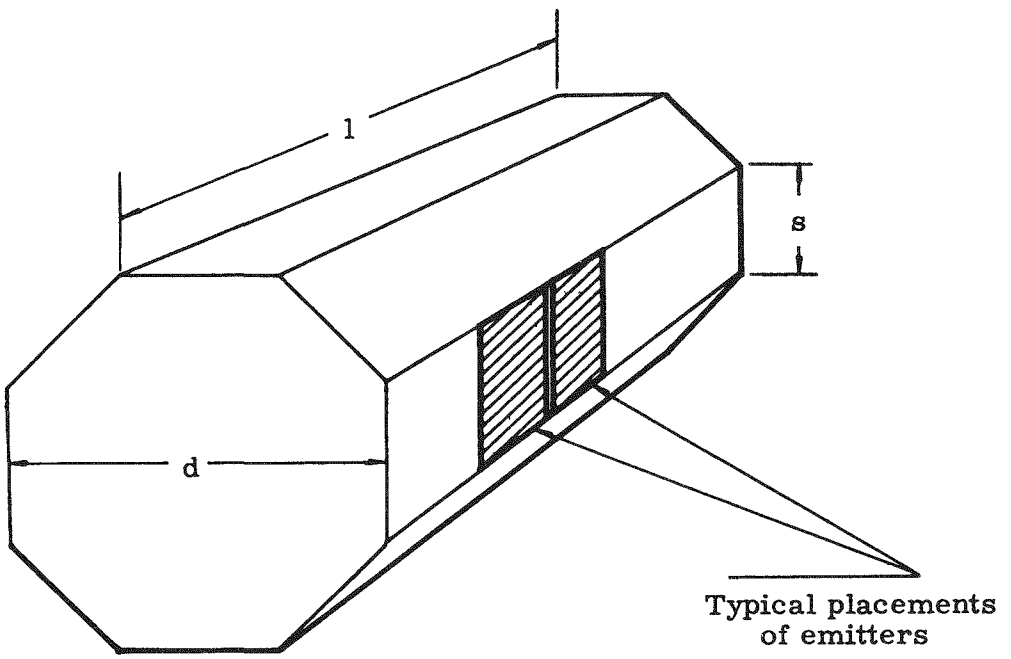

Fig. IV-29. Model for High Power Thermionic Generator

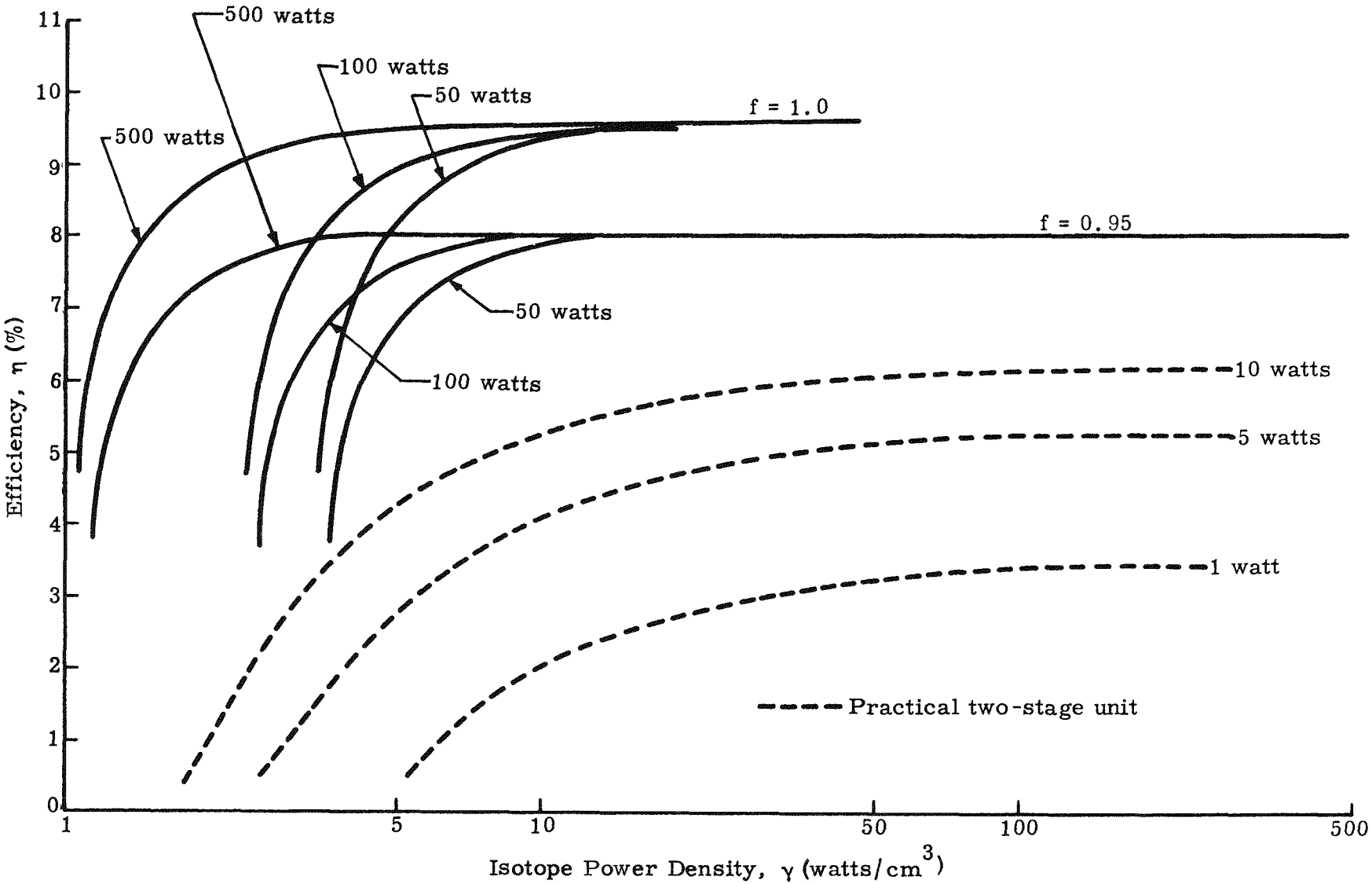

Fig. IV-30. Efficiency Versus Isotope Power Density

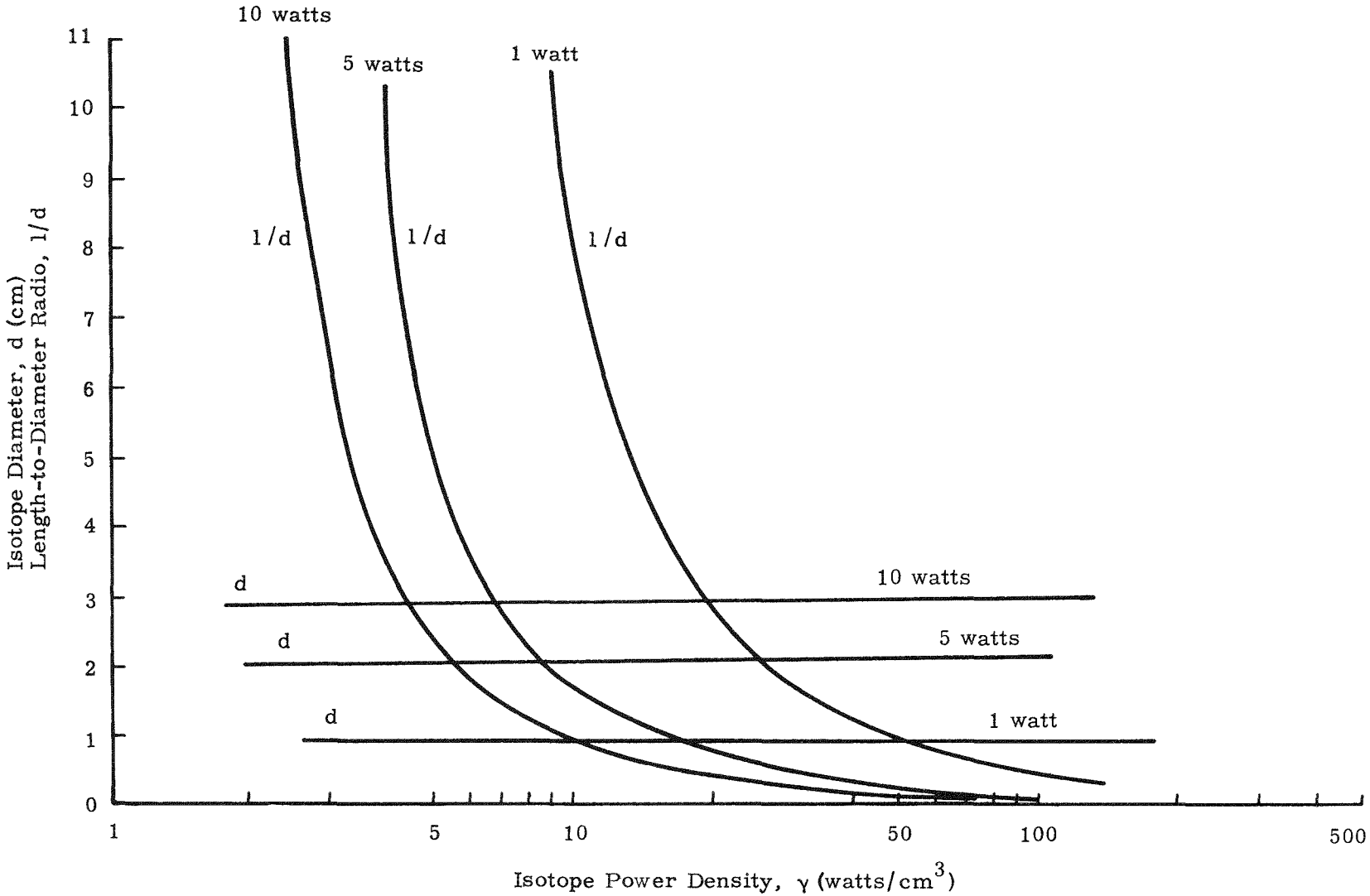

Fig. IV-31. Isotope Diameter and Length-to-Diameter Ratio Versus Isotope Power Density

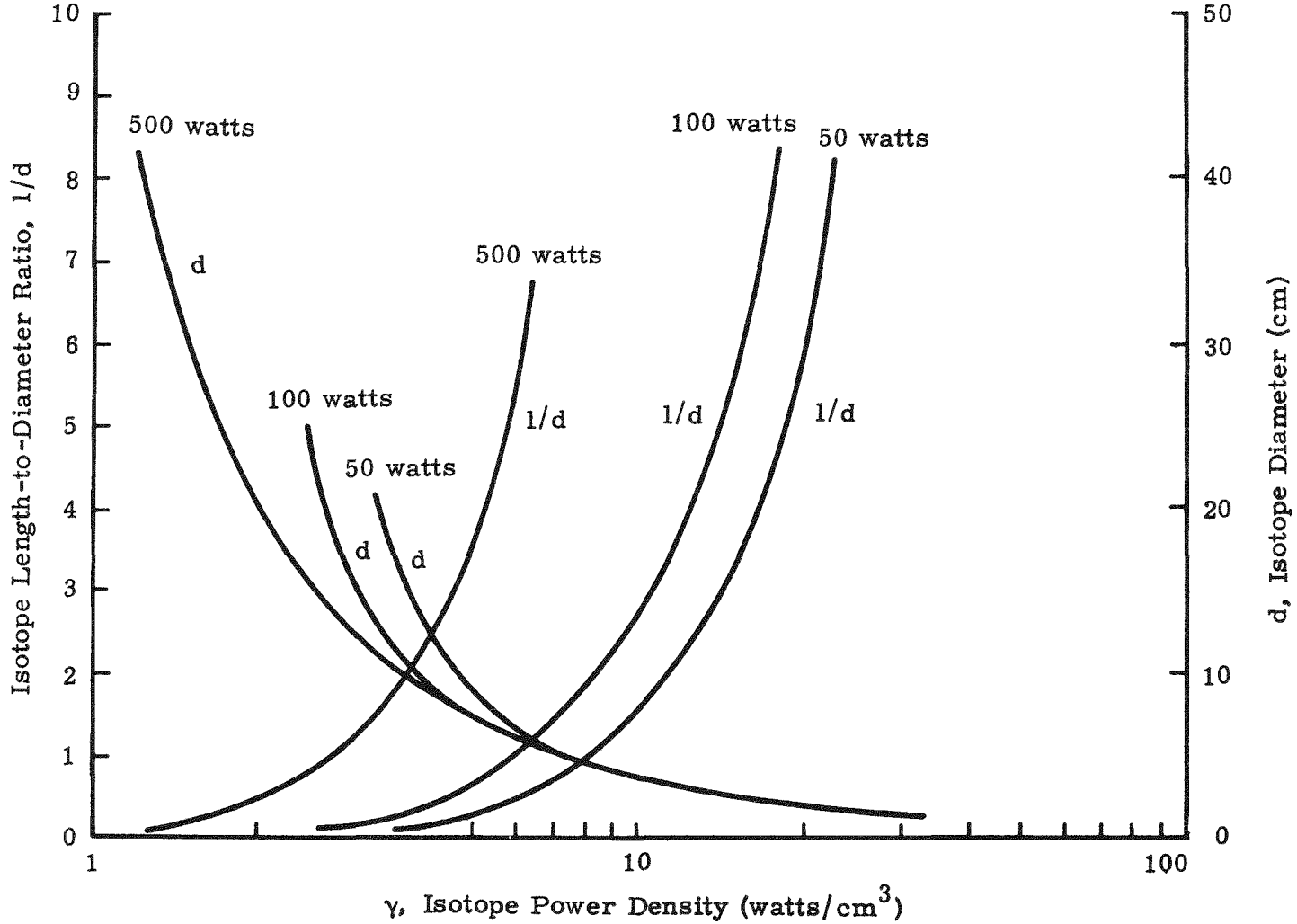

Fig. IV-32. Isotope Power Density Versus Isotope Diameter and Length-to-Diameter Ratio

There are two important differences between these two cases. An abrupt cutoff for the isotope power density exists in the case of the high output units (see Fig. IV-30). This value represents the smallest allowable isotope power density for operation at the assumed value of 1500°K under the assumed configuration, material properties and power output. If a value for isotope power density less than this cutoff value is chosen, the isotope will be unable to supply the necessary heat for operation at 1500°K at the specified power output, and the emitters will operate at some temperature less than 1500°K.

The second difference between the two cases is that, in the high power units, the same efficiency is approached regardless of the power output of the device. This is not true in the case of the low power units (see Fig. IV-30). The explanation for this phenomenon is that, in the case of the high power output units, where the size of the actual individual diodes is not specified, the spacing conduction loss has been reduced to a per unit area value, while in the other case, the spacing loss is constant for all power levels.

These efficiencies are based on a collector work function of 1.85 volts and a spacing of 0.001 centimeter. If the collector work function were 1.65 volts (a value achieved experimentally), then the efficiency would be as shown in Fig. IV-33. Figure IV-31 shows that the diameter of the isotope is determined principally by the power output of the unit and is affected only slightly by the isotope power density. The length, however, is strongly dependent upon the isotope power density. It is the practical limitation imposed by the required isotope length that may eventually determine the desired value of isotope power density.

As shown in Fig. IV-32, for the high power units, the diameter decreases and the length-to-diameter ratio increases as the isotope power density increases. Again, it can be seen that large values of isotope power density lead to impractical length-to-diameter ratios. It will be noticed that the two cases vary considerably. This is explained by the fact that, in the low power units, the emitter area is a function of the diameter only, while in the high power case the emitter area is dependent on both the length and diameter of the isotope.

To summarize the results of the parametric studies, it has been shown that the lower power, inherently less efficient devices require higher power density isotopes for operation near their maximum efficiency point than do the high power units. The high power, hexagonal units require an isotope power density of only 6 to 10 watts/cm^3 to achieve 95% of the maximum attainable efficiency, whereas a practical 5-watt, two-stage unit requires a power density of about 50 watts/cm^3

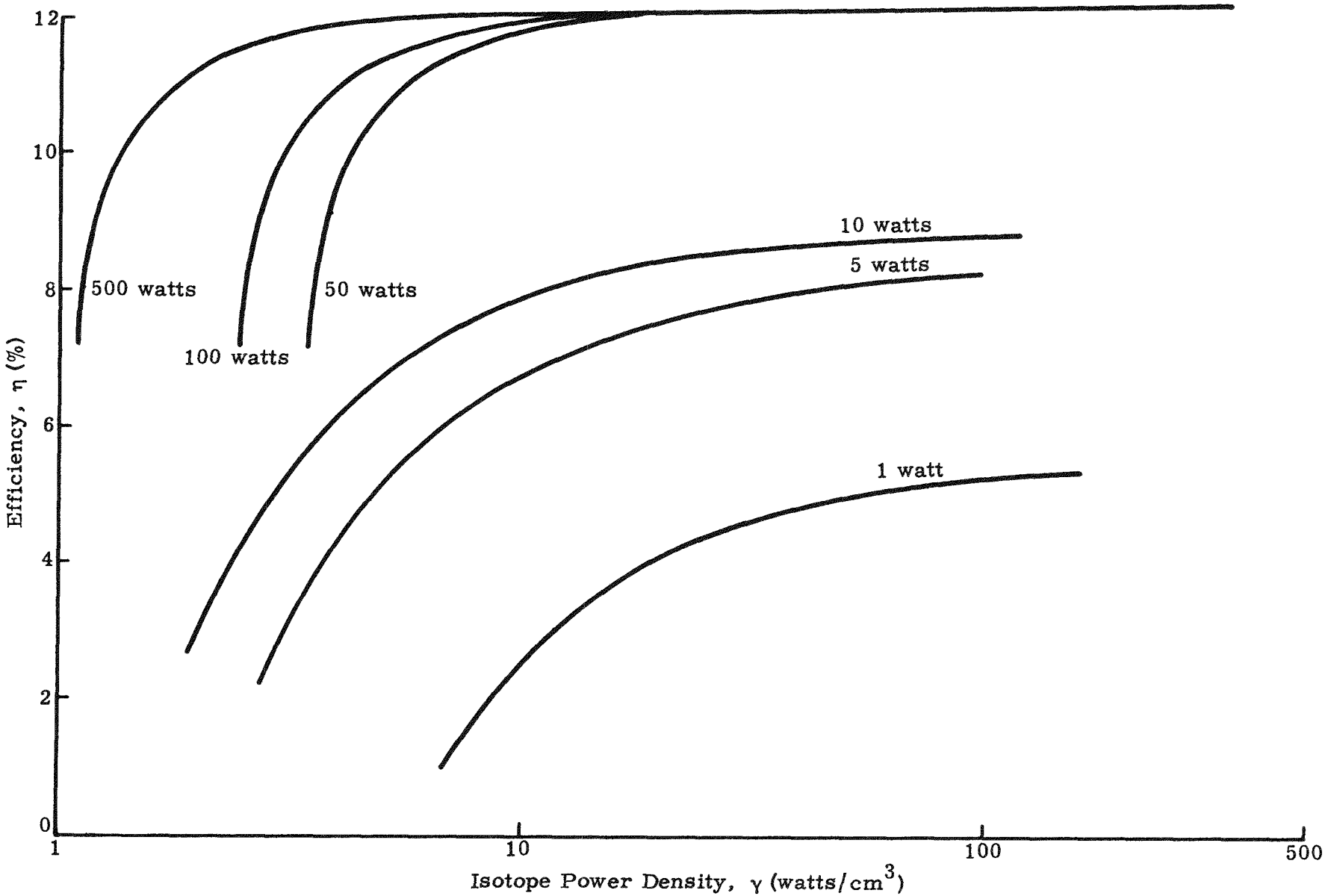

Fig. IV-33. Efficiency Versus Isotope Power Density for Collector Work Function = 1.65 V

to operate at 95% of its peak efficiency. It should be noted that the isotope power density referred to is the "effective" power density of the entire encapsulated heat source. This should not be confused with the power density of the actual isotope material itself, which would necessarily have to be somewhat higher than the "effective" power density.

The dimensions of the isotope, and hence the dimensions of the device, become impractical at high values of isotope power density, and will thus strongly influence the choice of isotope to be used in a thermionic generator.

2. Martin Nuclear Division Effort

All of the work to be performed by Martin Nuclear under this Subtask is now complete, except for the preliminary testing and fueling of the molybdenum fuel capsule with two Ce-144 fuel pellets, and the preparation of a topical report on the heliarc welding of molybdenum. This report on welding will be included in the final report for the work in Fiscal Year 1960.

Prior to the fueling of the molybdenum capsule with the ceric oxide fuel pellets already fabricated by ORNL, it was agreed that Martin Nuclear would accomplish the following:

(1) Make a device for measuring the thermal expansion of the radioisotope fuel pellets consisting of a dial indicator tool employing comparator techniques. The ambient conditions could be altered and the temperature and the length of the ceric oxide pellet would be observed.

(2) Expose a molybdenum capsule containing an inert ceric oxide pellet to a measured amount of oxygen, while maintaining a wall temperature of 2300° F. The formation of an oxidized surface on the molybdenum and the fusing of the ceric oxide to this surface will be studied.

(3) A device will be made to take a sample of the gas generated within the molybdenum capsule after a half life has elapsed.

The work this quarter was aimed at accomplishing these intermediate objectives. It is recognized that while work is being done in these areas, the actual fueling is being delayed which means the activity, and hence power output from the fuel pellets, will be reduced considerably. Therefore, to offset this effect, electrical heaters will be used in the storage container to supplement the heat of the isotope. This approach is preferred

rather than going ahead with the fueling and then determining how the tests will be performed or how to interpret the results.

In addition to work on the ceric oxide heat source, environmental tests were conducted on the 1B thermionic unit delivered to The Martin Company by Thermo Electron Engineering Corporation.

Device for measuring thermal expansion. A device to determine the coefficient of thermal expansion of the fuel pellets was fabricated and tested. This device is shown in Fig. IV-34. The lava blocks that had been machined for a sliding fit were judged to be a little too difficult an operation for hot cell manipulation. Considerable difficulty was also encountered in attempting to calibrate this device. Therefore, a new device was designed and fabricated. This unit is shown assembled in Fig. IV-35 and disassembled in Fig. IV-36. Some problems still remain, especially in regard to reproducibility of specific points and, therefore, calibration of the device.

The stacking of the lava block insulator parts, auxiliary heaters and the ceric oxide pellet is the major problem. It will be necessary to redesign these components so that the vibration and necessary adjustments will not affect the dimensions.

The National Bureau of Standards has been contacted in reference to this problem. To assist, they are forwarding complete fabrication drawings of a dilatometric device of similar design.

Effects of oxygen in the molybdenum encapsulated ceric oxide. The object of these tests is to determine the effects that the oxygen, which is liberated in the radioactive decay of the ceric oxide to neodymium oxide, has on the welded molybdenum capsule. Information concerning the depth of oxidation in molybdenum, the rate of oxygen conversion to molybdenum oxide, the anticipated internal pressures, the preferential attack in the weld area compared to the attack on the parent metal, and the reaction of the ceric oxide with the molybdenum or molybdenum oxide is to be obtained.

In discussions with ORNL personnel concerning the method of testing, it was suggested that the oxygen be added to a molybdenum capsule in measured amounts to serve as a comparison of the expected attack in the capsule actually fueled.

The initial approach required a thick-walled, small inside diameter, molybdenum tube welded to the capsule so that all gauges, valves and controls could operate at normal room temperature. The capsule in a vacuum atmosphere was to be heated by an induction coil for 24 hours

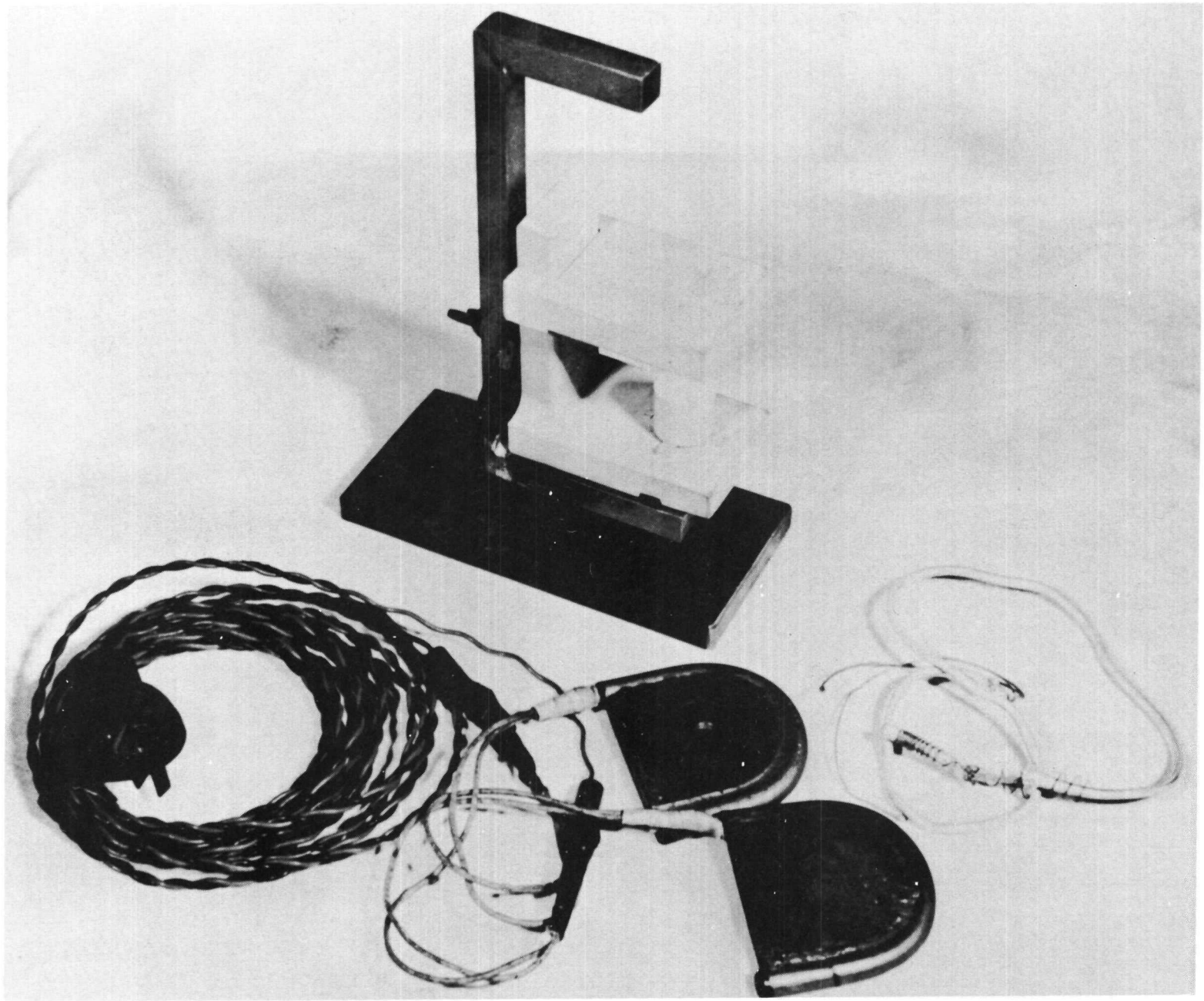

Fig. IV-34. Initial Thermal Expansion Device

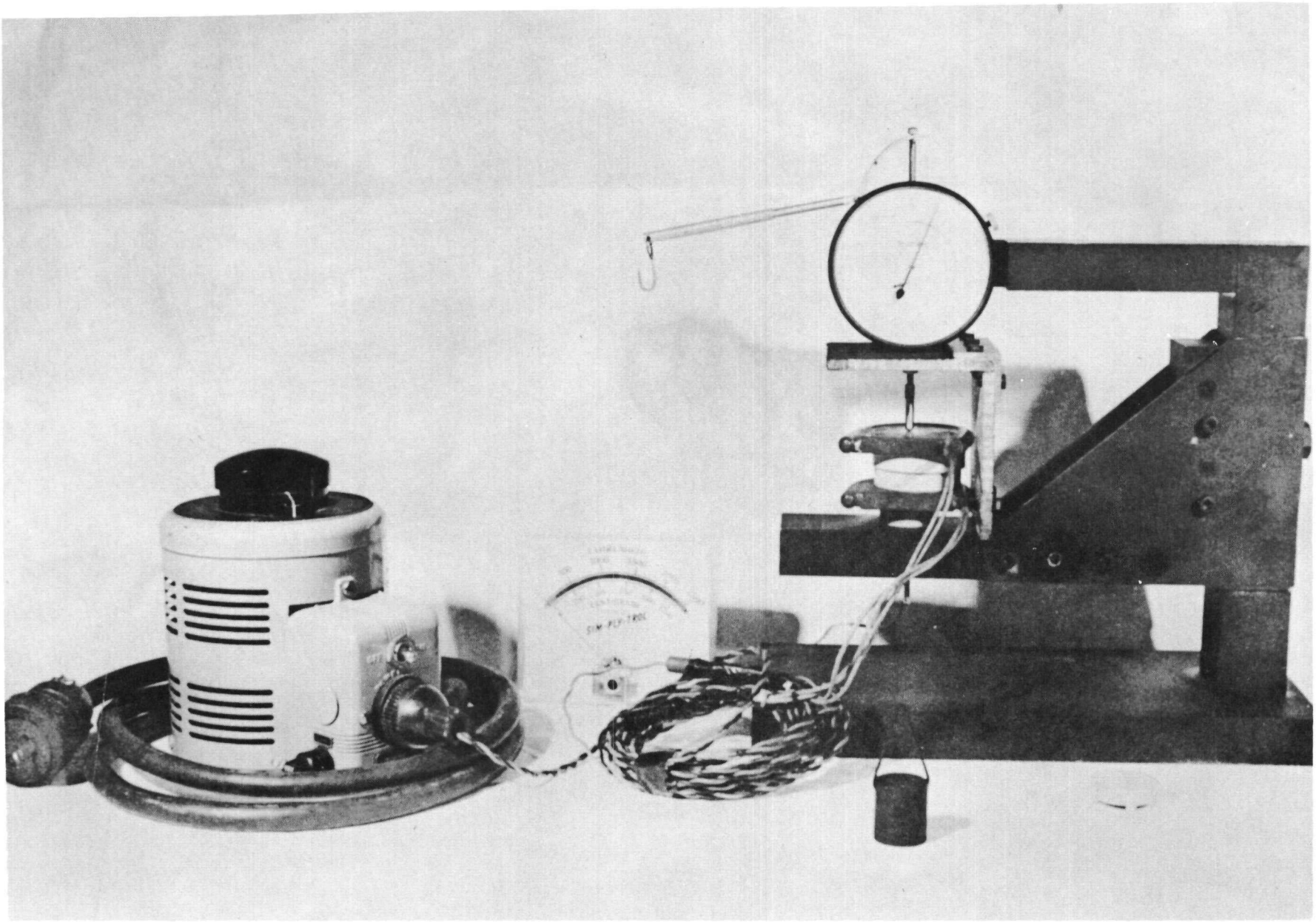

Fig. IV-35. Assembled View of Thermal Expansion Measuring Device

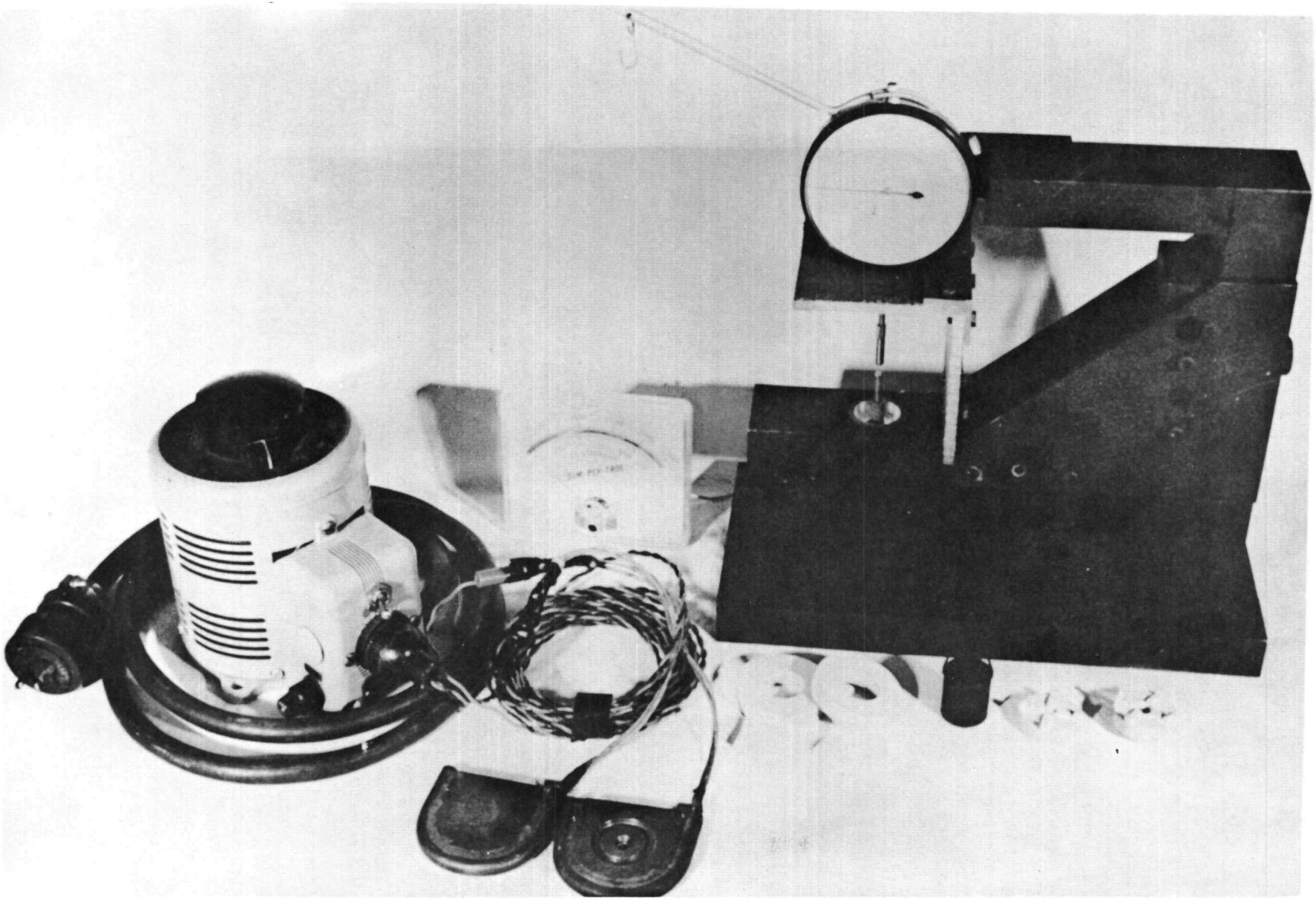

Fig. IV-36. Disassembled View of Thermal Expansion Measuring Device

of continuous operation, while oxygen was to be supplied under pressure from a gas bottle. This was simplified to a capsule inserted in a larger steel pressure container. This container, with an oxygen gas pressure of 15 psi, was then to be inserted in a resistance furnace.

A molybdenum capsule was then loaded with two stable ceric oxide pellets and heliarc welded. Two 1/8-inch diameter holes were drilled in both ends of the molybdenum capsule to allow the free passage of gas through the capsule. This capsule was then inserted in the steel pressure container; and the tubing, the necessary valves and gauges for charging, flushing and evacuating the container were attached. The welded can containing the molybdenum capsule was evacuated and backfilled with oxygen, after having been leak tested with helium. (A constant pressure drop of 0.2 psi per hour was observed when helium was used, although a leak detector indicated no leaks.) The unit was placed in a furnace and the temperature increased to 2000° F. After the temperature reached equilibrium, very little pressure drop was observed (on the same order of magnitude as with the helium gas). It was felt that gases evolved in the steel container may have formed a protective layer, and that the free oxygen, initially available, had been expended. If this were true, a method employing a purging system should produce different results. The valve was opened and the gas in the container allowed to escape. By successive pressurizing with oxygen and then rapid release, it was established that the gas in the steel container was oxygen. The rate of pressure drop at 2000° F remained the same as when checked with helium.

As the assembly was being cooled for examination, the pressure was noted to have dropped rapidly. When the temperature was stabilized at 675° F, pressure drops of 1 psi per minute as compared to 0.2 psi per hour were observed for the same gas at 2000° F.

In subsequent tests, it was found that the information was not reproducible at the lower temperatures, but in all cases the pressure drop was more rapid than the initial run with oxygen at 2000° F. In all, 50 experimental runs were conducted.

After a total of two weeks exposure to an oxygen rich atmosphere at elevated temperatures, the capsule was cut open and examined (see Figs. IV-37 and IV-38). This revealed only slight oxidation of the molybdenum capsule--an unexpected occurrence since it was expected that the molybdenum would have been completely consumed. The molybdenum was a violet-brown color due to the molybdenum dioxide (MoO_2) coating on the surface. Surprisingly enough, there was no indication of the formation of molybdenum trioxide (MoO_3) at all. The ceric oxide was the same color (violet-brown) except for a 3/8-inch diameter spot (see Fig. IV-38) that

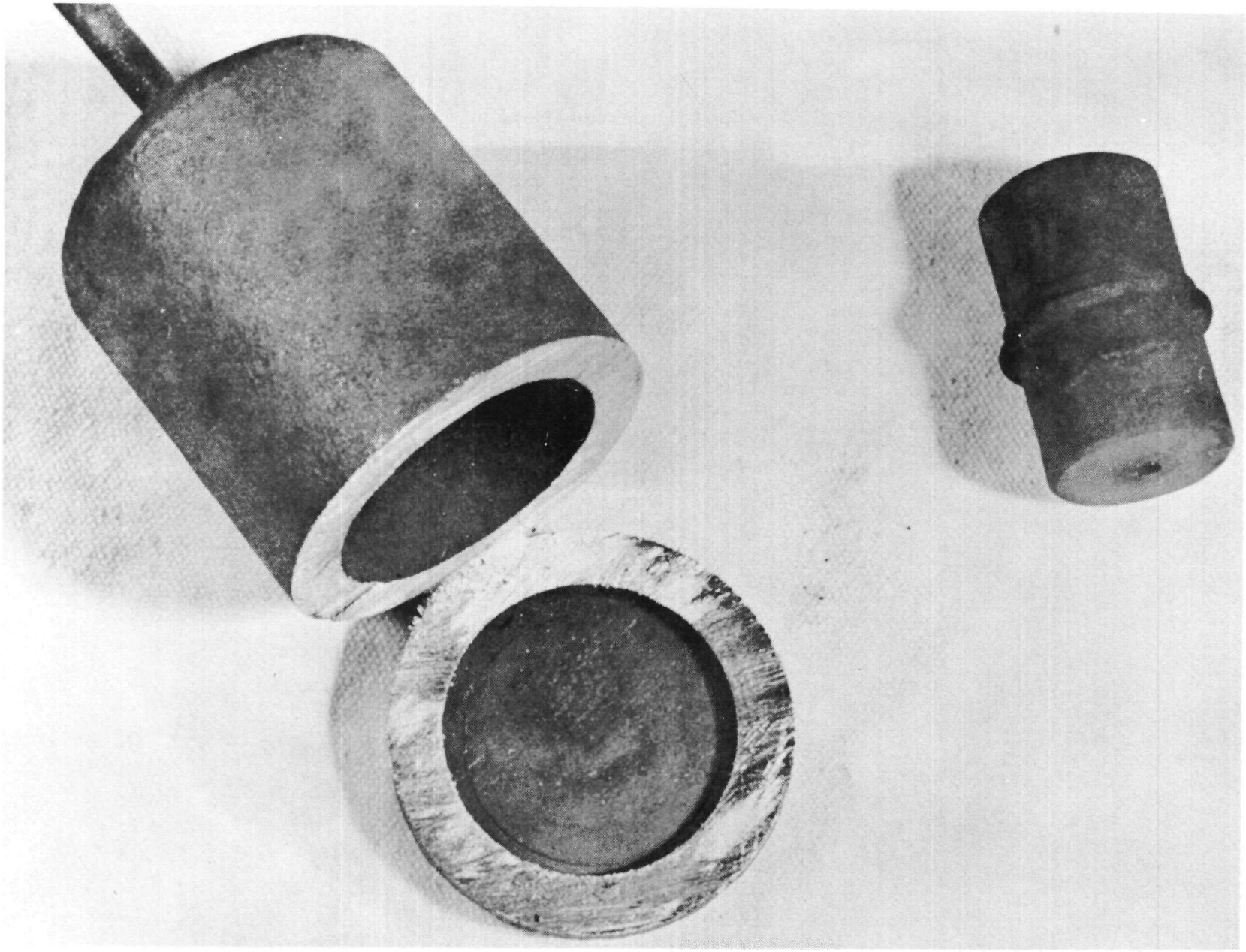

Fig. IV-37. Stainless Steel Container and Molybdenum Capsule After Test

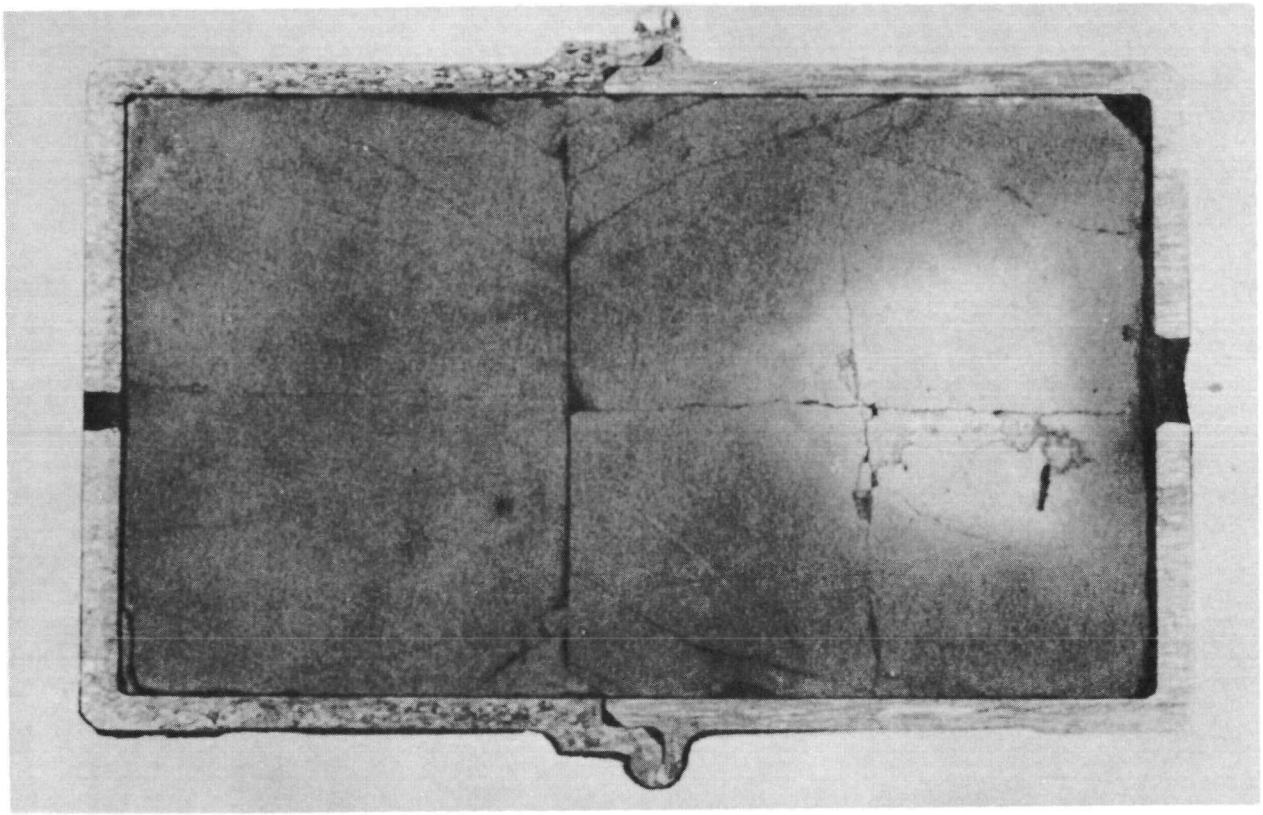

Fig. IV-38. Cross Section of Oxidation Sample

remained the light yellow color of the ceric oxide. The first observation was that the MoO_2 had permeated throughout the ceric oxide and caused the color change. However, an X-ray diffraction pattern taken on the material was identical to the control run of normal ceric oxide, indicating that the discoloration was not due to MoO_2.

Furthermore, measurements of the molybdenum indicated that only a 0.001-inch layer had been oxidized. By way of comparison, the interior of the stainless steel pressure container was badly oxidized while very little oxidation of the molybdenum had occurred even though exposed to oxygen for two weeks at 2000° F. This was considered highly unusual and unexpected. Therefore, one of the original two half-sections of the molybdenum capsule was stoked to 2000° F in a normal atmosphere furnace for comparison with the unusual exposure results of a very rich oxygen atmosphere. In a 24-hour period, the molybdenum metal had vaporized to molybdenum trioxide which then condensed at the ends of the furnace muffle. This run was more in line with the anticipated behavior of molybdenum. However, this still left the results of the first test unexplained. In an effort to explain these results, it was decided to repeat individual portions of the initial experiment. The first step was to leave out the ceric oxide pellets.

The same stainless steel container was used to hold a section of a molybdenum fuel capsule. The test setup was exactly the same as in the first experiment except an exhaust line and a flow meter on the oxygen supply line were added. The exhaust line permitted the purging of the container, and the flow meter made it possible to determine the relative oxidation rate under static conditions.

Tests were conducted at stabilized temperatures from 600 to 2000° F with an initial oxygen pressure of 15 psi. In the case of the sealed container with a fixed volume of oxygen, the pressure dropped off from 15 psi to zero in 10 seconds. Next, with the exhaust valve closed and the specimen at stabilized temperatures from 600 to 2000° F, the flow rates of oxygen were observed. At 600° F, the flow rate was slightly less than at 2000° F, with the intermediate points on a more or less linear relationship.

When oxygen gas was purged past the specimen, a white smoke identified as molybdenum trioxide (MoO_3) was blown out the exhaust. The previous run was repeated again observing the flow rate of oxygen immediately after the exhaust valve was closed. As expected, the flow rates in this dynamic purging setup exceeded those in the previous static run, but not by sufficient magnitude to explain the unusual results obtained in the first experiments, which included the ceric oxide pellets. The molybdenum capsule was completely consumed during these runs.

Sufficient work has not been done to draw definite conclusions concerning the phenomena taking place. The problem is certainly more complex than was originally anticipated. Because of the unusual results obtained, it raises some questions concerning the safety of such a heat source. Therefore, this phenomena should be understood prior to attempting to use such a heat source in a practical device.

Gas sampling device. The purpose of the device is to take a gas sample from the fueled capsule after it has decayed over approximately one half life. The first approach was to use a gland or gasket method of joining the gas sampling device to a tube that had been welded to the molybdenum capsule prior to the fueling. Difficulties were encountered in drilling open the capsule without admitting a contaminating gas or losing the gases present in the capsule. This would be a very difficult hot cell operation, and the approach was abandoned. It was decided to design a gas-tight container for the capsule such that when the time came to take the sample, the capsule could be placed in this container, sealed and a plunger struck to break open the capsule. A valved connection to an evacuated gas bottle would be attached to the container for taking the gas samples. A container was purchased commercially which only required the addition of a plunger. This setup is shown in Fig. IV-39. A welded capsule was placed in the container, the capsule broken and a gas sample successfully taken and analyzed (see Fig. IV-40). This portion of the work is complete and the device is ready for shipment to ORNL.

Environmental testing of unit 1B. Thermo Electron Engineering Corporation delivered Unit 1B, shown in Fig. IV-17, to Martin in the middle of March. On March 25, environmental dynamics tests were begun on this unit.

The generator was subjected to vibration and acceleration tests in each of the principal orthogonal planes. The test specifications were those developed by the Jet Propulsion Laboratories. The test equipment used included a Calidyne vibration shaker and a Genisco centrifuge.

A pretest electrical check of the generator was made using the test setup and actual equipment that would be used during the dynamic testing. This was done to provide a correlation with the test data supplied by TEE CO and to serve as a checkout of the circuitry and test setup employed. The results of these pretest data would then serve as a basis of comparison for during-test and post-test data. A constant load of two ohms was then applied to the generator, and this load was used during the entire test program. Five thermocouples were attached to the generator, which were continuously monitored and recorded on an oscillograph. The identification of the principal planes and the location of the thermocouples are shown in Fig. IV-41.

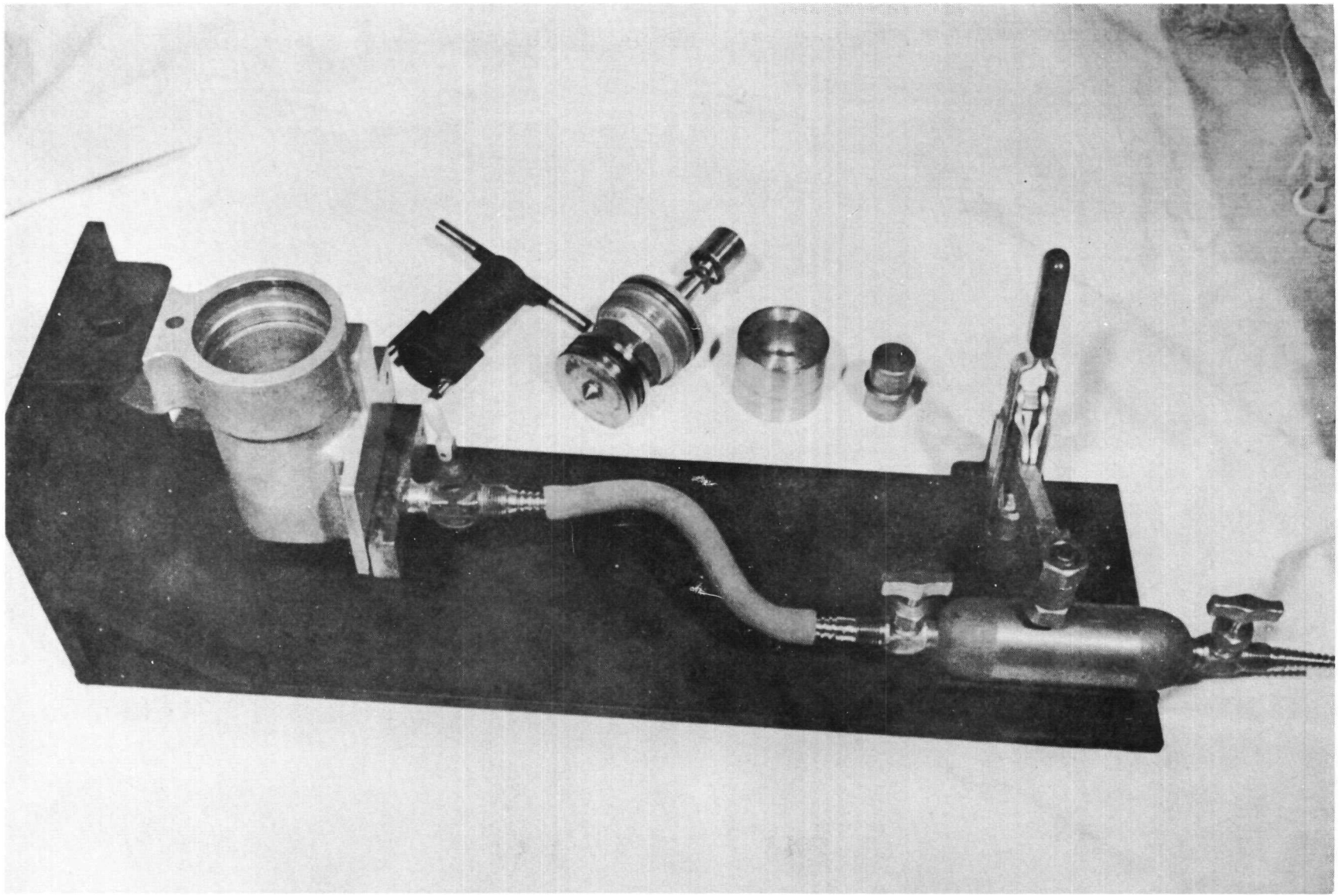

Fig. IV-39. Gas Sampling Device

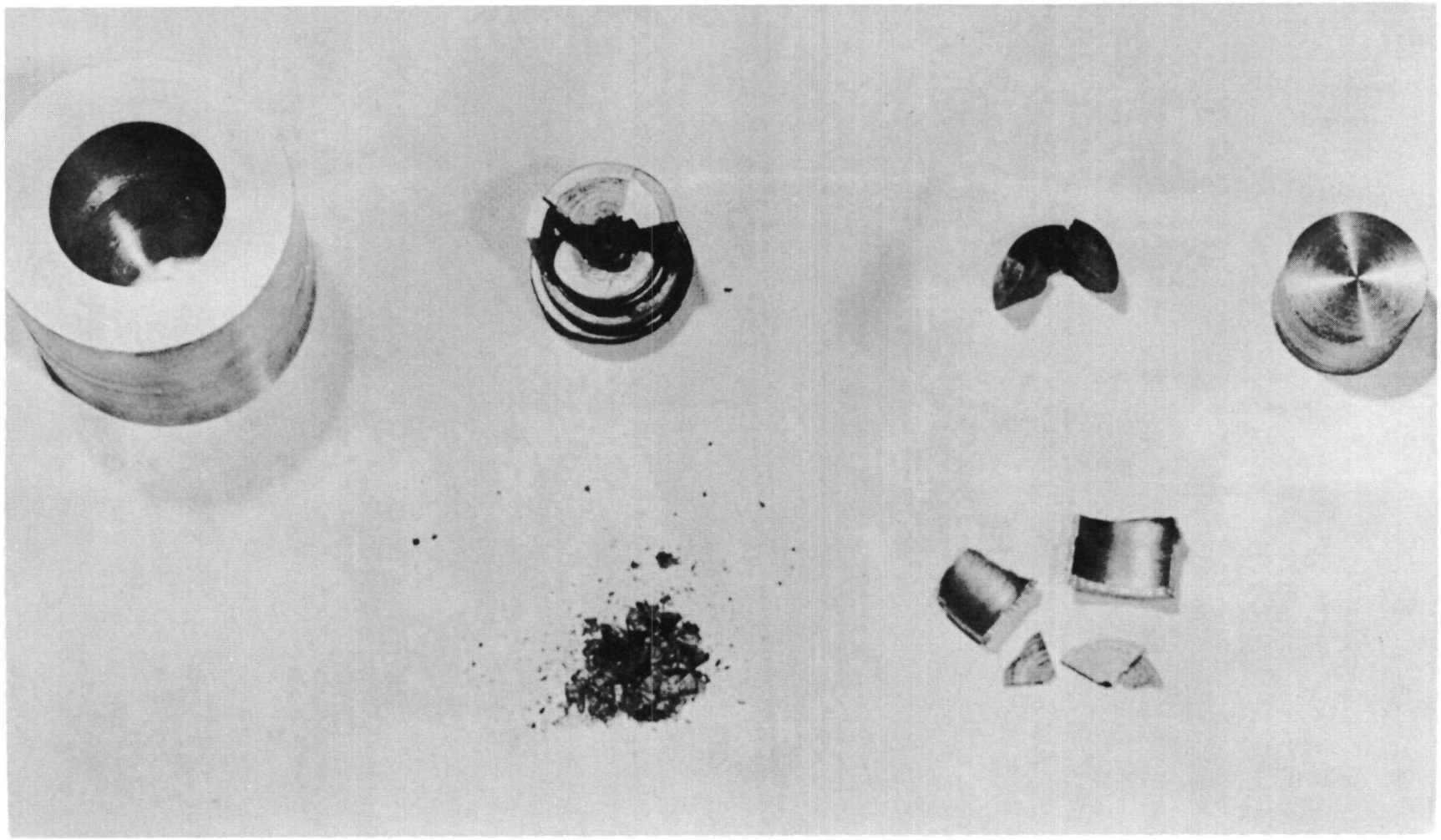

Fig. IV-40. Results of Operating Gas Sampling Device

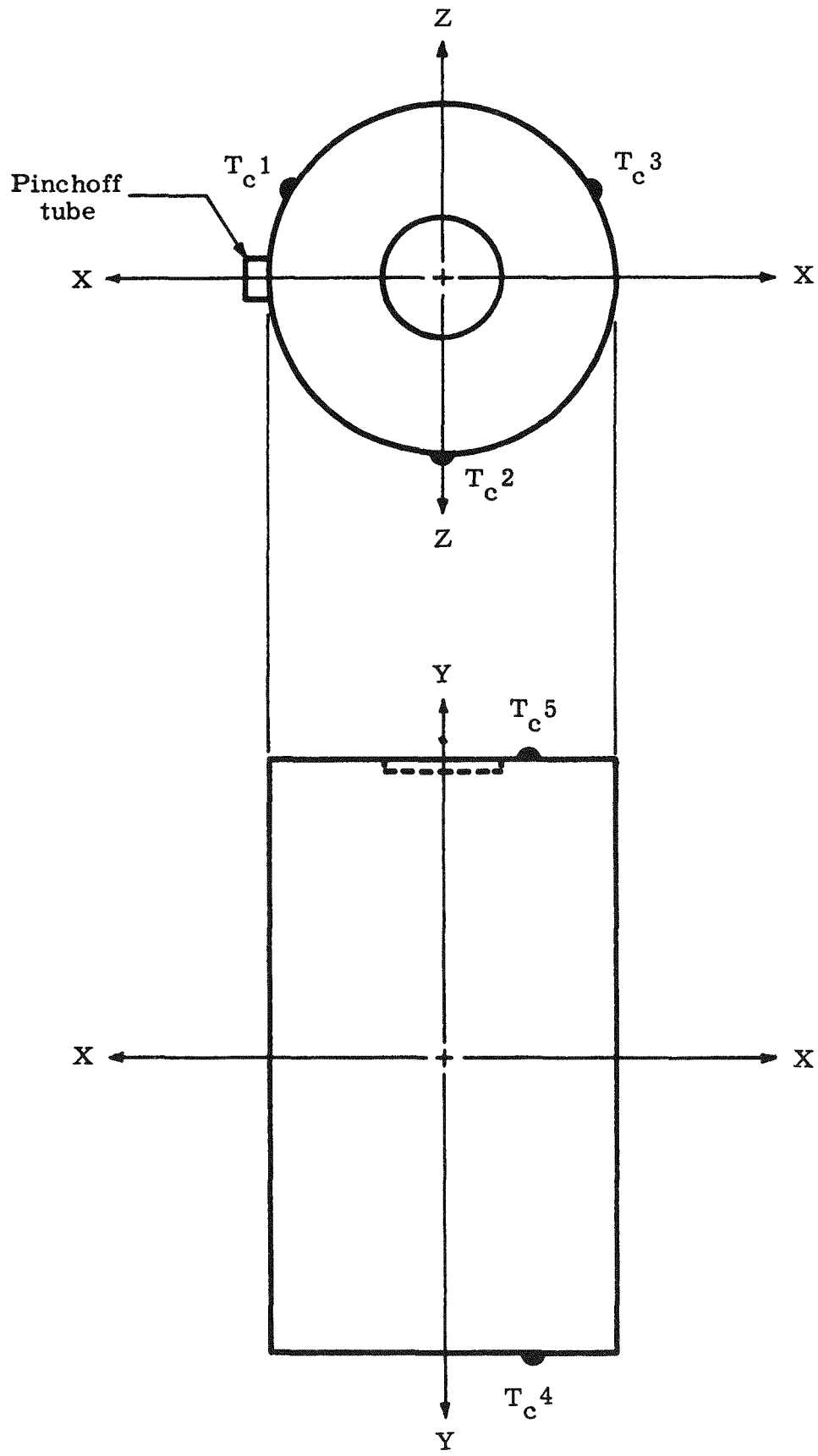

Fig. IV-41. Planes of Force

a. Acceleration tests

The specifications for the acceleration tests called for a maximum of 15-g static acceleration for five minutes in each of the three principal orthogonal planes. The tests were conducted in discrete steps as shown in Table IV-6.

TABLE IV-6

Acceleration Test Sequence

Step	1	2	3	4	5	6	7
Time--min	5	2	2	5	2	2	5
Level--g	0	5	10	15	10	5	0
RPM	0	76	105	125	105	75	0

Tests data were taken before, during and after each test to determine the effects of the simulated environment on the generator performance.

The output remained stable for the tests in the X and Z planes. Acceleration along the Y plane (the axis of the generator) resulted in erratic output. This is explained by a variation in the interelectrode spacing. The entire test cycle was completed for the Y plane even though the output was unstable. Upon completion of the test, the output immediately returned to its ambient level.

b. Vibration test

The vibration test was conducted using a Calidyne Model No. 177A vibration system. A magnetic tape of the vibration levels for this test was furnished by the Jet Propulsion Laboratory. The tape consisted of a sinusoidal vibration of 5 g rms from 15 to 500 cps, superimposed on a random signal of 5 g rms, band-limited between 15 to 1500 cps for five minutes. The second portion of the tape consisted of a sinusoidal vibration of 8 g rms from 500 to 1500 cps, superimposed on a random signal of 5 g rms, band-limited between 15 and 1500 cps for five minutes. Two test cycles, each 10 minutes in duration, were to be conducted in each of the three principal orthogonal planes. Again test data were taken before, during and after each test to determine the effects of the induced loads on the generator performance.

The vibration test was initiated in the Z plane. At approximately 500 cps, a resonant condition was noted within the generator. The generator output, which was stable at this point, immediately dropped off from 0.597 volt and 0.275 ampere to 0.163 volt and 0.075 ampere, a decrease

of approximately 94%. The test was discontinued at approximately 800 cps. The generator in the test fixture was removed from the Calidyne. The fixture was tapped lightly on the sides. The generator output returned to approximately 80% of its normal output. However, the output gradually dropped to 40% of the normal over a three-hour period and stabilized at 40% output. The generator was tapped lightly again, and the output climbed to 80%, but again fell to the 40% level over a three-hour period. The tests were discontinued and the generator returned to TEE CO for examination. This examination revealed that one cell was operating satisfactorily and accounted for the 40% output. An intermittent short had developed in the second cell. This accounted for the erratic behavior of the power output. The total operating time on the generator during the tests was 276 hours.

These tests have provided two vital inputs for the design of the curium-fueled unit. The design must be such that no serious resonant points exist between 15 and 1500 cps. This should not present any great difficulty and probably can be accomplished by breaking up the symmetry of the generator design. The second significant fact is that the means of spacing must be such that it provides positive restraint in all three planes. Several designs are now being evaluated to accomplish this.

D. SUBTASK 5.5--OPERATIONAL THERMOELECTRIC 2- TO 5-WATT GENERATOR FOR SPACE USE*

The objectives of this Subtask are to prove the operational capabilities of the SNAP-III-type generator through tests simulating the anticipated environments and to develop conceptual system designs.

1. Generator Operational Tests

Operational environments.

a. Vehicle induced

The final summary report, MND-P-2101, Volume III, has been distributed in accordance with the SNAP distribution list.

b. Ambient induced

The altitude chamber tests were completed using the 3M1G4 unit which had a black oxide coating on the external surface. This coating was formed using the Du-Lite Chemical process. A typical plot of output voltage versus amperage is shown by Fig. IV-42. The maximum generator outputs for each ambient temperature consistent with hot and cold junction temperature limitations are summarized by Fig. IV-43.

---

* R. J. Wilson

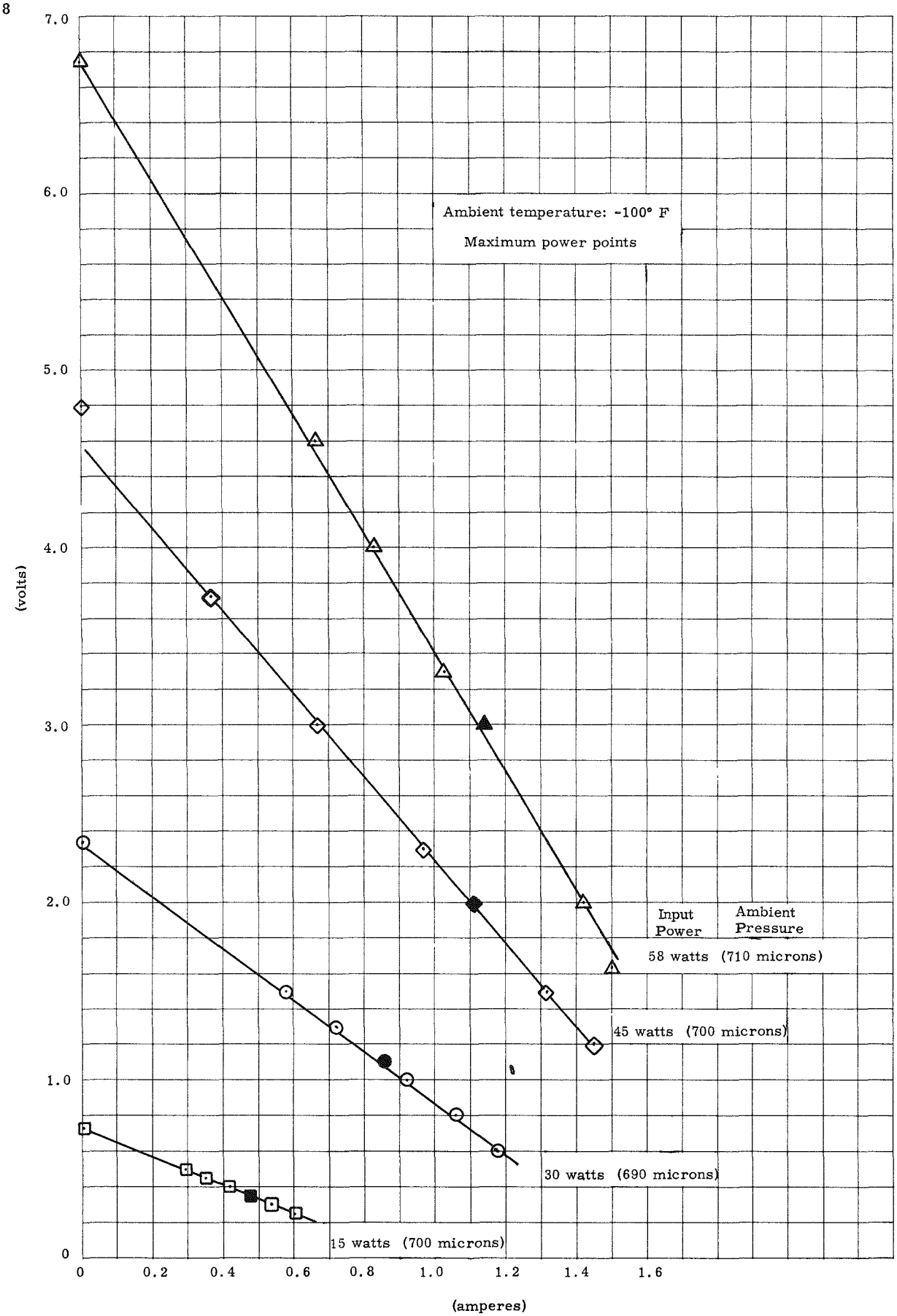

Fig. IV-42. Altitude Chamber Test Results, Oxide Coated Generator Surface

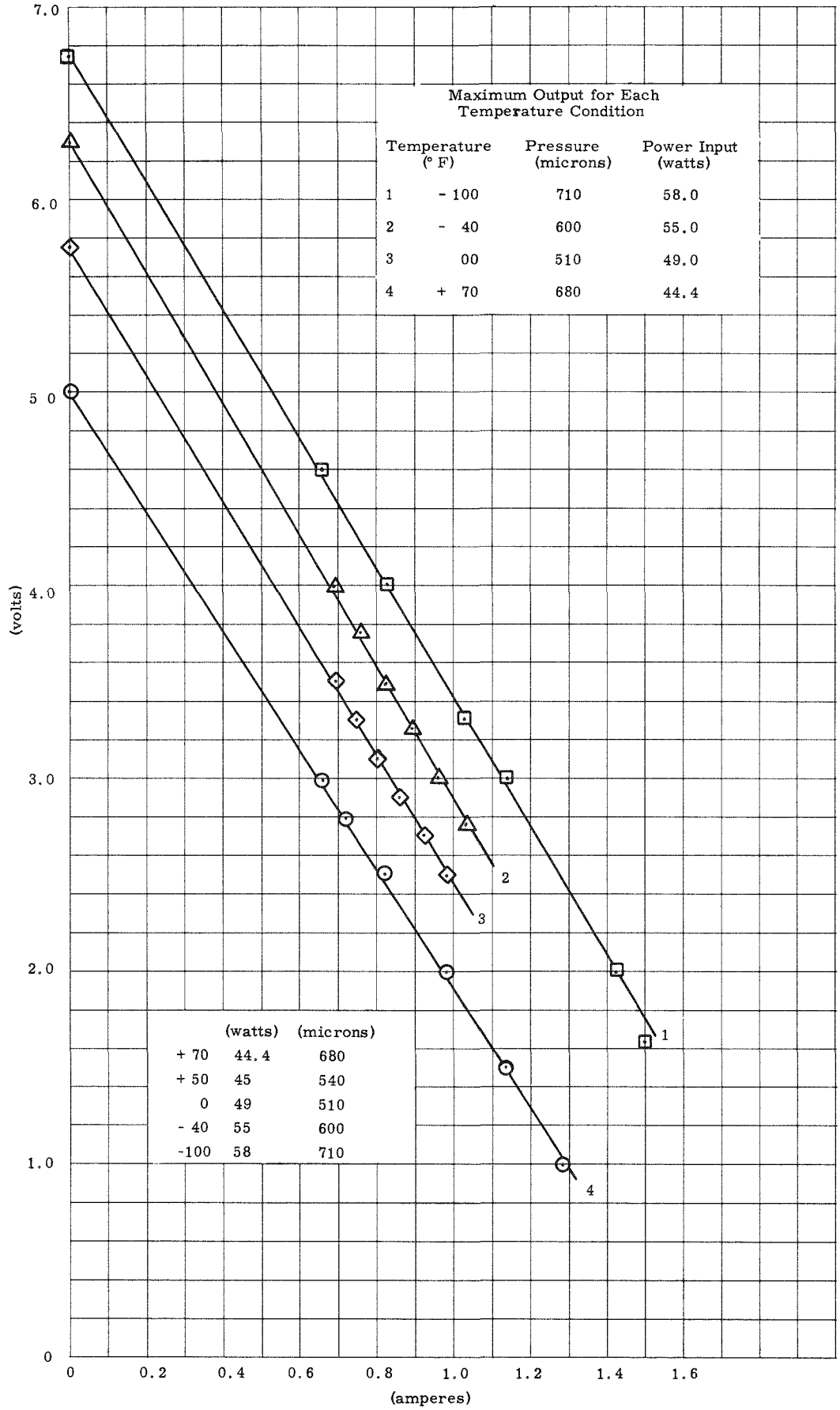

Fig. IV-43. Altitude Chamber Test Summary, Oxide-Coated Generator Surface

The generator electrical output reached a maximum of 3.39 watts as compared to 3.79 watts with the surface painted. This indicates that the copper oxide coating possesses a lower emissivity than the painted surface. An informal report summarizing these test results has been prepared for internal use by other projects.

Three sets of thermoelectric couples were prepared for sublimation testing in the electrically heated fixture. The Seebeck voltage output of the couples was checked prior to and after spraying with zirconium oxide. The checks were accomplished by applying a hot soldering iron tip to four places on one end of the element. The following results indicate that the coating does not significantly affect the performance of the thermoelectric.

Element Type and Number	Iron Temperature (°F)	Seebeck Voltage (millivolts)			
			Points		
		Centerline	1	2	3
		Before Coating			
P2	601	41.8	42.1	41.0	41.3
P5	601	38.0	37.7	39.5	37.2
N5	601	51.0	50.9	50.1	52.0
N6	602	53.0	54.0	53.8	52.9
		After Coating			
P2	606	42.8	44.9	44.6	44.1
P5	602	37.6	37.4	37.1	37.3
N5	605	52.1	51.4	51.1	50.0
N6	605	51.1	52.9	51.9	52.5

An encapsulated couple was also fabricated for testing in the electrically heated fixture. This couple uses an aluminum oxide ceramic sleeve to protect and support the element. Performance tests of the couple revealed inadequate output and rework was required before a continuity check indicated a satisfactory assembly. The couples were then inserted in the electrically heated test fixture and prepared for

test. This preparation consists of purging with a mixture of 85% nitrogen and 15% hydrogen gas while the unit is being heated. The first phase of the test consisted of 300 hours of operation at a hot junction temperature of 1000° F with the generator evacuated to 20-micron pressure. Originally, the first test phase planned was a 200-hour run at 900° F, but tests conducted by other projects under similar conditions indicated that sublimation effects were negligible over this time period. To accelerate the effect, the procedure was changed to incorporate two 300-hour runs at the higher hot junction temperatures.

After the hot junction temperature was stabilized at 1000° F, data were taken twice daily throughout the test. The output power decreased steadily from test initiation and could not be measured after 300 hours of operation. The encapsulated P element reversed polarity and a large increase occurred in the internal resistance of the entire unit. Upon disassembly, extensive sublimation effects were evident. An electrical short existed between the element cavities due to a deposit of sublimed material on the insulation block at roughly the 880° F isotherm. This deposit can be seen in Fig. IV-44. Extensive deterioration of the uncoated couple resulted in a 0.15-inch decrease in element length as shown by Fig. IV-45a. Figure IV-45b provides evidence that a similar but slightly inhibited reaction took place within the ceramic sleeve of the encapsulated couple. Sublimation effects were greatly reduced through the spray coating as depicted by Fig. IV-45c, but element performance was degraded by the increase in contact resistance. This disadvantage of spray coating may be offset by continuing the second coat of iron completely around the element hot end although the oxide coat is stopped short as before. Components for a second run to test this method are currently being prepared.

The life test of the generator and orifice combination to prove power flattening feasibility was halted after 24 days of operation. The generator output power deteriorated from 2.46 to 2.31 watts during this period. This deterioration became more significant than the change due to internal pressure variation and the test was halted. The generator internal resistance has increased from the original three to four ohms. However, sufficient data were recorded to indicate feasibility. An analysis was conducted to correct the power flattening test data for generator deterioration. When returned to the original conditions of internal gas pressure and input power, an output of 2.31 watts was obtained as compared to an initial output of 2.46 watts. Using these figures, a correction factor was applied to the recorded data. The net change in generator output attributable to the changing input was 1 to 2%. Generator internal pressure was 38 mm of mercury higher than optimum at termination of the test, although it was deliberately lowered a similar amount at the start of the test. This pressure variation amounted to 15% of that desired and contributed to the output variation. Test results are shown in Fig. IV-46.

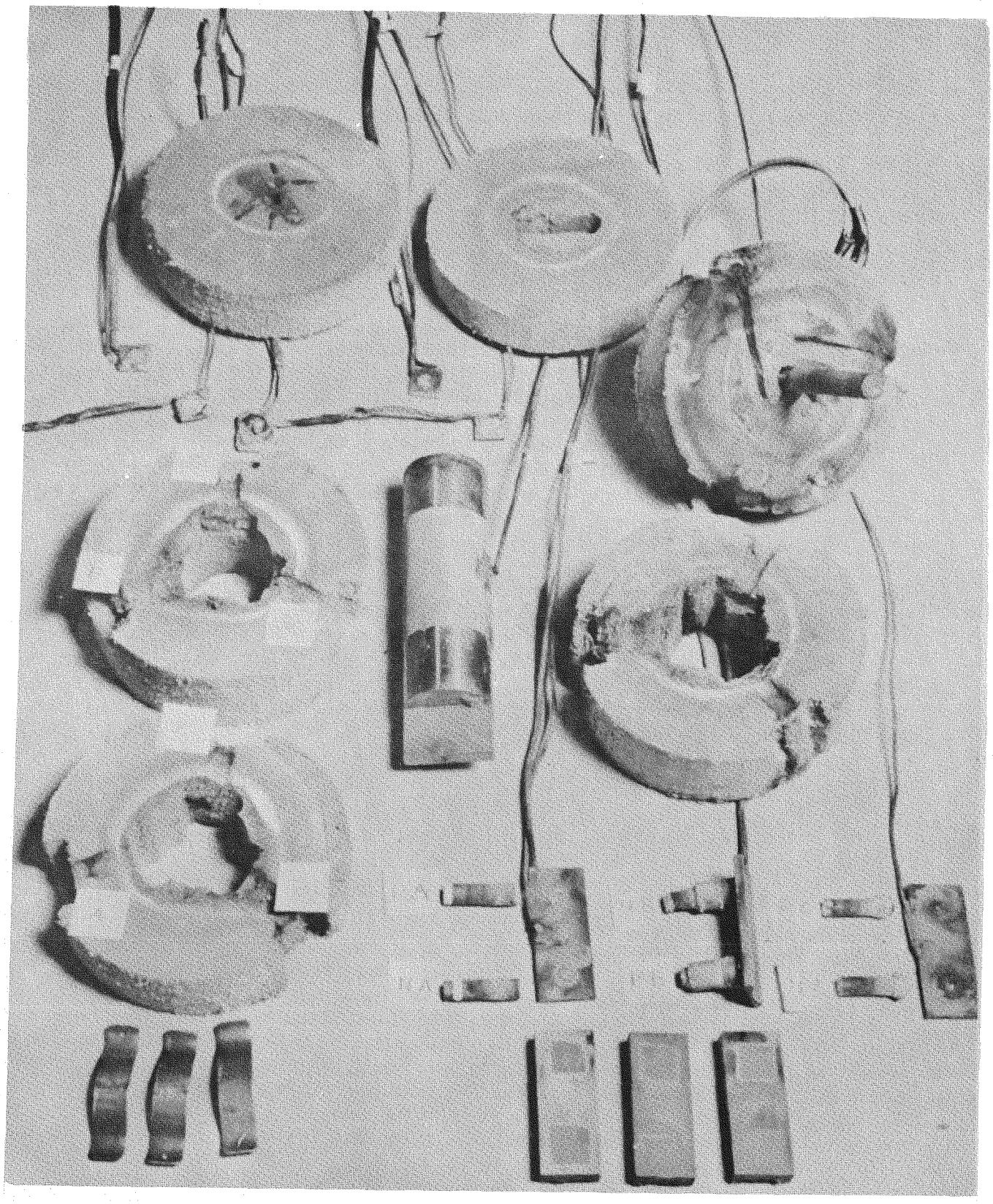

Fig. IV-44. Sublimation Test Fixture Components

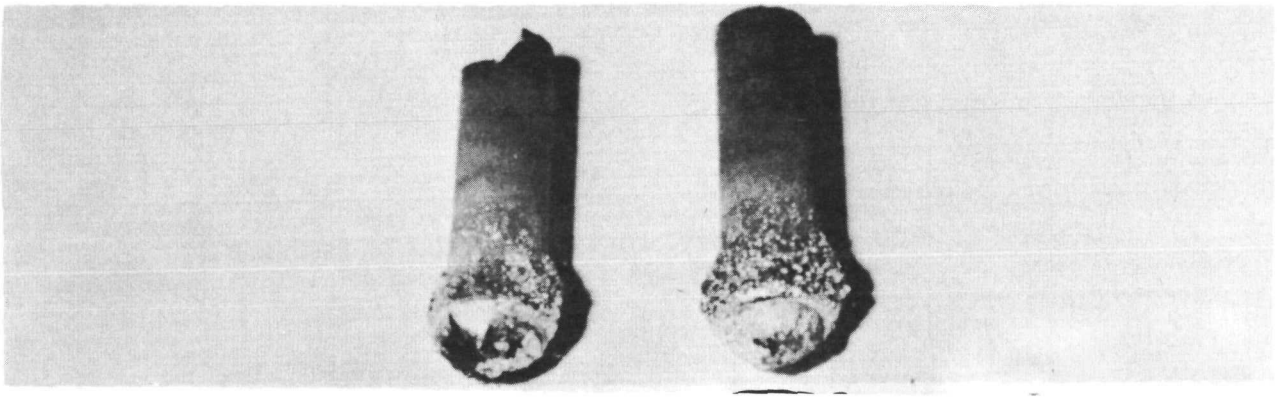

P-C N-C

Fig. IV-45a. Uncoated Elements, Sublimation Test

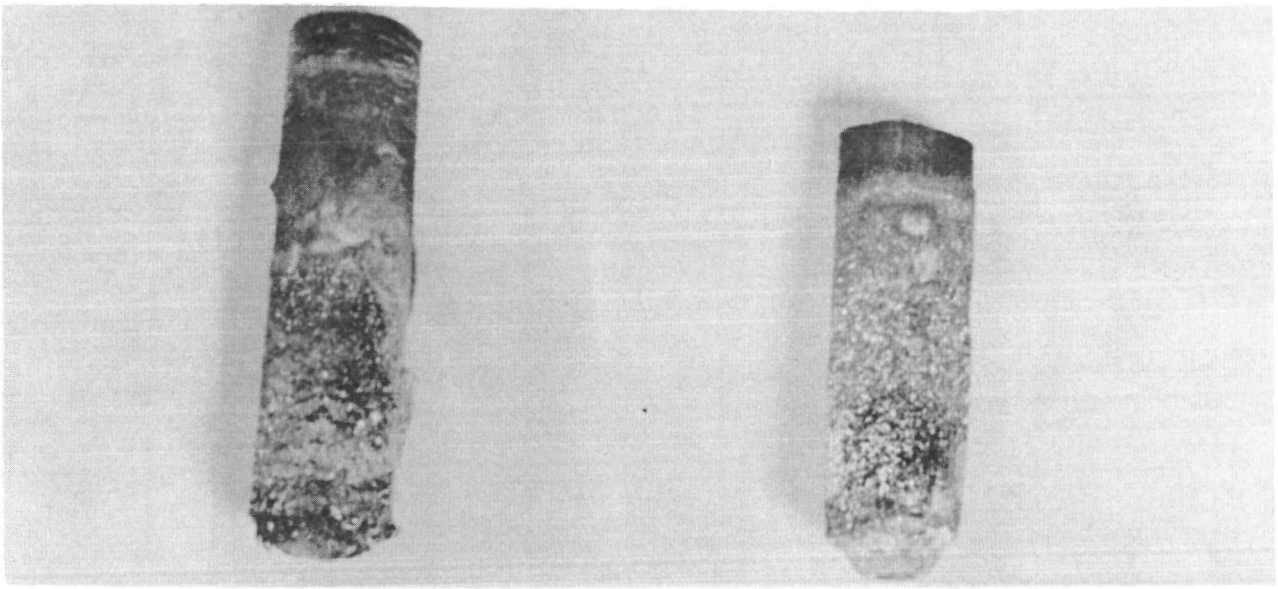

NB PB

Fig. IV-45b. Encapsulated Elements, Sublimation Test

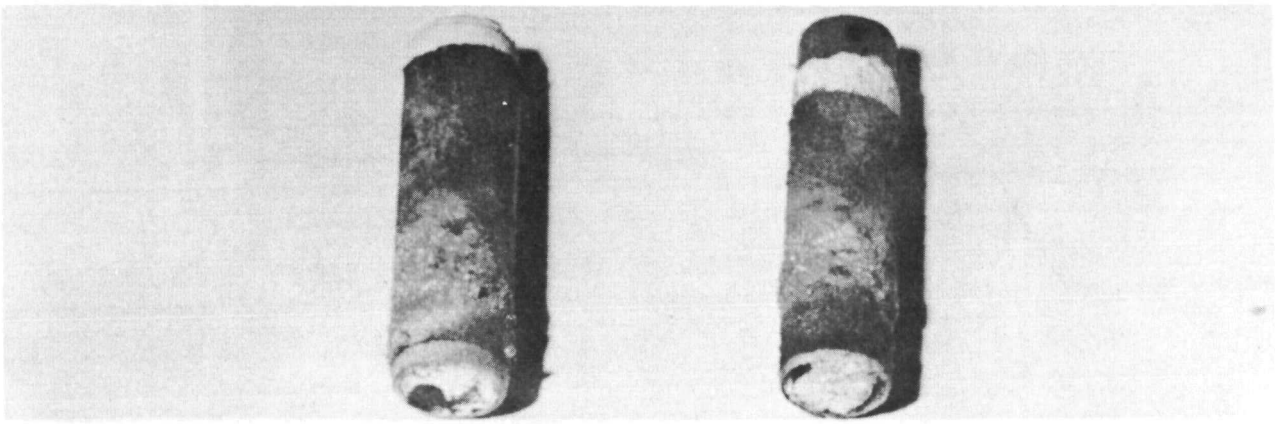

P-A N-A

Fig. IV-45c. Spray Coated Elements, Sublimation Test

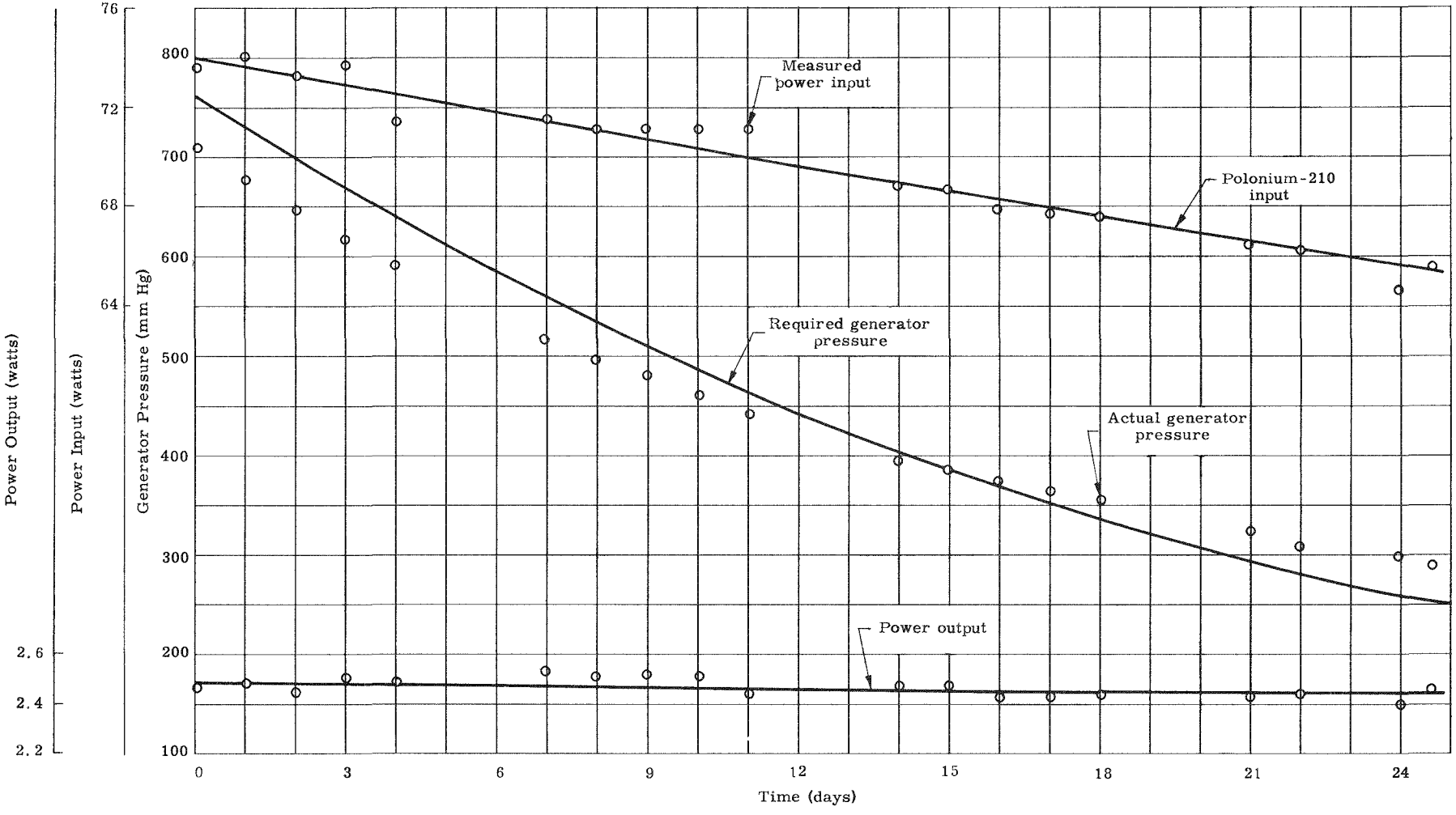

Fig. IV-46. SNAP-III Power Flattening Simulated Life Test

The generator deterioration is believed due to an increase in internal resistance as a result of sublimation. This generator has been operated at low internal pressures during the preliminary test phases for a period in excess of 1200 hours. Results of the power flattening tests are summarized in Report MND-P-2318. This control method is feasible although the hot junction temperature may have to be reduced to extend generator life at reduced internal pressure.

Missile failure environments.

a. Launch pad failure

The financial arrangements to transfer the necessary funds to Aberdeen Proving Ground were completed. The shock wave portion of these tests was successfully conducted late in the reporting period and only preliminary results are available. One-third-scale specimens of both generator and bare capsule were included as shown in Fig. IV-47. An oxide coating, sprayed over the heater wire wrapped around the capsule, is apparent on Specimen No. 3. Blast effect, apparent in Fig. IV-48, scoured the bare capsule specimen but did not completely remove this oxide coat from the capsule in the generator specimen due to the protection afforded by the shell. Final results will be available when the Aberdeen report is received.

The preliminary results of the plasma jet tests discussed in the next section indicated that it may be desirable to change the generator shell material from copper to aluminum. The most significant effect of this material change on the integrity of the isotope capsule would be during a fire resulting from a launch pad abort. To determine this effect, two additional specimens were fabricated for inclusion in the high temperature test. The specimens were similar to those previously assembled except aluminum is used in lieu of copper for the outer shell. These additional specimens will not affect the test procedure or cost.

b. Impact

These tests were successfully conducted in conjunction with Task 2 early in the period. A final report giving test details has not been received from Aberdeen. Figure IV-49 shows the result of impact of bare capsule specimens against granite and concrete. Although extensive abrasion and weld deformation were caused by the granite impact, leak tests proved that capsule integrity had been maintained.

c. Corrosion

The salt water corrosion test was concluded after 720 hours of operation. The specimens were removed, cleaned, vacuum dried and

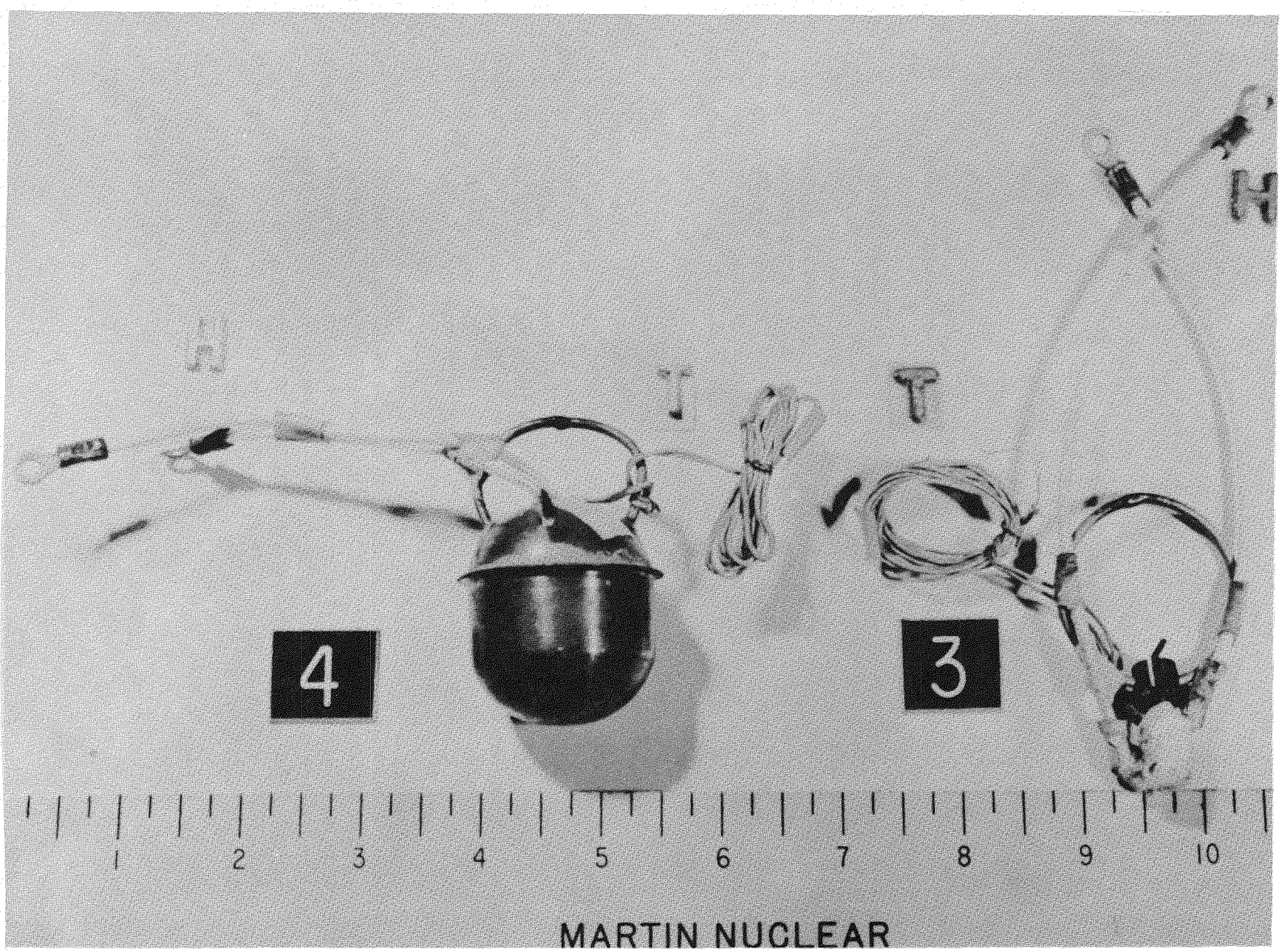

Fig. IV-47. Shock Wave Specimens Before Test

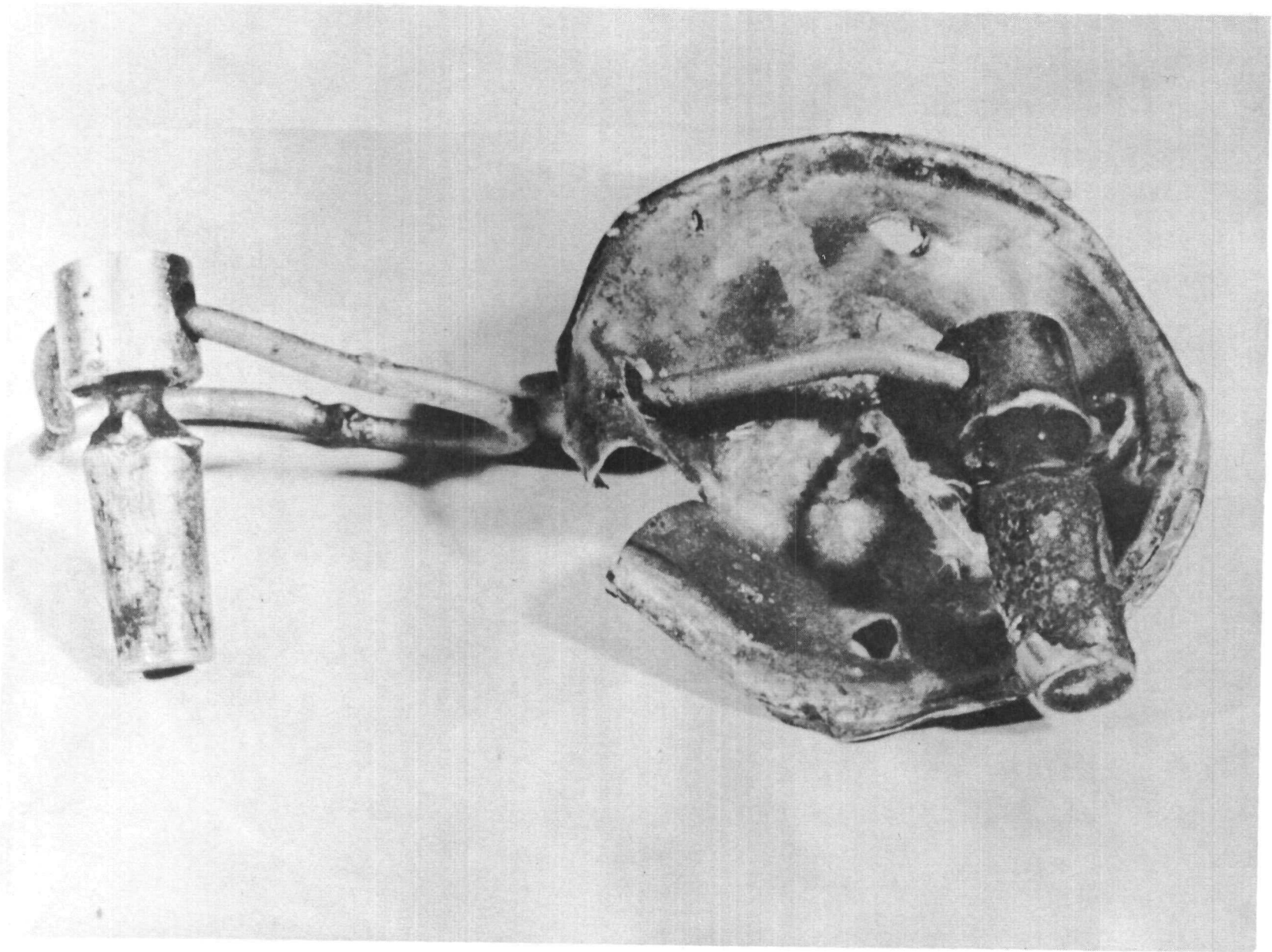

Fig. IV-48. Shock Wave Specimens After Test

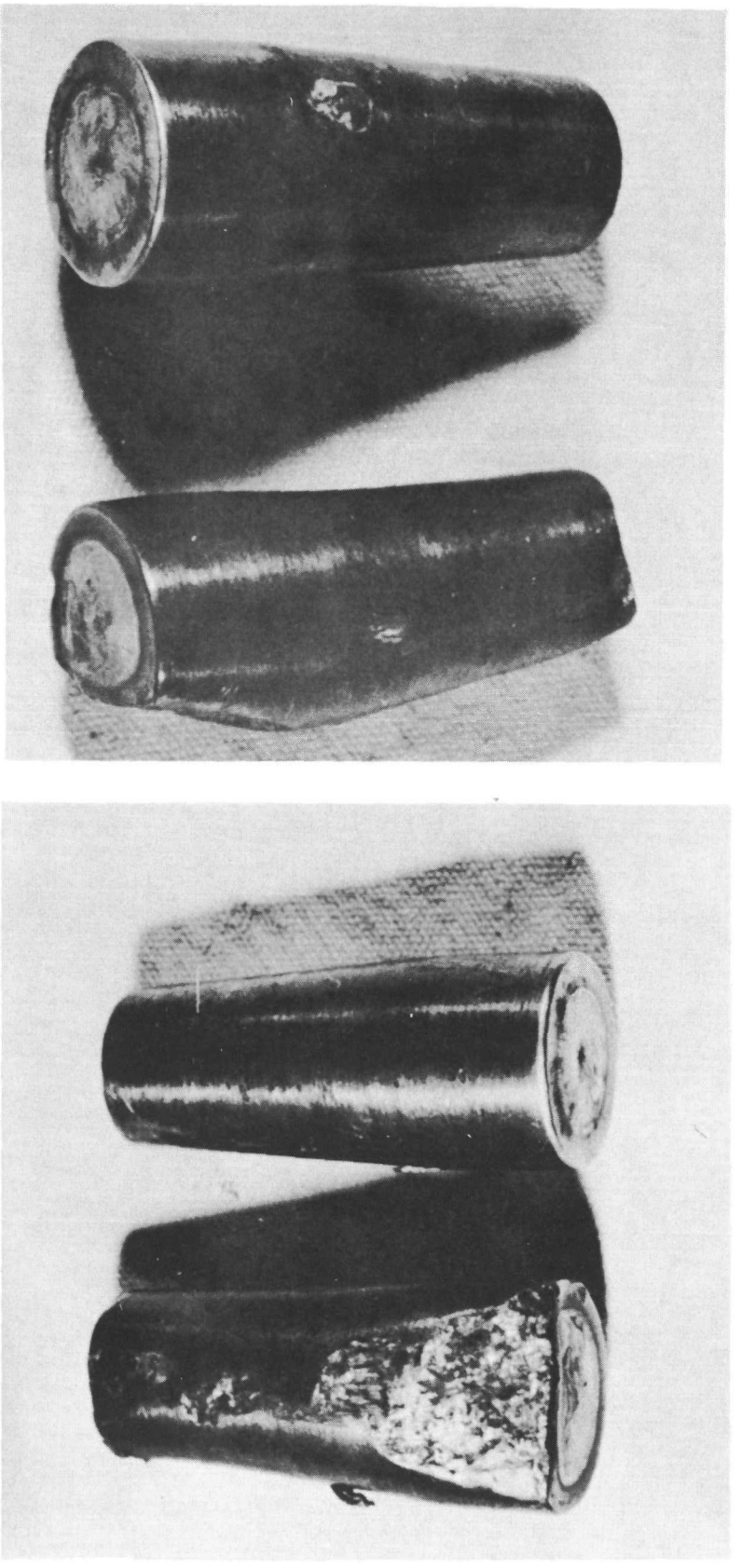

Fig. IV-49. Impact Test Specimens

weighed. The weight change and corresponding corrosion rate is as follows:

Material	Weight Change (gm)	Corrosion Rate (mg/sq decimeter/day)
	Test samples (internally heated)	
Haynes-25	-0.0094	0.6
Haynes-25	-0.0108	0.7
Type 304 SS	-0.0217	1.5
Type 304 SS	-0.0266	1.9
	Control specimens (unheated)	
Haynes-25	-0.0006	< 0.1
Haynes-25	-0.0010	< 0.1
Type 304 SS	-0.0008	< 0.1
Type 304 SS	-0.0010	< 0.1

Several conclusions may be drawn from the data:

(1) Haynes-25 was generally unaffected. Examination of a cross section of the sample showed no penetration.

(2) The Type 304 stainless steel showed some attack in the area of the weld and severe crevice corrosion at the junction of the rubber tubing and the Type 304 stainless steel tube as shown in Figs. IV-50a and IV-50b. The deepest penetration was 22 mils, nearly one-half the tube thickness. Crevice corrosion was found on both stainless steel specimens.

The salt spray corrosion test was concluded after 720 hours of operation using a 20% salt solution. The test specimens were removed and chemically cleaned. Blanks of each material were simultaneously cleaned to verify that the cleaning solution removed only the oxide. The samples were then rinsed, vacuum dried and weighed. The weight change and corresponding corrosion rate is as follows:

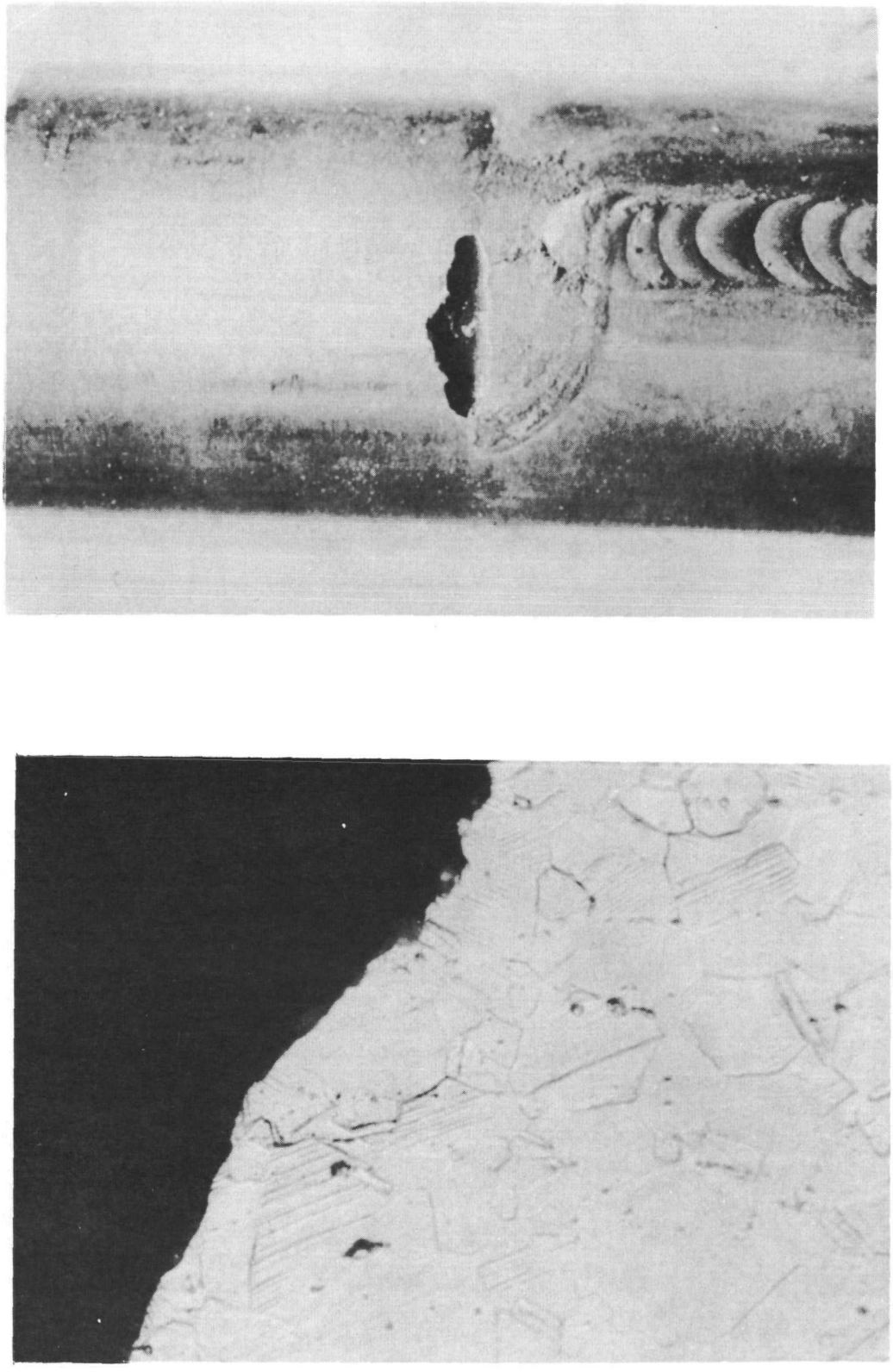

Fig. IV-50. Salt Water Test Specimen--Type 304 Stainless Steel Material

Material	Weight Change (gm)	Corrosion Rate (mg/sq decimeter/day)
	Test samples (internally heated)	
Haynes-25	-0.0186	0.6
Haynes-25	-0.0180	0.6
Type 304 SS	-0.0846	3.0
Type 304 SS	-0.1134	4.0
	Control specimens (unheated)	
Haynes-25	-0.0010	0.1
Haynes-25	-0.0002	0.1
Type 304 SS	-0.0109	1.3
Type 304 SS	-0.0103	1.2

Several conclusions may be drawn from the data:

(1) The test had a negligible effect on Haynes-25. Examination showed some very slight general corrosion as shown in Fig. IV-51.

(2) The Type 304 stainless steel was heavily oxidized, although at 600° F there was no indication of sensitization of the material. The material was badly pitted as shown in Fig. IV-52a. Pits as deep as eight mils were found. Stress corrosion cracking was noted at several points as shown in Fig. IV-52b. Depth of penetration was found to average 17 mils.

d. Ejection

The ejection system tests were resumed using the modified thruster. These modifications were designed to effect a 15% increase in the initial velocity while holding an acceleration level of 400 g. Three shots resulted in no increase in vertical rise height. This indicates that the limits of this thruster configuration were reached and no significant increase in thruster performance could be anticipated from these units.

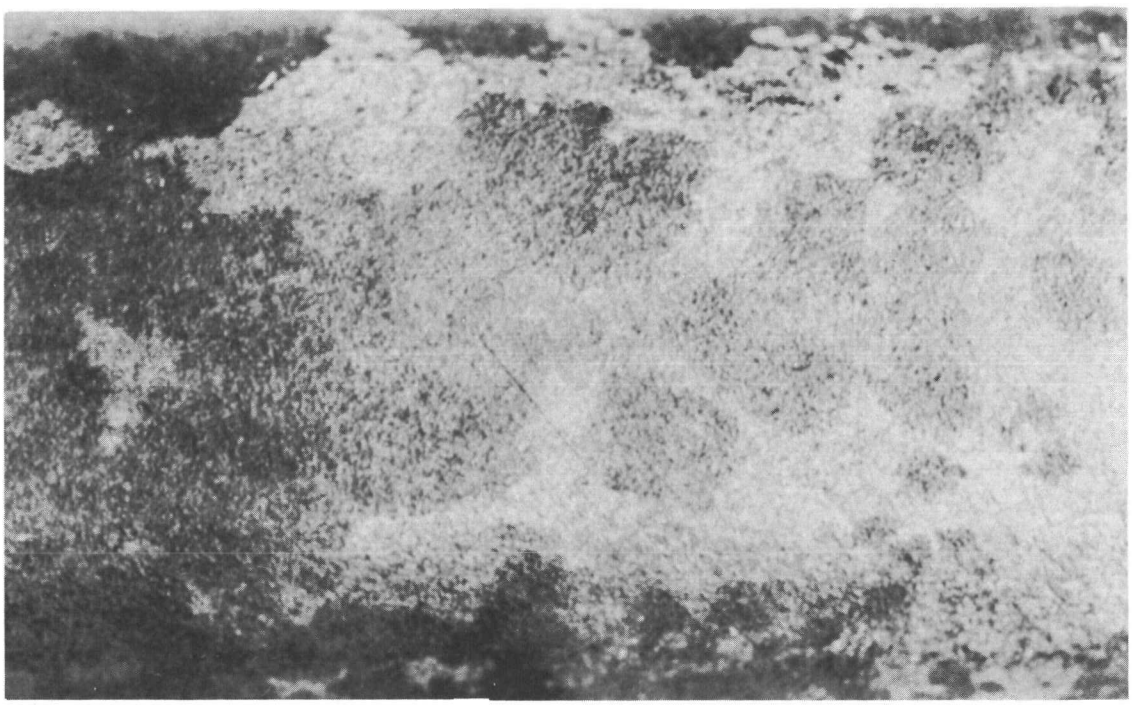

Fig. IV-51. Salt Spray Test Specimen--Haynes-25 Material, Magn 4X

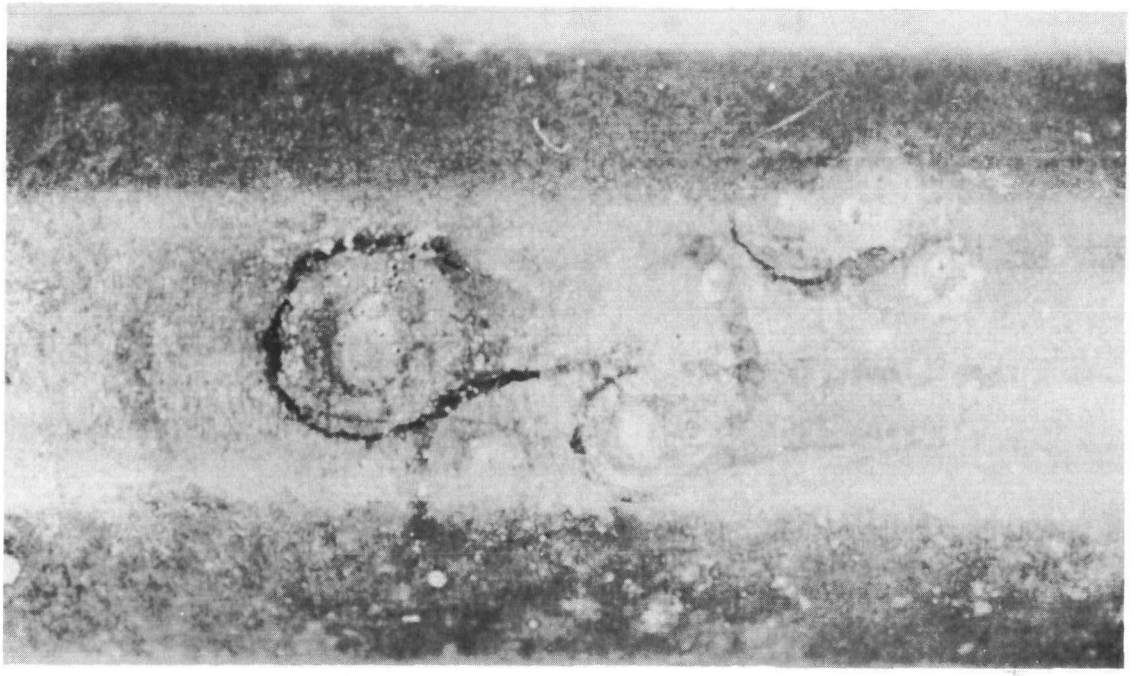

Fig. IV-52a. Salt Spray Test Specimen--Type 304 Stainless Steel Material

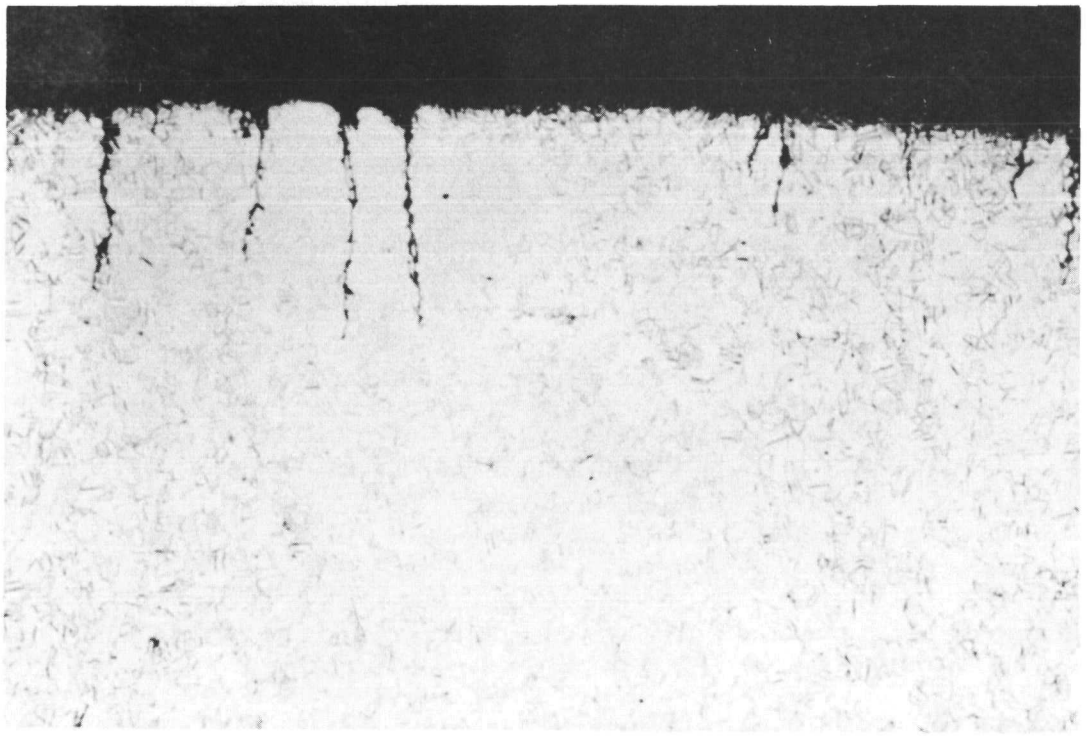

Fig. IV-52b. Photomicrograph of Salt Spray Test Specimen--Type 304 Stainless Steel Material, Magn 100X

A new thruster unit was designed to use two M-48 squibs yielding increased performance. Deformation of the simulated generator shell and bearing cap have been negligible, which allowed the 400-g initial acceleration limit to be increased to obtain improved performance. Four shots were conducted with the following results:

Test Number	Date	Orientation	Results
1	3-24-60	Vertical	Rise 75 to 100 ft
2	3-28-60	Vertical	Rise indefinite--support bolts sheared
3	3-28-60	45 deg	Range 170 ft--support bolts sheared
4	3-31-60	45 deg	Range 271 ft

Although the range achieved on Test No. 4 is greater than the 200 feet desired, additional shots next period will determine the reproduction capability.

Re-entry environments.

a. Plasma jet tests

Testing was initiated and completed at the General Electric Aeroscience Laboratory. The heating curve derived from the trajectory studies was simulated by a square-shaped heating pulse, i.e., constant with time. This simulation provides the same total integrated heat input. Preliminary examination of the test report indicated that the copper shell maintained its integrity longer than calculated. This variation was reduced in the cases where the specimens contained only Min-K insulation by accounting for heat lost through conduction. However, the specimens containing an aluminum slug, simulating the generator cold junction, reacted in a manner not predicted by the machine calculations. The digital program utilized the simplifying assumption that the generator was composed of a homogeneous material which combined the properties of the aluminum cold junction ring and the copper shell. Although digital programs can determine the behavior of layers of different materials, a case where the inner layer has a lower melting point cannot be considered. This is especially true when the materials involved possess high heat capacity and thermal conductivity. The tests showed that this was the case as the conductivity of the copper was sufficient to melt the adjacent

aluminum. This phase change provided a sufficient heat sink to delay failure of the copper shell until the vapor pressure of the molten aluminum caused it to rupture. Although the ratio of aluminum to copper is lower in the actual generator, this situation may delay failure of the generator due to aerodynamic heating. Two methods of decreasing the heat input and, consequently, the time required for failure of the copper shell are feasible and may easily be incorporated in the generator construction. The first is to divide the shell into segments joined by solder connections. The solder may be selected to have a melting point so that failure will occur prior to the melting point of aluminum. The second method is to use aluminum rather than copper for the outer shell.

The test report and documentary film footage received from General Electric Aeroscience Laboratory is being utilized to correlate test data with the vehicle trajectories studied to determine final burnup or impact locations.

b. Internal pressure tests

Assembly of the test fixture was completed, but a portion of stainless steel hydraulic tubing failed during a test run at 1700° F. A special tube was fabricated of Inconel material by successive swaging operations using tubes with increasing diameters. The end of this tube was welded to the bottom of the capsule specimen through which a 1/8-inch diameter hole had been drilled. This arrangement proved satisfactory and pressure tests were initiated. Micrometer measurements accurate to 0.0001 inch were made and no permanent change in either diameter or length occurred. A Rockwell hardness check indicated a 9-point increase during the first 240 hours but only a 1-point increase during the next cycle of 144 hours. The capsule was maintained at 1100° F with an internal pressure of 9400 psi for a total of 528 hours. Temperature was increased to 1700° F, but failure of the Inconel connecting tube occurred after 12 hours. After repair, the pressure was increased to 30,000 psi for a 100-hour period. To prevent tube failure, the temperature was limited to 1100° F during this last phase.

Testing was continued using hydraulic fluid at room temperature to pressurize the capsule to 78,000 psi. At this point, valve failure interrupted the test. Diameter of the specimens midway in the tapered length increased from 0.8375 to 0.8390 inch, which was the first dimensional change observed. Testing will continue after valve repair.

c. Destruct system tests

The destruct tests were resumed using the isotope capsule and generator specimens. The effect of three different charges directed against bare isotope capsules was determined as follows:

Test Number	Charge Weight (gm)	Results
1	33	Complete penetration. Extensive flowering at entrance.
2	18	Complete penetration. 1/4-in. diameter minimum.
3	10.5	Similar to Test No. 2.

The explosive used in all cases was RDX manufactured by E. I. DuPont De Nemours and Company. The standoff in all cases was 2-1/2 inches since this distance is required to locate the charge external to the generator.

In the next series of shots, charges of various weights were directed against simulated generator specimens containing an isotope capsule. The test arrangement used a wooden block to support the specimen as illustrated by Fig. IV-53. Plywood sheets located behind the generator collected the debris expelled by the gas jet. The results are listed and illustrated by Fig. IV-54.

Test Number	Charge Weight (gm)	Results
1	34	Complete penetration. Exit 3/8-in. diameter.
2	34	Complete penetration. Exit 3/8-in. diameter.
3	18	Complete penetration. Exit 1/4-in. diameter.
4	10.5	Penetration depth 1-7/16 in. off center.

Since the last shot resulted in an off-center condition, the original location of the capsule within the shell was questioned. X-ray inspection of the remaining three specimens showed the capsule to be slightly misaligned. The location is currently being corrected. Specimen support will be revised for the three remaining shots to more accurately simulate the final mounting anticipated. The specimen will be supported only by the bearing cap with the shaped charge directed through a hole in the cup.

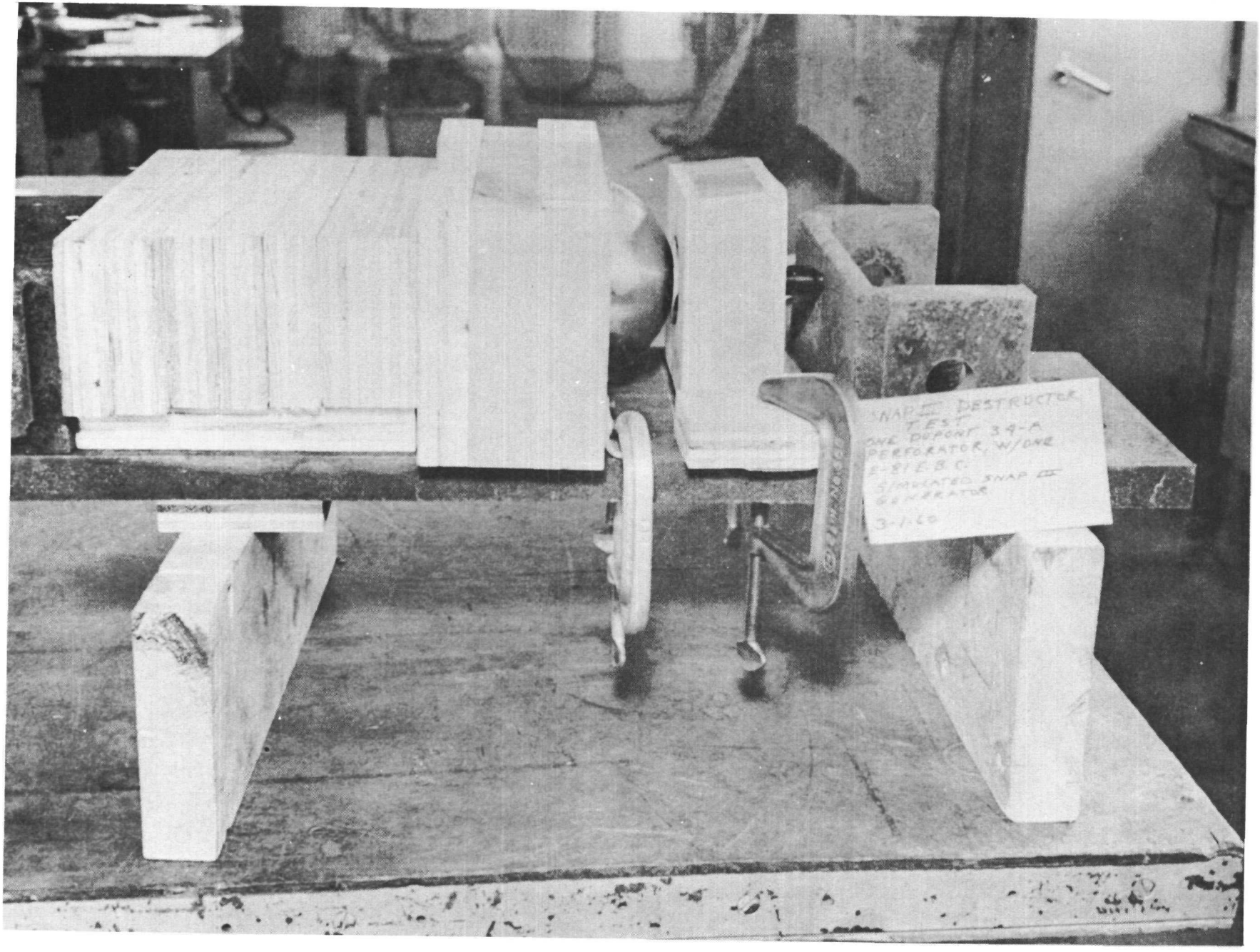

Fig. IV-53. Destruct Test Arrangement

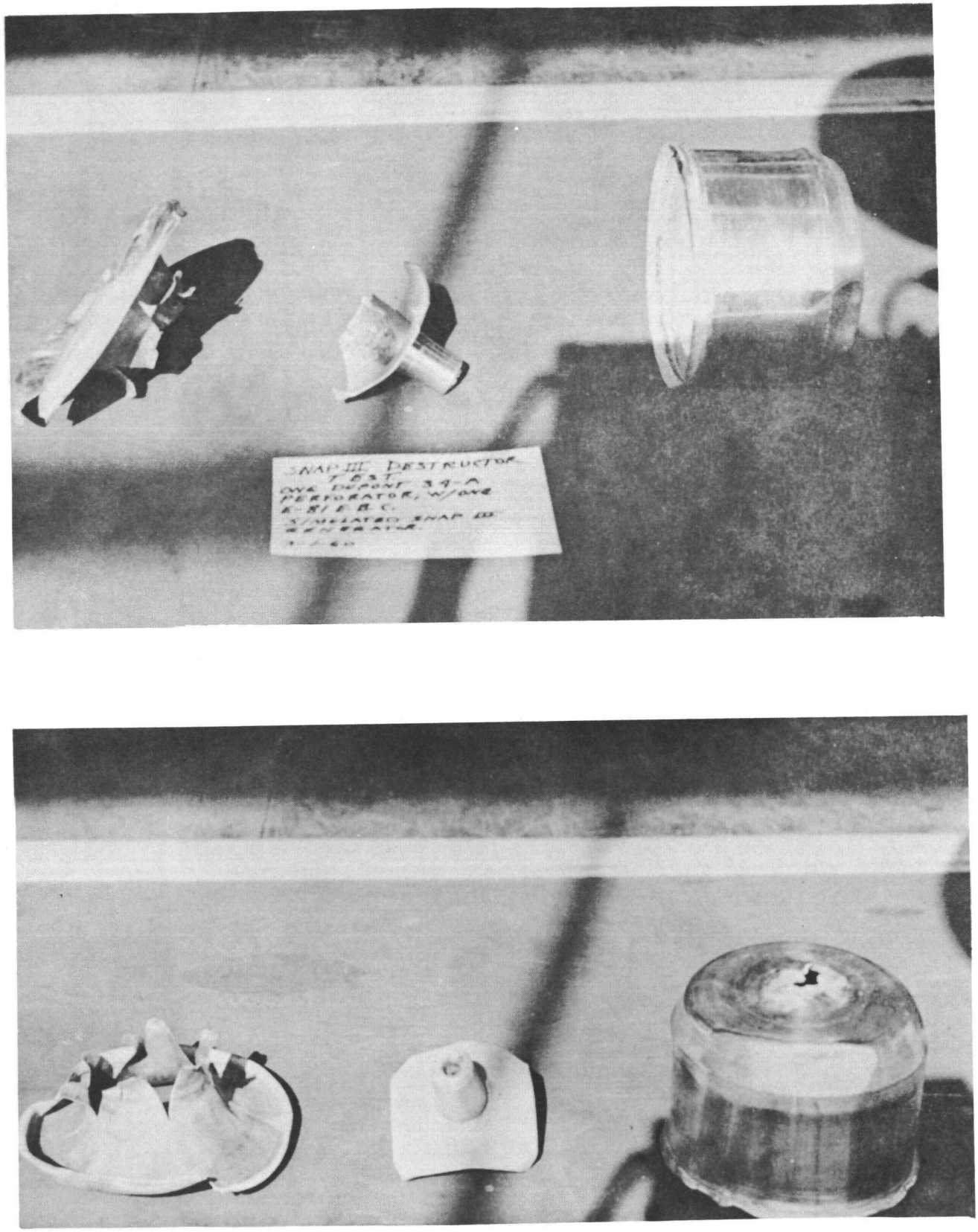

Fig. IV-54. Destruct Test Results

2. System Conceptual Design

Cerium-fueled system. The preliminary data from the altitude chamber tests were utilized to develop a plot of power output versus time using the heat input derived from Cerium-144 decay. This plot is presented in Fig. IV-55.

Polonium-fueled system. A similar plot has been developed using the heat input derived from Polonium-210 decay and is illustrated by Fig. IV-56.

An analysis of the aerodynamic burnup characteristics of the SNAP-III-type generator has been completed. This analysis was based on a circular polar orbit of 275 statute miles altitude. A vehicle similar to that used for the Discoverer series was synthesized to yield this orbit from a Vandenberg Air Force Base launch. Knowing the required orbital injection velocity and altitude, the final-stage trajectory was calculated using two-dimensional trajectory equations to fly the final stage back to the point of ignition. Using this trajectory, the thrust vector of the final stage was instantaneously deflected in pitch or yaw or was terminated at various times after ignition. Eighty-six different variations of missile failure were analyzed to obtain the maximum possible dispersion of the generator.

Equations to determine the temperature environment of a generator mounted in a missile nose cone, as depicted in Fig. IV-57 have been derived. For an extensive study, the problem should be programmed for computer solution. The equations are currently being evaluated by approximate methods to determine if a practical solution of this complex problem is feasible.

The generator mounting selected for heat transfer studies is illustrated by Fig. IV-58. For purposes of correlation with the altitude chamber tests, an equivalent space temperature was established. This temperature is a purely fictitious quantity which is determined by the generator surface temperature and the heat radiated from its surface. It represents the temperature of the imaginary spherical surface to which the generator radiates heat and takes into account the incoming radiation from the sun and other objects within view of the generator. The equivalent space temperature calculated was -135° F with the generator exposed to the radiation of the sun. The conclusion drawn is that the generator output in space will be equivalent to that achieved in the altitude chamber tests with an ambient temperature of -100° F.

Results of the ejection and destruction system tests have indicated that the larger thruster with M-48 squibs and the 34-gram shaped charge

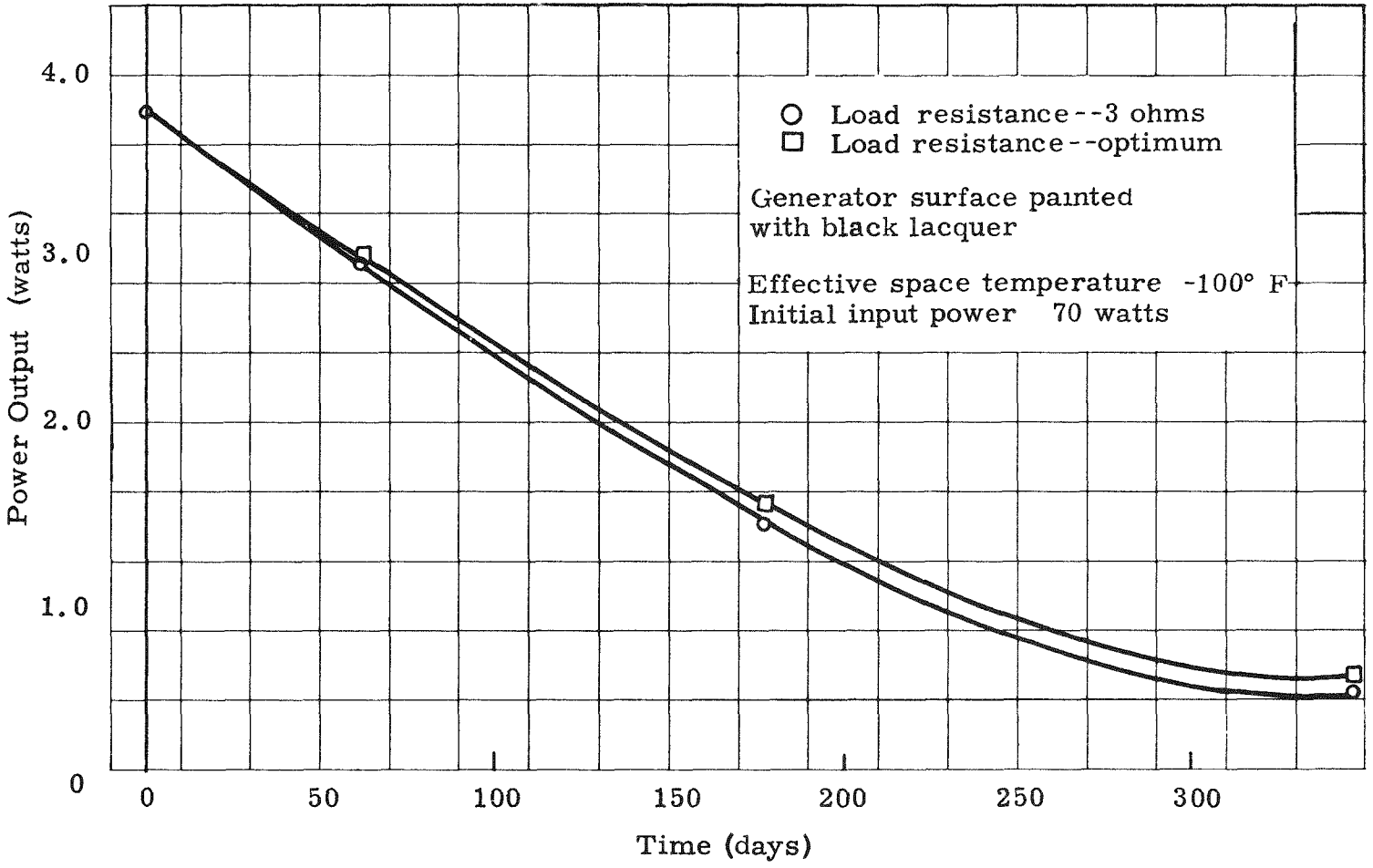

Fig. IV-55. Power Time History for Cerium-Fueled System

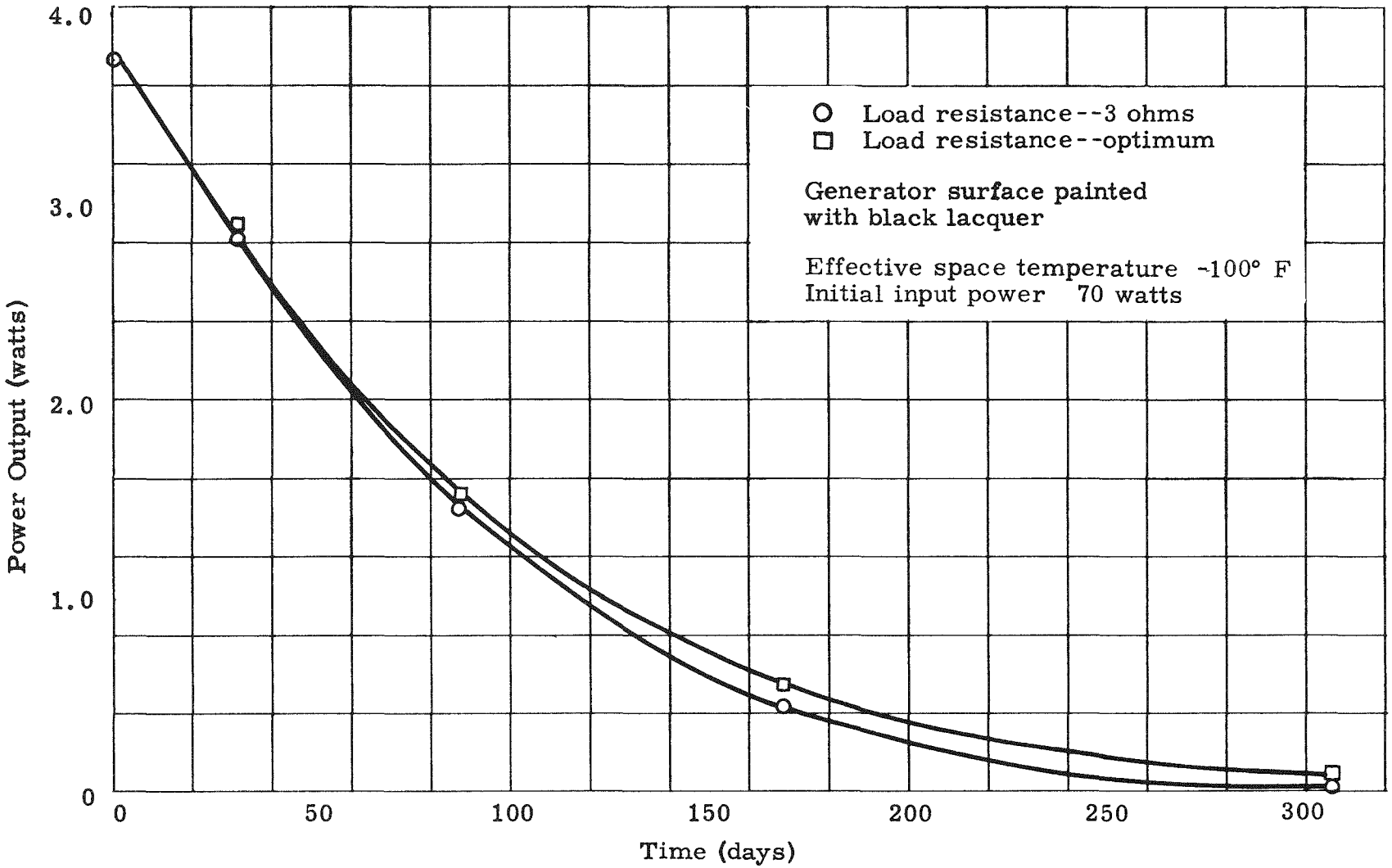

Fig. IV-56. Power Time History for Polonium-Fueled System

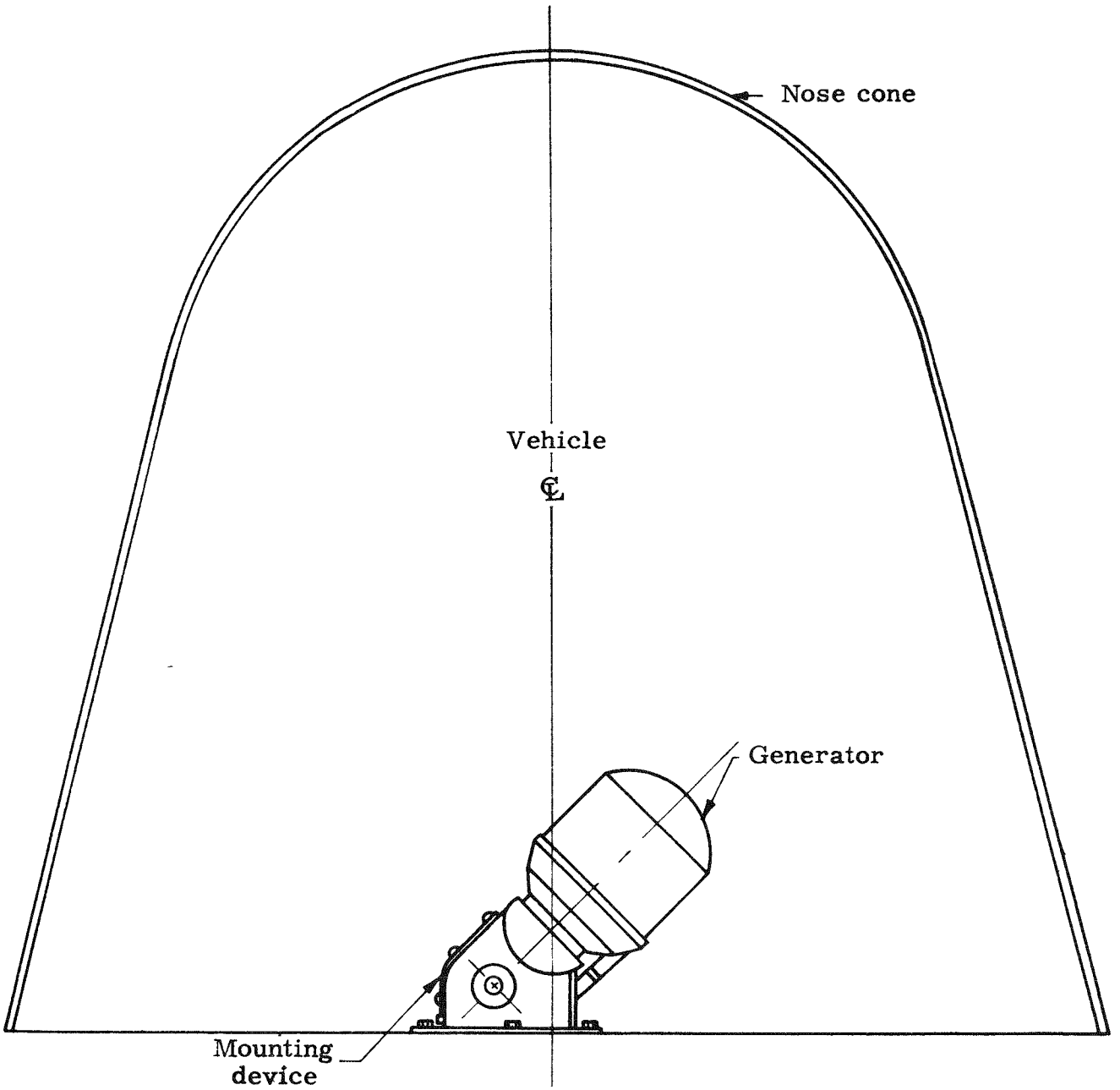

Fig. IV-57. Nose Cone Mounting Arrangement

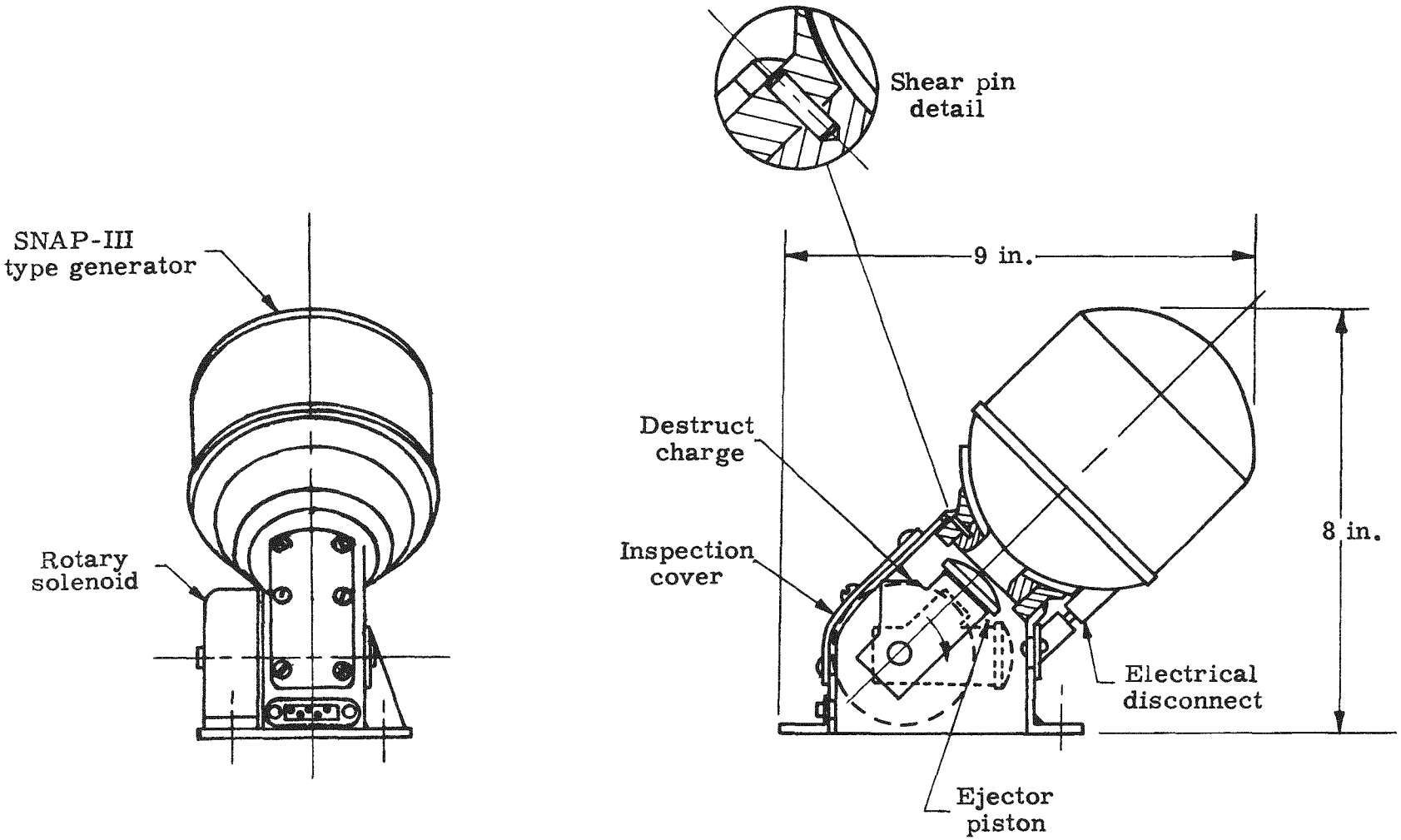

Fig. IV-58. Generator Mounting Arrangement

are required to provide adequate safety margins. These units are larger than those in the mounting arrangement depicted by Fig. IV-58. This arrangement is being modified and designed in greater detail for the final report.

Original plans called for determining the total emissivity of the various generator surface coating materials by testing, but this study could not be scheduled. A calculated emissivity of the black oxide coat on copper was obtained by equating heat transfer relationships and temperatures obtained during altitude chamber tests. Assuming an emissivity of 0.94 for the black lacquer finish, emissivity of the oxide coat was calculated to be 0.61. This compares well with reference values for heavily oxidized copper.

3. Converter and Battery System Studies

The generator output curve for maximum power transfer has been analyzed for the Polonium-210 system. An empirical equation has been developed for output power at any time with variable resistance loads. With all constants evaluated except k, the equation is as follows:

$$P_o = \frac{4 R_e P_i E_o e^{-t\,(0.00502 + 0.00086\, t^{0.383})}}{(R_e + R_g\, e^{-kt})^2}$$

where

P_o = output power at any time--watts

P_i = input power at time zero--watts

E_o = efficiency at time zero

e = 2.71828

t = time--days

R_e = load resistance--ohms

R_g = generator internal resistance at time zero--ohms

k = internal resistance decay constant.

Attempts to determine converter transfer functions through a literature search were unsuccessful since published data at the low input voltages considered were inadequate. Using the converter developed and described in the Subtask 5.6 Progress Report, additional parametric tests were conducted to provide data on performance over a wider range of input voltages. These data are being correlated using equivalent circuits to obtain transfer functions. This study is aimed at developing an empirical equation for converter performance that may be combined with the equation given to define the overall system performance. The equations may become too cumbersome for general use, in which case a graphical method of presentation will be investigated.

E. SUBTASK 5.6--ONE-WATT NUCLEAR POWER SUPPLY FOR SPACE APPLICATION

The purpose of Subtask 5.6 is to analyze and design a nuclear-thermoelectric power supply for a 2- to 5-year space mission. This power supply consists of a 1.5-watt(e), 1.5-volt d-c radioisotope-powered generator and a static voltage converter whose output is 1 watt(e), 15 volts dc. The radioisotope selected for this task is Plutonium-238 which is primarily an alpha emitter whose average energy is 5.48 Mev.

The technologies developed for the SNAP-III and Strontium-90 generators under Atomic Energy Commission contracts have been utilized in the design of the proposed unit.

The preliminary generator design fully described in the first quarterly report was reviewed during this period with The Johns Hopkins University Applied Physics Laboratory (JHUAPL). The compact Mod I generator, Fig. IV-59, then evolved as a result of integrating the power supply in the JHUAPL satellite system.

Using the configuration established for the Mod I design, a thermoelectric radiator breadboard device has been engineered and manufactured and is presently being made ready for testing so the actual electrical characteristics can be determined.

The design of the converter has been completed and a breadboard test of the converter hardware has shown that an efficiency of 75% is realistic for low wattage power supplies.

Hazards and shielding evaluations which were started late in this quarter will be mentioned briefly at the end of this report.

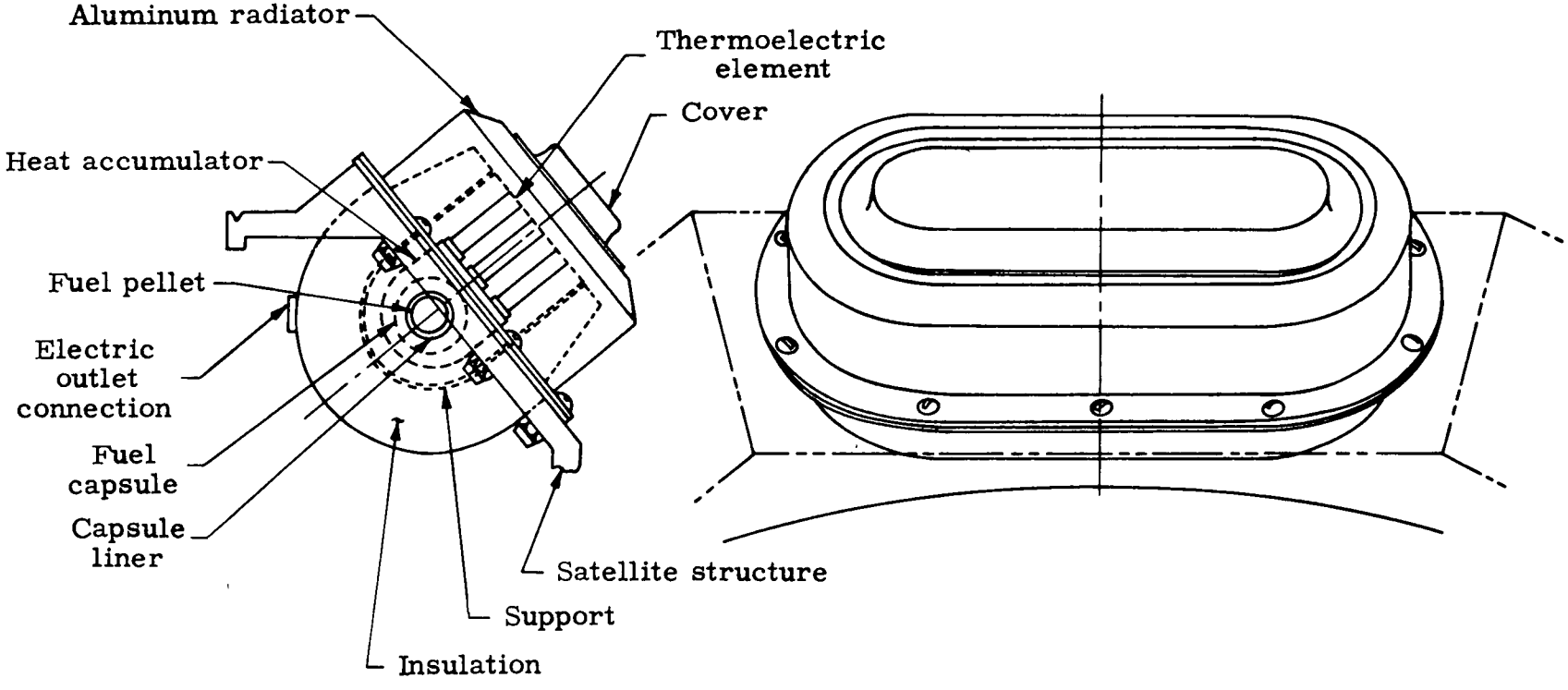

Fig. IV-59. MOD I Generator

1. Systems Integration in a Satellite

Liaison was conducted during the month of January 1960 with a satellite contractor, The Johns Hopkins University Applied Physics Laboratory, to ensure the compatibility of the 1-watt(e) power supply with a satellite system.

During several meetings, the first of which was attended by Atomic Energy Commission representatives, an increased power supply of 2.22 watts(e), the space allocation for the generators and a proposed hardware production schedule were discussed. Between meetings, a design study was conducted at The Martin Company which revealed that two reshaped 1.5-watt, 1.5-volt generators connected in series to a converter would satisfy the larger power requirement. Also, the generators would be mounted on the existing satellite external structure; moreover, a satellite weight balance would be maintained by spacing them at positions which were diametrically opposite. As to power supply delivery, a 2.22-watt(e) radioisotope-fueled power supply could be manufactured, environmentally tested and delivered by The Martin Company within one year from contract approval.

2. Mod I Generator

The design of the integrated or reshaped Mod I generator differs from the preliminary generator design described in the first quarterly report as it can no longer be mounted with the radiator flush to the external skin of the satellite. Because the reshaped generator must be mounted in the external solar cell support structure, the generator is now a rectangular-shaped box as shown in Fig. IV-59. The radiator is a hat-shaped section having an excellent mean radiation area-to-absorption area ratio of about 5.5. Vertical space limitations between the bottom of the generator and the satellite shell structure have necessitated a slight reduction in insulation material thickness.

An analysis has been made for the reshaped generator configuration. Results of tests conducted under Task 2 and the Strontium-90 test generator programs have been reviewed, and a factor of 1.5 x R_{PbTe} has been used for the total lead telluride electrical resistance. This factor necessitated the reduction in length of the 15 pairs of 1/4-inch diameter PbTe elements from 1.5 to 1.04 inches. A summary of the data for the Mod I nuclear-powered generator is shown in Table IV-7. The thermal analysis may be found in Appendix IV-A.

The Plutonium-238 source material is encapsulated in three successive containers. The inner container consists of two welded tantalum cylinders which contain the pelletized Pu-238 fuel. Tantalum is used to prevent the

TABLE IV-7

Mod I Nuclear-Powered Generator Data

Generator dimensions		
Overall size--in.		
Height	4.5	
Width	4.5	
Length	9.0	
Radiator--sq in.		
Effective absorption area	Varies from 36.8 to 0	
Effective radiating area	~ 58.9	
Electrical conversion system		
Lead telluride semiconductors	N-Type	P-Type
Diameter--in.	0.25	0.25
Length--in.	1.04	1.04
Elements--No.	15	15
Radioisotope		
Plutonium-238		
Half life--yr	86.4	
Volume (pure Pu-238)--cc	3.54	
Volume (including 15% impurities and 90% compaction of pellets)--cc	5.62	
Weight (pure Pu-238)--gm	58.40	
Weight (including 15%--5 gm/cc impurities)--gm	68.80	
Quantity of Pu-238--curies	1017	
Thermal properties		
Input power--watts	33	
Hot junction temperature--°F	1000	
Cold junction temperature--°F	300	
Electrical properties		
Output power--watts	1.5	
Voltage, dc--volts	1.5	
Overall efficiency of generator--%	4.54	
Thermoelectric efficiency--%	6.05	

alloying of the plutonium with the outer structural containers, which consist of two welded Haynes-25 impact resistant capsules. The impact tests conducted under Subtask 5.5 revealed that Haynes-25 was the best material to use for high velocity impaction on granite at 600° C capsule temperatures.

The Haynes-25 capsules are then encapsulated in a highly corrosion resistant Hastelloy C material. This material has been selected on the basis that 10-year sea water corrosion tests, conducted at Wrightsville Beach, North Carolina, revealed that Hastelloy C has a corrosion rate of only 1/10,000 inch per year. Short term (700 hours) simulated sea water corrosion tests have been conducted on the Haynes-25 material and similar corrosion rates have been measured. However, at this time, due to the requirement that the capsule remain intact after an abort in sea water for a period of 10 half lives for Pu-238, the tests performed on Haynes-25 have not proceeded for a sufficiently long time to permit elimination of the outer Hastelloy C jacket.

An analytical objective in the generator design was to minimize heat flow to the inside of the satellite. This was accomplished by the use of a reflective gold surface on the stainless steel capsule support and Owens-Corning Fiberglas AAAA insulation, and by the evacuation of the generator to a pressure of 100 microns of mercury.

A summation of heat flow will give the required heat source power. The calculated heat flows are as follows:

	(watts)
Heat flow through elements	24.80
Heat flow through Min-K to radiator	1.10
Heat flow through structure to radiator	4.10
Heat flow converted to electricity	1.50
Heat flow to satellite structure	1.50
	33.00

The average radiator temperature has been calculated from a heat balance on the radiator. The heat flow to the radiator is the sum of heat flow from the internal heat source plus the absorbed solar energy. The

heat flow into the radiator must be radiated to space. The heat from the internal source is assumed to be constant at 31.5 watts. The solar heat absorbed is dependent on orbital conditions, radiator configuration and position of radiator surface relative to the sun and earth.

Definition of orbit. The satellite carrier, established by conferences with the satellite contractor, would be launched in a near polar orbit (or a 67-1/2-degree SE inclination to the earth's equator) as shown in the sketch.

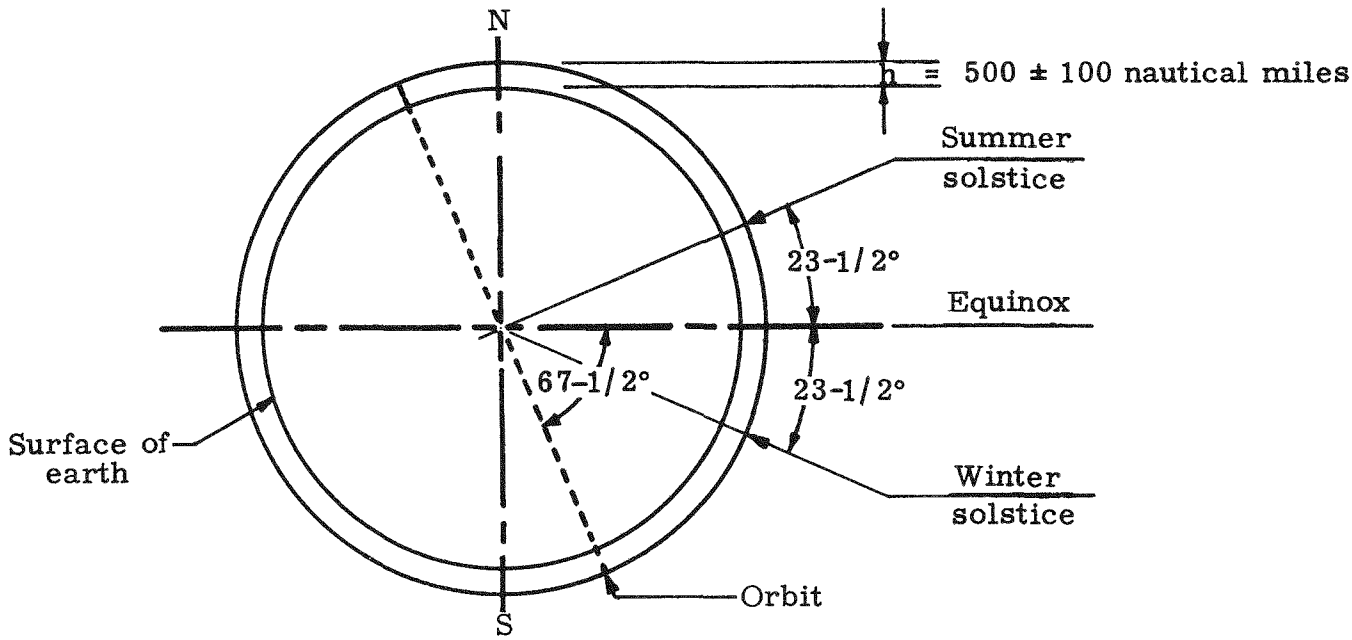

Satellite orbit

For this orbit, the satellite will have an eclipse factor (μ) per orbital revolution for various times of the year as shown in Fig. IV-60.

To establish a relationship for the solar heat absorbed, it is assumed that the satellite is spinning (at 2 rpm) and that there is no heat transfer between the generator and the satellite structure.

The analysis has been carried out for 0- to 90-degree orbital inclinations, and the radiator average temperature was computed to be 376 ± 10°K. The analytical study which defines the radiator temperatures may be found in Appendix IV-B.

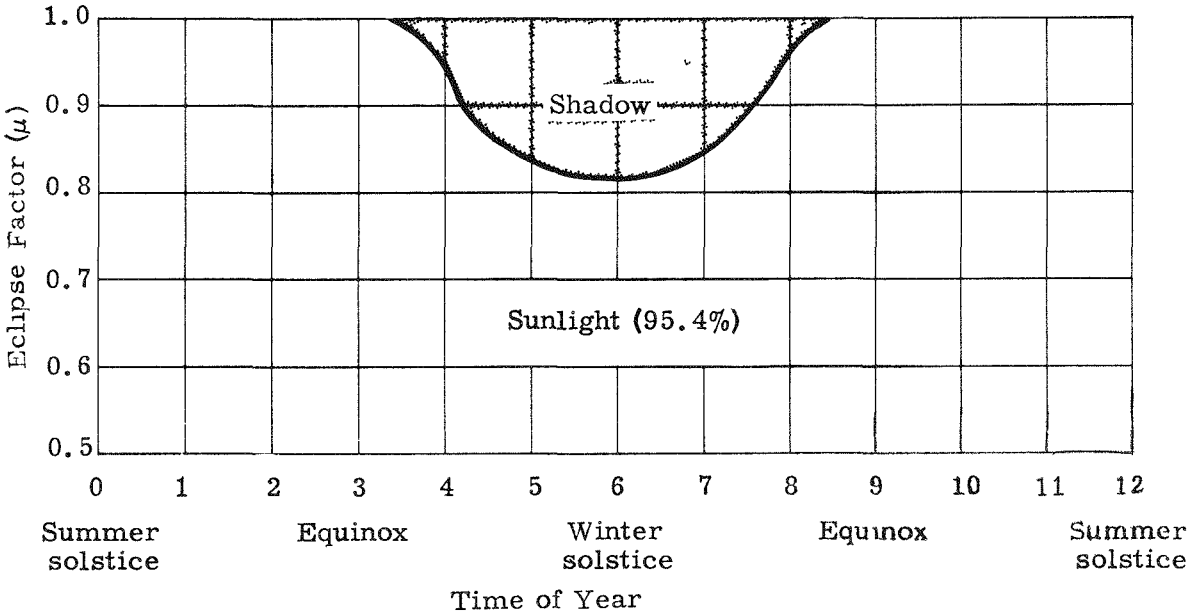

Fig. IV-60. Satellite's Eclipse Factor Versus Time of Year

3. Thermoelectric Radiator Test Device

A breadboard test device has been designed and manufactured. This device, which will be tested electrically during the next reporting period, has been designed primarily to measure the electrical characteristics of the thermoelectric elements used in the Mod I generator configuration. The test unit, Fig. IV-61, consists of a flat aluminum radiator, 1/4-inch diameter by 1-inch long thermoelectric elements, Min-K-1302 insulation, a gold-plated stainless steel support and an electrically heated stainless steel core.

The design of the heater core incorporates molybdenum hot shoes which have been flame sprayed in the required pattern over an Al_2O_3 electrical insulator coating. A fixture has been manufactured for soldering copper cold shoes to the thermoelectric elements to maintain the required alignment.

The thermoelectric radiator breadboard unit is to be tested in a Bell jar which permits purging with a 25% H_2, 75% N_2 reducing gas. After the purging operation, sufficient electrical heat will be supplied to maintain a steady hot junction temperature of 1000° F. When this condition is reached, measurements will be taken of the radiator and cold junction temperatures, the Seebeck emf and the electrical resistance of the elements.

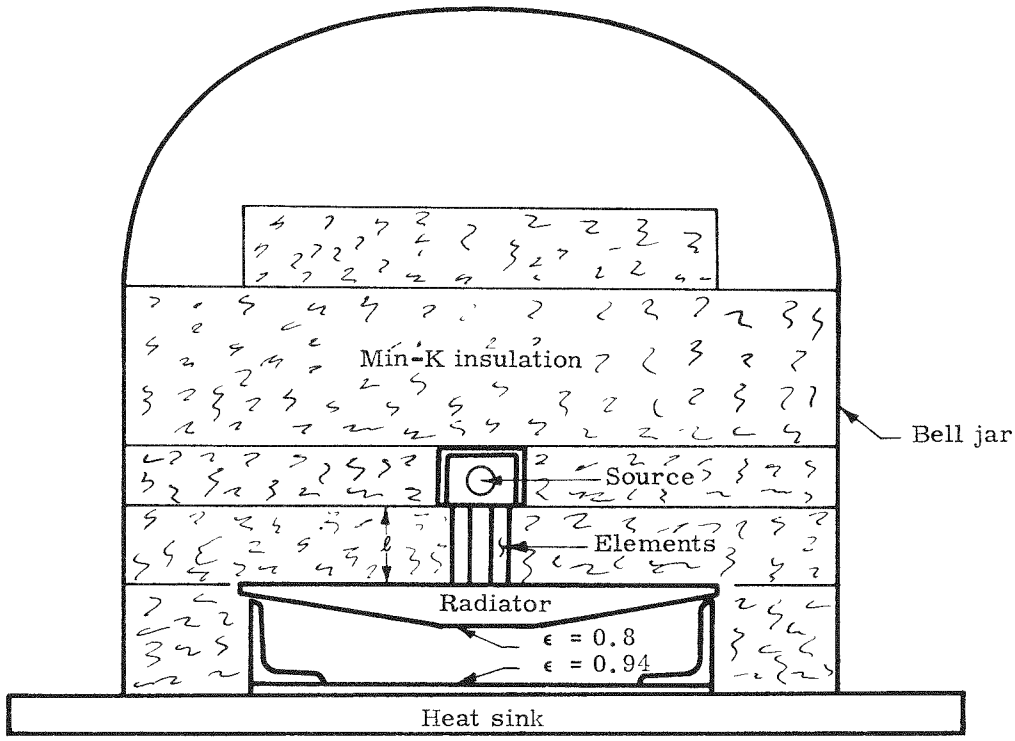

Section B-B

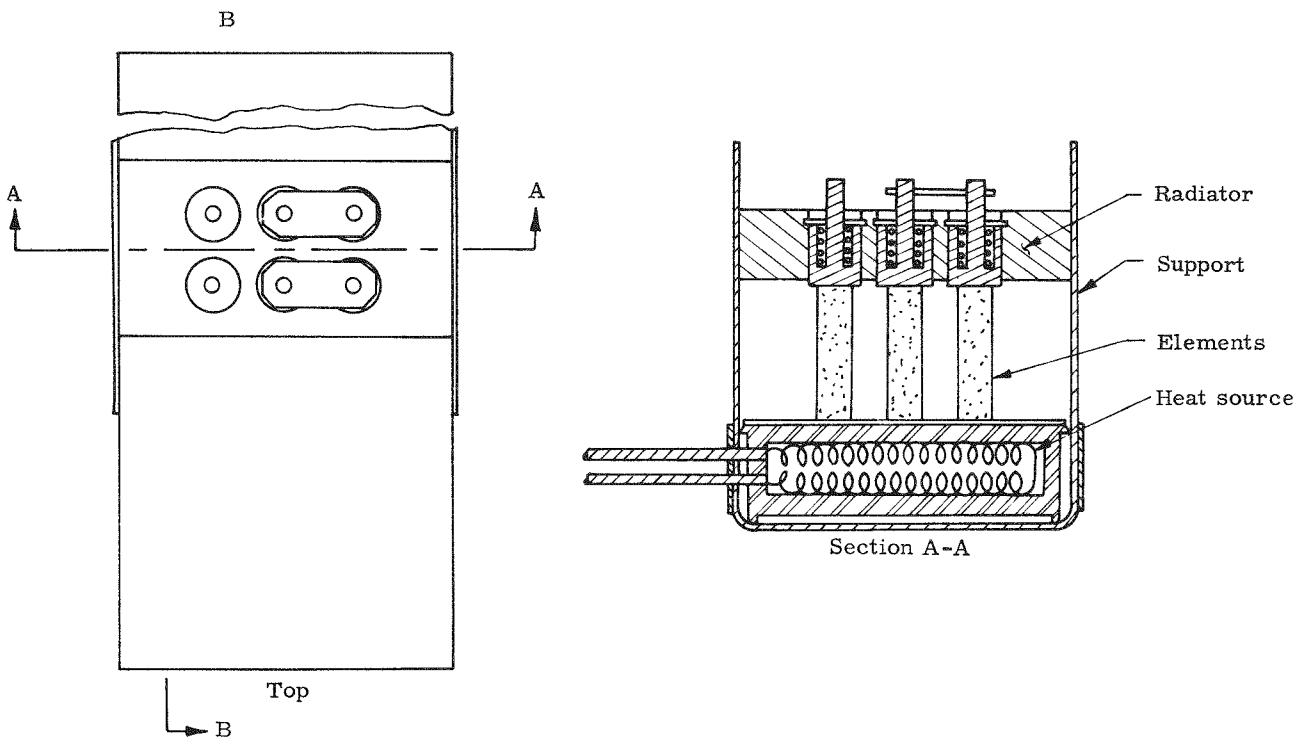

Section A-A

Fig. IV-61. Generator Test Model

4. D-C to D-C Converter

The Subtask 5.6 electrical generator system for a 2- to 5-year space application consists of a 1.5-watt(e), 1.5-volt d-c nuclear powered thermoelectric generator and a d-c to d-c static converter whose output is to be 1 watt(e), 15 volts of direct current. The maximum peak-to-peak a-c voltage ripple was limited to 350 millivolts. The converter specification which was prepared for this Task may be found in Appendix IV-C.

Converter design. The d-c to d-c converter essentially consists of an oscillator circuit, a transformer and a rectifying circuit as shown in Fig. IV-62. The oscillator circuit (2 germanium transistors, transformer primary and feedback windings) converts the d-c input from the radioisotope-powered generator into ac. This ac is then stepped up by a factor of 10 by the transformer (primary and secondary windings of copper wire around a toroidal iron core). The stepped up a-c voltage is then passed through the rectifying diodes to achieve the desired output of 1 watt(e), 15 volts dc.

Converter test. Breadboard tests have been conducted on the converter to determine the electrical transformation characteristics of the d-c converter.

The test rig consists of a d-c power supply, the converter breadboard, input and output voltage and current meters, and an oscilloscope which visually displays the a-c peak-to-peak ripple.

Results of the tests conducted have proven that, with a low d-c input of 1.5 watts, 1.5 volts, the assembled converter components have the capability of operating at an efficiency of 77%, thereby producing 1.15 watts at 15 volts dc. This amounted to a realization of 11% greater converter efficiency than expected.

Furthermore, the output a-c peak-to-peak ripple which was superimposed on the d-c voltage output amounted to only 110 millivolts, or less than 1% of the output voltage.

The converter design and analysis and test data may be found in Appendix IV-C.

5. Hazards and Shielding Evaluations

Hazards and shielding evaluations are in progress on the Mod I generator design. These evaluations are being made to determine transportation safety, the effects of missile failure forces upon the fuel capsule, the helium pressure buildup within the fuel capsule, the encapsulated fuel burnup upon the satellite orbital decay and return to earth, and the resultant fallout pattern and dose rate.

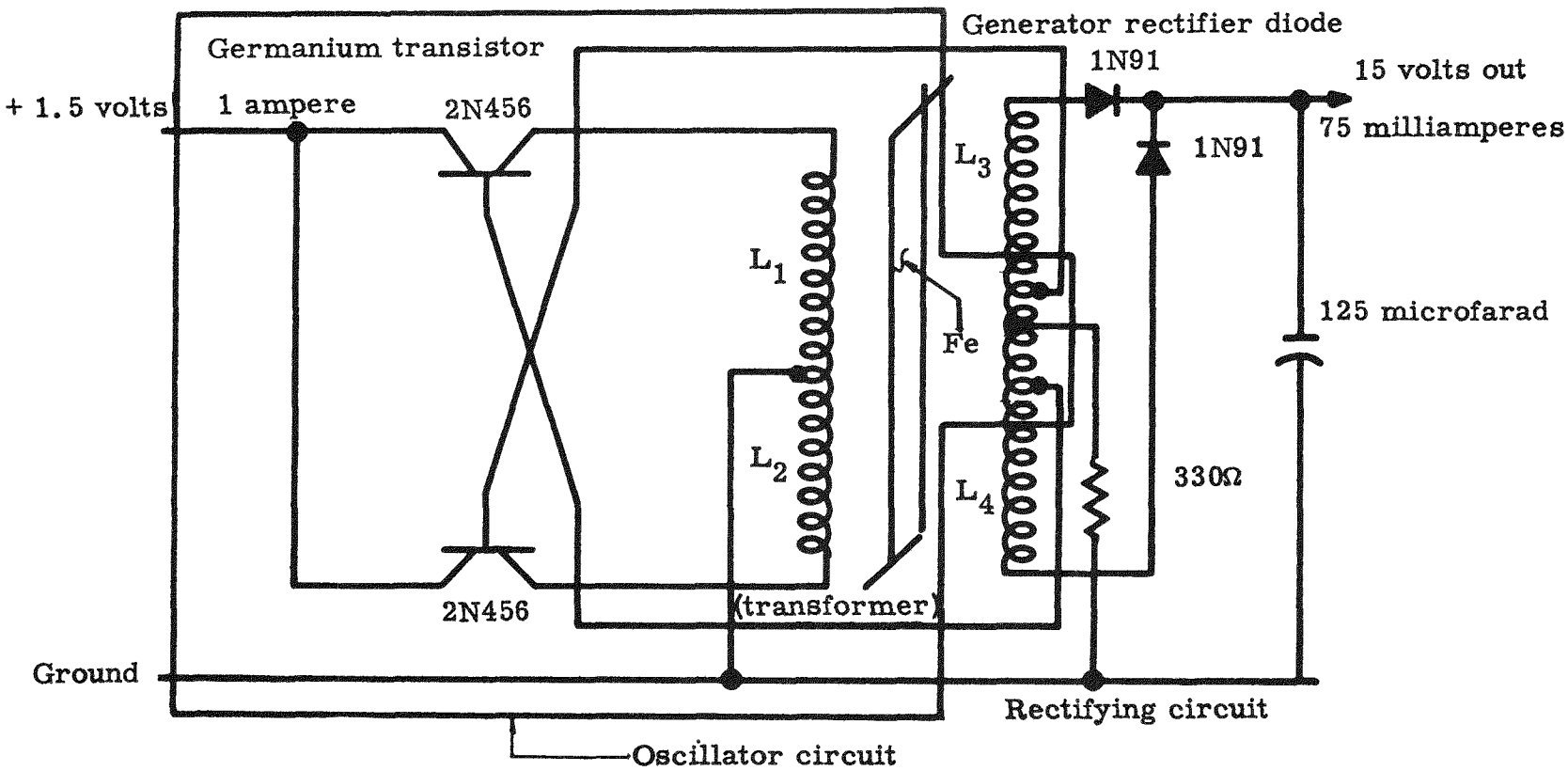

Fig. IV-62. Converter Schematic

Fuel capsule analysis. A study has been made to evaluate the capability of the fuel capsule design to withstand various types of forces imposed upon it (Fig. IV-63). Helium buildup was predicated on an intact condition upon impacting into dry soil. Figure IV-64 graphically displays time in years, capsule temperature decay, capsule internal pressure and radial stress buildup for impacting in dry soil. A resume of the maximum stresses imposed on the capsule design is as follows:

Helium buildup	
Peak pressure--psi	27,600
Time--yr	700
Radial stress--psi (inner Haynes-25 capsule only)	52,100
Allowable--psi	70,000
Temperature--°K	300
Impact	
Maximum impact pressure--psi	27,750
Maximum velocity--ft/sec	460
Modulus of elasticity (1600° F)--psi	24×10^6
Maximum impact stress--psi	21,700
Allowable stress (est)--psi	50,000

Aerodynamic heating. Post-orbital re-entry of the satellite will subject the generator to aerodynamic heating which will burn up at altitudes in excess of 100,000 feet. However, the generator must be ejected from the satellite to effect positive burnup.

The aerodynamic analysis, using the techniques performed for the Task 2.3 re-entry investigation from a 300-statute mile orbital condition, shows that the complete Mod I generator, capsule and fuel pellet will be consumed at an altitude of approximately 200,000 feet.

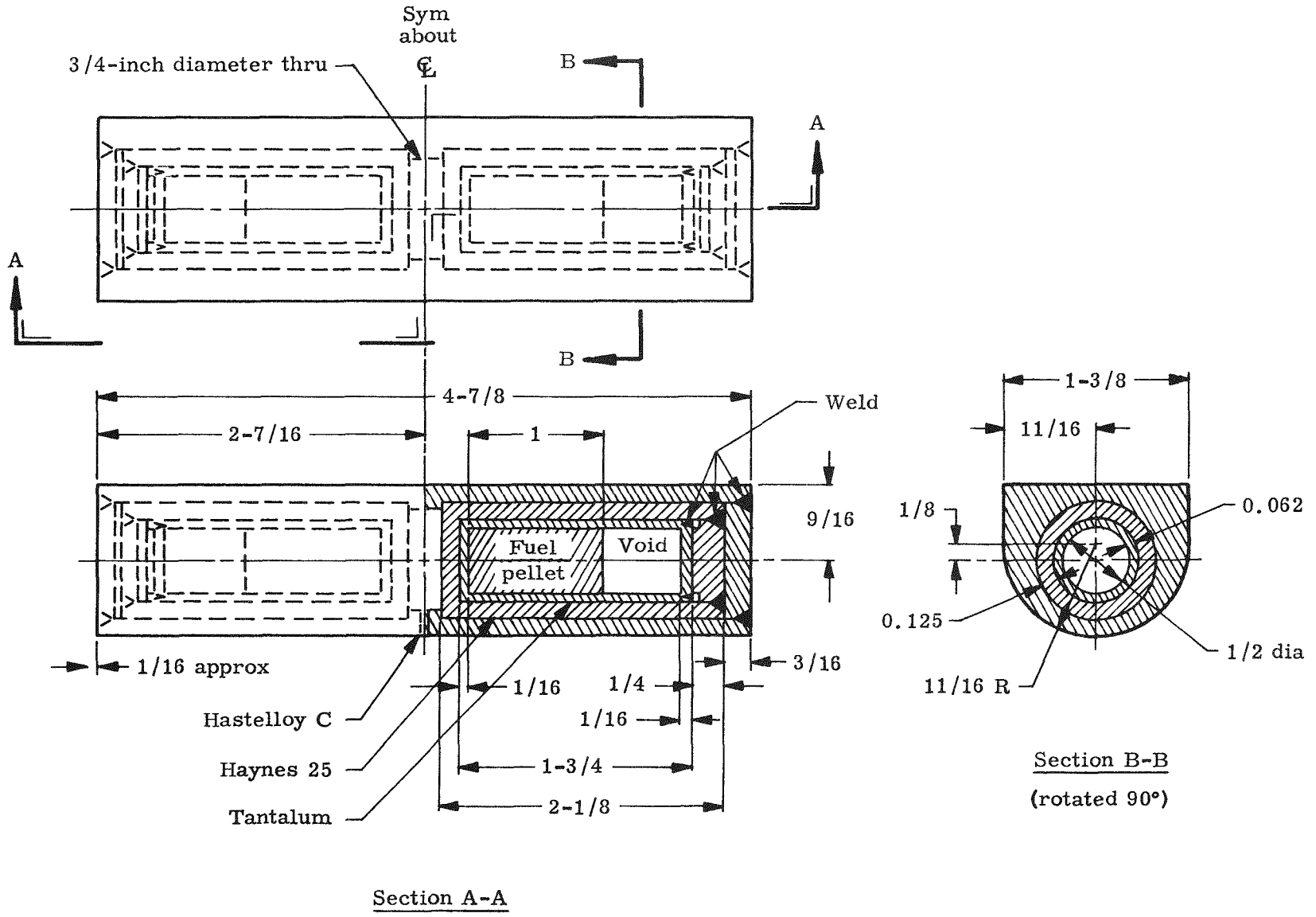

Fig. IV-63. Mod I Fuel Capsule

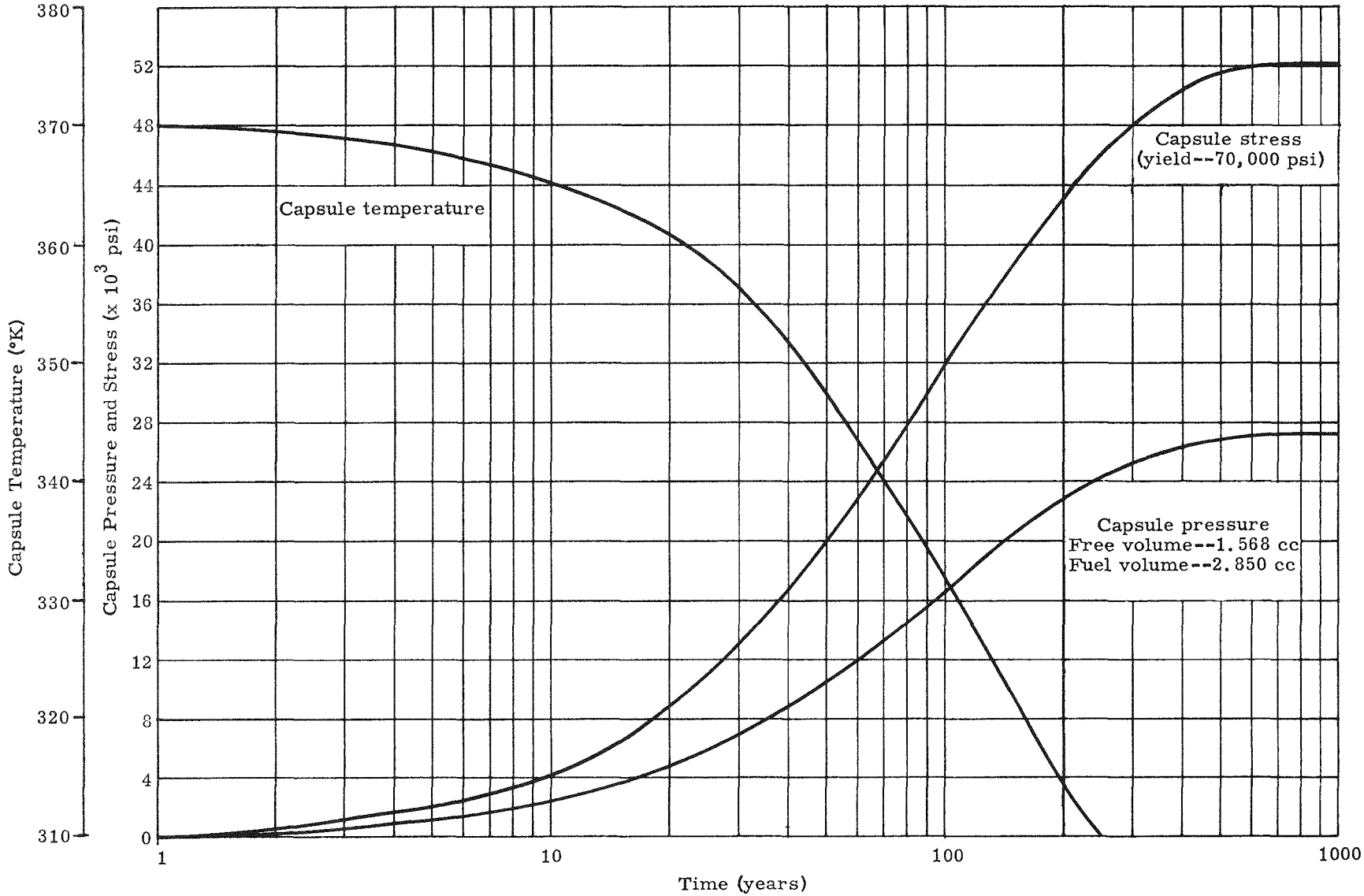

Fig. IV-64. Capsule Pressure Buildup, Stress and Temperature Decay upon Impacting on Dry Soil

A study has been completed to determine the fallout pattern resulting from post-orbital re-entry or aborts resulting from near orbital injection. Based on the complete burnup of the fuel pellet at an altitude above 100,000 feet, 1017 curies of Pu-238 will result in approximately 0.0205-millicurie per square mile fallout. This rate will be in the maximum fallout area lying between 30 and 60 degrees latitude. Studies have shown that any fallout tends to concentrate selectively in these latitudinal bands in the Northern and Southern Hemispheres. For near orbital abort, this condition will be in the Southern Hemisphere while post-orbital re-entry may cause fallout in either zone.

The appropriate curves of heating rate, altitude, and velocity versus time; and fallout density versus time and location are being summarized and will be included in the hazards report.

Shielding analysis. The decay scheme for Pu-238 is as shown.

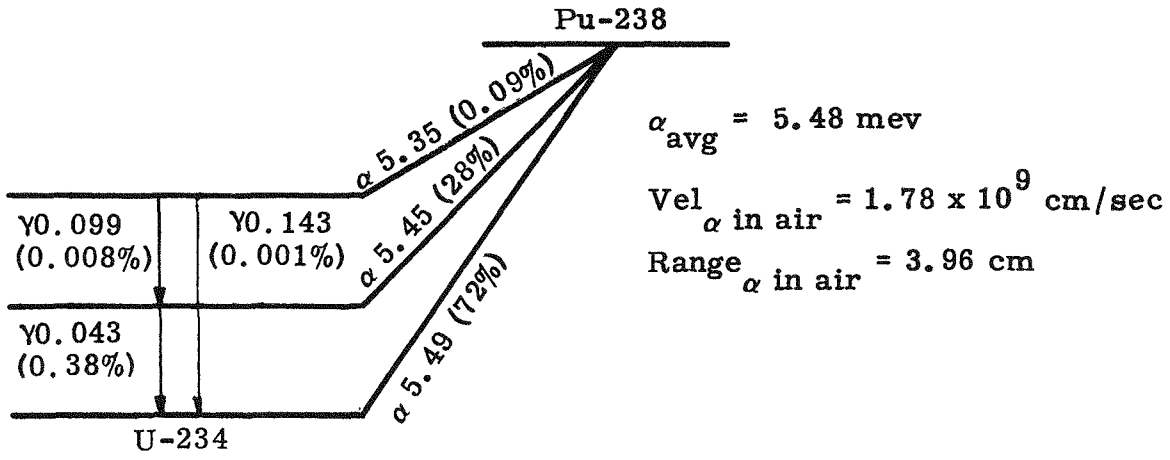

($T_{1/2}$ = 2.48 x 10^5 year)

Decays to Th-230 by α emission

Neutron radiation from the fuel capsule comes from (α, n) reactions and from spontaneous fission. The former contributes an insignificant number of neutrons. The spontaneous fission half life is 10^{10} years. Neutron emission due to this spontaneous fission contributes 130 mrem/hour and decay gammas contribute 58 mrem/hour. This results in a total of 188 mrem/hour at the surface of the generator.

Using the approved tolerances for safe handling of 1500 mrem/week for hands and forearms, it is therefore possible for a person to hold the generator for about 8 hours in any one week without exceeding the accepted tolerance.

F. SUBTASK 5.8--CONCEPTUAL DESIGN OF A 13-WATT THERMOELECTRIC GENERATOR*

1. General Status

The general objective of this Subtask is to develop a conceptual design of a thermoelectric generator fueled with Curium-242, to deliver 13 watts of d-c electric power during a space mission. Until late in January 1960, the objectives further required the generator to operate for a period of six months while in some trajectory in space. The photon flux from the isotope fuel was restricted to 7 photons/cm^2-sec (over 100 kev) on an area of 100 cm^2, 10 centimeters distance from the generator surface. The generator weight was limited to 15 pounds.

Following a redefinition of the anticipated requirements by Jet Propulsion Laboratory, the objective of the Subtask was altered to provide for operation of the generator on the moon for at least 30 days and preferably 60 days following impact at a velocity of 500 ft/sec. The time of arrival was to be randomly related to the lunar day at the impact point which may lie anywhere on the surface of the moon visible from the earth. The weight of the generator may be as much as 18 pounds. The photon flux requirement, which previously led to a significant shielding design problem, was relaxed to:

1 photon/cm^2-sec of energy--0.4 to 3 mev

0.5 photon/cm^2-sec of energy--3 to 10 mev

all on an area of 100 cm^2 at a distance of 5 meters from the generator.

Before December 31, 1959, several configurations for the space probe mission had been examined. Analysis of the thermoelectric conversion systems and heat source designs had led to the selection of the optimum cylindrical generator described in the previous Quarterly Report (MND-P-3009-1). Preparation of the final detailed conceptual design of this generator was under way. Liaison with JPL had established the design criteria for the lunar impact mission.

As of March 31, 1960, the design of the space probe generator was complete, except that details of the variable heat dump mechanism and heat source, thermoelectric analysis of the final detailed design, and some aspects of hazards evaluation were omitted by agreement. A shipping container for the generator was designed. Several configurations for the lunar impact generator were proposed, and two of these were analyzed

---

* J. B. Weddell and J. L. Bloom

in some detail. The development of a generalized thermoelement optimization code, previously conducted as part of Subtask 5.7, was carried forward under the present task.

In the next quarter, the work on the lunar impact generator will be completed. The most reliable configuration will be selected and optimized by means of parametric analysis. Detailed design drawings will be prepared. Shielding and hazards analyses will be completed and a shipping container designed.*

2. Space Probe Unit (cylindrical radiative type)**

Generator analysis. This design was based on maximum thermoelectric efficiency for a radiator area which was fixed by the number of lead telluride couples needed to produce the 13 watts of electrical power. Other factors that dictated the radiator area were the shielding requirements and thermal loss through the insulation. This particular design configuration is a result of previous work and is a compromise between the design and analysis requirements. Assumptions for this design are:

(1) The temperature drop through the hot and cold junction shoes is small in comparison to the temperature drop through the thermoelectric element.

(2) No heat is lost except that which passes through the insulation.

(3) The fuel element and radiator area have a uniform temperature.

(4) The hot junction temperature is 1000° F.

(5) The unit internal pressure is 0.5 atmosphere (inert).

(6) The inner and outer shells are aluminum.***

---

*Subsequent to the end of the report period, the AEC determined that the scope of Subtask 5.8 would be extended to cover completion of the design effort on the generator for the six-month space mission and the preparation of a final report.

** M. Peiffer

***Stainless steel was subsequently adopted for the inner shell.

Using the quantity of fuel determined for the previous designs and incorporating the shielding requirements, the fuel element was sized. A radiator area was then chosen with respect to the number and length of thermoelements. After the radiator size was fixed, a heat loss equation was derived (see Appendix IV-D).

To initiate the design, a hot junction temperature of 1000° F (which is a practical temperature for lead telluride thermoelements) was chosen. With this temperature and several assumed cold junction temperatures, the thermoelectric efficiency curve (Fig. IV-65) was determined.

To initiate the calculation, an overall efficiency was assumed and a cold junction temperature determined by employing Singer's equation for satellite temperature. This temperature fixed the thermoelectric and thermal efficiencies. If the calculated overall efficiency did not agree with the assumed overall value, another efficiency was chosen and the entire procedure was repeated. This trial and error process was continued until the assumed and the calculated overall efficiency were in agreement, thus giving a generator design optimized on the basis of thermoelectric efficiency.

The analytical results are shown in Table IV-8.

TABLE IV-8

Summary of Results Cylindrical Radiative-Type Generator

Unit size--in.	
Height	7.5
Diameter	6
Efficiency--%	
Thermoelectric	6.51
Thermal	92
Overall	6.1
Temperature--°F	
Hot junction	1000
Cold junction	370
Heat loss--watts	16
Weight--lb	
Insulation	1.9
Outer skin	0.8

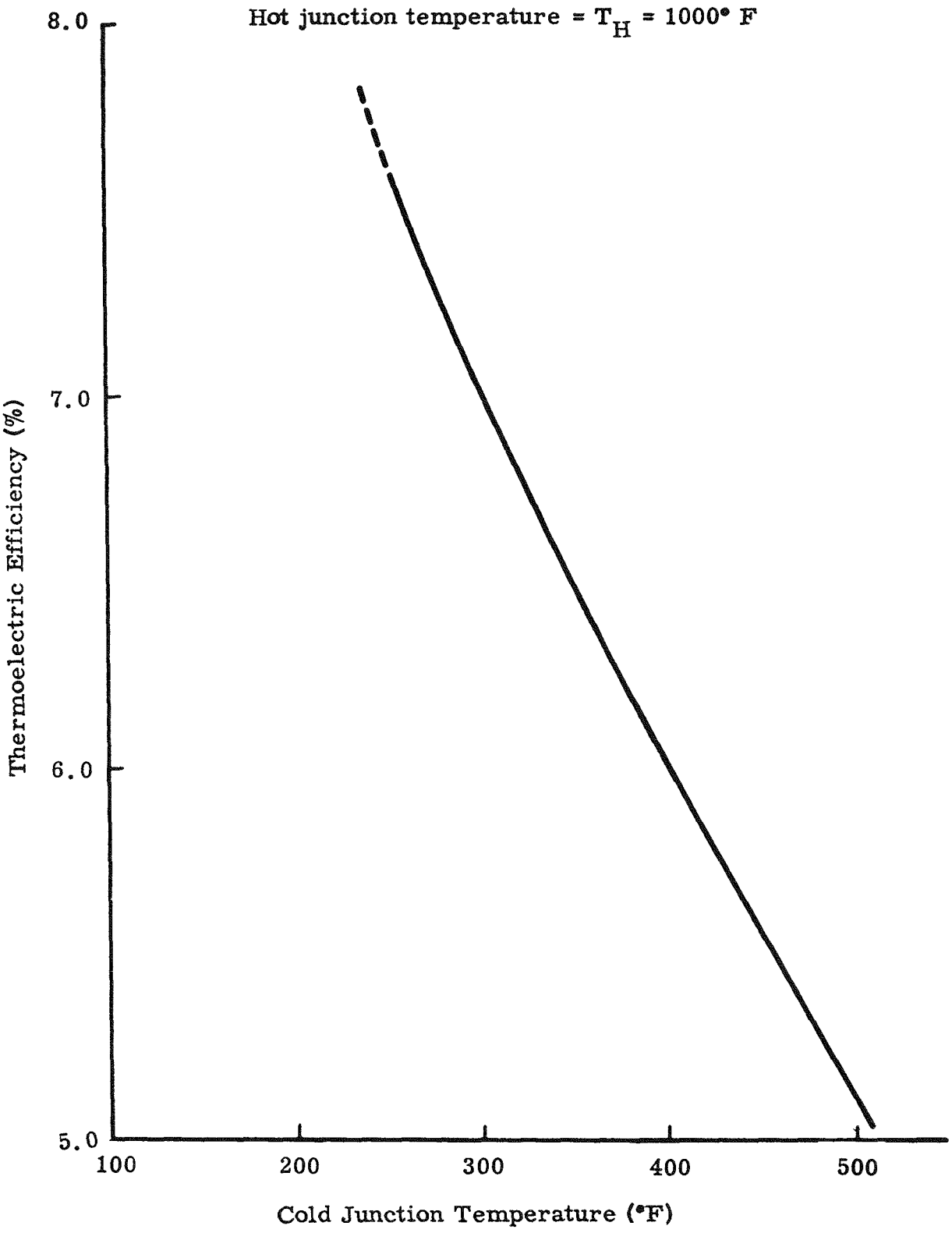

Fig. IV-65. Thermoelectric Efficiency Versus Cold Junction Temperature for PbTe Elements

TABLE IV-8 (continued)

Inner skin	0.30
Thermoelectrics	1.58
Fuel container	2.41
	6.99
*35% structure	2.44
Total	9.43

Thermoelectrics

Pairs--No.	30
Length--in.	0.75

	Doping (%)	Area ($in.^2$)
P-element (lead telluride)	1 sodium	0.1300
N-element (lead telluride)	0.03 lead iodide	0.1089

*25% structures weight was used in previous calculations. This was found to be optimistic and has been increased to 35%. The figures shown do not include an allowance for the heat dump mechanism.

Shipping cask analysis. This analysis was based on the cask configuration described. The primary objective was to incorporate a cooling technique for the generator during shipping and storage prior to vehicle launch.

The calculation technique employed consisted of assuming an ambient temperature of 70° F, choosing several surface temperatures, and then calculating the heat flow from the surface to the surroundings. Figure IV-66 is a plot of surface temperature versus heat flow for the ground handling cask. With the outer surface temperature fixed, the temperature of the inner surface was determined by using McAdams' correlation for natural convection of cylinders and the film coefficient concept. Appendix IV-D describes the calculation technique employed. In determining the film coefficient for the shipping cask, two correlations from McAdams were investigated but the more conservative correlation was

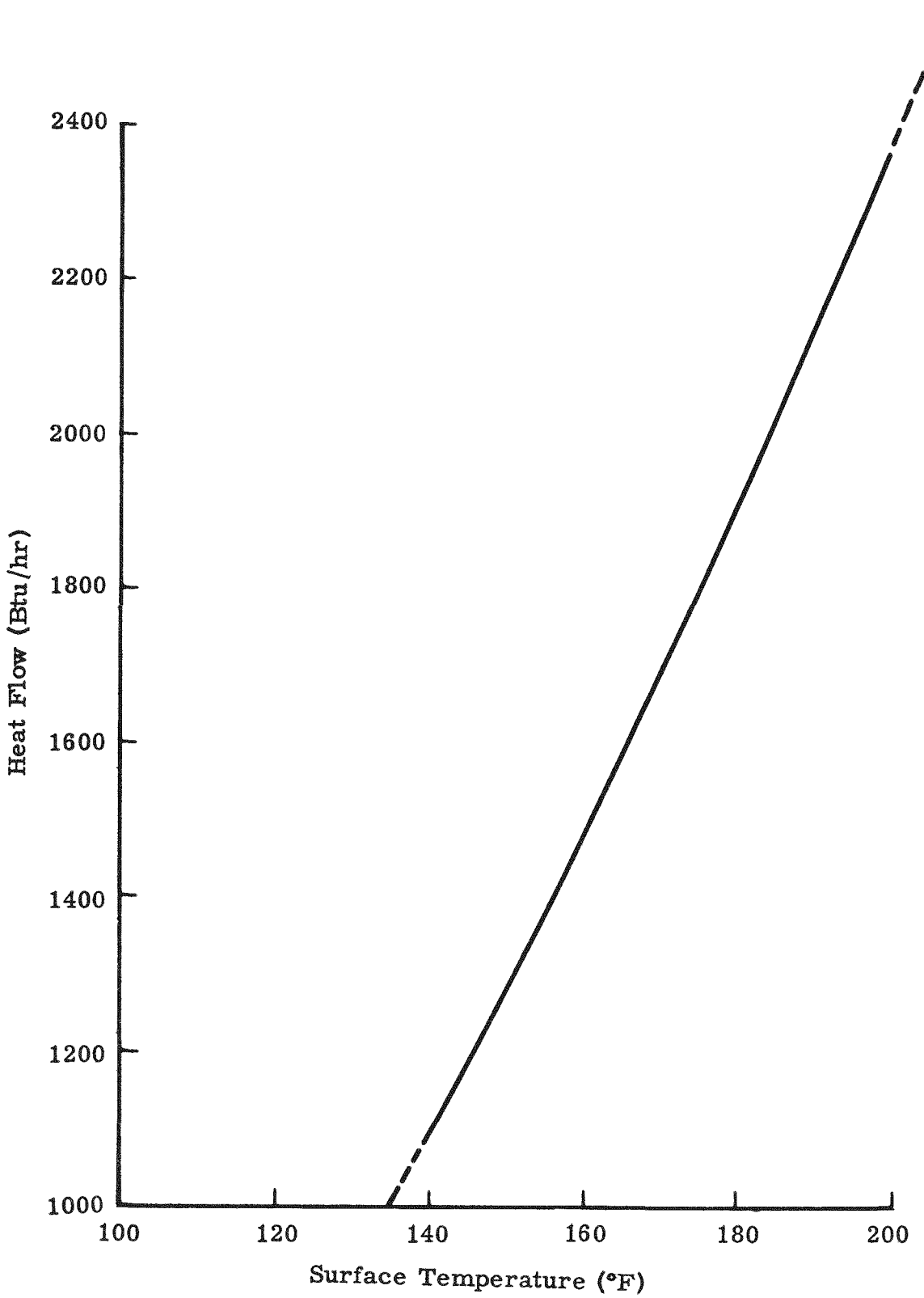

Fig. IV-66. Heat Flow Versus Surface Temperature for Ground Handling Cask

employed to determine the inner surface temperature. Several stagnant cylinder* temperatures were assumed, and the film coefficient was determined by each method mentioned previously. Figure IV-67 is an illustrative plot of the two film coefficients, and the point where the two lines cross is the temperature of the stagnant cylinder. Using temperatures calculated by this technique, the inner temperatures were determined.

Analysis of fuel block**. The objective of this analysis was to determine the centerline temperature of the fuel element with 20-to-1 and 5-to-1 ratios of nickel and curium metal.

Assuming a hot junction temperature of 1000° F, the outer surface temperature of the fuel element was determined using the radiation equation for concentric cylinders. With this temperature, the inner surface temperature of the cladding was determined by Fourier's Third Law. The equation employed is given in Appendix IV-D.

Summary of Results

Centerline Temperature (° F)		Ratio
1600	160	20 to 1
1630		5 to 1

Generator design***. At the end of the reporting period, the design of the generator was at the stage shown in Fig. IV-68.

The overall design of the generator shell was based on two criteria, the radiating surface required to maintain the cold junction temperature at a reasonably low level (about 300° F) and the number of thermoelements required to produce the desired output of 13 watts.

The configuration of the heat source is a function of fuel volume and gamma shielding material desired. Uniform temperature distribution on the hot junction surface was also taken into consideration.

---

* A stagnant cylinder is a fictitious stationary hollow cylinder made up of a thin layer of water located between the outer and inner surface.

** D. Tupper

***J. Peters

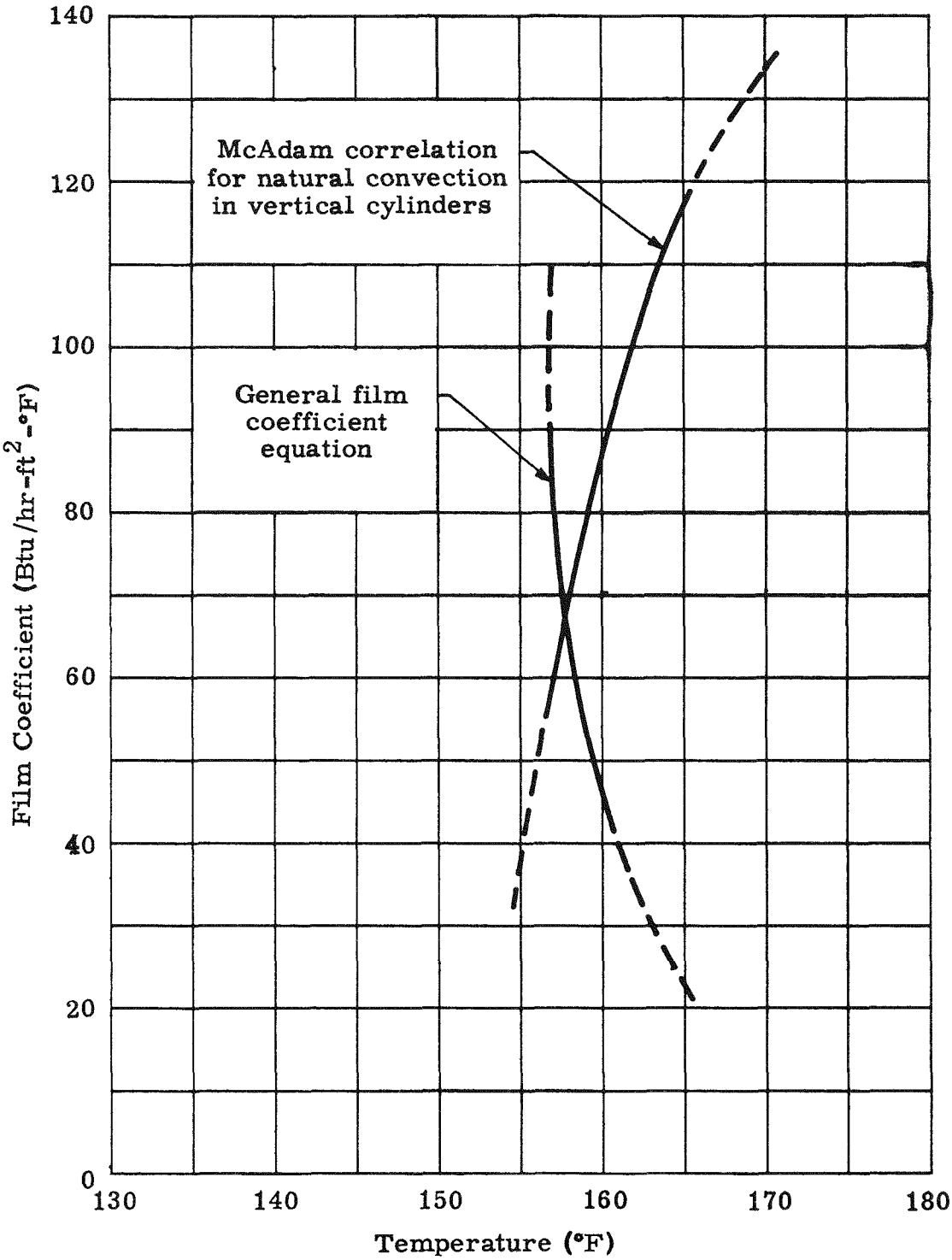

Fig. IV-67. Film Coefficient Determination Between Outside and Stationary Fluid

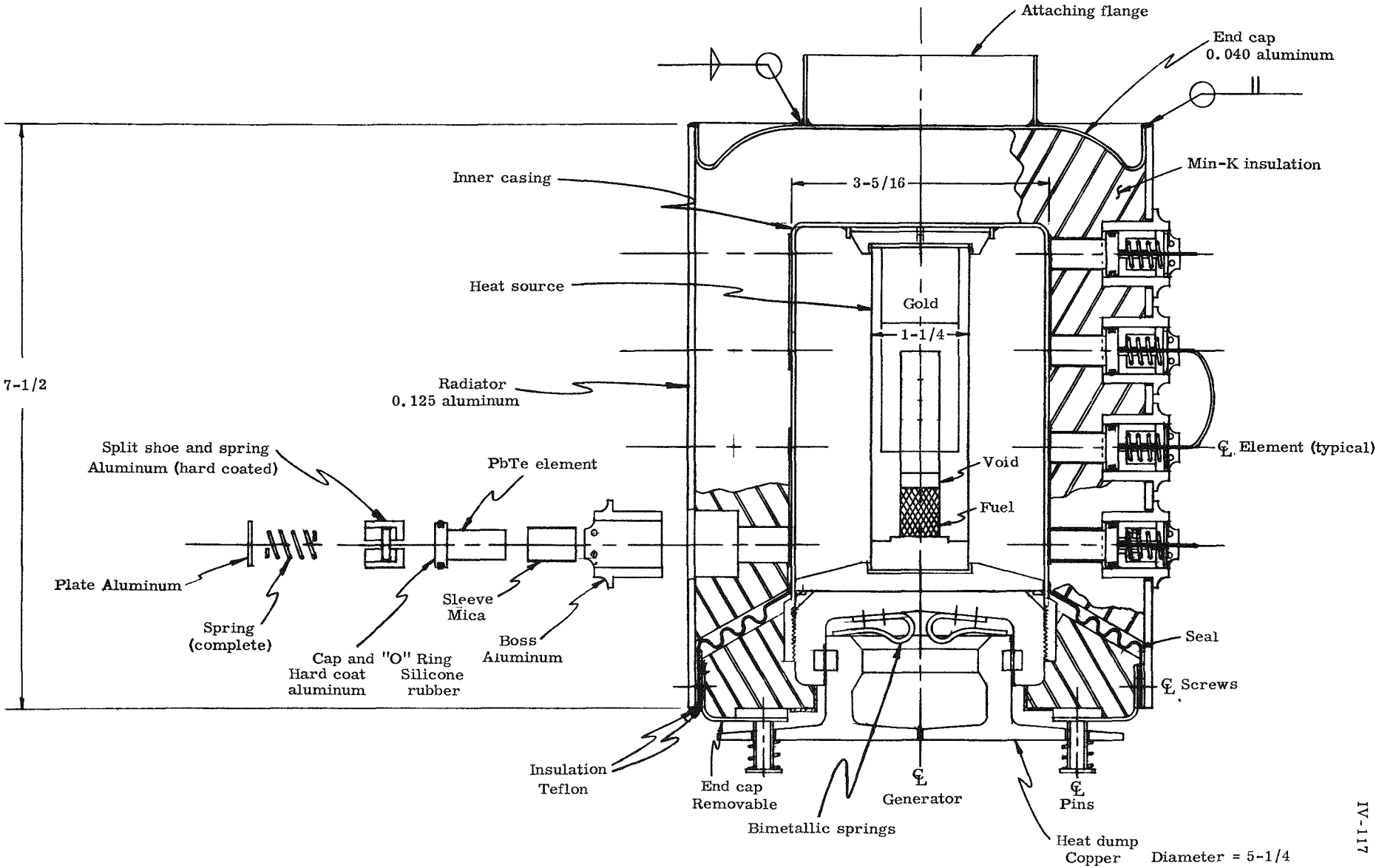

Fig. IV-68. Cylindrical 13-Watt Generator

Innovations in the design include the ability to individually adjust each thermoelement and the insertion of the heat source and heat dump into the generator as one piece. The assembly of the generator is completed by fastening the heat source-heat dump part in place with screws. This simple procedure would be well suited to hot cell operations.

The design of the heat dump is not final. It has not been analyzed to determine the temperatures in the system, its heat dumping ability and heat losses at end of life.

3. Lunar Impact Unit

Analysis*. A preliminary configuration of a generator for the lunar probe mission was drawn up (Fig. IV-69), and the analysis of it was initiated. Cobalt silicide was the material selected for thermoelectric elements insofar as the calculations were concerned.

Thermal conductivity data for cobalt silicide elements are limited, and an attempt was therefore made to calculate this parameter by means of the Wiedemann-Franz ratio. The value of 0.056 watt/cm-°C at 20° C so obtained is substantially higher than the figure of 0.04 reported unofficially by the element supplier. The curve of thermal conductivity versus temperature obtained by the calculation was, therefore, normalized to the single value reported by the supplier and to the mean of the theoretical and reported figures (see Fig. IV-70). The three sets of data so obtained were then employed individually to arrive at separate thermoelectric designs (Table IV-9). These designs formed the basis for determining requisite radiator area in the preliminary configuration.

In previous considerations, the dumping of excess heat was of primary importance in the generator design. Since this generator is being designed to operate for 60 days, an effort is being made to eliminate an excess heat dump mechanism. First results indicated this was possible. Figure IV-71 is a plot of cold junction temperature versus heat input in watts for various ambient temperatures, determined partially by use of Singer's equation. The range of particular interest (200 to 300 watts) indicates that the cold junction temperature varies about 100° F for the 500°-F differential (+250 to - 250° F) in the moon's environmental temperature. With a temperature change of only 100° F in the cold junction, it was felt that the heat dump could be eliminated.

---

*M. Peiffer, L. Lee

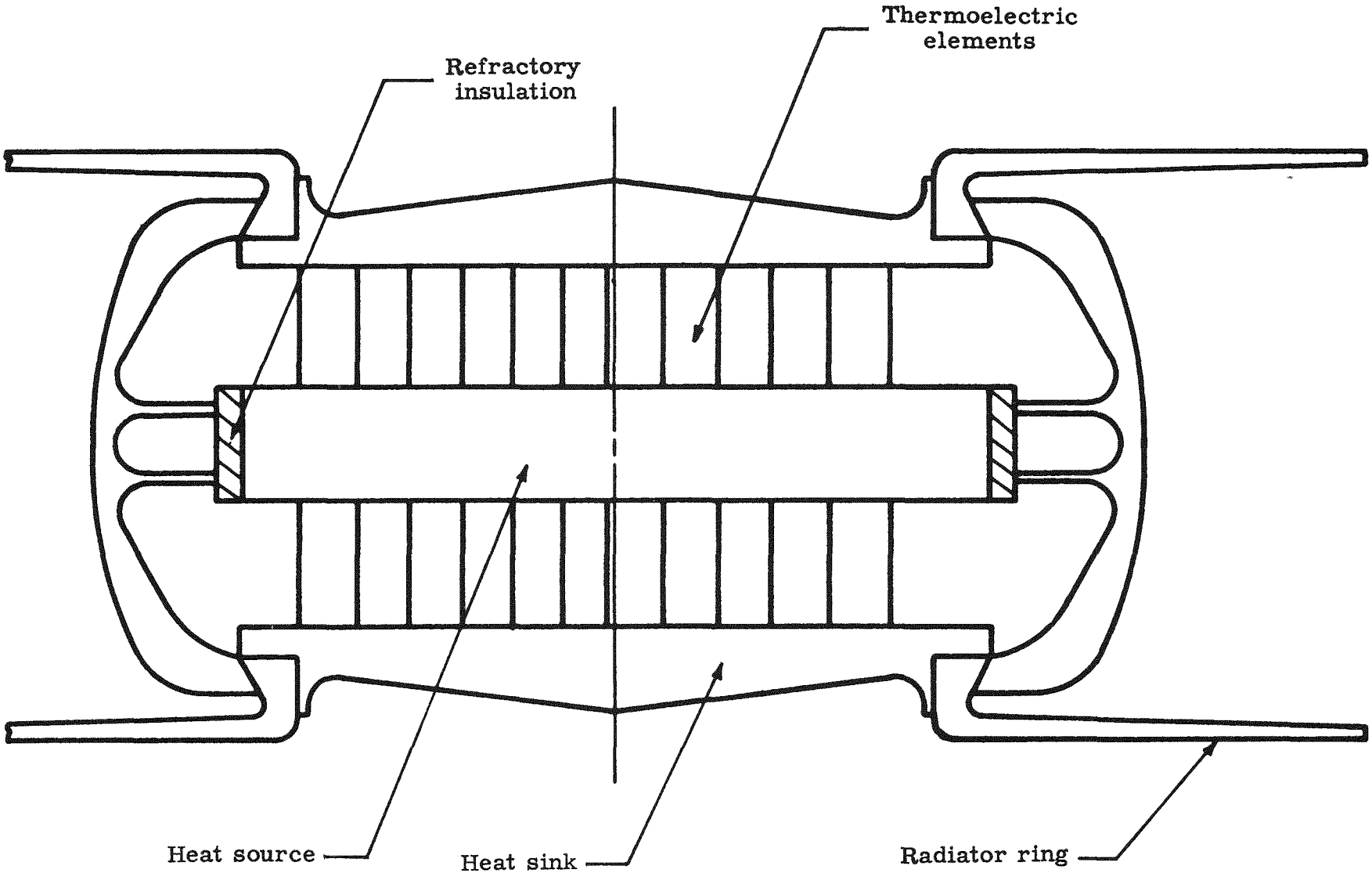

Fig. IV-69. Preliminary Cylindrical Configuration--13-Watt (e) Thermoelectric Generator for Lunar Impact Mission

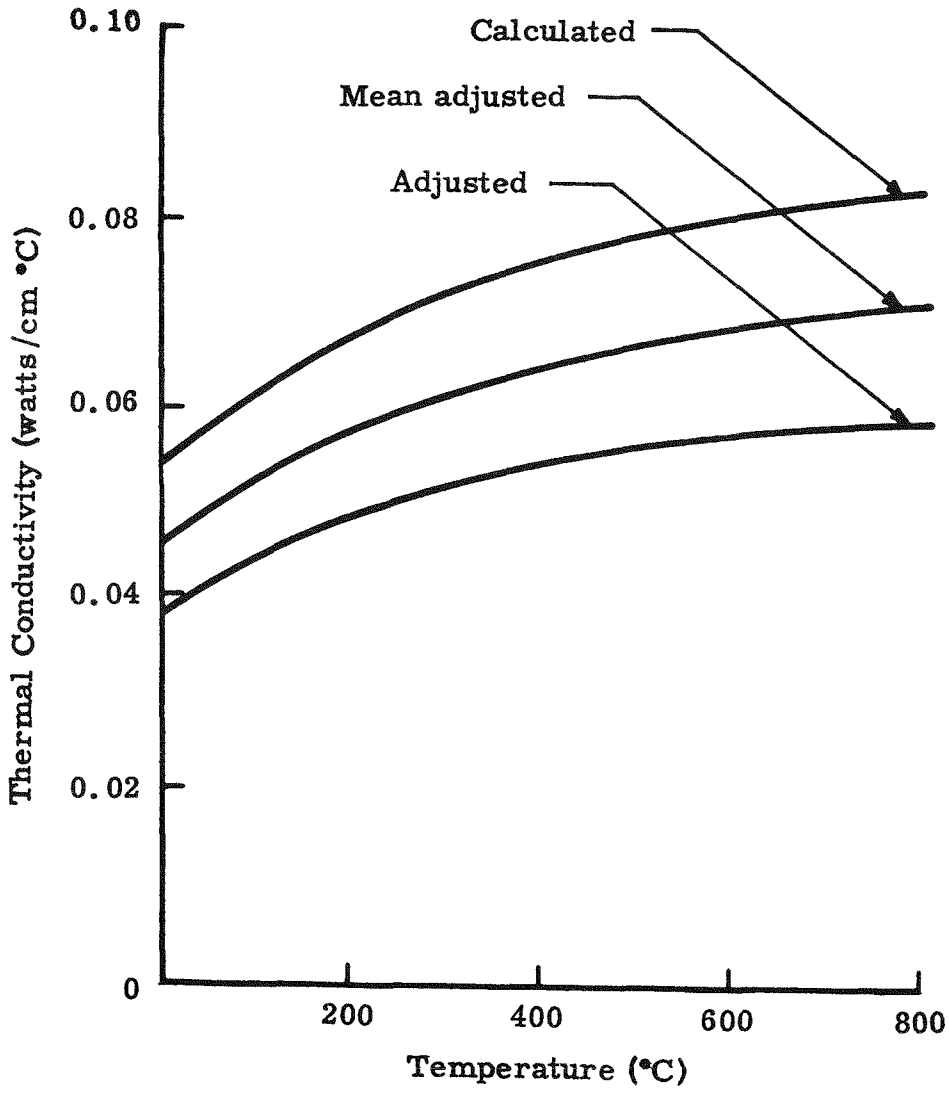

Fig. IV-70. Calculated Thermal Conductivity for Cobalt Silicide

TABLE IV-9

Calculation of Design Parameters

Cobalt Silicide Thermoelements, P and N Type
Heat Loss = 44 watts

Case I (Calculated Thermal Conductivity)

Elements (no.)	Dimensions of Elements: Length (in.)	Diameter (in.)	Efficiencies (%)	
105	1	0.1948	Thermal	84.1
	or 1.25	0.218	Thermoelectric	5.69
			Overall	4.78

Case II (Adjusted Thermal Conductivity)

Elements (no.)	Dimensions of Elements: Length (in.)	Diameter (in.)	Efficiencies (%)	
94	1	0.1829	Thermal	78.7
	or 1.25	0.2044	Thermoelectric	7.83
			Overall	6.16

Case III (Adjusted Mean Thermal Conductivity)

Elements (no.)	Dimensions of Elements: Length (in.)	Diameter (in.)	Efficiencies (%)	
98	1	0.1874	Thermal	81.2
	or 1.25	0.2095	Thermoelectric	6.84
			Overall	5.55

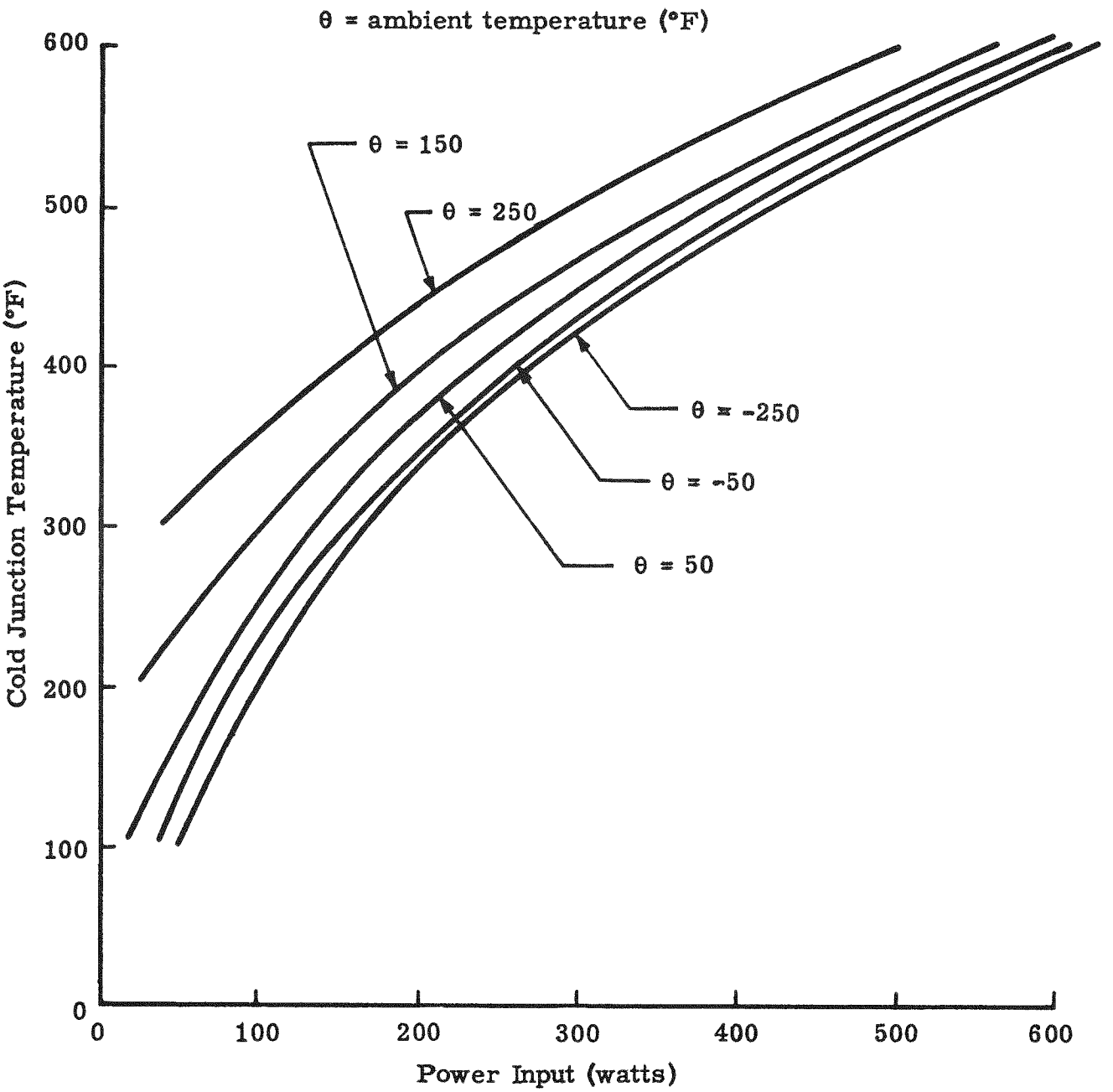

Fig. IV-71. Lunar Probe Generator

Since Singer's equation is not exact for a generator resting on the moon's surface, more detailed calculations were then undertaken in which the equation for radiation to an infinite sink was used to determine cold junction temperatures as a function of lunar ambient conditions. Other refining assumptions were:

(1) The adjusted mean thermal conductivity curve for cobalt silicide was utilized in all calculations.

(2) All thermoelectric power was generated by N-type elements, with the return wires neither contributing to nor reducing thermoelectric efficiency.

(3) Hot junction temperatures for the generator under the poorest ambient condition at end of life were assumed to be in the range of 1200 to 1400° F, and the thermoelectric design was then varied to give 13 watts of electrical power under these conditions. Four designs covering the hot junction temperature range were obtained, and their performance at significant points in time prior to end of life was computed.

(4) No loss of heat through insulation or structure is considered, pending determination of the actual design to be used.

The significant results obtained are shown in Table IV-10.

Design. Since essentially no published information on the thermoelectric characteristics of cobalt silicide is available, a program has been initiated to measure k, ρ , and α for the N-type material. The program is being supported out of overhead funds, and the information obtained will be made available to this Subtask. Experimental data are vital to the further consideration of this material.

The approach to design that has been followed is the use of all N-type elements connected in series with a metallic conductor. The first material considered for the wire was iron, but the optimum size with respect to electrical resistivity and thermal conductivity still permits 26% of the heat flux to bypass the thermoelectric elements. The use of a return wire also complicates the installation of the thermoelectric elements.

As an alternative, the use of the more conventional P and N element arrangement has been studied, and two designs have been completed.

The first one uses "nested" elements. A P-type lead telluride element is placed inside a previously drilled N-type cobalt silicide element. The two elements are electrically insulated from each other by a lavite sleeve, except at the hot shoe junction. At the hot junction, the metal shoe is shaped to act as an electrical jumper and to produce a temperature gradient of sufficient magnitude to permit the use of lead telluride.

TABLE IV-10

Results of Parametric Study Based on Mean Thermal Conductivity Curve

Original Design at End of Life in 250° F Ambient

Temperature--°F				
Hot Junction	1200	1250	1300	1400
Cold Junction	493	488	485	474
Thermoelectric efficiency--%	4.64	5.04	5.13	5.54
Output power--watts	13	13	13	13
Elements--no.	156	142	135	121
Current--amperes	4.3	4.3	4.3	4.3
Voltage--volts	3	3	3	3

Design Characteristics 60 Days Prior to End of Life in 250° F Ambient

Temperature--°F				
Hot Junction	1530	1675	1800	1940
Cold Junction	540	531	529	516
Thermoelectric efficiency--%	5.30	5.68	5.69	5.74
Output power--watts	21.3	22.5	22.7	21.24
Elements--no.	156	142	135	121
Current--amperes	5.55	5.7	5.73	5.56
Voltage--volts	3.84	3.95	3.97	3.82

Design Characteristics at End of Life in -250° F Ambient

Temperature--°F				
Hot Junction	1125	1250	1260	1410
Cold Junction	413	403	399	385
Thermoelectric efficiency--%	5.26	5.84	5.97	6.34
Output power--watts	14.7	16.6	15.5	16.49
Elements--no.	156	142	135	121
Current--amperes	4.61	4.9	4.73	4.9
Voltage--volts	3.19	3.4	3.27	3.36

Design Characteristics 60 Days Prior to End of Life in -250°F Ambient

Temperature--°F				
Hot Junction	1460	1575	1675	1875
Cold Junction	471	459	454	440

TABLE IV-10 (continued)

Thermoelectric efficiency--%	5.77	5.95	6.32	6.22
Output power--watts	22.9	21.6	22.9	23.08
Elements--no.	156	142	135	121
Current--amperes	5.75	5.59	5.75	5.8
Voltage--volts	3.98	3.87	4.00	3.98

Design Characteristics at Launch in 80° F Ambient

(60 Days Prior to End of Life)

Temperature--°F				
Hot Junction	1450	1580	1650	1850
Cold Junction	452	443	437	427
Thermoelectric efficiency--%	5.9	6.14	6.16	6.25
Output power--watts	24.4	23.99	23.6	23.4
Elements--no.	156	142	135	121
Current--amperes	6.02	5.89	5.84	5.84
Voltage--volts	24.4	23.99	23.6	23.4

In the second design, the wiring is also eliminated by substituting P-type elements. The design involves the use of rectangular elements about 1 inch long. (A P-element is 0.35 inch by 0.4 inch by 1.0 inch and an N-element is 0.05 inch by 0.4 inch by 1.0 inch.) The difference in area results from the difference in the thermoelectric properties of the two materials. The rectangular elements are insulated from each other and bonded together with a ceramic cement. This type construction would contribute quite significantly to the strength of the generator.

Both designs use the cobalt silicide to strengthen the lead telluride element and prevent sublimation at elevated temperatures. Substitution of the P-element for the wire has the effect of appreciably reducing heat loss while increasing the total power output of the generator.

Still another area to be explored is the use of cobalt silicide in the form of both P- and N-type elements, provided that data on P-type material can be obtained.

4. Thermoelectric Optimization Code*

In the course of literature surveys pertaining to thermoelectric operation, it became apparent that no uniform convention had been selected to indicate the direction of heat or current flow within and external to the elements. A meaningful convention has therefore been established which will be employed henceforth in all computations and in development of the IBM code. The convention is as follows.

*T. Bustard, L. Lee

The thermoelectric properties designated as the Seebeck, Peltier and Thomson coefficients will be considered positive for a P-type element and negative for an N-type element. The distance variable, x, is chosen to be positive in the direction of decreasing temperature, i.e., from the hot to cold junction. Heat flow will also be positive in the direction of decreasing temperature, regardless of the thermoelement type. Current flow will be positive in the circuit from plus to minus, positive in a P-element from minus to plus, and positive in an N-element from plus to minus. The given sign convention will correlate all of the observed thermoelectric phenomena consistently. That is,the Thomson, Joule and Peltier effects (at x = 0) will release or generate heat and the Peltier effect (at x = L) at the cold junction will absorb heat.

Detailed and extensive computations have resulted in the first set of equations to be utilized in programming the IBM-709 for thermoelement optimization. The more important equations represent:

(1) Thermoelement energy balance.

(2) Differential equation for heat flow in a thermoelement.

(3) Thermoelectric efficiency of the system.

They have been modified as appropriate to permit numerical solution and will be utilized to maximize the thermoelectric efficiency in terms of the physical parameters included.

Appendix B shows the derivation of the equations and the flow chart to be employed in the code.

5. Hazards Evaluation*

An analysis of the hazards resulting from a launch pad accident or abort and ensuing fire is presented in Appendix C.

A study of the launch-to-space flight hazard conditions which arise from the operation of the Atlas-Agena B (with Bell Hustler engine) rocket system has defined the environments of temperature, pressure, velocity and chemical action the generator would experience as a result of malfunction in the rocket at any point in the sequence. The system studied is considered representative of the type which could be used to carry a 300-pound payload to the moon.

---

*C. Riggs.

The following accidents are considered feasible:

(1) Launch failures (flight distance = 0 to 1000 feet; time = -15 minutes to +15 seconds from zero countdown).

(a) Propellant tank failure.
First-stage fire of LOX and RP-1 fuel, followed by ignition of second-stage fuel (unsymmetrical dimethylhydrazine and red fuming nitric acid). Duration of 20 minutes, T_{max} = ~ 6000° F, T_{avg} = ~ 3000° F. Fuel capsule may melt, depending upon insulation provided by surrounding material.

(b) Propulsion failure.
Similar to Item a but with decreasing severity as height increases. In addition, probability of impact of payload or generator on launch pad becomes reasonable after fall from 1000 feet. Velocity at impact = 250 feet/second. Fuel capsule probably retains integrity.

(c) Guidance failure.
Same as Item b except debris scattered over slightly larger area due to firing of destruct charges. Fuel capsule probably retains integrity.

(2) Ascent failures (altitude = 1000 feet to 1.58×10^6 feet, time = +15 to +585 seconds).

(a) Failure at pitchover (point of departure from vertical trajectory) (altitude = 1000 feet, velocity = 200 feet/second). Same as (1, b) above, except that point of impact is probably down range from launch pad.

(b) Failure at maximum dynamic pressure (altitude = 38,000 feet, velocity = 957 feet/second, range = 0.1 nautical mile). Vehicle coasts to a 41,000 foot altitude, then falls to earth about one nautical mile down range. Fire will not be a severe problem. The ability of fuel capsule to withstand impact on a hard surface is dependent upon deceleration provided by vehicle and generator-fuel capsule design payload structure. Accurate analyses of the drag factors and resulting impact velocity have not been made.

(c) Failure at booster separation (altitude = 250,000 feet; velocity = 10,890 feet/second, range = 60 nautical miles). The vehicle coasts to 586,000 feet altitude and falls to earth 640 miles down range. Aerodynamic heating results from re-entry. Whether burnup of the fuel capsule in the stratosphere occurs is contingent upon the relative orientations of the generator, payload and rocket structure. Impact of residual material in the ocean is assumed.

(d) Subsequent failure during ascent.
The failure of the final stage to ignite results in a fall to earth of the vehicle from an altitude of 1,584,000 feet and at a range of 2500 nautical miles. Aerodynamic heating is more severe than in (c) above, and the same remarks apply.

(3) Final-stage failure after ignition.
Three cases result:

(a) Final velocity greater than 25,000 feet/seconds and less than 35,390 feet/second.
The vehicle becomes a satellite of the earth, with the possibility of impacting on the moon at the intersection of the trajectories if its velocity is greater than 35,092 feet/second and proper orientation is maintained. Failure to impact probably results in a stable earth orbit persisting over many Cm-242 half lives. Burnup upon re-entry is probable, with Pu-238 being dispersed into the atmosphere. Maximum Pu-238 activity occurs at seven years.

(b) Final velocity greater than 35,390 feet/second.
The vehicle escapes from gravitational pull of the earth and becomes a satellite of the sun. There is a possibility of lunar impact if proper orientation is maintained. The possibility of its recapture by earth is extremely unlikely.

(c) Final velocity less than 25,000 feet/second.
Re-entry to the earth occurs in less than one revolution. Conditions are the same as in (2, d) above, except that the impact area has not been determined.

APPENDIX IV-A--THERMAL ANALYSIS-MOD I GENERATOR

A. THERMOELECTRIC ELEMENTS

1. Thermoelectric Coefficients--Electrical and Thermal

The thermoelectric elements considered for the Mod I generator are manufactured by Transitron Electronic Corporation.

The integrated average values of resistivity, Seebeck coefficient and thermal conductivity between 538°C (1000°F) and 149°C (300°F) are as follows:

	Resistivity (ρ, ohm-cm)		Seebeck Coefficient (e, volts/°C)		Thermal Conductivity (k, watts/cm-°C)	
Values	N	P	N	P	N	P
Theoretical	3.03×10^{-3}	3.72×10^{-3}	2.36×10^{-4}	2.37×10^{-4}	1.93×10^{-2}	1.63×10^{-2}

2. Calculation of Optimum Element Sizes

An algebraic summation of the voltages in the equivalent circuit diagram for a one-generator system

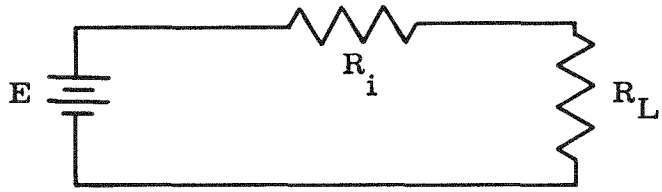

gives the equation:

$$E = E_i + E_L = I(R_i + R_L)$$

$$= N\alpha\Delta T$$

E = total emf of thermoelectric elements

E_i = voltage drop across elements

E_L = voltage drop across load

I = current

R = electrical resistance

R_i = internal resistance

R_L = load resistance

N = number of couples (a couple is one N-type element and one P-type element)

α = Seebeck coefficient per couple ($|e_P| + |e_N|$)

e = electricity produced per element

ΔT = temperature drop between the hot and cold junctions of the elements

$$I = \frac{E_L}{R_L}$$

$$N\alpha\Delta T = \frac{E_L}{R_L}(R_i + R_L)$$

$$= E_L \left(\frac{1 + R_L/R_i}{R_L/R_i} \right)$$

For maximum generator efficiency

$$\frac{R_L}{R_i} = \left[1 + \left(\frac{T_h + T_c}{2} \right) \frac{\alpha}{\sqrt{K_P \rho'_P} + \sqrt{K_N \rho'_N}} \right]^{2} 1/2$$

T_h = hot junction temperature (811 °K)

T_c = cold junction temperature (422 °K)

$\alpha = (2.36 + 2.37) \times 10^{-4} = 4.73 \times 10^{-4}$ volts/°C

$K_P = 1.63 \times 10^{-2}$ watts/cm-°C

$K_N = 1.93 \times 10^{-2}$ watts/cm-°C

$\rho'_P = \rho_P (1.5) = 3.72 (1.5) \times 10^{-3} = 5.58 \times 10^{-3}$ ohm-cm

$\rho'_N = \rho_N (1.5) = 3.03 (1.5) \times 10^{-3} = 4.54 \times 10^{-3}$ ohm-cm

The 1.5 coefficient is a factor used to adjust internal resistance to a laboratory measured values.

$$\frac{R_L}{R_i} = 1.18$$

$$N = \frac{E_L}{\alpha \Delta T} \left(\frac{1 + 1.18}{1.18}\right)$$

$N = 15$ couples

$$\text{Output power } W = \frac{E_L^2}{R_L}$$

$$R_L = \frac{E_L^2}{W} = \frac{(1.5)^2}{1.5} = 1.5 \text{ ohms} = 1.18\ R_i$$

$$R_i = \left(\frac{\rho'_P \ell_P}{A_P} + \frac{\rho'_N \ell_N}{A_N}\right) \times N = \frac{1.5}{1.18}$$

For practical purposes, let $\ell_P = \ell_N$ and $A_P = A_N$

$$R_i = (\rho'_P + \rho'_N) \frac{\ell_N}{A} = \frac{1.5}{1.18}$$

$$\frac{\ell}{A} = \frac{1.5 \times 10^3}{1.18(15)(10.12)} = 8.37$$

Since available space for mounting the generator is a critical factor, it is necessary that the length be kept to a minimum. The length varies directly as the square of the diameter; therefore, the smallest practical diameter of 1/4 inch will be used. The length must be 1.04 inches.

For an output of 1.5 watts at 1.5 volts, 15 pairs of thermoelectric elements are required. The nominal dimensions of these elements are 1/4-inch diameter by 1.04 inches long. Element arrangement will be three rows of 10 elements each.

B. HEAT FLOW CALCULATIONS

Heat losses for the Mod I generator were calculated on the basis of the following assumptions:

(1) Steady-state heat flow.

(2) Parallel heat flow.

(3) Temperature of satellite structure is 300 °K (27 °C).

(4) The hot junction temperature is 811 °K (538 °C).

(5) The cold junction temperature is 422 °K (149 °C).

(6) The temperature of the heat source surface opposite the hot junction is 860 °K.

1. Flow Through Elements

The heat flow through the 30 thermoelectric elements is

$$q_A = \frac{N(K_P + K_N)}{\ell/A} \Delta T$$

$$= \frac{15\,(3.56 \times 10^{-2})\,(389)}{8.37}$$

$$= 24.8 \text{ watts}$$

2. Flow Through Min-K Insulation

The heat flow through the Min-K insulation surrounding the 30 thermoelectric elements is

$$q_B = \frac{KA\Delta T}{\ell}$$

$K = 3.3 \times 10^{-4}$ watts/cm-°C

$\Delta T = 389\,°C$

$\ell = 2.54$ cm

$A = 2(6)(2.54) - 30(0.786)(0.25)^2(6.45)$

$A = 30.48 - 9.506$

$= 20.97 \text{ cm}^2$

$$q_B = \frac{3.3 \times 10^{-4}\,(20.97)(389)}{2.54}$$

$$= \frac{3.3\,(2.097)(0.389)}{2.54} = 1.06 \text{ watts}$$

3. Flow Through Structure

The structure that holds the heat source in place is a stainless steel cradle attached to the radiator. The stainless steel heat path has an effective area of 0.244 cm^2 and a length of 3 centimeters.

$$q_c = \frac{KA\Delta T}{\ell}$$

$K = 0.265$ watts/cm-°C

$T = 600\,°K - 410\,°K = 190\,°C$

$$q_c = \frac{0.265\,(0.2)\,(190)}{3}$$

$= 4.1$ watts

4. Other Heat Losses

The design details of the Mod I generator have not yet been completely defined; therefore, it is necessary to estimate the heat loss to the interior of the satellite on the basis of the previous preliminary generator calculations. It is reasonable to assume that these losses are not greater than 1.5 watts.

5. Summary of Heat Losses

	(watts)
Through elements (q_A)	24.8
Through Min-K (q_B)	1.1
Through structure (q_c)	4.1
Other losses (q_D)	1.5
Conversion to power	1.5
Total or source power required	33.0

Overall generator efficiency $= \frac{1.5\,(100)}{33} = 4.54\%$.

APPENDIX IV-B--RADIATOR TEMPERATURE VERSUS ORBITAL CONDITION

This analysis defines the equilibrium radiator temperature for use in predicting the nominal generator output. A temperature range is also defined which can be used to evaluate the possible variation of the generator output due to changes in orbital conditions.

A. ORBIT LOCATION

The orbital path of the satellite has been defined to lie in a plane which is inclined to the earth's equator at 67-1/2 degrees SE. The altitude of the satellite is to be 500 ± 100 nautical miles. However, for the purposes of this analysis, the satellite path was varied from an equatorial to a polar orbit. Thus, this study has been accomplished to determine the relationship between the average equilibrium radiator temperature and variables resulting from orbital conditions and the orientation of the radiator surfaces relative to the incoming solar energy.

B. THERMAL CALCULATIONS

The solar power absorbed on the radiator surface is calculated by use of the Goldman-Singer equation.

where $$q_a = \left[(1 - \alpha_v)\,(1400)\,(\mu + \frac{\alpha_E}{\pi}\cos\xi) + \varepsilon_{IR}\,188.5\right] A_a$$

$(1 - \alpha_v)\ 1400\,\mu$ is direct radiation from the sun

$(1 - \alpha_v)\,(1400)\frac{\alpha_E}{\pi}\cos\xi$ is reflected energy from earth

$\varepsilon_{IR}\,(188.5)$ is energy radiated from the earth

$1 - \alpha_v = 0.3$

$\alpha_E = 0.34$

$\varepsilon_{IR} = 0.8$

A_a = effective radiator surface for absorption (M^2)

The substitution of these known values into the equation reduces it to

$$q_a = \left[420\ (\mu + 0.11 \cos \xi) + 151\right]\ A_a$$

The properties of this relationship which are functions of orbital conditions are μ (eclipse factor) and ξ (angle between the orbit and the sun's radiation).

The total energy to the radiator is equal to the energy radiated from it, thus:

where $q_a + q_b = \varepsilon_{IR}\ A_r\ \sigma\ T^4$

q_b = power from internal source--watts

A_r = effective area for radiation (M^2)

$\sigma = 5.67 \times 10^{-8}$ watts/M^2 °K^4

T = average equilibrium temperature of the radiator surface--°K

By combining these equations, the average equilibrium temperature of the radiator can be calculated for various orbital conditions. The orientation of the radiator surface relative to the sun's rays is considered on the basis of the ratio A_r/A_a. The resulting relationship is:

$$T = \left[\frac{q_b + \left[420\ (\mu + 0.11 \cos \xi) + 151\right] A_a}{\varepsilon_{IR}\ A_r\ \sigma}\right]^{1/4}$$

This study has been extended for all angles between an equatorial and a polar orbit. For orbit altitudes greater than 400 miles, μ varies between 1 and 0.7.

Since the value of ξ can only vary between 0 and 90 degrees, the possible extreme conditions are:

$\xi = 0°$; $\mu = 1$

$\xi = 0°$; $\mu = 0.7$

$\xi = 90°$; $\mu = 1$

$\xi = 90°$; $\mu = 0.7$

The value of the ratio, A_r/A_a, for the radiator shape proposed for the

Mod I generator varies between 1.6 and infinity. A_r is defined as the actual area of the radiator which is 380 cm^2. For a flat plate, $A_r = A_a$, and A_r/A_a is 1. For a sphere, $A_r = 4A_a$, and A_r/A_a is 4.

From these data, a family of curves has been plotted in Fig. B-1 showing the relationship between radiator temperature and all anticipated orbital conditions.

C. CONCLUSIONS

This analysis reveals a possible temperature range for the radiator surface of 402 to 366° K. Temperatures within this range represent equilibrium conditions. The satellite on which the generator will be mounted will orbit the earth approximately every two hours and will rotate about one of its own axes at a rate of 2 rpm. This means that the temperature of the radiator will never reach an equilibrium condition. Instead, it will oscillate about some mean temperature.

For design purposes, the value of the mean temperature has been defined as 376° ±10° K. This temperature was selected because the probability that the radiator will be oriented toward "black space" (no solar heat absorption) is 0.5. Therefore, this should place the mean temperature in the bottom part of the possible temperature range of 402 to 366° K.

Figure B-1 shows the variation of the radiator temperature as a function of the eclipse factor (μ) and the angle between the orbit and the sun's radiation (ξ) as well as the ratio of effective radiator surface for radiation to effective radiator surface for absorption (A_r/A_a). The change in temperature due to ξ and μ is small (1-1/2 to 3° K) and, therefore, the orientation of the radiator surface relative to the sun's radiation is the only significant variable.

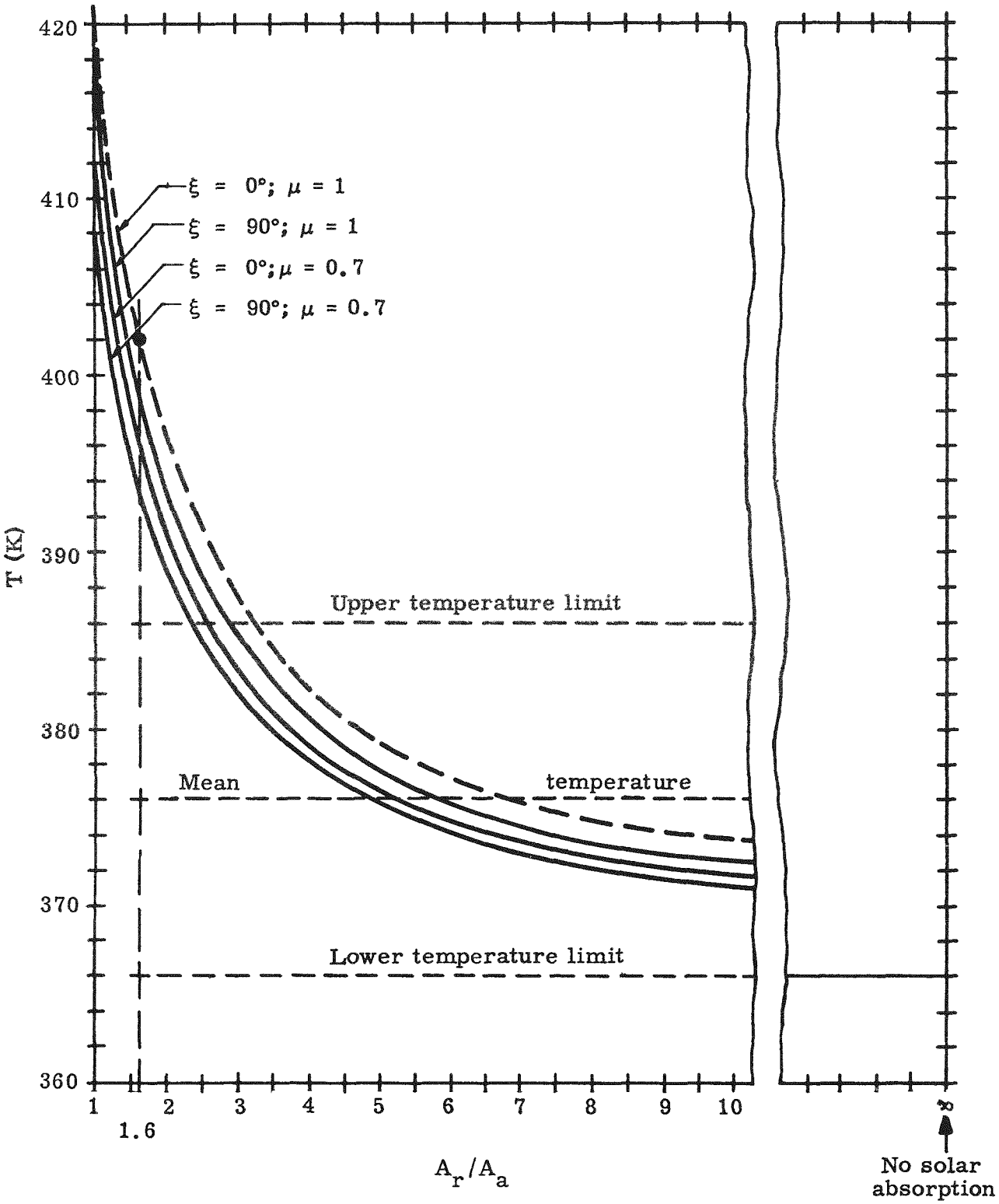

Fig. B-1. Radiator Temperature Versus Orbital Condition

APPENDIX IV-C--DC-TO-DC CONVERTER DESIGN AND ANALYSIS

A. CONVERTER DESIGN AND ANALYSIS

The dc-to-dc converter design program consisted of component selection and converter design analysis. The purpose was to design a unit capable of providing an efficient voltage conversion from a 1.5-volt input source. The design was analyzed for operation at one ampere of input current.

The physical characteristics of the converter may be found in the converter specification at the back of this appendix.

The following elements were studied for their loss characteristics to maintain as low a loss function as possible.

(1) Transistor loss--This loss is created by the saturation resistance in the collector of the transistor. To minimize this loss, transistors with low saturation resistance are desired. The T12N511 and T12N456 series are ideal for this application with respective resistances of 0.025 and 0.048 ohm.

(2) Core loss--This loss is attributed to the core geometry and electrical characteristics. When these two factors are established by core selection the loss will be found to vary almost directly as the volts per turn ratio. Therefore, a transformer with low core loss must have a low volts per turn ratio.

(3) Copper loss--This loss is caused by the resistivity of copper increasing directly with the length and inversely as the cross sectional area of the wire. This means a high volts per turn ratio should be used for low copper loss.

(4) Rectifier loss--All rectifier diodes have a forward drop creating a loss equal to the product of the load current and the forward drop. Low drop germanium diodes such as the GEIN91 series have been selected for this application.

(5) Driving power--This loss is created due to the need for using some of the available power to drive the converter oscillator. Additional loss is necessary for regulating the drive such that the converter may tolerate a reasonable load, temperature and transistor variation.

(6) Other losses--Losses due to transistor switching and leakage are present but are negligible if moderate power outputs are maintained.

A basic converter oscillator is shown in Fig. C-1. The feed-back windings, L_3 and L_4, permit the circuit to oscillate. The power consumed by the oscillator is approximately equal to the sum of the power dissipated in R_1 and the core loss.

The secondary winding circuit may have either of two configurations shown in Fig. C-1. The bridge circuit requires half the number of turns, thus reducing copper loss but the diode loss is doubled. The full-wave circuit is preferred for low voltage applications because the reduction in diode loss can more than make up the increase in copper loss.

Itemizing and anticipating the various losses, a reasonable estimate of the total loss expected can be calculated.

Transistor loss is equal to the square of the current times the saturation resistance. For a 2N456 transistor, the loss is:

where I^2R

I = collector current (1 ampere)

R = collector resistance (0.048 ohm)

$\therefore I^2R = 1^2 \times 0.048 = 48$ milliwatts.

Diode loss is equal to the load current times the forward drop (I x E). Load current was estimated at 75 milliamperes and the forward drop at 0.6 volt.

Therefore, the diode loss is:

$0.075 \times 0.6 = 45$ milliwatts.

The drive power is approximately:

$E_{in}^2 \div R = 1.5^2 \div 30 = 0.075 = 75$ milliwatts.

The core and copper loss can be anticipated with reasonable accuracy.

Core loss = 100 milliwatts

Copper loss = 80 milliwatts.

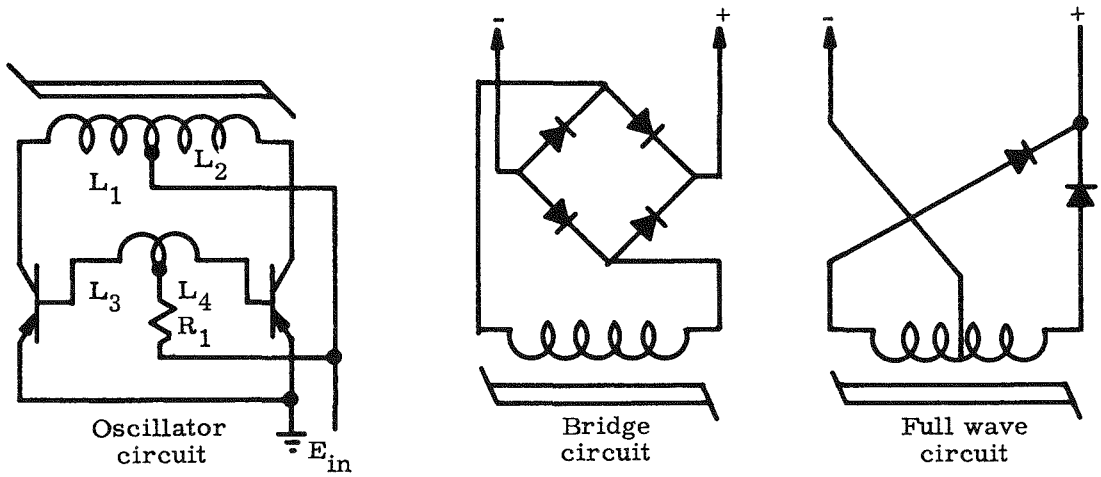

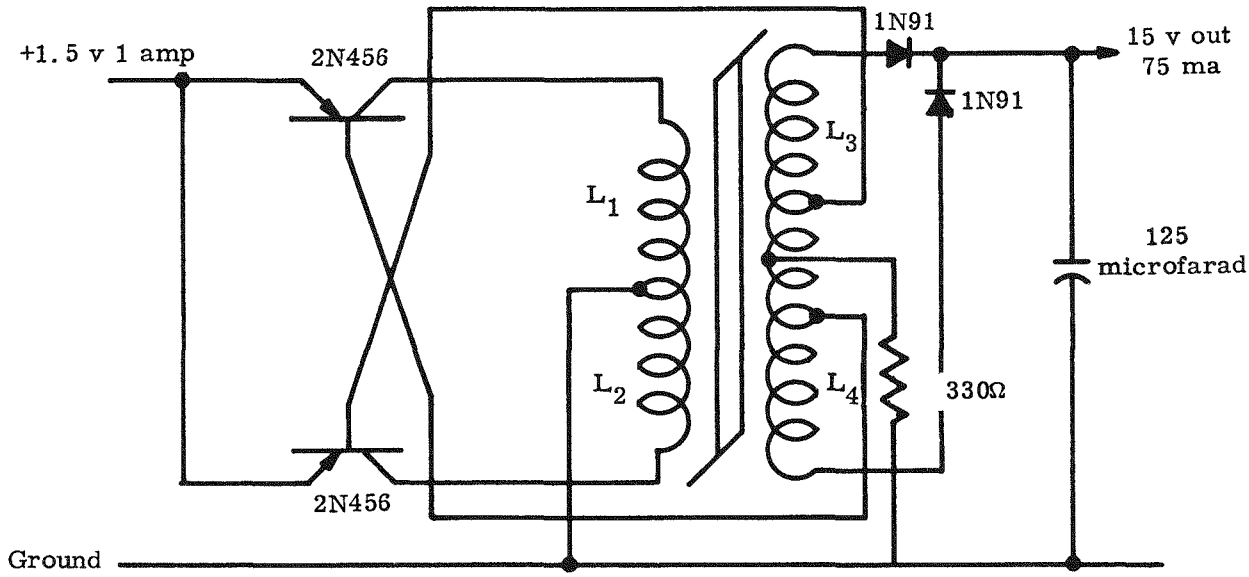

L_1, L_2 = 43 turns No. 18
L_3, L_4 = 430 turns No. 28
Feedback tap at 14 turns from centertap

Fig. C-1. Converter Circuits

Summing all the losses:

Transistor	48
Diode	45
Drive	75
Core	100
Copper	80
Total	348 milliwatts

The efficiency of the converter would then be:

$$\frac{\text{Power input - power loss}}{\text{Power input}} \times 100\%$$

$$\frac{1.5 - 0.348}{1.5} \times 100\% = 77\%.$$

The 77% efficiency figure is not intended as the maximum, but merely as an expectant figure for a conventional circuit using ideal components. The efficiency can, however, be increased to some extent by utilizing certain techniques. For instance, if the load current could be drawn through the source, the converter would be required to draw a decreased current. This would reduce the transistor and copper loss by 10% for a saving of 12 milliwatts. The load current can be used to regulate the drive power such that R_1 in Fig. C-1 could be increased by 10 times. This will permit a reduction in drive power by about 30%. The overall efficiency could then be increased by:

$$\frac{12 \text{ mw} + 25 \text{ mw}}{1.5 \text{ watts}} \times 100\% = 2.5\%.$$

The transformer design was based on the following minimum loss formula:

$$\text{Core loss} = K E + N$$

K = amperes--turns of core required (2.6)
E = winding voltage (1.5)
N = number of turns.

$$\text{Copper loss} = \frac{R \ell N^2}{A}$$

R = resistivity (0.68×10^{-6} ohms)
ℓ = mean length per turn (1.8 inches)
A = available copper area (0.049 sq in.).

Differentiating:

where $\frac{d L_{core}}{d N} = \frac{-KE}{N^2}$ and $\frac{d L_{copper}}{d N} = \frac{2R\ell N}{A}$

L_{core} = core loss

L_{copper} = copper winding loss.

Maximizing:

$$\frac{KE}{N^2} = \frac{2R\ell N}{A}$$

$$\frac{AKE}{2R\ell} = N^3 = \frac{0.49 \times 2.6 \times 1.5}{2 \times 0.68 \times 10^{-6} \times 1.8}$$

$\therefore$ N = 43 turns

Wire cross section area $= \frac{A}{N} = \frac{0.049}{43} = 0.00114$ sq in.

NOTE: The transformer was designed to have a core with a 1-inch ID and a 1.5-inch OD with a 0.4-inch height. The copper area is computed by dividing the window area by four to permit two primary and two secondary windings. This figure is again divided by 4 to allow for space between windings and unorderly wire placement. Since K, ℓ and A are functions of the core geometry, the turns (N) and, hence, the losses will vary with the shape and size of the core.

1. Converter Tests

The transformer was wound in accordance with the calculated requirements. Figure C-1 shows the diagram of the circuit used to construct a breadboard model. The test data from this model are tabulated in Table C-1. Figure C-2a illustrates efficiency versus power output at 15 and 25 volts. Figure C-2b shows the input voltage versus output current at constant output voltages.

Even though tests were conducted at voltages other than 1.5 and an efficiency figure was computed, it must be remembered that the transformer design was optimized for a 1.5-volt input. Higher efficiencies can be generally expected for higher input voltages.

TABLE C-1

Converter Test Data

E_{in}	I_{in}	P_{in}	E_{out}	$I_{out_{(ma)}}$	P_{out}	Eff %
1.453	0.140	0.223	15.0	8.5	0.127	67
1.485	0.275	0.438	15.0	20.5	0.308	70.6
1.525	0.440	0.700	15.0	35.0	0.525	75
1.565	0.640	1.00	15.0	52.5	0.789	78.9
1.590	0.830	1.32	15.0	67.5	1.01	76.6
1.625	1.01	1.61	15.0	83.5	1.25	77.8
1.645	1.115	1.77	15.0	92.0	1.38	78
1.7	1.48	2.52	15.25	127.0	1.94	77
1.75	2.23	3.9	14.9	145.0	2.16	55
1.85	3.07	5.68	15.1	160.0	2.42	42.5
1.95	4.05	7.9	15.1	187.0	2.82	35.7
4.05	5.05	20.45	17.1	345.0	5.9	28.8
2.32	0.115	0.267	25.0	5.5	0.138	51.5
2.35	0.215	0.506	25.0	13.6	0.340	67.2
2.38	0.31	0.740	25.0	22	0.550	74.3
2.42	0.47	1.14	25.0	35.6	0.890	78.1
2.43	0.56	1.36	25.0	43.5	1.09	80.2
2.49	0.73	1.80	25.0	58.3	1.46	81.1
2.49	0.89	2.22	25.0	71.5	1.79	80.6
2.55	1.25	3.19	25.0	1.01	2.52	79.0
3.78	0.300	1.13	40.0	19.6	0.784	69.3
3.81	0.415	1.58	40.0	29.6	1.184	75.1
3.85	0.504	1.94	40.0	40.3	1.612	83.2
3.87	0.67	2.59	40.0	51.6	2.064	79.8
3.88	0.75	2.91	40.0	58.3	2.232	80.7
3.90	0.88	3.43	40.0	68.7	2.744	80.2
3.92	1.04	4.08	40.0	80.5	3.22	79.1
3.93	1.07	4.21	40.0	85.0	3.40	80.8
3.95	1.245	4.92	40.0	97.0	3.88	79.0
5.7	0.110	0.625	63.8	0	0	0
5.68	0.171	0.972	62.2	10.5	0.653	67.2
5.62	0.340	1.91	60.8	19.8	1.204	63.2
5.6	0.450	2.52	59.8	29.3	1.75	69.6
5.55	0.560	3.105	59.2	38.3	2.265	73.0
5.5	0.700	3.85	58.1	50.0	2.905	75.5
5.45	0.820	4.47	57.3	60.0	3.44	77.0
5.4	0.940	5.07	56.8	70.0	3.975	78.4
5.35	1.07	5.73	55.8	80.0	4.465	78.0
5.3	1.2	6.37	55.0	90.0	4.95	77.8
5.27	1.32	6.96	54.2	100.0	5.42	78.0

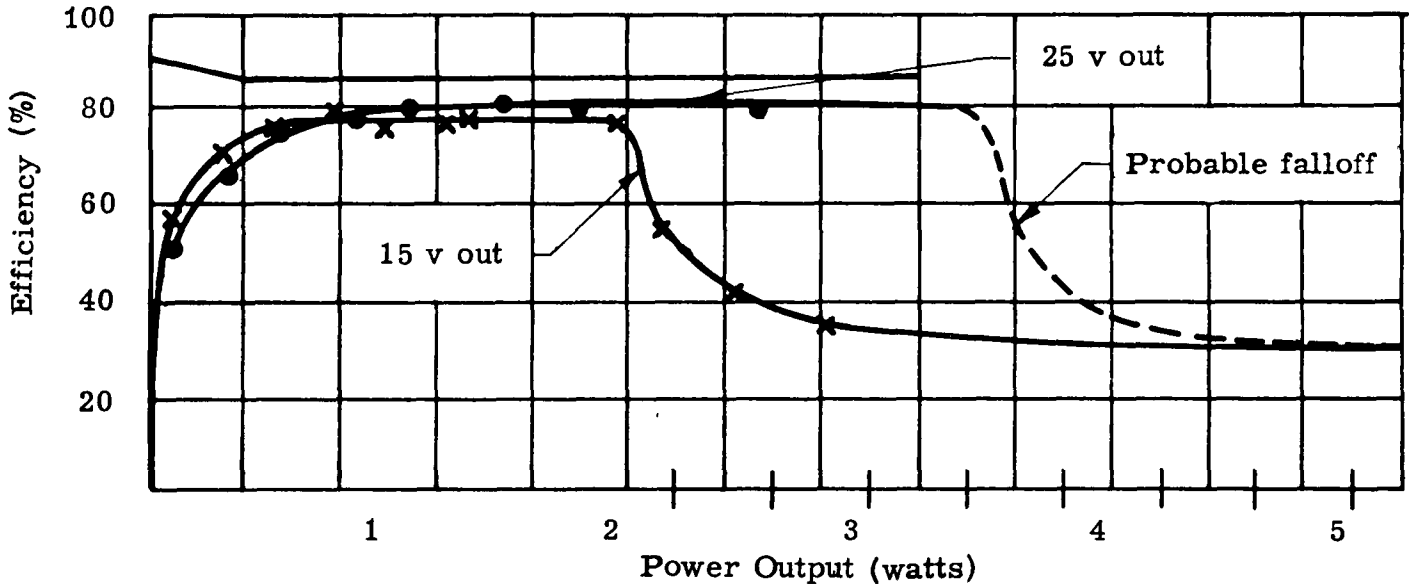

(a) Efficiency Versus Power Output (for 15 and 25 volts out)

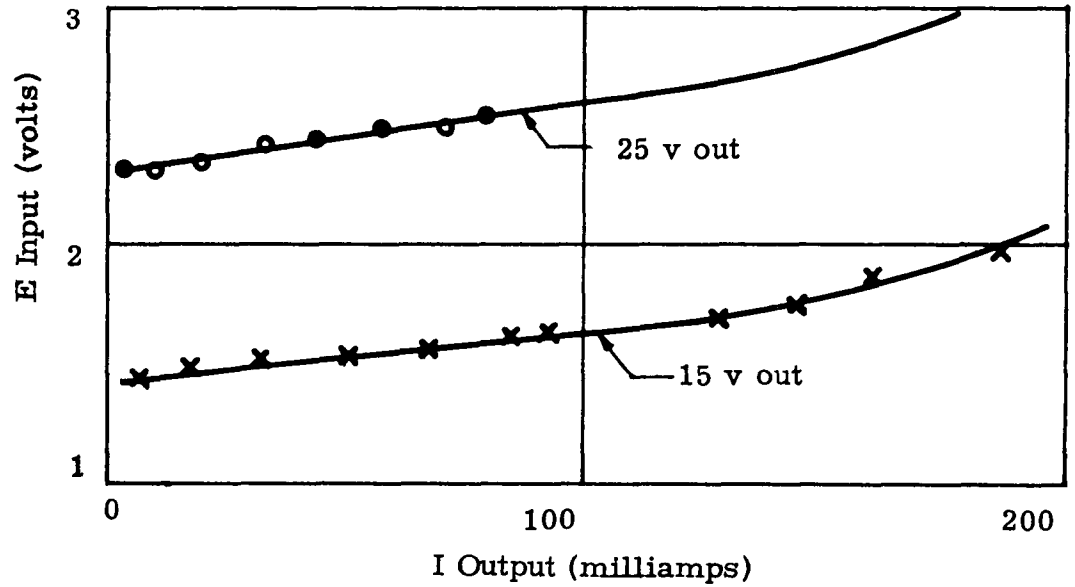

(b) Voltage Input Versus Current Output (for 15 and 25 volts out)

Fig. C-2. Converter Test Data Curves

2. Conclusion

It can be determined from the tests that converters for a 1.5-volt, 1-ampere input can provide efficiencies greater than 75% at an output voltage of 15 volts. It should be possible to maintain voltage regulation of 5 to 10% over a range of input power by placing a 15-volt Zener diode at the output. The transistors are capable of handling 50 watts of power such that transistor overload can be almost eliminated.

SPECIFICATION

The specification prepared for the dc-to-dc converter follows.

I. Purpose

To convert a low voltage D.C. input to higher voltage D.C. output.

II. Physical Description

A. The converter shall approximate the general configuration but not exceed the envelope of the outline dimensions shown in figure 1.

B. Weight - minimum consistent with good design, but not more than 0.6 lbs.

C. Pigtail leads for connecting converter shall come from top of unit as shown in figure 1.

D. Pigtail leads shall be 2 feet long and printed every 3 inches with the identifying voltage or color coded as follows:

Input		Output	
+ 1.5 Volts	White	+ 15 Volts	Red
GND	Black	GND	Brn.

E. Converter end of pigtail leads shall be embedded in the potting encapsulating the converter and physically secured to the converter so that suspending the converter by any pigtail lead shall in no way damage connection or converter.

F. Pigtails shall be made from 20 gage MIL-W-16878 type B, or NSA702 class C or equivalent wire.

G. The converter shall be potted so as to completely encapsulate all components. A thirty pound compressional load applied to any surface of the converter shall in no way damage or impair its performance. Unit shall be capable of operating under same loading.

III. Electrical Requirements

A. Input: Input to the converter shall be a generator capable of supplying 1.5V at 1 amp.

B. Output: The converter shall be capable of supplying the following load within the voltage tolerance specified herein at the generator power level described above under paragraph A "input".

$15V \pm .5$ VDC at 75 ∓ 2.5 ma.

C. Efficiency: 75% minimum efficiency at the above output.

D. Regulation: Output voltage may vary with input power. However, at a constant input, the output voltage regulation shall not exceed 10% no load to full load.

E. Overload: No damage or subsequent impairment to performance of the converter shall result from overloads or short circuits (up to the duration of one minute), or any transients therefrom.

F. Starting ability: The unit shall be capable of starting immediately after the removal of any overload or short circuit as described in paragraph E, above, or after interruption of the input power source (for any length of time).

IV. Environmental Requirements

A. The performance of the converter shall meet all the requirements of Paragraph III Electrical Requirements while operating in the environment as specified herein:

(1) Temperature range: -40 to +176° F

(2) Humidity: Up to 100% relative humidity for 24 hours.

B. The converter shall not be damaged or its performance impaired by exposure to the following environments (converter not required to operate under environments specified herein).

(1) Vibration--Four minutes in each of three mutually perpendicular axes at the following frequencies and accelerations:

10 to 40 cps at ± 5 g

40 to 200 cps at ± 10 g

200 to 2000 cps at ± 20 g

(2) Shock--Shock loading of 20 g along each of the three mutually perpendicuolar axes in both directions for a total of 6 directions. Rise time less than 1 millisecond, dwell time greater than 10 milliseconds.

(3) Acceleration--g forces along the axis of thrust and along an axis perpendicular to thrust at the following times:

40 seconds at 15 g along axis of thrust

4 minutes at 7.5 g perpendicular to axis of thrust

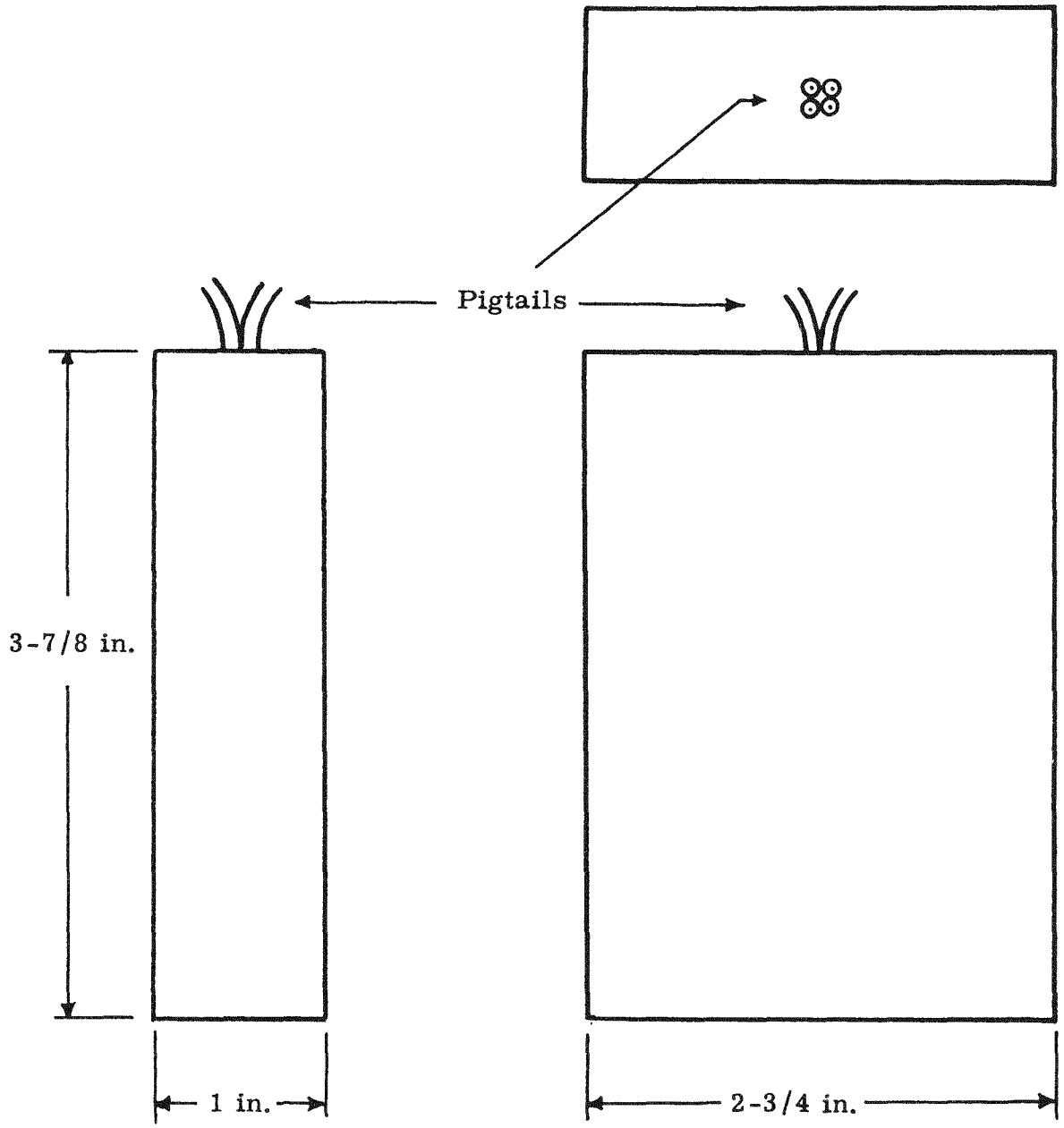

Fig. 1. DC-to-DC Converter

(4) Temperature--Storage at -40° to +160° F.

V. Life

A. The unit shall be capable of meeting the requirements of this specification while continuously in operation for a period of 2 to 5 years.

B. Storage for a period of 5 years under temperature conditions of paragraph 3 of IV B above shall in no way reduce life as specified under paragraph A of V above.

VI. Workmanship

Workmanship shall be in accordance with high grade manufacturing practice.

VII. Drawings and Specifications

The vendor shall supply with each shipment:

A. Two outline drawings and schematic of converter.

B. Specification control drawing used for the manufacture and inspection of the complete converter assembly.

C. Final inspection data sheet for each completed unit.

APPENDIX IV-D--EQUATIONS EMPLOYED IN ANALYSIS OF SPACE PROBE UNIT

A. HEAT LOSS

Fourier's law for conduction through a homogeneous solid is given as:

$$Q = -k\,A(r)\,\frac{dT(r)}{dr}$$

where

Q = heat flow

k = thermal conductivity

r = radius or thickness

A = area as a function of position

T = temperature as a function of position.

Integration between the inner and outer surfaces gives

$$\int_{r_1}^{r_2} \frac{dr}{A(r)} = \frac{k}{Q}\,(T_1 - T_2)$$

where

r_1 = distance from center to inner shell

r_2 = distance from center to outer shell

T_1 = inner shell temperature

T_2 = outer shell temperature.

This equation can be used to compute the heat loss when the area term has been expressed so as to include heat flow through the sides and ends.

B. HEAT TRANSFER IN GROUND HANDLING CASK

Film coefficients for the ground handling cask were calculated using the following equations:

$$Q = h A \Delta T$$

where

Q = heat flow

h = film coefficient

A = heat transfer surface area

ΔT = temperature potential.

McAdams' correlation for vertical cylinders is given as:

$$\frac{h_c L}{k_f} = 0.13 \left[\frac{L^3 \rho_f^2 g \beta_f \Delta T}{\mu_f^2} \left(\frac{C_p \mu}{k_f} \right) \right]^{1/3}$$

where

h_c = film coefficient for natural convection

L = height of vertical surface

k_f = thermal conductivity of fluid at film temperature

ρ_f = density of fluid at film temperature

g = acceleration of gravity

β_f = coefficient of volumetric expansion at film temperature

ΔT = temperature potential

μ_f = viscosity of fluid at film temperature

C_{p_f} = specific heat of fluid at film temperature.

C. CENTERLINE TEMPERATURE OF HEAT SOURCE

Centerline temperature of the fuel element was determined using the following equation:

$$T = \frac{S(R^2 - r^2)}{4k}$$

where

S = volumetric heat production rate

R = radius of the fuel element

r = radius at which the temperature is evaluated

k = thermal conductivity.

APPENDIX IV-E--DEVELOPMENT OF THERMOELECTRIC OPTIMIZATION CODE

Consider Fig. E-1 for purposes of drawing an energy balance over the section of the thermoelement.

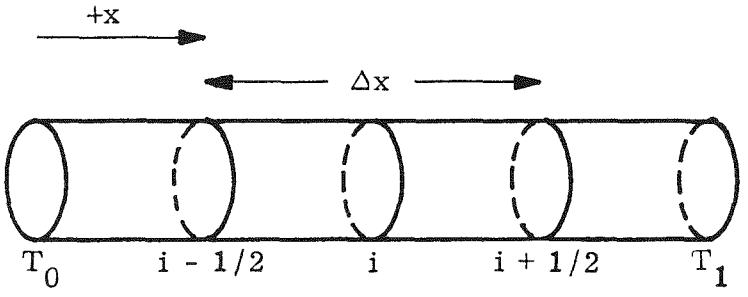

where

T_0 = hot junction temperature

T_1 = cold junction temperature

Δx = incremental segment.

It may then be stated that:

> Energy into face (i - 1/2) + energy generated in i = energy out of face (i + 1/2), purely from an energy balance standpoint. Note also that the current, I, is continuous throughout any circuit regardless of the sign convention. This is true as the current is not created or destroyed within a simple loop circuit. (1)

Utilizing the applicable physical laws, Eq (1) may be expressed in the following form:

$$-k_{i-1/2} A_{i-1/2} \left.\frac{dT}{dx}\right|_{i-1/2} + I^2 R_i + \tau_i I \left.\frac{dT}{dx}\right|_i \Delta x = \tag{2}$$

$$-k_{i+1/2} A_{i+1/2} \left.\frac{dT}{dx}\right|_{i+1/2}$$

where

k = thermal conductivity

A = cross-sectional area

T = temperature

R_i = resistance

τ = Thomson coefficient

x = distance or length variable

$I^2 R_i$ = Joule heat.

$\Delta x \tau I \frac{dT}{dx}$ = Thomson heat

$k A \frac{dT}{dx}$ = conducted heat.

From the definition of the resistivity of a material:

$$R_i = \frac{\rho_i \Delta x}{A_i} \tag{3}$$

where

ρ_i = material resistivity.

Substituting Eq (3) into Eq (2) and rearranging, the following is obtained:

$$\frac{k_{i+1/2} A_{i+1/2} \left.\frac{dT}{dx}\right|_{i+1/2} - k_{i-1/2} A_{i-1/2} \left.\frac{dT}{dx}\right|_{i-1/2}}{\Delta x} + \frac{I^2 \rho_i}{A_i} + \tau_i I \left.\frac{dT}{dx}\right|_i = 0. \tag{4}$$

Taking Eq (4) in the limit as $\Delta x \to 0$, it is found that:

$$\frac{d}{dx}\left(k(T)\, A(x)\, \frac{dT(x)}{dx}\right) + \frac{I^2 \rho(T)}{A(x)} + \tau(T)\, I\, \frac{dT(x)}{dx} = 0 \tag{5}$$

which is the governing differential equation for heat flow in a thermoelement. It may be noted that this equation was arrived at independently of element-type considerations, and employing the given sign convention, Eq (5) will hold for either type.

Equation (5), however, happens to be a second-order, nonlinear, nonhomogeneous differential equation with variable coefficients for which there is no obvious solution. Therefore, a numerical technique will be used for the solution to this equation when programmed for the digital computer. Equation (2) shall be converted into complete numerical form:

$$-k_{i-1/2} A_{i-1/2} \left[\frac{T_i - T_{i-1}}{\Delta x}\right] + \frac{I^2 \rho_i \Delta x}{A_i} + \tau_i I \left[\frac{T_{i+1/2} - T_{i-1/2}}{\Delta x}\right] \Delta x + k_{i+1/2} A_{i+1/2} \left[\frac{T_{i+1} - T_i}{\Delta x}\right] = 0 \tag{6}$$

Assuming

$$k_{i-1/2} = \frac{k_i + k_{i-1}}{2}$$

$$k_{i+1/2} = \frac{k_{i+1} + k_i}{2}$$

$$A_{i-1/2} = \frac{A_i + A_{i-1}}{2}$$

etc.

Equation (6) may then be expressed in the form:

$$a_i T_{i+1} + b_i T_i + c_i T_{i-1} + d_i = 0 \qquad (7)$$

where the forms of a_i, b_i, c_i and d_i are obvious. Equation (7) is suitable for digital programming, and any one of several numerical techniques may be employed to obtain a solution. As T_0 and T_1 are planned inputs into the code, Eq (7) may be solved as N_0 equations in N_0 unknowns, with N_0 being determined by $L/\Delta x$.

Thermoelectric efficiency is defined as being the electrical output divided by the energy passing through the thermoelement. It is not planned to consider thermal losses through the insulation, or lateral losses from the element itself in this code, and efficiency will then be given by the electrical output divided by the source input. In the design of most isotopic direct conversion generators, the desired electrical output is known and would be an input for the program. This leaves only the source input to be calculated. For a thermoelement, the source input per element may be expressed as follows:

$$\frac{Q_0}{N} = -k_0 A_0 \left.\frac{dT}{dx}\right|_{x=0} + \pi_0 I - I^2 R_{CO} \qquad (8)$$

where π_0 is the Peltier coefficient at the hot junction and is equivalent to $\alpha_0 T_0$. The hot junction contact resistance is denoted by R_{CO}. Equation (8) is also applicable to N- or P-type elements if the given sign convention is adhered to. Equation (8) may be expressed in difference form for purposes of programming as:

$$\frac{Q_0}{N} = \frac{k_0 A_0 T_{0-1} - k_0 A_0 T_{0+1}}{\Delta x} + \alpha_0 I T_0 - I^2 R_{CO} \qquad (9)$$

The number of thermoelements, N, may be deduced solely from external power requirements by means of the following relationships:

$$R_{iT} = N \left(\int_{T_1}^{T_0} \frac{\rho_N(T)}{A(x)}\, dx + R_{NCI} + R_{NCO} \right.$$

$$+ \int_{T_1}^{T_0} \frac{\rho_P(T)}{A(x)}\, dx + R_{PCI} + R_{PCO} \Bigg) \qquad (10)$$

$$E_{OCT} = N \left(\left| \int_{T_1}^{T_0} \alpha_N(T)\, dT \right| + \left| \int_{T_1}^{T_0} \alpha_P(T)\, dT \right| \right) \qquad (11)$$

$$E_{eT} = \frac{E_{OCT} R_e}{R_e + R_{iT}} \qquad (12)$$

where

R_{iT} = total internal resistance of the generator

R_{NCI} = cold junction contact resistance of an N element

R_{NCO} = hot junction contact resistance of an N element

R_{PCI} = cold junction contact resistance of a P element

R_{PCO} = hot junction contact resistance of a P element

E_{OCT} = open circuit voltage of the generator

E_e = external voltage

R_e = external voltag e

N = number of thermoelement pairs

From the previous relationships, the thermoelectric efficiency is given by:

$$\eta = \frac{\text{Electrical Power Output}}{\text{Thermal Power Input}} \qquad (13)$$

Or in mathematical terms:

$$\eta = \frac{E_{OCT}^2 R_e/(R_e + R_{iT})^2}{Q_0} \qquad (14)$$

All mathematical relationships required for programming have now been derived. For purposes of simplification, many steps have been excluded from this derivation. However, it is felt that the key points are clearly outlined and may be reproduced by anyone possessing a working knowledge of thermoelectricity.

The primary purpose of this program will be to maximize the thermoelectric efficiency. This may be accomplished employing an iterative manipulation of the derived equations.

Equations (5), (9) and (13) demonstrate that the performance or efficiency of a thermoelectric generator is dependent upon the geometry of the individual thermoelements. Ioffe shows that the efficiency of a thermoelement is dependent upon what is commonly termed the shape factor of the element; the shape factor being the cross-sectional area-to-length ratio of the thermoelement. It should be noted at this point that the shape factor may be made to assume any positive value by independently varying either the cross-sectional area or the length of the element. In this manner, the thermoelectric efficiency may be maximized based upon this parameter, assuming such a maximum to exist.

Therefore, to avoid overrestriction of the problem, either the cross-sectional area or the length of the thermoelements will be inputs to the code. The solution to the problem then becomes a trial and error type as the geometric parameter which is not an input must be varied to obtain the maximum efficiency point.

A flow chart outlining the basic steps of the code is found in Fig. E-2. This should complete all of the preliminary investigation prior to the actual writing of the code.

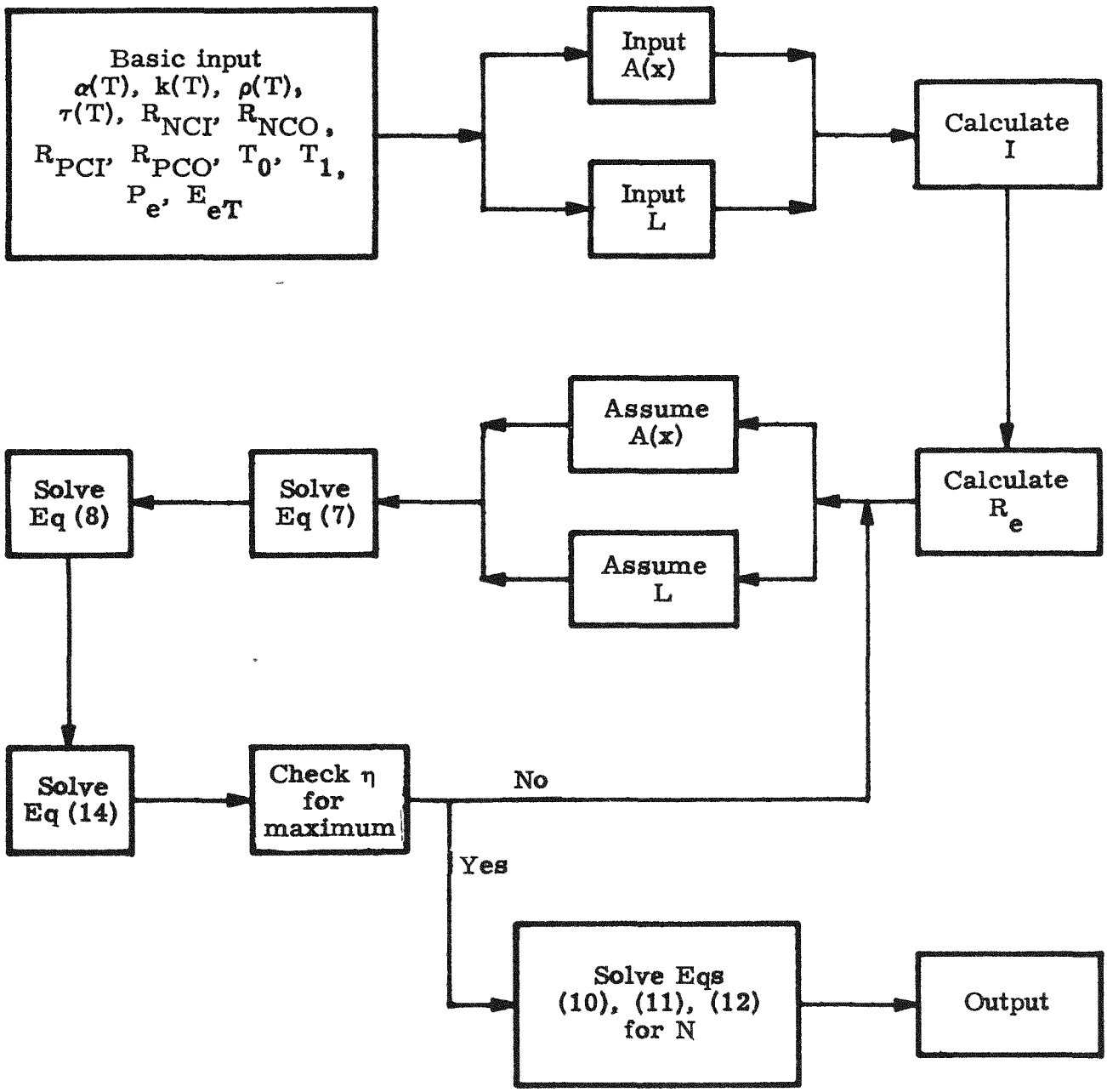

Fig. E-2. Code Flow Chart

APPENDIX IV-F--RADIOLOGICAL HAZARD FROM LAUNCH PAD FIRE

In case the generator and fuel container should be exposed to a fire resulting from the destruction of the space vehicle on the launch pad, it is almost certain that the fuel container would remain intact and preserve the containment of the isotope fuel. However, it will be assumed that the fuel container is melted or broken open and the fuel exposed. Even in this case, the fuel would be dispersed in massive form over only a small area, producing a localized contamination.

In order that the fuel be vaporized, producing a cloud of active material, a large heat input is required. This heat input may be calculated from the thermal properties of nickel--of which the fuel form is largely composed--to be 1.9×10^5 calories. It might be argued that the fuel slug would not reach the boiling point of nickel, but would be oxidized at some lower temperature. The heat input required would not be greatly different since the heat of formation of nickel oxide, NiO, is 58,830 calories per mole and consequently 0.61×10^5 calories are required to oxidize the nickel in the fuel.

For a known heat input, the height to which the cloud formed will rise can be calculated by means of an equation due to Sutton (Ref. 1, 2 and 3).

$$Z = \left(\frac{Q_h}{2C_p \rho \ \pi^{3/2} \ C^3 \ \theta'} \right)^{0.276}$$

where

Z = height--meters

Q_h = heat input--calories

C_p = specific heat at constant pressure

ρ = ambient air density--gm/in.^{3}

C = diffusion coefficient

θ' = vertical temperature gradient--°C/m.

For a neutral or average atmosphere, the temperature gradient is 0.0035° C/m. The diffusion coefficient varies from 0.3 for a stable atmosphere to 0.6 for a highly unstable one; 0.50 is a reasonable

value for the neutral atmosphere. The specific heat is taken to be $0.25 \frac{cal}{gm-°C}$, and the air density as 1.18×10^3 gm/m^3. Then

$$Z = \left(\frac{1.9 \times 10^5}{2 \times 0.25 \times 1.18 \times 10^3 \times \pi^{3/2} \times 0.5^3 \times 3.5 \times 10^{-3}} \right)^{0.276}$$

This cloud, at a height of approximately 26 m, will move downwind and increase in size due to diffusion. Sutton relates the volume of the cloud to the distance moved by the equation:

$$V = \left(\pi^{1/2} \, Cd^{(2 - n)/2} \right)^3$$

where

V = volume of the cloud--m^3

d = distance--meters

n = stability parameter which can vary from zero to unity. For a neutral atmosphere, 0.25 is a reasonable value.

The distance, d, should be calculated from the point at which the cloud can be considered a point source. In this case the cloud is initially small and no appreciable error is introduced by considering it a point source directly above the fire.

The launching of the vehicle is expected to take place 60 days after the encapsulation of the fuel. At this time the activity of the curium is 8.6×10^3 curies. The concentration within the cloud can be calculated directly. It is conventionally expressed in microcuries per cubic centimeter. Thus

$$X = \frac{Q}{V}$$

where

X = concentration--curies/cm^3

Q = activity--curies

V = cloud volume--m^3.

Deposition from the cloud will take place as it moves downwind. By a modification of Sutton's equations, the maximum deposition that can take place is expressed by:

$$w = \frac{nQ}{2e\pi^{1/2}Cd^{(2 - n/2)}}$$

where

w = deposition--curies/m^2

e = base of natural logarithms.

The internal dosage received by an individual in the path of the fuel cloud may be approximated by:

$$D = \frac{2r}{\mu} \times bf$$

where

D = internal dosage received--microcuries

r = radius of cloud--meters

μ = wind velocity

b = breathing rate--cm^3/sec

f = fraction of inhaled isotope taken up by the body.

The wind velocity has been taken as 3.8 m/sec, the average ground velocity at Cape Canaveral. The breathing rate has been taken to be 500 cm^3/sec. The biological effects of curium have not been studied extensively, but the value 0.12 has been suggested for f (Ref. 5). The factor $(2r/\mu)$ represents the time of exposure of an individual to the cloud.

In the table, the results of calculation of the cloud volume, radius, concentration, deposition and dosage are presented. It is evident that there is a hazard presented by the radioactive deposition. While this material presents a significant hazard by means of external exposure, it would be subject to redispersal by wind and movement through the area. It would be deposited in a narrow strip downwind from the source. This contamination would have to be removed or covered. While the Curium-242 has a half life of 162.5 days, the daughter, Plutonium-238, with a half life of 86 years, also presents a serious hazard. The total body burden permitted for Curium-242 is 0.2 microcurie (Ref. 6).

It is seen from the table that a dosage exceeding this may be received by personnel exposed to the cloud within 3000 meters of the source.

In conclusion, it is found that serious hazards would be encountered if a radionuclide of a few kilocuries activity were to be dispersed at the launch pad. It is necessary that the fuel container be able to contain the fuel safely under any such conditions. A maximum possible incident has been presented here; further investigations will be made for a refinement of this incident into a maximum credible incident.

TABLE E-1

Parameters for the Release of a Nickel-Curium-242 Alloy Fuel of 8.6 Kilocuries as a Cloud

d	V	r	X	w	D
Distance from Source (m)	Volume of cloud (m^3)	Radius of Cloud (m)	Concentration ($\mu c/cm^3$)	Deposition* ($\mu c/m^2$)	Internal dosage (μc)
10	293	4.1	29.3	5.95	3800
20	1770	7.5	4.8	1.63	1150
30	5160	10.7	1.66	0.76	562
50	2.03×10^4	16.9	0.424	0.29	227
60	3.20×10^4	19.7	0.268	0.21	167
100	1.03×10^5	29.0	8.35×10^{-2}	8.43×10^{-2}	76.8
200	7.58×10^5	56.5	1.13×10^{-2}	2.17×10^{-2}	20.2
300	2.20×10^6	80.5	3.91×10^{-3}	1.01×10^{-2}	9.95
500	8.50×10^6	126	1.01×10^{-3}	3.88×10^{-3}	4.03
1,000	5.15×10^7	240	1.67×10^{-4}	1.06×10^{-3}	1.27
2,000	3.16×10^8	422	2.72×10^{-5}	2.90×10^{-4}	0.36
3,000	9.2×10^8	602	9.35×10^{-6}	1.35×10^{-4}	0.18
5,000	3.43×10^9	935	2.51×10^{-6}	5.23×10^{-5}	0.07
10,000	2.22×10^{10}	1740	3.88×10^{-7}	1.40×10^{-5}	0.02
20,000	1.73×10^{11}	3450	4.97×10^{-8}	3.54×10^{-6}	0.005

* Deposition in a narrow strip downwind from the source.

REFERENCES

1. Sutton, O. G., "A Theory of Eddy Diffusion in the Atmosphere," Proc Roy Soc London A, 135, 143, 1932.

2. Sutton, O. G., "The Theoretical Distribution of Airborne Pollution from Factory Chimneys," Quart Jour Royal Met Soc 73, 426, 1947.

3. Sutton, O. G., "Atmosphere Turbulence," Methuen and Company, Ltd, London, 1949.

4. "Meteorology and Atomic Energy," U. S. Weather Bureau, 1955.

5. "Recommendations of the International Commission on Radiological Protection," Supplement No. 6, 1954.

6. "Maximum Permissible Body Burdens and Maximum Permissible Concentrations of Radionuclides in Air and Water for Occupational Exposure," National Bureau of Standards Handbook 69.

V. TASK 6--FUEL TECHNOLOGY DEVELOPMENT*

The purpose of this Task is to investigate and develop suitable radioisotope fuels for use in thermoelectric and thermionic generators, specifically designed to meet the demands of the various SNAP Programs. At present, the primary effort is directed towards utilization of isotopes such as Curium-242 and Plutonium-238 because of their attractive power characteristics and half lives.

In accordance with the Task 6 Contract, Americium-241 will be processed and irradiated to obtain gram quantities of the Curium-242 isotope. Subsequently, purification and encapsulation of the curium will be accomplished at The Martin Company to provide an optimized power source suitable for use in a variety of direct conversion generators.

A similar effort is underway on Plutonium-238.

During this quarter, a radioisotope laboratory (Heavy Elements Processing Laboratory) was designed for processing americium and developing plutonium and curium fuel forms. Construction of this facility at The Martin Company, Baltimore site will begin in May 1960.

Design, fabrication and installation of the equipment to produce capsules for irradiation has progressed to the point where preliminary dummy capsules are being made for purposes of optimizing the process. An aluminum chloride volatilization system for recovery of curium from aluminum in the irradiated capsules has been constructed and is in operation. Numerous runs have been made on dummy samples to establish volatilization characteristics and evaluate process techniques.

Considerable effort has been devoted to the development of purification techniques for americium and curium. Results to date have progressed satisfactorily by using chemically similar elements to simulate these materials. However, firm process specifications must be established later when americium and curium are available for evaluation, since a by-product material license is required for handling such elements. An application for this license has been submitted along with a Summary Report covering the americium processing to be performed.

Fuel form investigations for both curium and plutonium were initiated. Major emphasis has been placed on cermet and ceramic systems, with the intention of exploring metallic systems later.

---

* W. Bowes

Evaluation of containment materials was begun. A compressive impact test facility has been designed and constructed to investigate the high velocity deformation of the various metals which appear most suitable for SNAP applications. This system will facilitate screening the different materials under consideration in addition to providing valuable engineering data for future design of power capsules.

Two shielding casks were designed; one for transportation of the americium capsules to an irradiation facility and the other for return of the irradiated capsules to Martin-Baltimore. Both the casks and irradiated capsules have undergone rigorous radiation and thermal analyses employing "worst case" conditions; results in all cases were favorable.

Work was initiated on arranging an irradiation program for the americium capsules in the Materials Testing Reactor or Engineering Test Reactor at Idaho Falls, Idaho. Thermal, activation and neutron depression analyses were conducted on the capsules to assure hazard-free performance and determine reactor flux requirements. A trip is planned to the National Reactor Testing Station to establish criteria and program requirements.

A. SUBTASK 6.1--GENERAL DEVELOPMENT AND MATERIALS REQUIREMENTS

The objectives of the Subtask 6.1 program are to:

(1) Examine the physical, chemical and nuclear properties of the pure metals and compound forms of Curium-242, Americium-241 and Plutonium-238. In addition, compare these with other suitable radioisotopes that can be used for isotopic power.

(2) Determine the types of matrix materials which can be used with curium and plutonium fuels and establish the container materials which are compatible with the internal and external environmental conditions.

(3) Select purification processes for americium and curium which are capable of removing fission products, rare earths and other undesirable radioisotopes such as cerium, plutonium, strontium, etc.

1. Americium Purification Process Selection

During this quarter, several methods reported in the literature for purifying americium sufficiently for irradiation and conversion to curium

were reviewed. The most feasible method was a process used by the University of California, Lawrence Radiation Laboratories at the Livermore Site. This method has been demonstrated to give yields in excess of 90%. The Martin Company is currently attempting to improve the yield and purity of the product and to establish the procedure necessary to place it on a production basis. This effort will be described in detail under Subtask 6.2.

2. Curium Purification Process Selection

The methods for separating the neutron irradiation products of americium in the americium-aluminum capsules are being studied to determine how curium can best be isolated from aluminum and the residual isotopes. There are numerous processes described in the literature for purifying microgram quantities of curium and a few methods for milligram quantities, but little reported data exist on handling gram quantities. Considerable development work has been done on curium, however, at both Los Alamos Scientific Laboratory and University of California, Lawrence Radiation Laboratories, Livermore Site. The maximum quantities processed at these installations is a few kilocuries. It is desired to increase these amounts by an order of magnitude and to develop a production-type process for handling quantities up to a magacurie. All reports on the ion exchange methods for purifying curium which is contaminated with fission products, americium and plutonium have been limited to only milligram quantities of curium. In addition, the ion exchange methods described gave only partial separation of the impurities. Similarly, solvent extraction methods have not offered a sharp separation of curium from fission products and plutonium. Experimenters at both Los Alamos Scientific Laboratory and the Lawrence Radiation Laboratory have achieved only partial success using either the solvent extraction or the ion exchange method. It is therefore planned to use a combination of both methods to separate the americium-curium from the fission products and plutonium. One of the more promising methods which was described in the last quarterly progress report utilizes diethyl hexyl-orthophosphoric acid (HDEHP) in carbon tetrachloride (CCL_4). Laboratory tests indicate 99% of the fission products were extracted by the solvent phase without the use of any carrier. Other solvents such as thenoyl trifluoroacetone (TTA) and tributyl phosphate (TBP) also have been tested but do not appear as promising.

Further studies are required on both ion exchange and solvent extraction methods since decontamination factors of the order of 10^6 must be achieved before a suitable process can be recommended for curium purification. Details of some of the experiments conducted during this period are described under Subtask 6.2.

3. Plutonium-238 Process Selection

Under this phase of the program, it is anticipated that further purification of the plutonium will be unnecessary since high quality material is already available as either the chloride or nitrate. However, a standby method has been selected in case it becomes necessary to remove small amounts of fission products. According to the proposed method, adjustment of the original solution to a nitric acid concentration of 7.5 to 9.0 N will cause the plutonium to be absorbed on a strong base anion exchange resin column, Dowex 1, 50 to 100 mesh. The plutonium is eluted by first washing the column with 1 N nitric acid solution several times, followed by an 0.3 M hydroxylamine nitrate solution.

The resultant plutonium nitrate solution is adjusted to the proper acidity and treated with an excess of hydrogen peroxide to effect a precipitation of plutonium peroxide. The slurry is then filtered, washed and finally air dried.

4. Processes for Conversion of Plutonium-238 to the Desired Chemical Compounds

Several procedures for preparation of the carbide, fluoride, nitride and oxide have been reviewed. Of those studied, several were immediately eliminated on the basis of the hazard or risk involved; others were rejected because of the poor yield and/or slow reaction rates. A few are considered feasible and are described under Subtask 6.3.

In all of the plutonium laboratory experiments, Plutonium-239 will be substituted for the much more expensive Plutonium-238 since their physical properties are identical. The physical properties of some plutonium compounds are listed in Table V-1.

TABLE V-1

Physical Properties of Plutonium

Compound	Melting Point (°C)	Boiling Point (°C)	Densities
Pu_2O_3	1649	---	11.47
PuF_3	1425	2228	9.32
PuF_4	1038	1427	7.0

TABLE V-1 (continued)

Compound	Melting Point (°C)	Boiling Point (°C)	Densities
$PuCl_3$	732	1753	5.70
PuC	1850	---	13.6
Pu_2C_3	1900	---	12.70
Pu	639	3235	19.74 (alpha)

The literature search on the physical properties, potential fabrication methods, and methods of containment for curium and plutonium and their compounds was continued during this quarter. Special emphasis was placed on plutonium metal and its compounds, which may be utilized for the Task 5.6 mission requiring a radioisotope heat source for a thermoelectric generator with a mission life of 5 to 10 years. A flow sheet of potential methods for the preparation of plutonium metal, oxides, fluorides, carbides and nitrides is shown in Fig. V-1.

Work on this task will be terminated in April, and a topical report will be issued which will cover all of the data collected to date on curium, and plutonium and their compounds.

B. SUBTASK 6.2--AMERICIUM AND CURIUM RADIOISOTOPE PREPARATION PROCESSES

The objectives to be achieved under Subtask 6.2 include:

(1) Design of radioisotope laboratory.

(2) Design and installation of americium processing and capsule fabrication equipment.

(3) Design of shipping casks for irradiated and unirradiated americium capsules.

(4) Development of techniques for purification of curium.

(5) Development of an aluminum chloride sublimation process for recovery of curium.

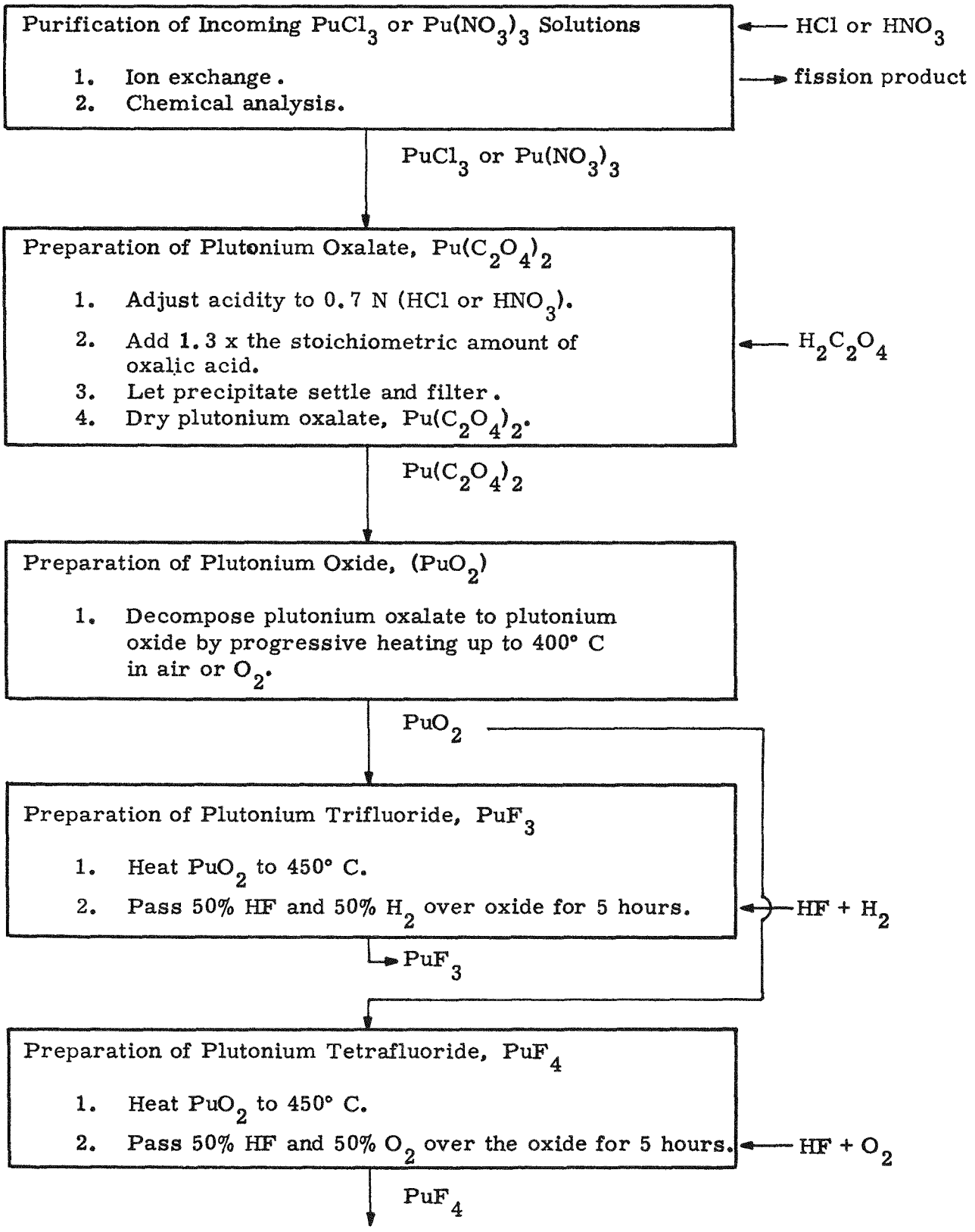

Fig. V-1. Method of Preparation for Plutonium and Its Compounds

Preparation of Plutonium Metal

1. Blend PuF_4 + 25 molar percent excess calcium chips and 0.1 to 0.5 moles of iodine per mol of PuF_4. ← Ca, ← I_2
2. Load mixture into bomb.
3. Reduce PuF_4 to Pu by heating to 400° C.
4. Discharge bomb contents and separate the plutonium metal from the slag.
5. Vacuum distill excess calcium from plutonium. → CaF_2 + CaO
6. Cast Pu into desired shape. ← Ca

↓ Pu (metal)

Preparation of Plutonium Monocarbide

(Method a)

1. Blend plutonium hydride with graphite. ← C
2. Heat to 800° C for 4 hours in an inert atmosphere.

(Method b)

1. Blend plutonium oxide with graphite. ← C
2. Heat in an inert atmosphere to 1800° C for 10 minutes.

(Method c)

1. Blend plutonium metal with graphite. ← C
2. Heat in an inert atmosphere to 1000° C for 5 hours.

(Method d)

1. Heat plutonium metal to 800° C.
2. Pass hydrocarbon gas over molten metal. ← CH_4

↳ PuC

Preparation of Plutonium Nitride

(Method a)

1. Heat plutonium metal to 800 to 1000° C.
2. Pass nitrogen gas over molten metal. ← N_2

(Method b)

1. Heat plutonium hydride in a nitrogen atmosphere to a temperature greater than 230° C.

1. Radioisotope Laboratory Layout

Plans for installing the heavy elements processing facility in an existing building at The Martin Company had to be abandoned because the building in the desired location was unavailable. A new building has now been proposed which is 25 x 50 feet with 1250 square feet of floor space and will be located near the present critical facility. The americium purification equipment, the weighing and blending apparatus, along with the pelletizing press, welding box and sand blast apparatus are to be placed on one side of the laboratory. The plutonium dry boxes and furnace are to be located on the other side. A clean area has been provided in the front section of the building to accommodate two desks, a table for counting equipment, a washroom and a clean change room. A mechanical equipment room and another change room with provisions for laboratory coat storage are located to the rear of this area.

2. Americium Processing Equipment

The equipment for americium processing is separated into five stages:

(1) Purification units and equipment for conversion of americium oxalate to americium oxide (AmO_2).

(2) A blending unit which mixes AmO_2 with powdered aluminum and a weighing unit.

(3) The pelletizing and compacting units which form the capsules for irradiation.

(4) The unit for welding of the end cap to the aluminum shell.

(5) The cleaning and surface finishing unit designed to remove contamination and give the final shell an emissivity of 0.6 or higher as oxidized.

After the capsules of americium have been processed through these stages, they will be ready for shipment to an irradiation facility. A schematic of the processing equipment is shown in Fig. V-2.

In the second stage, the AmO_2 is weighed and mixed with aluminum powder in the proportion of 26.5 Al to 1 AmO_2 by weight. Subsequent blending of the mixture is accomplished in the blending and dispensing unit. The volume capacity of the unit is sufficient to completely fill four

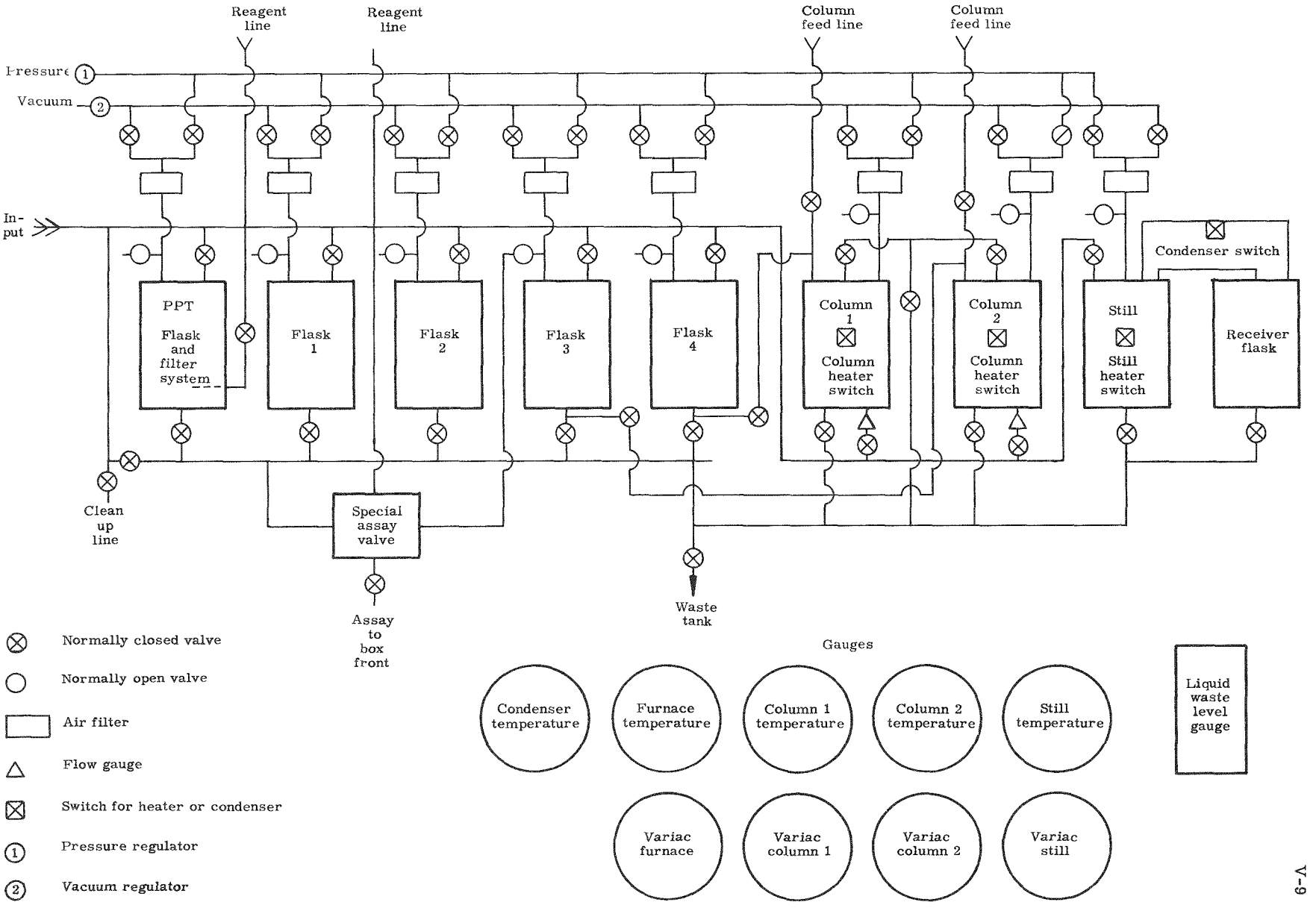

Fig. V-2. Processing Equipment for Purification of Americium.

capsules with the Al-AmO_2 mixture. Tests to determine the optimum speed, time, percent volume and other factors are planned.

In the third stage, the blending container with dispenser valve is connected to the die block of the Denison Press. An air cylinder operates the dispenser and feeds the blended powder into an aluminum shell mounted in the die block. Small quantities of the Al-AmO_2 powder are intermittently dispensed into the aluminum shell and compacted until the capsule is filled with high density material (95% of theoretical). The proposed schedule for the compacting press has been set up in the following steps:

(1) On the up stroke of the press ram, a measured volume of charge is dispensed into the capsule shell.

(2) The complete assembly is then vibrated, to ensure that all of the blended powder is uniformly deposited in the aluminum shell prior to compacting.

(3) The press ram is then lowered to compact the powder charge.

(4) On the down stroke of the ram, the dispenser valve is automatically returned to the refill position. This cycle is repeated 10 times to completely fill each aluminum capsule shell with compacted americium-aluminum powder.

Twenty-eight capsules will be fabricated for irradiation, and the amounts of the material required are as follows:

Material	Total (gm)	Per Capsule (gm)
AmO_2	113	4.045
Calculated as americium	100	3.571
Aluminum powder	3000	107.14
Aluminum shell	1470	52.50

Ratio of aluminum (including clad material) to americium

$$\frac{3000 + 1470}{100} = 44.7 \text{ to } 1$$

In the fourth stage, the capsule top end cap is pressed into position and subsequently fusion-welded into place. The capsule is now ready for cleaning and surface finishing.

In the fifth stage, the capsule is sandblasted to remove possible contamination of americium on the exterior. Upon oxidation of the aluminum capsule the surface finish is estimated to have emissivity of 0.6 or greater. After a preirradiation inspection for defects, the capsules are transferred to a shipping cask and transported to the irradiation facility.

3. Shipping Casks

The 28 americium tubes, 1 inch in diameter by 5-inches long, will be transported in a special cask from Martin-Baltimore to Arco for irradiation. This cask is constructed of 6061 aluminum and has a cover which is hermetically sealed by a rubber "O" ring. This cask will be shipped in a welded steel outer case.

A conceptual design is being developed for a shielding cask to permit transporting 14 irradiated capsules to the Martin-Baltimore plant. The biological shielding consists of 8.25 inches of lead completely surrounding the source, and 11 inches of borated water outside of the lead for protection against fission neutrons from the contained curium. The internal frame is of welded carbon steel plate construction, with stainless-clad steel plates on all outside surfaces. A pressure relief valve installed in the water jacket provides a safety measure against vapor pressure buildup in the event of steam formation. Suitable drains have been incorporated for the shield water and specimen cavity. Four hook eyes and a sling chain have been included to facilitate handling of the cask into and out of the pools. Also, a steel skid (removable) has been designed to facilitate handling by lift trucks. The assembled gross weight is approximately 12,200 pounds.

4. Curium Purification Development

A preliminary literature survey indicated that practically all of the work accomplished on the separation of curium from fission products had been done using trace quantities of curium. Ion exchange methods gave only partial separations, as did solvent extraction methods. It is the plan of this laboratory to utilize both methods of separation in an overall purification system. Such a plan should involve the least amount of work with better results when large quantities of curium are involved.

Several of the more promising solvent extraction procedures have been investigated, using a chemically similar alpha-emitting isotope to simulate curium and a depleted fission product mixture as the contami-

nants. A summary covering the experiments conducted during this period is presented in Table V-2.

The extraction experiments with radioactive tracers resulted in separations up to 70% of the tracer in a single batch extraction from aqueous solution. The solvent mixture used was 1.5 molar diethylhexylphosphoric acid (HDEHP)-carbon tetrachloride. Triple-batch extraction of the aqueous phase with this mixture satisfactorily removed almost 100% of the radioisotope tracer.

Similar single separations of the radioisotope from an aqueous solution with concentrated tributyl phosphate (TBP) produced only a 15% extraction.

Single extractions of radioactive fission products and gadolinium from aqueous solutions with thenoyl trifluoroacetone (TTA) and other solvents all showed less than 50% extraction of the fission products. A much higher percentage separation is needed before the solvents are considered suitable for isotope purification.

5. Solvent Extraction--Ion Exchange Systems

A new approach to the ion exchange purification of Cm-242 was tested using a concentrated lithium chloride (LiCl) solution to form complexes with americium-curium in several ion exchange separation systems. If this complex is substantially stronger than other rare earth or fission product-lithium chloride complexes, then it would be possible to extract one of the complexes from the other with an organic solvent.

Investigation of TBP Solvent. This approach was initially investigated using TBP as the organic solvent. The first step was to determine if this method would effect a separation of curium, so an aliquot of alpha emitter (to simulate curium) was mixed with gadolinium carrier (a bulk agent), and the resulting solution treated with a large excess of LiCl (11.5 M) whose pH was adjusted to 6.6. The combined mixture was then extracted with concentrated TBP. The organic phase was stripped with water and the extracted elements precipitated and counted. It was found that approximately 98% of the alpha activity had been extracted by the TBP.

The next step was to determine if this new method would separate curium from fission product contaminants by exhibiting a lack of affinity for the fission products. Consequently, the experiment was repeated using an aliquot of beta-gamma emitting fission products, instead of an alpha emitter. It was found that the fission product activity was also removed, so in this case separation between curium and fission products cannot be effected because the process removes both alpha and fission products equally well. These results, however, were encouraging in the

TABLE V-2

Solvent Extraction--Experiments to Determine Decontamination Efficiencies

Aqueous Phase	Solvent Phase	Activity C/M After Mixing Phases		Separation (%)
		In Solvent	In Aqueous	
Alpha emitter + gadolinium carrier (in 0.5N nitric acid) 27,000 C/M	1.5M diethylhexyl orthophosphoric acid (HDEHP) in carbon tetrachloride (CCl_4)	19,000 C/M	8,000 C/M	70 extracted into solvent
Alpha emitter without gadolinium (in 0.5N nitric acid)	1.5M HDEHP in CCl_4	--	--	55 after first extraction 99 after third extraction
Fission product (FP) with gadolinium at pH4 (156,000 C/M)	0.2M thenoyl trifluoro acetone (TTA) in benzene	900 C/M 6N/HCl was used to strip the solvent of F.P.	155,100 C/M	0.58 extracted
Fission products with gadolinium at pH4 (156,000 C/M)	0.2M TTA in CCl_4	2,057 C/M	153,943 C/M	1.3 extracted
Alpha emitter	0.2M TTA in CCl_4	--	--	55 after second extraction
Alpha emitter (in 0.5N nitric acid)	Concentrated tributyl phosphate (TBP)	--	--	15 after first extraction 50 after second extraction

sense that previous extractions in the absence of LiCl gave only a 15% removal of the alpha emitter--not nearly so efficient as this new method.

Investigation of HDEHP Solvent. Since the HDEHP system appeared to be a favorable medium in earlier work, the described experiment was repeated substituting HDEHP for TBP. A number of runs were made on solutions containing only fission products in one case, and alpha emitters in the other, to determine the optimum conditions for maximum extraction of the alpha emitters and minimum extraction of the fission products. Various rare earth elements such as yttrium, gadolinium, lanthanum and praseodymium were added to the radioactive solutions to act as carriers. In all cases, the concentration of the LiCl complexing agent added to the solutions was 11.5 M. The pH values of both the radioactive solutions and the LiCl complexing solution were varied for the different runs. It was found that optimum separation conditions existed when the radioactive solution was adjusted to an acidity sufficient to obtain a yellow color from bromthymol blue indicator and the LiCl complexing solution adjusted to a pH of 7.5. After combining these two solutions, extraction with HDEHP in CCl_4 resulted in a 95% pickup of the alpha emitter and only 0.4% pickup of the fission products. In the following run, fission products and alpha emitters were mixed together and the experiment repeated. This time, the extract layer was eluted and the eluent passed through an ammonia form Dowex A-1 chelating resin column. The alpha emitter was thereby recovered, and only a trace quantity of beta-gamma emitting elements (fission products) could be detected.

6. Ion Exchange Purification of Curium

Experiments were conducted employing an ammonia form Dowex A-1 chelating resin to treat solutions of gadolinium and alpha emitter. Both constituents were absorbed on the column, but subsequent elution with 0.2% citric acid resulted in retention of the gadolinium while the alpha emitter was expelled. Gadolinium was later eluted with HCl and the alpha activity in the solution determined. No alpha activity remained with the gadolinium, so that an excellent separation between these two constituents was obtained. Since gadolinium will be a contaminant in the eventual curium purification process, this experiment is significant in the sense that it may provide a means for separating curium from gadolinium.

Several experiments were run using oxides of titanium, zirconium and aluminum as column material. Due to the fineness of the powders, however, flow through the columns was obstructed and the experiments were discontinued.

An investigation was made into the use of LiCl (11.5M) as an elutrient. In this case a solution comprised of fission products, alpha emitters and gadolinium carrier was passed through an ammonia form Dowex column. Some of the fission products passed through without the aid of the elutrient. Subsequent application of the LiCl solution further increased the rate of removal, but not to the extent that the process would be feasible for production purposes. Future experiments in this area are planned in which column and elutrient temperatures will be varied along with pH values and LiCl concentrations.

Work was also initiated on the procedure outlined by Dr. W. W. T. Crane (Ref. V-2). A test mixture of fission products, alpha emitters and gadolinium was precipitated with oxalic acid. The filtrate was found to contain substantial amounts of beta-gamma activity but no alpha activity. The oxalate precipitate was dissolved with an acidified LiCl solution and passed through a Dowex 1 x 10 anion resin column. Contrary to results obtained by earlier experimenters, washing the column with acidified LiCl solution resulted in removal of both gadolinium and alpha emitter. It was found that this can be prevented by use of a finer mesh resin and by maintaining column and solution temperatures at 90° C. Further investigations are required in this area because these finer resins obstruct flow to the point where several days are required for one column separation.

7. Americium Slug Fabrication

Previous galling and warpage of the die assembly has delayed progress to some extent on the pelletizing of americium-aluminum powders. A new approach to the mode of operation led to a redesign of the die, such that the compacting and assembly of the green compacts will be combined into one operation by compacting the powders directly within the tube. If successful, this technique will eliminate several steps from the old process and will result in less contamination within the dry box.

8. Aluminum Chloride Sublimation Process

Due to severe corrosion of the reaction vessel during the previous period, it was imperative that the system be redesigned and dismantled for incorporation of more resistant construction materials. The reaction vessel was replaced with a 24-inch long by 2-inch diameter Vycor tube employing Teflon gaskets for all seals. A split-type furnace having three independently controlled heating zones and a sight glass in the center was also obtained to gain a more uniform reaction temperature. Figure V-3 shows a closeup view of the new Vycor tube and furnace, while Fig. V-4 shows an overall view of the equipment installed.

The condenser design was modified to a cold finger type to eliminate

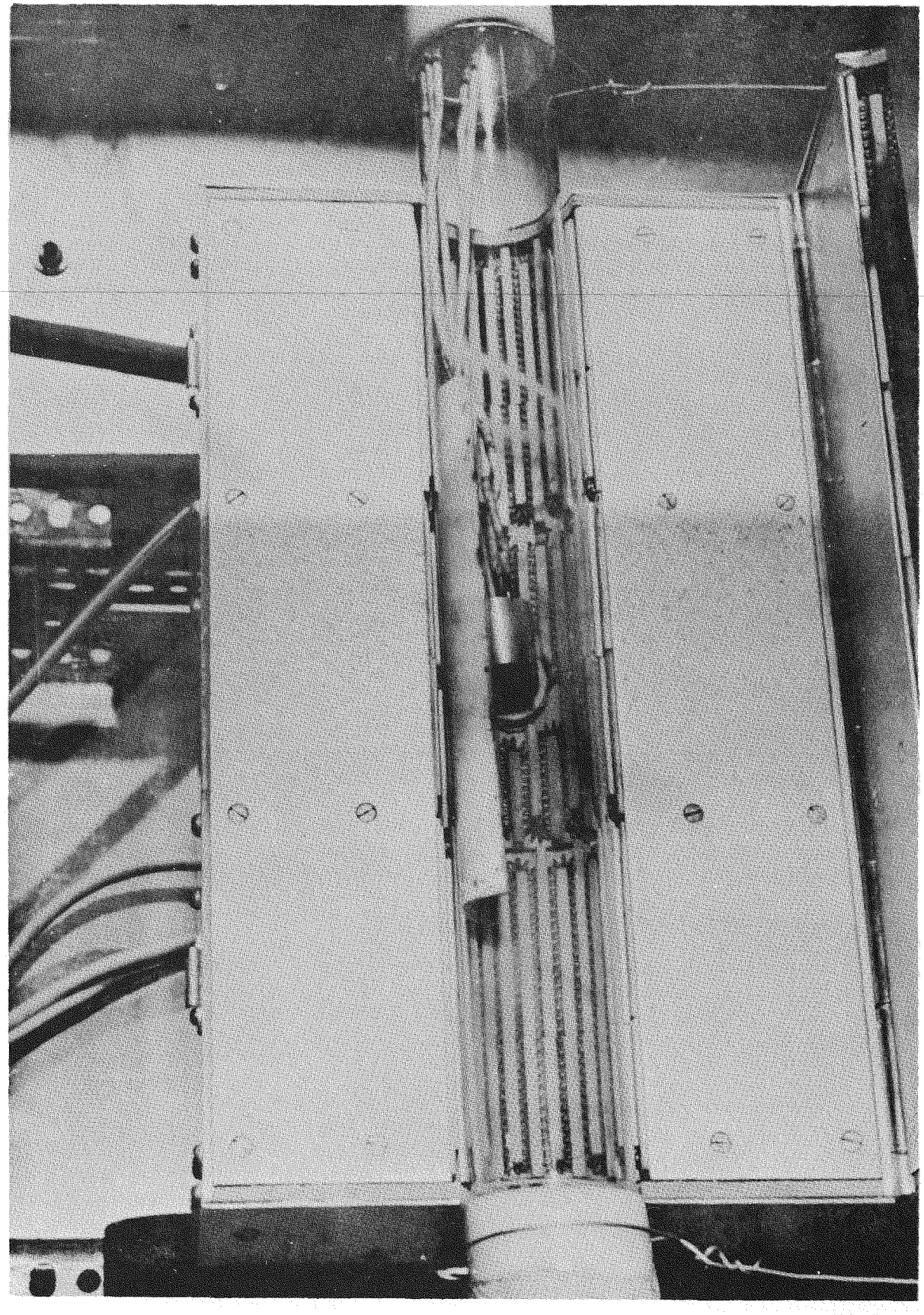

Fig. V-3. Reaction Tube and Furnace for Volatilization of Aluminum Capsules

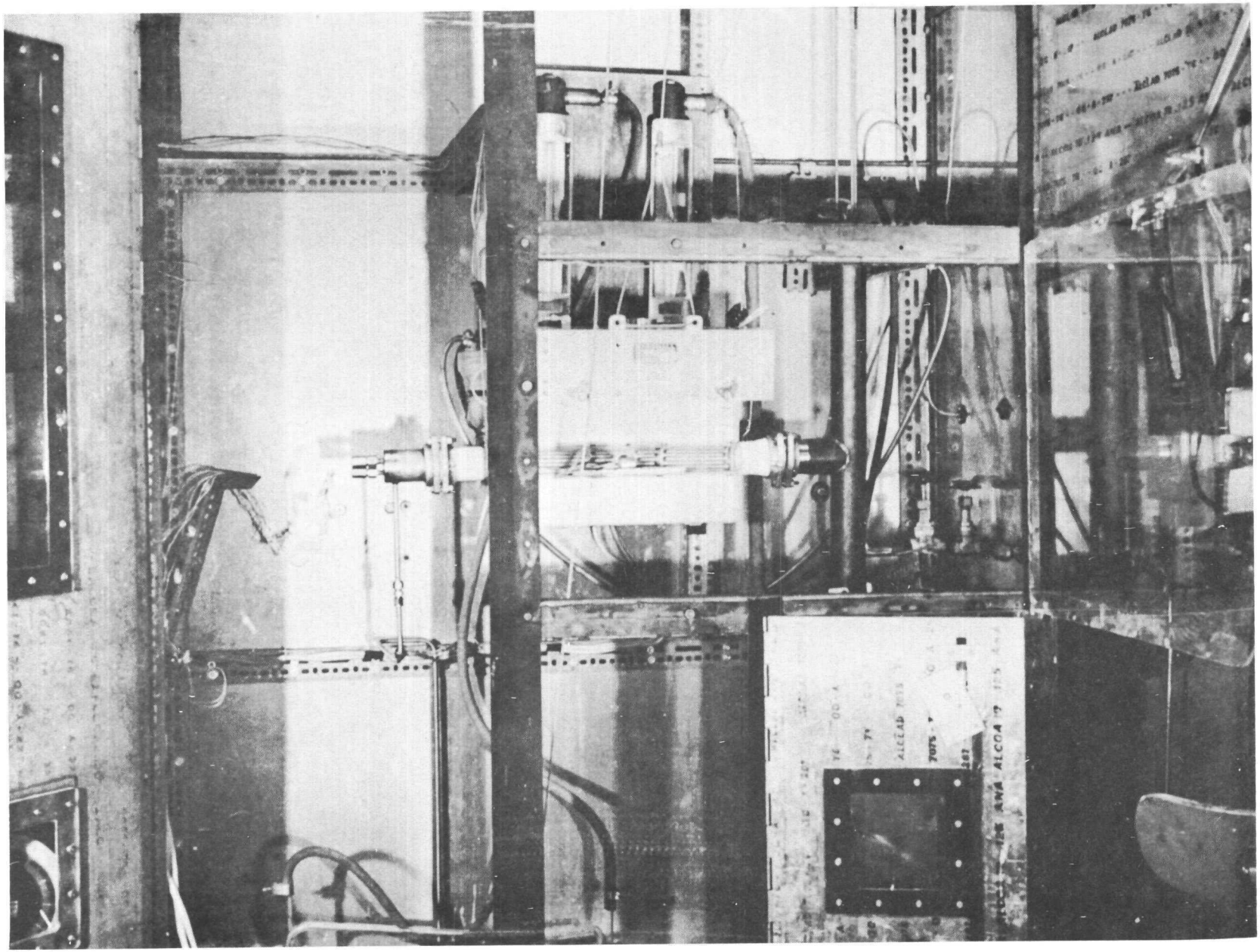

Fig. V-4. Overall View of Aluminum Volatilization Installation

clogging of the inlet caused by external cooling of the old baffle type condenser. This new condenser is constructed from Hastelloy C and has a cylindrical sliding knife on the cold finger to remove the condensate. The outlet end is open to the aluminum chloride collection unit. Under these conditions the condenser capacity is governed by the size of collection flask or air-lock arrangement.

The fabrication, installation and testing of all new components for the volatilization apparatus was completed during this period. Twelve runs were made with the apparatus and the following results were obtained:

(1) The minimum temperature required to initiate the reaction of chlorine with aluminum is 460° F. Even though the reaction could be started at this temperature, additional heat was required to bring the samples up to an operating temperature of 1200° F.

(2) X-ray diffraction, emission spectroscopy and chemical analyses indicate that the black scale coatings found on the aluminum surface are complex intermetallic compounds of aluminum, iron, copper, nickel and silicon. They are for the most part amorphous, with faint patterns of copper-aluminum complexes and aluminum oxide being detected.

(3) The sublimation or reaction rate decreases with time and appears to be a function of exposed surface area.

(4) The percentage of specimens converted to $AlCl_3$ which is sublimed away also decreases exponentially with time, and extrapolation of present data, as shown in Fig. V-5, indicates that it will take 10 to 12 hours to completely react a 1-inch diameter by 1-inch long aluminum slug (1100 wrought aluminum). Figure V-6 makes a comparison of actual specimens after given intervals of reaction time.

(5) Slow flow rates of chlorine and helium yielded better reaction rates than fast flow rates; the optimum rates were found to be 1 cfh chlorine and 2 cfh helium.

C. SUBTASK 6.3--FUEL FORM AND CONTAINMENT INVESTIGATION

The objectives to be attained on Subtask 6.3 are:

(1) Initiation of fuel form investigations.

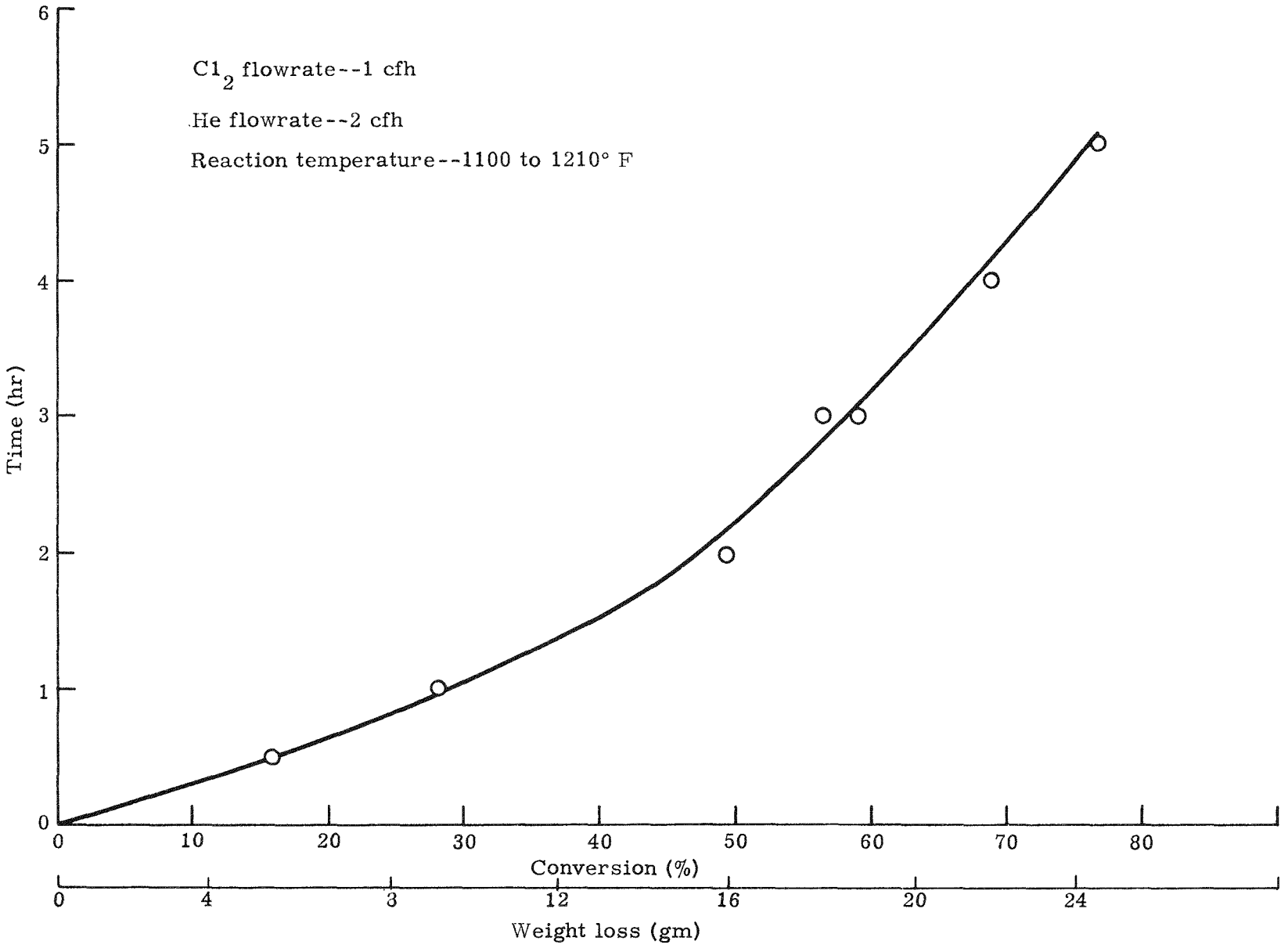

Fig. V-5. Volatilization Rate of Aluminum in Chlorine-Helium Gas

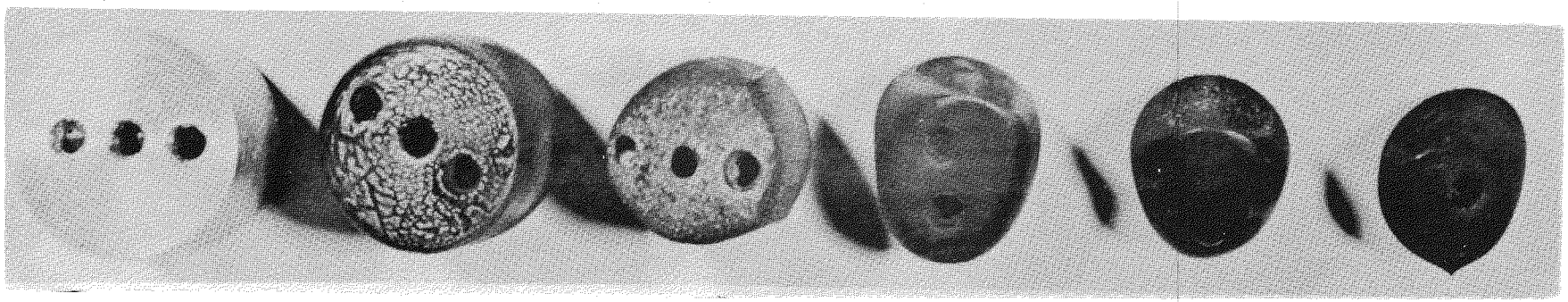

Original 1/2 hr 2 hr 3 hr 4 hr 5 hr

Rx temperature--1200° F±20° F

Chlorine flowrate--1 cfh

Helium flowrate--2 cfh

Fig. V-6. Comparative Reaction of Aluminum Slugs with Chlorine Gas

(2) Design and construction of a compressive impact test facility and initiation of impact testing.

(3) Development of welding schedules for containment materials.

1. Fuel Form Investigation

Work was initiated on the fuel form phase of Task 6.3 during this period. In view of the fact that this program is in the early development stages, several assumptions were made as to criteria for the selection of fuel compounds and matrix materials. A program plan for this effort was then prepared. Main emphasis of the program was placed on the development of cermet and ceramic systems, with metallic systems to be investigated later. Since the actual use of plutonium and curium and their compounds cannot be handled until facilities are available and a facility license is approved by the AEC, natural uranium and its compounds will be used as substitutes for the actual fuel compounds.

Plans have been made to survey various possible alloying constituents for curium and plutonium and to develop capabilities for the bomb reduction of reactive metals. Combinations of uranium dioxide (UO_2), uranium carbide (UC), and uranium tetrafluoride (UF_4) with copper, titanium, vanadium, iron, nickel and molybdenum will be investigated as potential fuel forms.

Procurement of long lead items and work in the laboratory involving preparation of materials on hand and assembly of equipment was initiated.

2. Containment

Compressive Impact Testing. A preliminary evaluation was made of possible tests to determine or predict impact characteristics of materials. The problem of correlating impact phenomenon for different materials with existing natural or statistical laws was discussed with the consultants within The Martin Company and from Johns Hopkins University. In general, the consensus of opinion was unfavorable toward any direct correlation for the following reasons:

(1) No simple laws can be used to explain deformation of materials undergoing high velocity impact.

(2) Velocity, geometric shape and size of a specimen cannot be readily scaled down or up.

(3) Existing theories are based primarily on statistical relations for independently controlled conditions.

Based on these facts, it was decided that drop-impact tests should be conducted to screen materials with respect to their relative behavior for similar conditions. This type of testing will be more economical than an extensive series of sled tests and will give an insight as to impact behavior for various materials. Impact results will be complemented in the final selection of materials by sled testing of full-scale dummy units.

During this period the design, fabrication and assembly of a compressive drop test facility was completed. The facility consists of the following components:

(1) An anvil of hardened steel.

(2) A drop weight or hammer.

(3) A guide tube.

(4) A quick release mechanism for the hammer.

(5) A 1/4-ton hoist.

Figure V-7 shows an overall view of the apparatus and the arrangement of the components which constitute the compressive impact facility. Figure V-8 shows a closeup view of the anvil and the protective shield surrounding it.

The guide tube has a 6-inch internal diameter and the hammer weight can be varied from 35 to approximately 150 pounds. This weight, coupled with a free fall distance of about 96 inches, will give a maximum impact energy of 1200 foot-pounds and an impact velocity of 22.6 feet per second.

Samples of 3/8 inch-diameter type 1018 steel, type 303 stainless steel and Monel deformed at 1700° F with an impact load of 282 foot-pounds (35.2 pound weight dropped 8 feet) were compared in Fig. V-9 with a cold compressed sample of type 1018 steel and the original size specimen. Tests have also been made on 1020 steel to determine the amount of deformation versus the impact energy. Figure V-10 makes a comparison of the original sample through progressive stages of testing with impact energies of approximately 280, 400, 800, 1200 and 1600 foot-pounds. In this case, the tests were accomplished at room temperature.

Welding development. Work was begun on a welding development program aimed at developing welding schedules for different materials, i.e., Mo, Ti, Ta, Ni, etc., and different type seal designs. Procurement of material was started and a "Pauling and Harnischfeger," 300 ampere, a-c d-c welding power supply with an automatic sequence time control has been received. This unit can program a complete weld cycle automatically to a welding head or torch. This unit will also be utilized in the Nuclear Laboratory hot cells when the facility is completed.

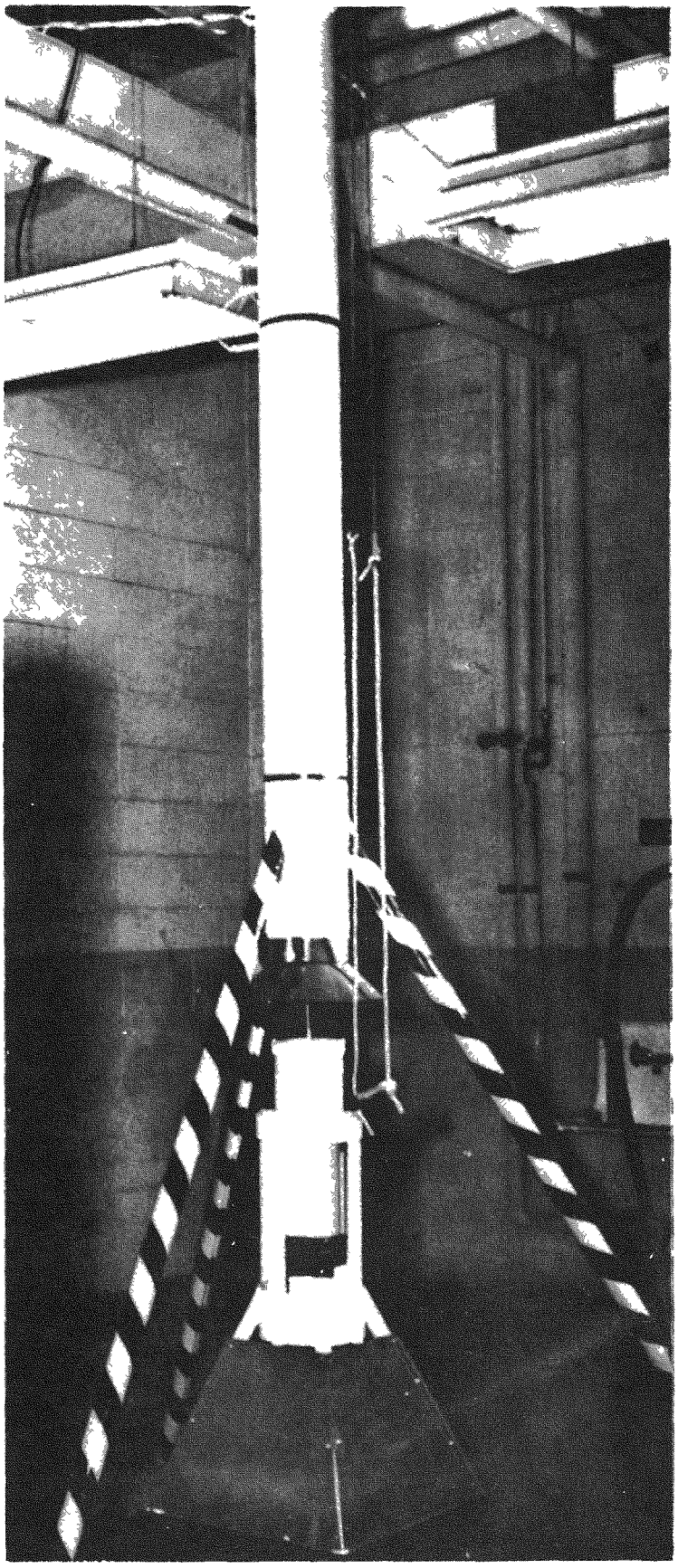

Fig. V-7. Overall View of Compressive (Impact) Drop Test Facility

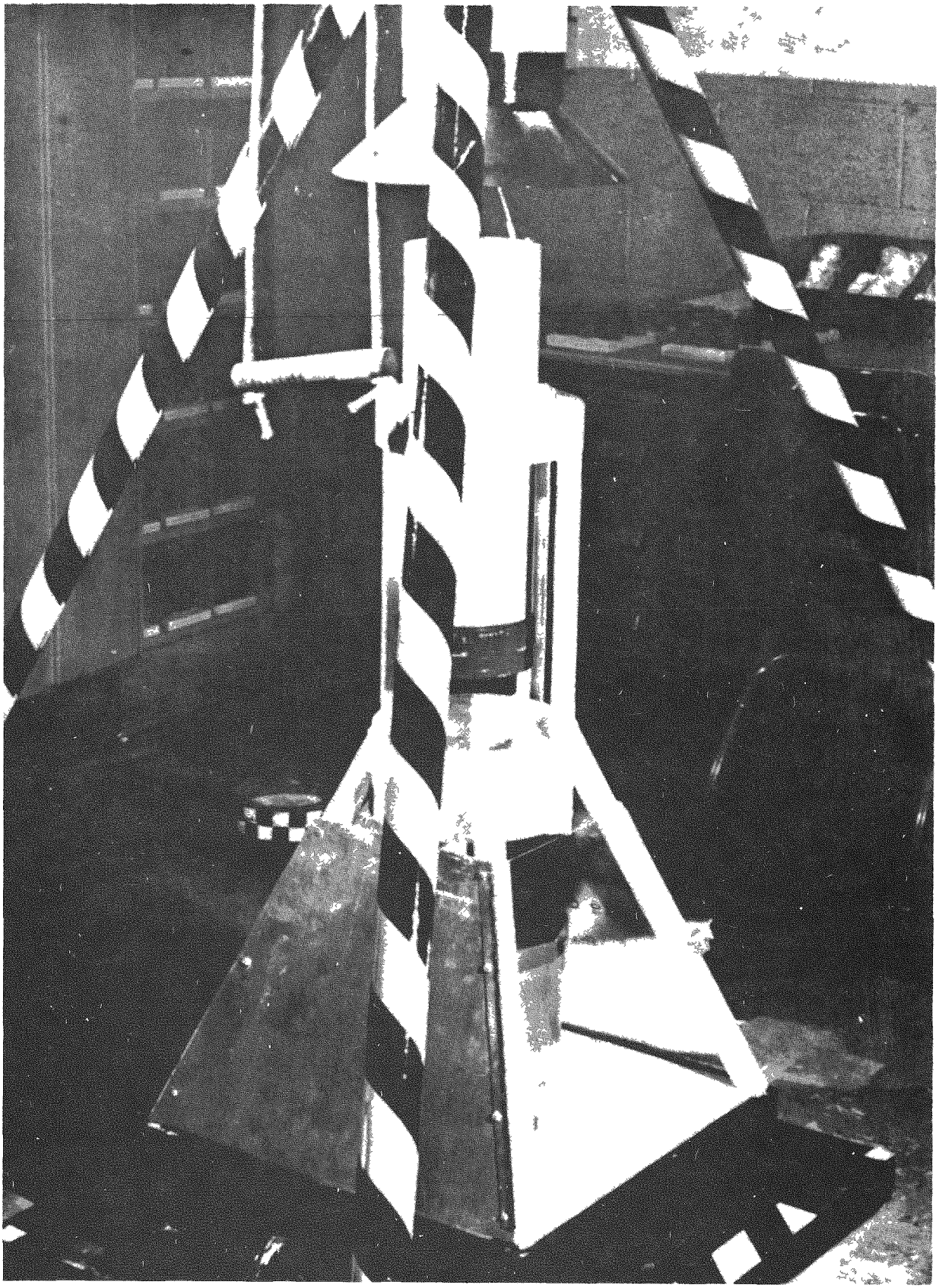

Fig. V-8. Anvil and Protective Shield Detail of Drop Test Facility

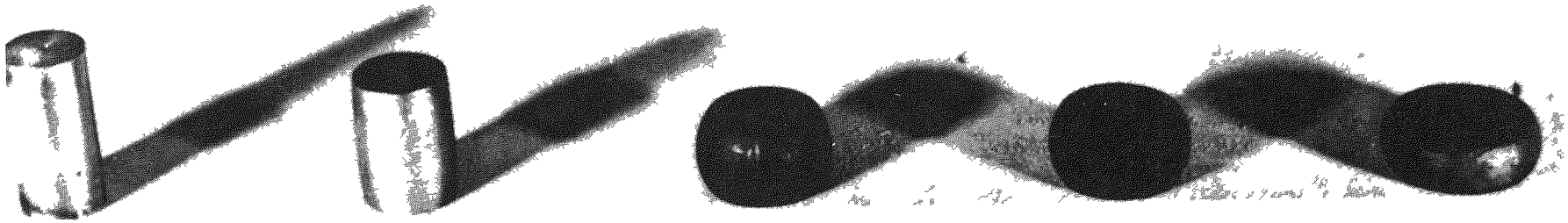

Fig. V-9. Impact Test Results on Different Materials at 1700° F and Room Temperature

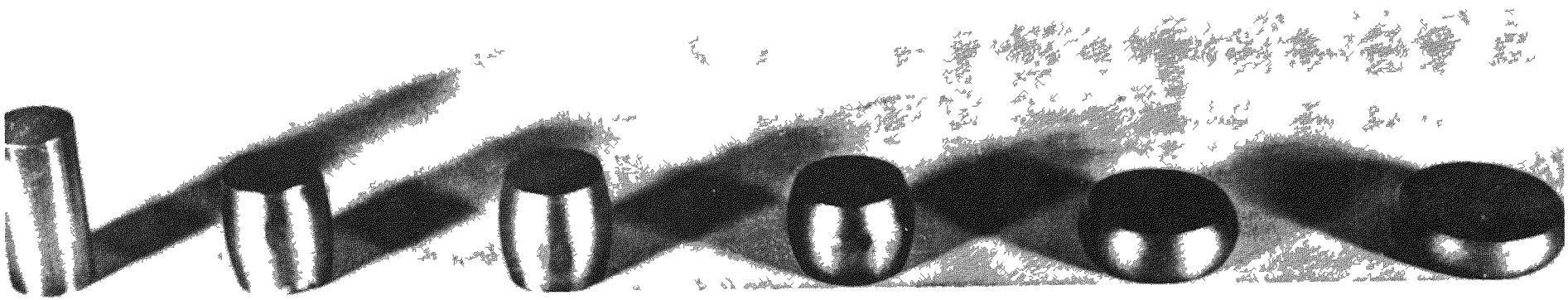

Fig. V-10. Progressive Impact Deformation Tests on Low Carbon Steel 1018 at Room Temperature

D. SUBTASK 6.4--SHIELDING AND SAFETY ANALYSIS FOR CURIUM, PLUTONIUM AND AMERICIUM

The objectives during this report period for Subtask 6.4 were:

(1) Complete the summary report on americium processing.

(2) Apply for by-product material license--Form AEC-313(5-58).

(3) Complete integrity analysis of containment materials for Pu-238.

(4) Investigate He buildup in the americium capsules for irradiation.

(5) Investigate isotope decay products and associated radioactivity.

(6) Do shielding analysis of shipping casks.

(7) Do thermal analyses of americium capsules, shipping cask and volatilization process.

1. Preliminary Hazards Analysis

The primary effort during the report period resulted in a document entitled "Summary Report of Americium Processing to be Performed by The Martin Company," (Ref. V-1). This report was submitted with and as part of the application for the by-product material license, Form AEC-313(5-58), and presents the initial americium processing to be accomplished under the fuel technology program.

An analysis of the mechanical integrity of a Haynes-25 capsule containing 470 curies of metallic Pu-238 was also initiated during this quarter. It was shown that the capsule could withstand 12,780 psi for a period of 1000 hours operating at a temperature of 1350° F, and 6737 psi for a period of 1000 hours operating at a temperature of 1500° F. These values indicate that an adequate margin of safety exists at the actual operating temperature of 860° K (1088° F). The maximum impact pressure to which this capsule will be subjected during re-entry is 1732 psi.

Investigations of the amount of helium pressure buildup from alpha particles within the irradiated AmO_2-Al elements versus time and the effective neutron flux versus time required for 43% conversion of Am-241 to Cm-242 were initiated. No definite results have been obtained as yet.

2. Growth of Decay Products

A study was made covering the growth of decay products of Cm-242, Pu-238, Pu-241, Am-241 and Cm-244. The effective radiation from the parent and daughter isotopes was determined to obtain the biological dose rates. Growth of successive decay products was calculated by means of Bateman's generalized equations for multiple radioactive decay (Ref. V-3). Calculations were based upon the assumption that no decay products were initially present.

Tables A-1, A-2 and A-3 of Appendix V-A give the decay products of these isotopes and their corresponding gamma radiation. Table A-1 gives the decay of Cm-242 and Pu-238, Table A-2 the decay of Pu-241 and Am-241, and Table A-3 the decay of Cm-244. The decay chains of Cm-242 and Pu-238 were terminated at Radium-226, since the daughters of Ra-226 have very short half lives and are considered to disintegrate simultaneously with Ra-226. The decay chains of Pu-241 and Am-241 were terminated at Np-237 because of the long half life of this daughter, and the decay of Cm-244 was carried no further than U-236 for the same reason. Figures V-11 and V-12 show the growth of decay products per original gram of Cm-242 from 10^{-2} to 10^{2} and 10^{2} to 10^{6} years, respectively. Figures V-13 and V-14 show the dose rates per original gram of the parent for corresponding decay times. Dose rates were calculated for only the gamma rays above 100 kilovolts since self-absorption will remove most of the gammas below this energy. Inspection of Fig. V-14 shows that the total dose rate decreases until 375 years have passed. The dose rate then increases and reaches a peak at about 200,000 years. This increase is due to the buildup of Ra-226.

Figures V-15, V-16 and V-17 show similar information for the decay of Pu-238.

The decay chains of Pu-241 and Cm-244 contain elements with half lives longer than any member of the Cm-242 chain. Consequently, the growth of decay products will be delayed for longer periods of time. Figures V-18, V-19 and V-20 show the decay product growth of Pu-241, Am-241 and Cm-244, respectively. Figure V-21 shows the dose rates for these isotopes and their decay products. The increase in dose rate of the Pu-241 chain, which peaks at 70 to 80 years, is due to the growth of Am-241.

With the exception of Pu-241, dose rates at the start of the lifetime of pure isotopes are the highest for all practical purposes. The increase in dose rate of Pu-241 is not significant because the gamma energies associated with its daughter, Am-241, are relatively low and may be removed by small thicknesses of a heavy element.

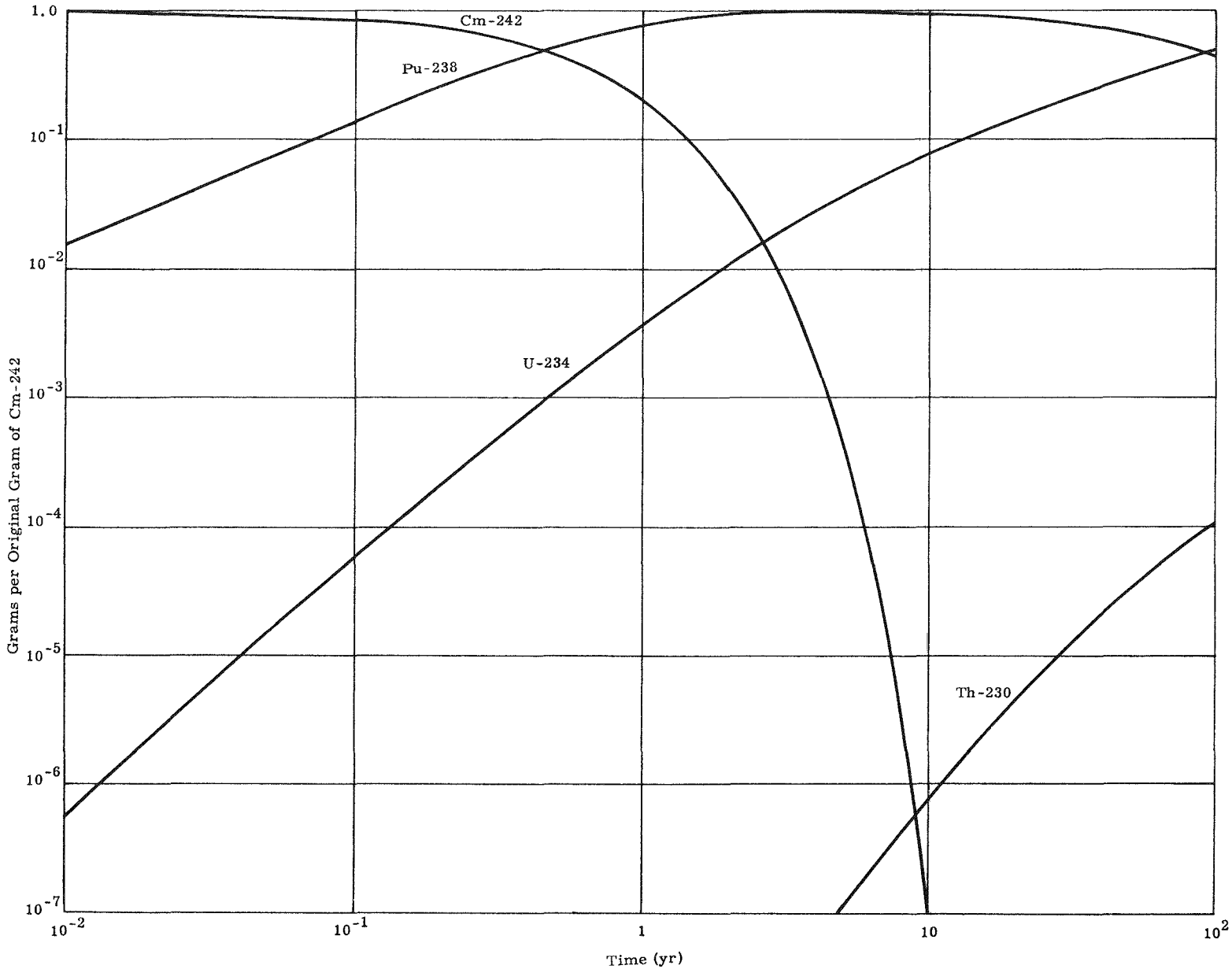

Fig. V-11. Decay of Cm-242 and Growth of Decay Products (10^{-2} to 10^{2} yr)

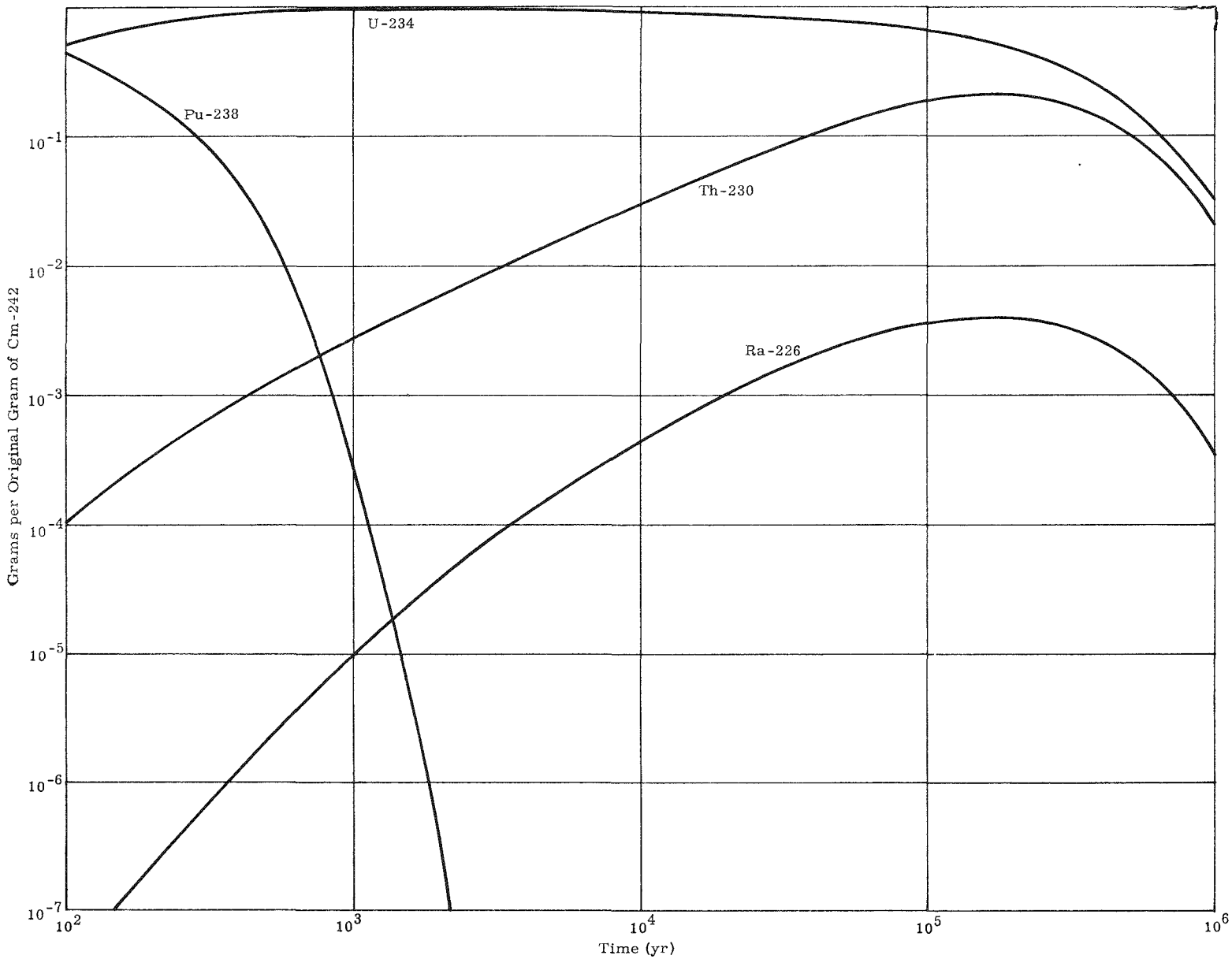

Fig. V-12. Decay of Cm-242 and Growth of Decay Products (10^2 to 10^6 yr)

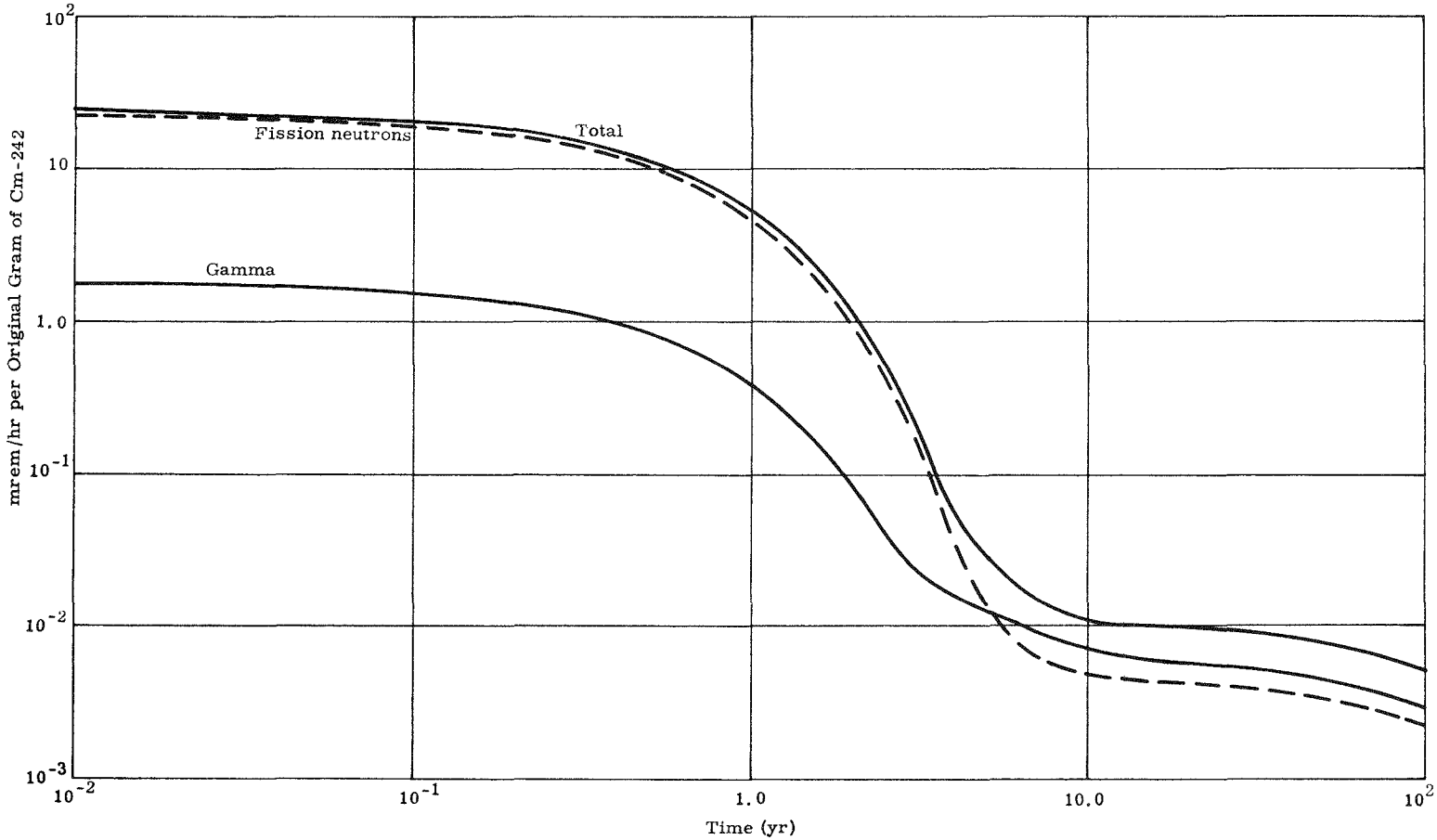

Fig. V-13. Dose Rate from Cm-242 and Its Decay Products (10^{-2} to 10^2 yr)

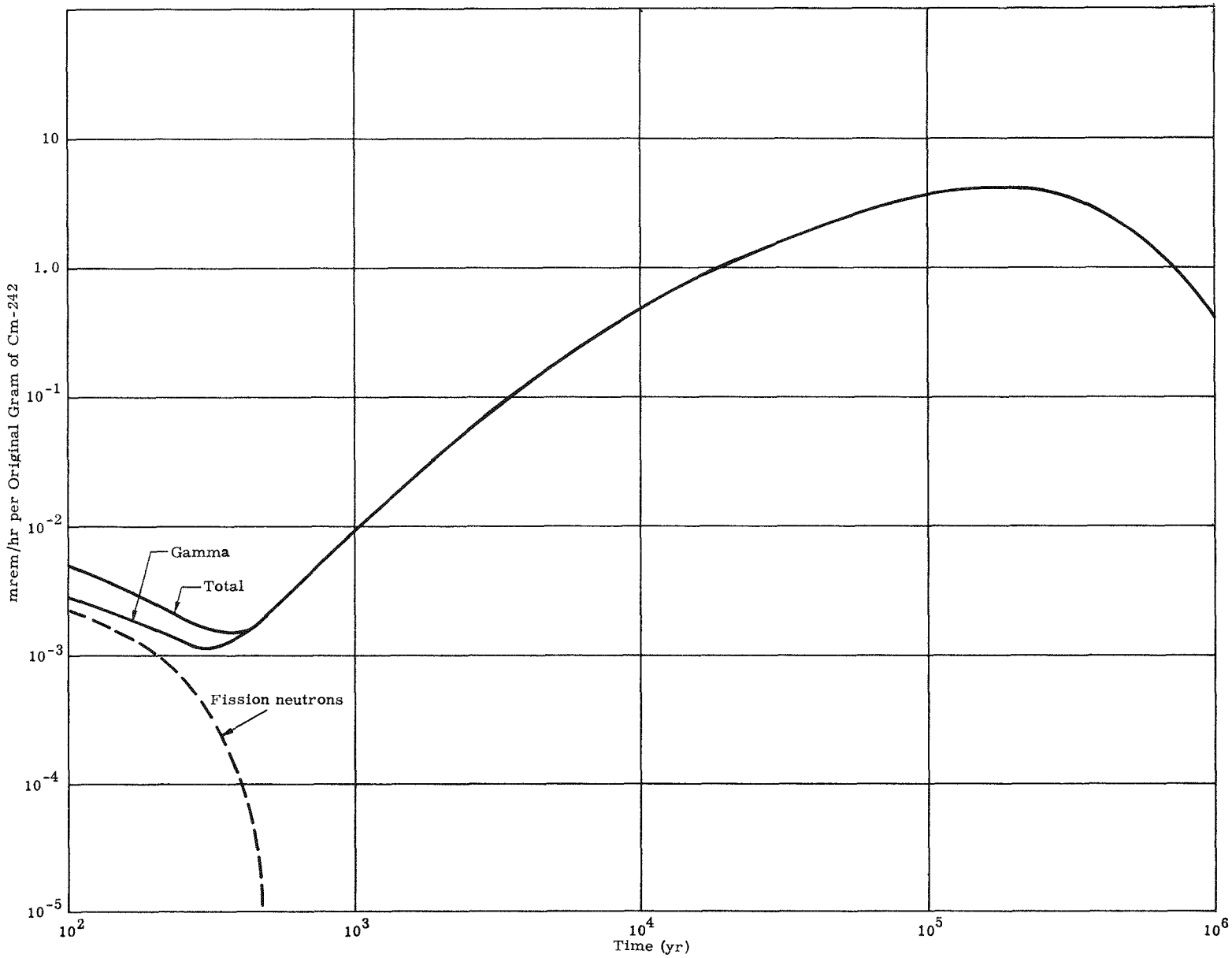

Fig. V-14. Dose Rate from Cm-242 and Its Decay Products (10^2 to 10^6 yr)

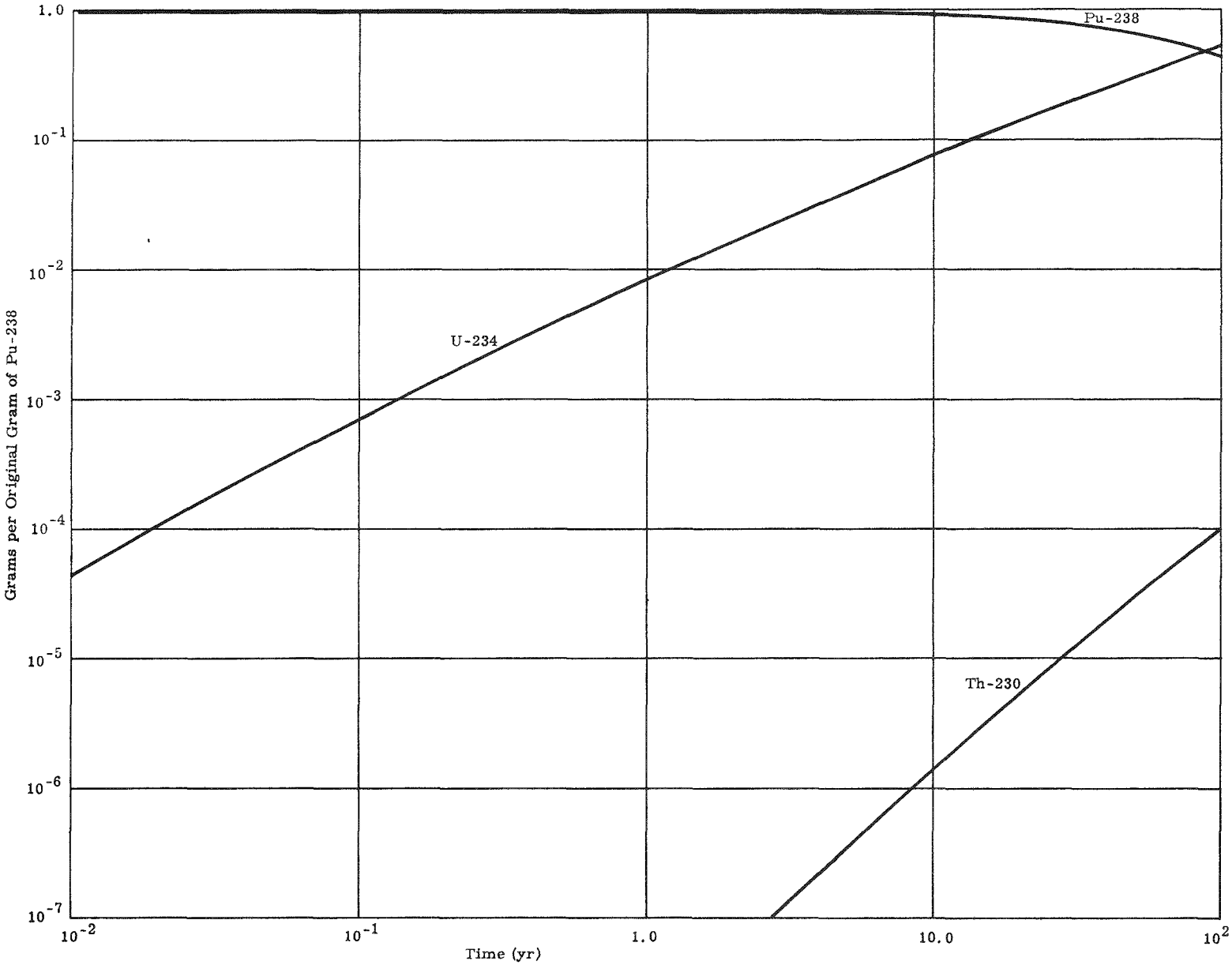

Fig. V-15. Decay of Pu-238 and Growth of Decay Products (10^{-2} to 10^{2} yr)

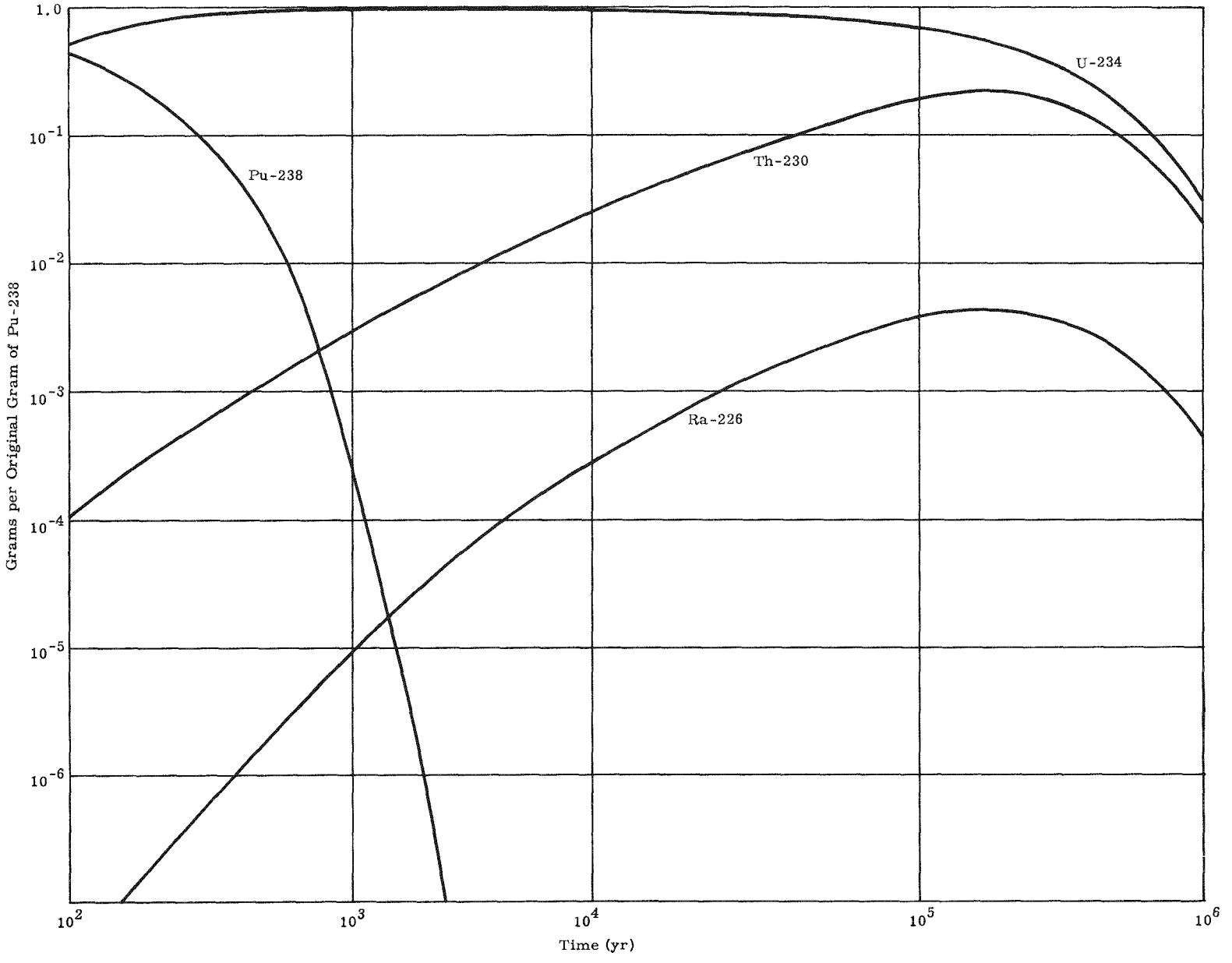

Fig. V-16. Decay of Pu-238 and Growth of Decay Products (10^2 to 10^6 yr)

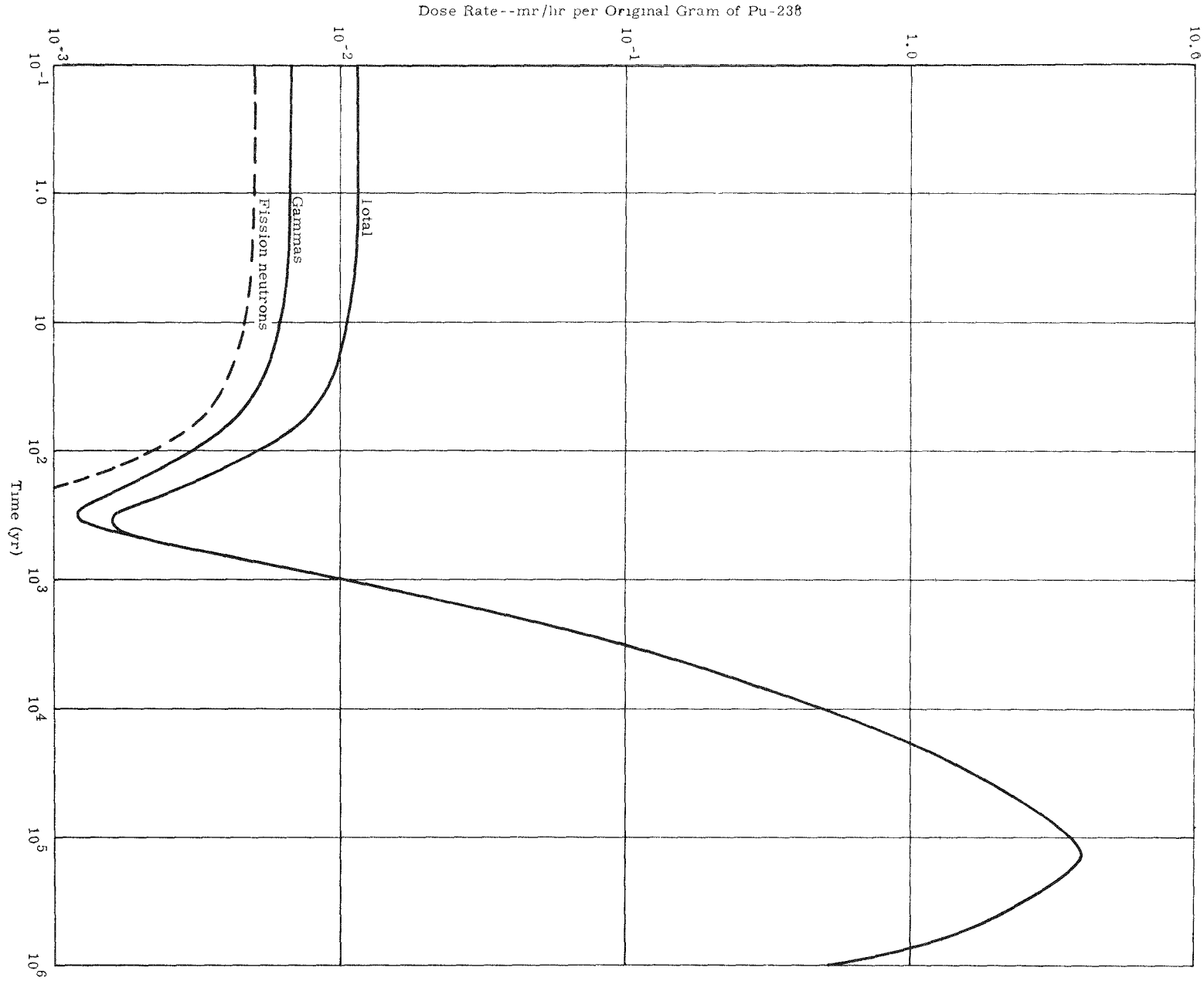

Fig. V-17. Dose Rate from Pu-238 and Its Decay Products (10^{-1} to 10^{6} yr)

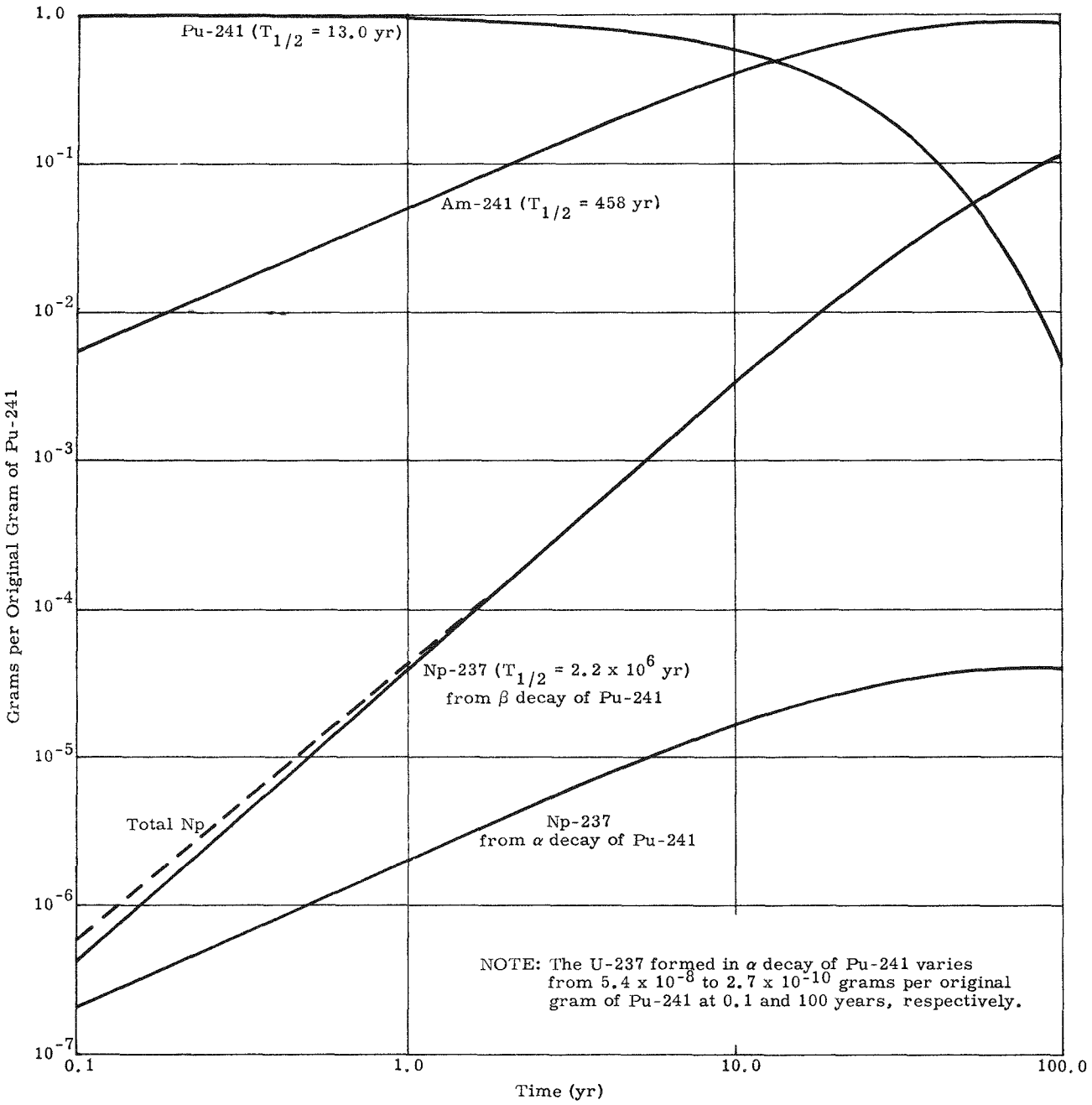

Fig. V-18. Decay of Pu-241 and Growth of Its Decay Products

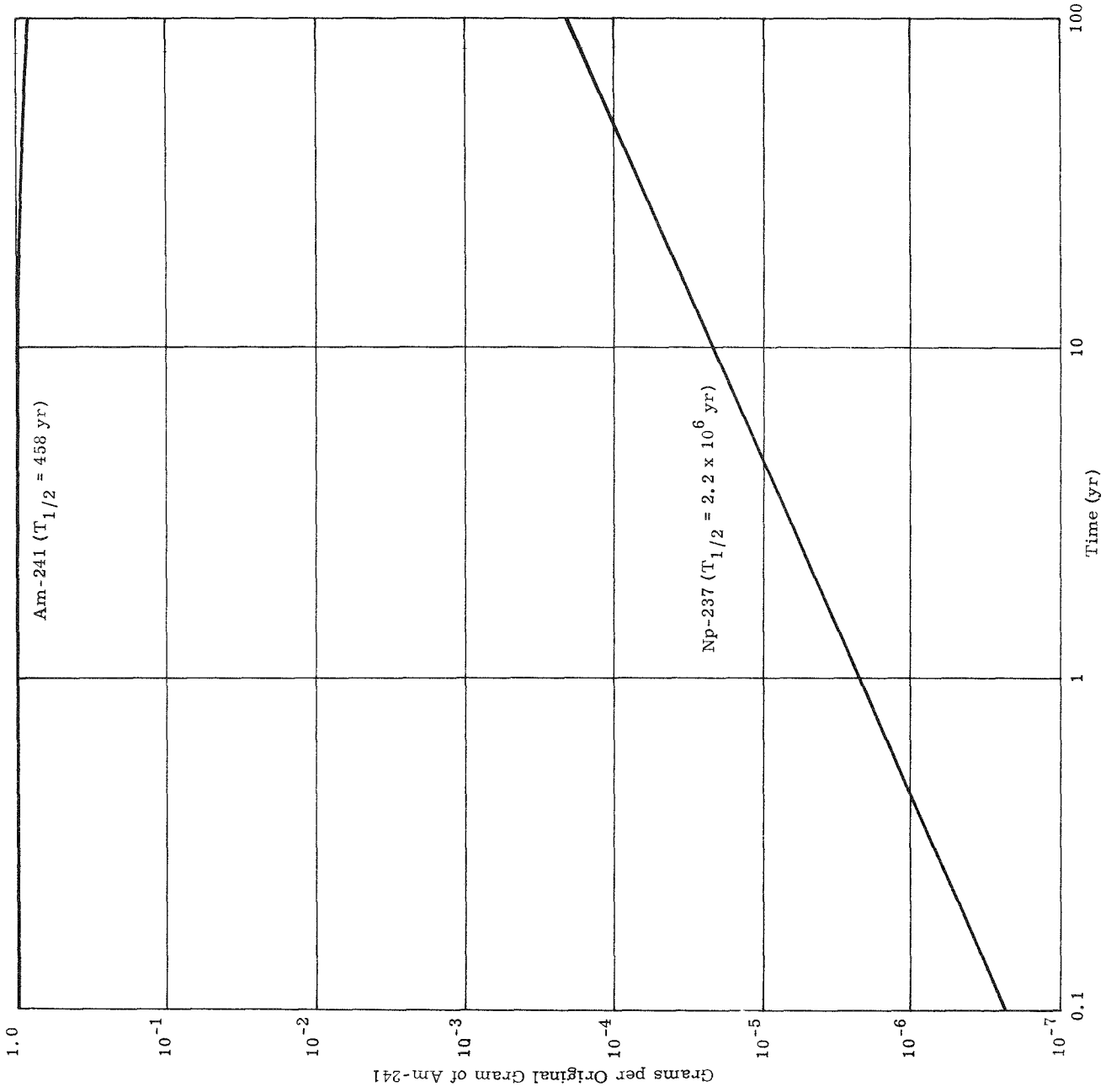

Fig. V-19. Decay of Am-241 and Growth of Its Decay Products

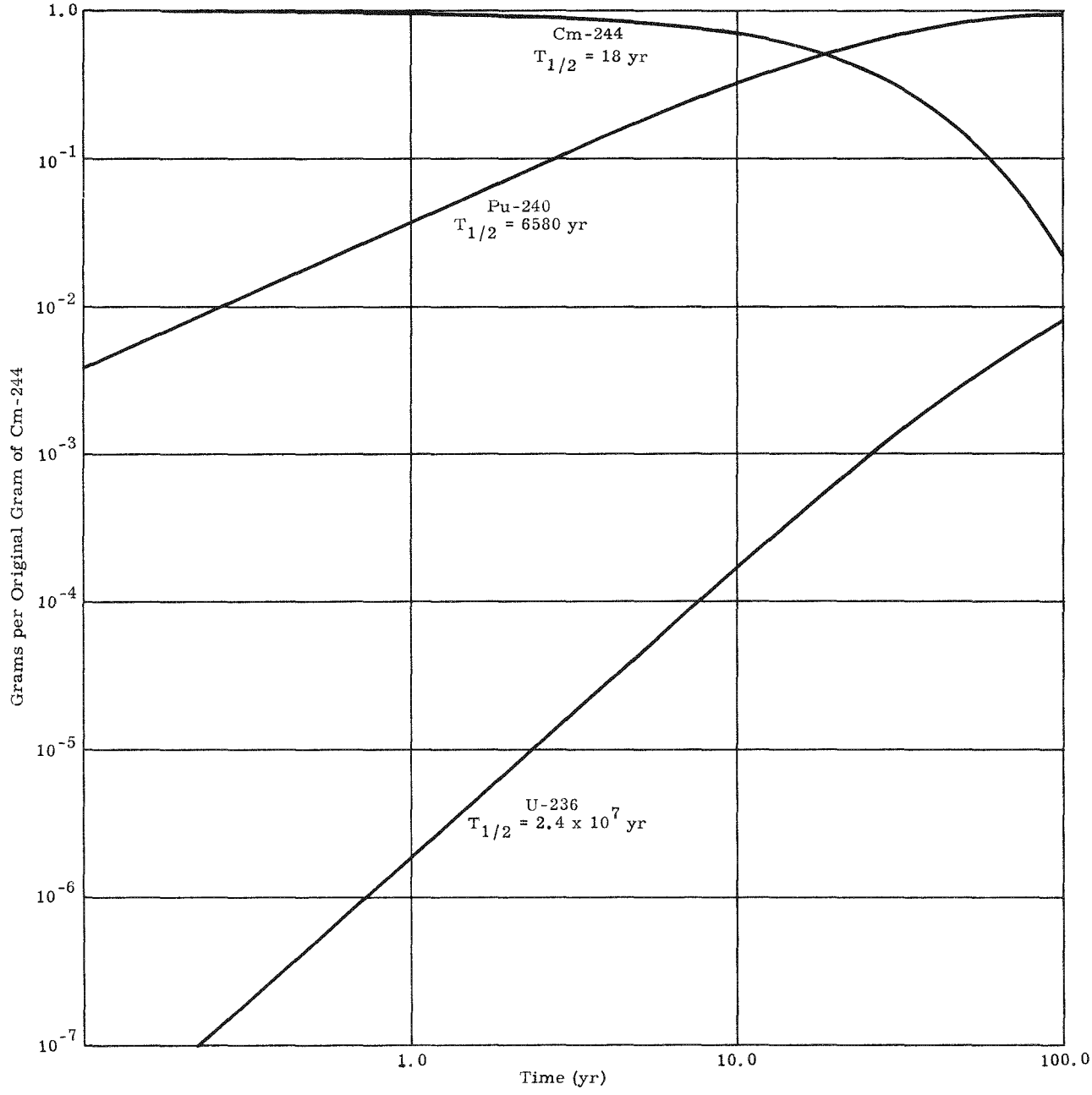

Fig. V-20. Decay of Cm-244 and Growth of Its Decay Products

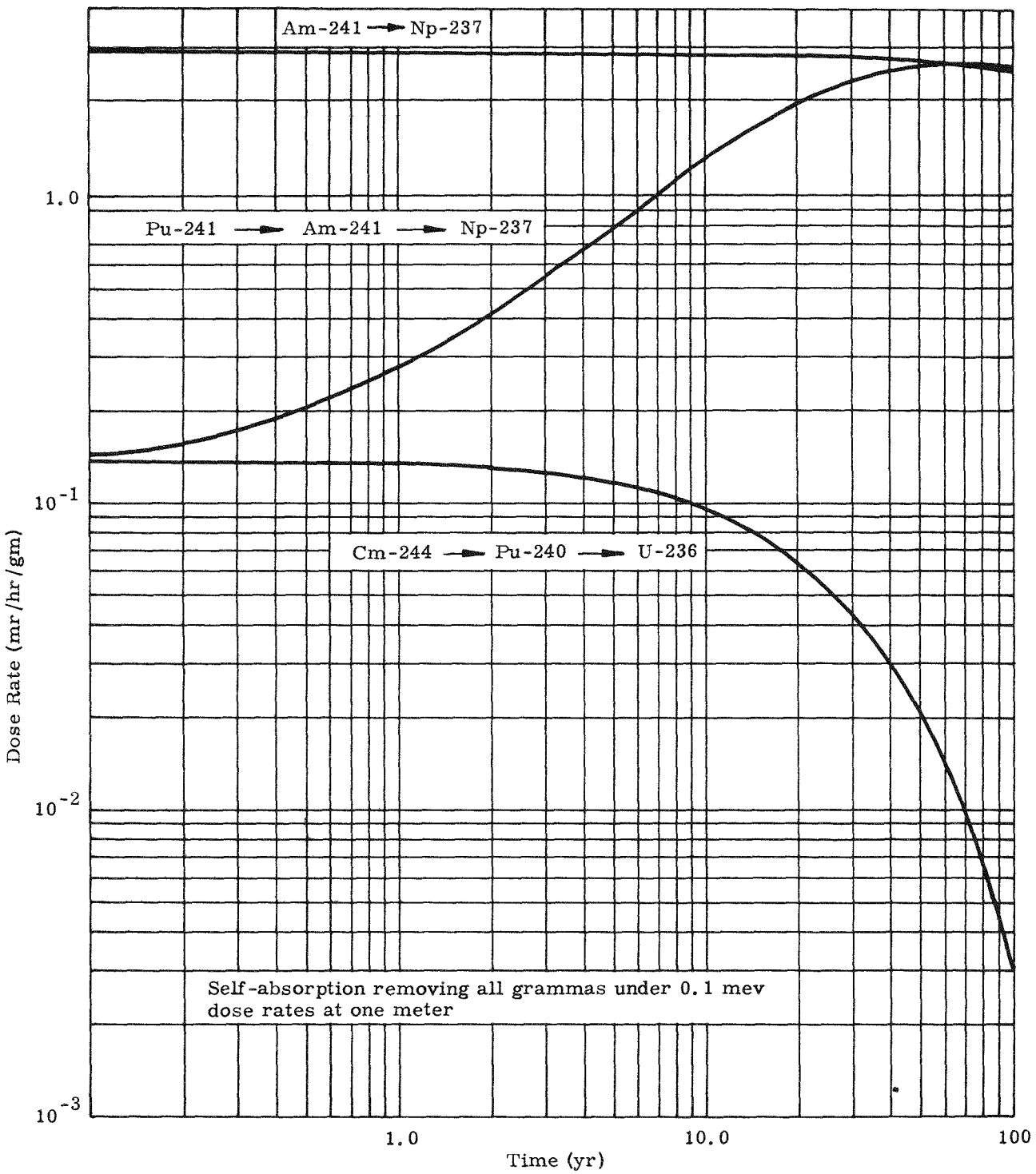

Fig. V-21. Dose Rates--mr/hr per Original Gram of Pu-241, Am-241 and Cm-244

3. Shielding Analysis of Shipping Casks

A cask for shipping irradiated Am-241 from a reactor site to The Martin Company was designed to hold 14 irradiated slugs. Each slug contains about 1.4 grams of Cm-242. From data given in Ref. 2, it was determined that this amount of irradiated material will give a gamma dose rate of 400 roentgens per hour at four feet and a dose rate, due to fast neutrons, of 3000 mrem/hr. Knowing the half value thicknesses of lead and water, it was possible to ascertain the various thicknesses of these materials required to reduce the combined neutron and gamma ray dose rate to 10 mrem/hr at four feet. The results are plotted in Fig. V-22. The data presented were based upon the amount of radiation present 30 days after removing the slugs from the reactor and the shielding should be more than adequate after greater periods of time.

A cask was also designed to ship unirradiated Am-241 from The Martin Company to the reactor site. Dose rates at one meter from the top and bottom were calculated and are given in Fig. V-23.

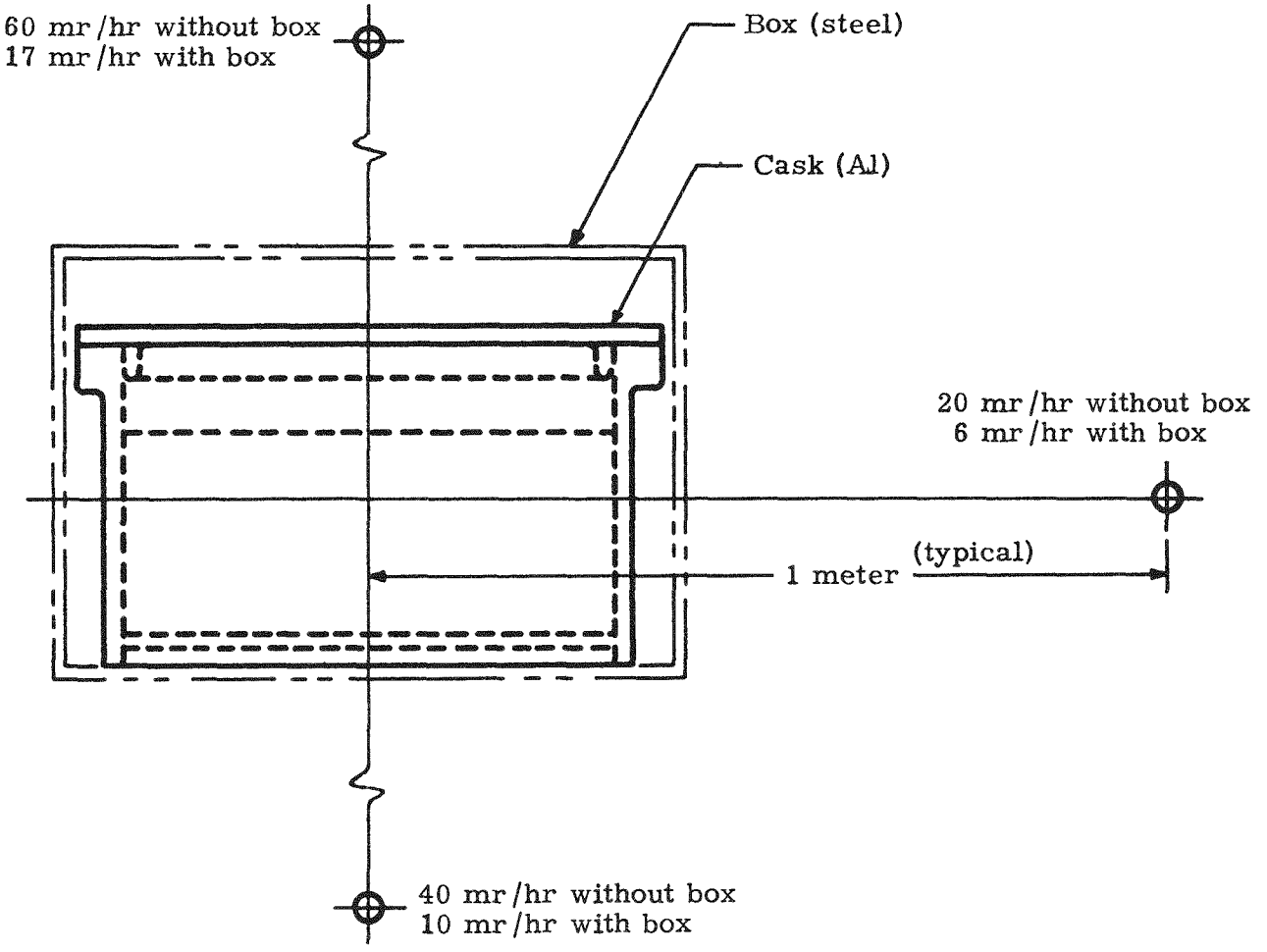

Fig. V-23. Dose Rates Around Americium Shipping Cask

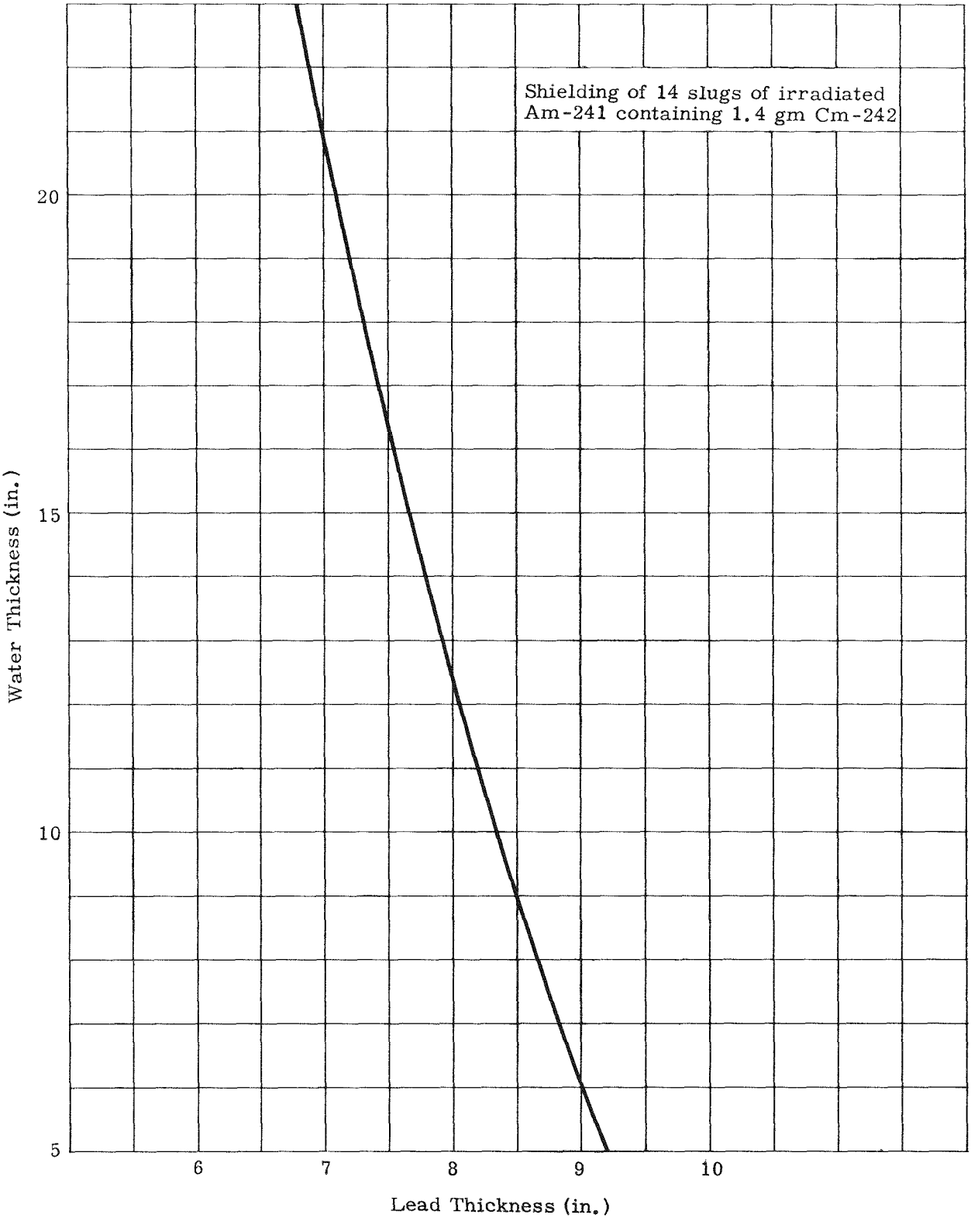

Fig. V-22. Thickness of Water Versus Thickness of Lead to Give 10 mrem/hr at Four Feet

4. Dose Rates from Irradiated Fuel Slugs While in Storage Pool

After the shipping container is received at The Martin Company, it will be placed in the Hot Laboratory storage pool and opened. Therefore, it is desirable to know the radiation level above the pool. Figure V-24 shows the variation of dose rates with thickness of water. The dose rates shown in this figure may be greater than what will actually exist since the shipping time must be added to the 30-day cool-down period.

5. Comparison of Isotopes

A comparison of isotopic heat sources was made by calculating the curies, weight of pure isotope and the shielding required for a 10-thermal watt unit. The results are shown in Table A-4 of Appendix V-A.

It should be remembered that the shielding requirements will vary as the power of the unit and the distance of the dose point from the source changes.

6. Thermal Analyses

Thermal analysis of irradiated capsules. An investigation was made to determine the surface temperature of a 5 inches long by 1-inch diameter aluminum capsule containing irradiated americium. It was assumed the capsule initially contained 3.571 grams of Americium-241, of which 43% was converted to Curium-242 after 84 days irradiation time.

The capsule surface temperatures in still air were determined for heat production rates of 630 and 800 Btu/hr. The Curium-242 will produce 630 Btu/hr, but residual fission products also contained in the capsule may increase this figure to 800 Btu/hr. If the capsule is allowed to cool for 30 days, the power level of the curium drops from 630 to 555 Btu/hr. The surface temperatures for various surface emissivities are plotted in Fig. V-25 and film coefficients are listed in Table V-3. For purposes of this analysis, only convection and radiation losses were considered.

The theoretical capsule surface temperature was determined by finding the film coefficient for radiation and convection to infinite surroundings at 100° F. The radiation film coefficient is:

$$h_R = \sigma \epsilon \quad (T_1^2 + T_2^2)(T_1 + T_2)$$

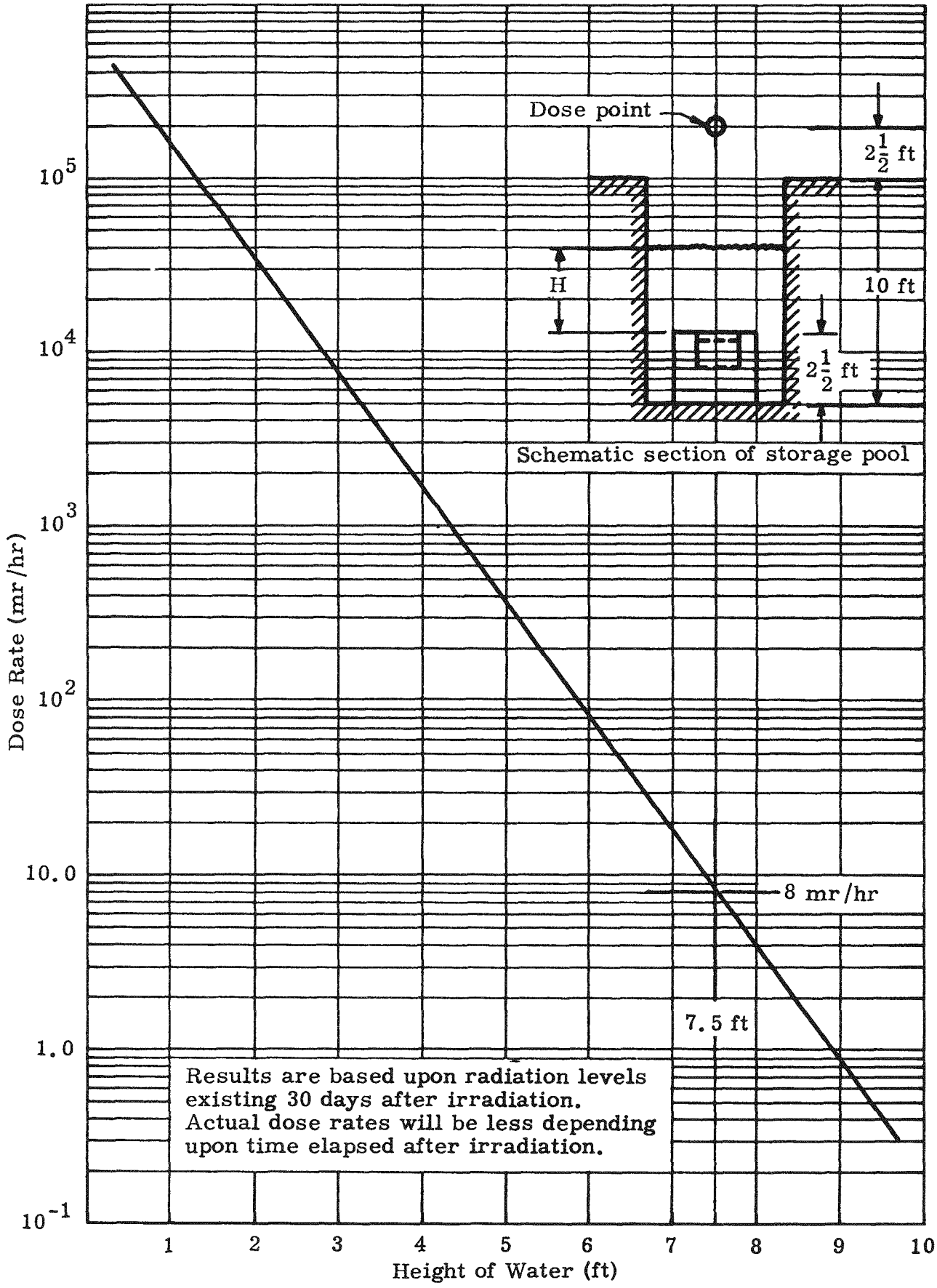

Fig. V-24. Dose Rate Above Storage Pool

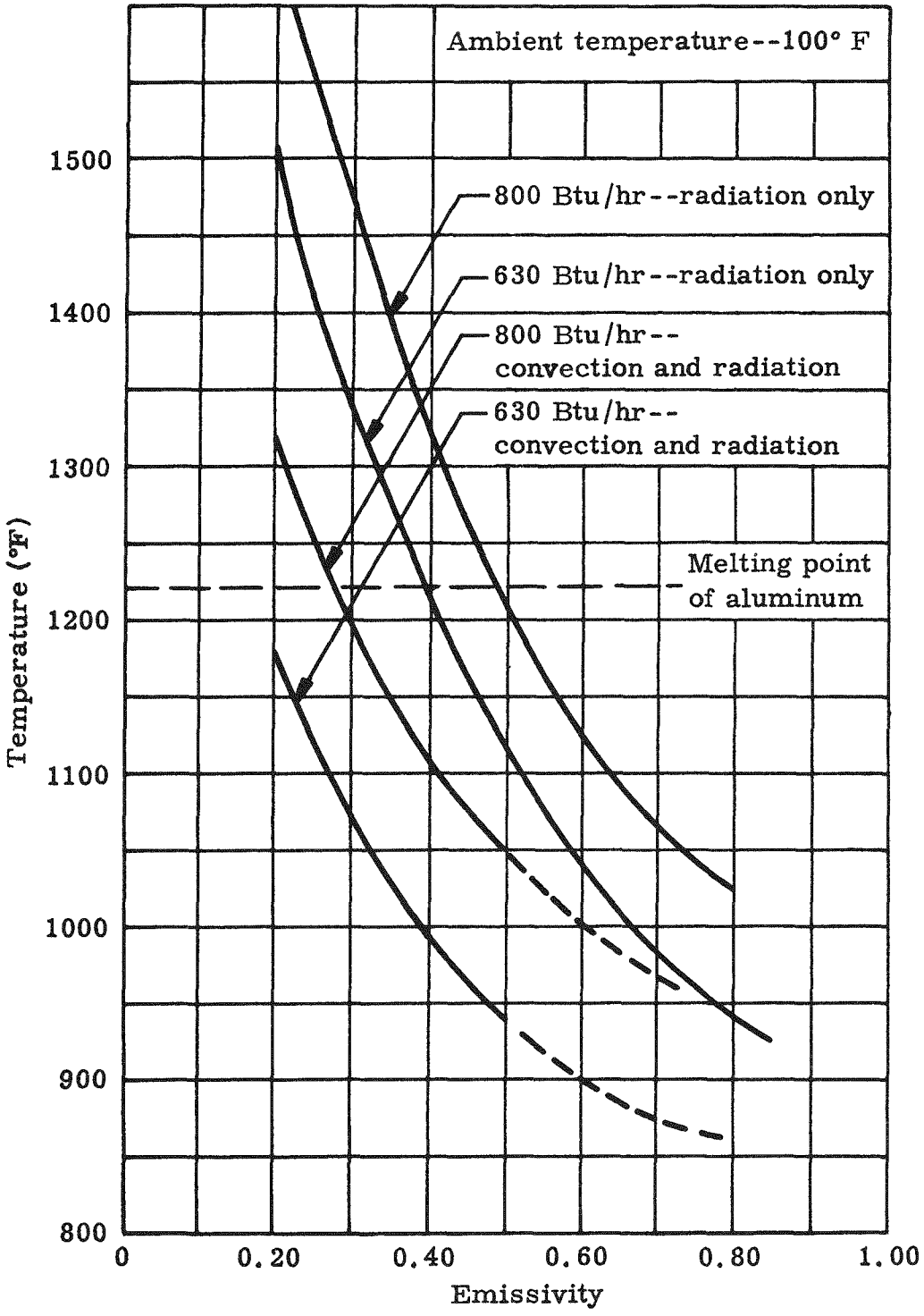

Fig. V-25. Surface Temperatures of Irradiated Capsules in Air

and the convection film coefficient for a cylinder (horizontal or vertical) in the laminar region is:

$$h_{cv} = 0.24 \left(\frac{T_1 - T_2}{d}\right) 0.25 \qquad \text{(Ref. 4)}$$

Then, by trial and error computations:

$$q = h_f \, A \, (T_1 - T_2)$$

where

σ = Stefan-Boltzmann constant

ϵ = surface emissivity

T_1 = absolute capsule surface temperature

T_2 = absolute ambient temperature

d = capsule diameter

A = capsule surface area

q = heat production rate

$h_f = h_R + h_{cv}$.

The capsule surface temperature was determined for emissivities of 0.20, 0.35, 0.50 and 0.85. Emissivities of normally oxidized aluminum at greater than 1000° F are in the range of 0.20 to 0.30 and somewhat higher for a heavily oxidized surface. Decontamination of the capsule by sandblasting will roughen the surface and probably give an increase in emissivity. Table V-3 lists the film coefficients for several temperatures and emissivities.

Thermal analysis of shipping cask for irradiated capsules. The equilibrium temperatures in the proposed curium shipping cask have been determined. The shipping cask is being designed for the specific purpose of providing adequate shielding and heat dissipation during the shipment of 14 aluminum capsules containing irradiated americium, of which approximately 22 grams have been converted to Curium-242. The thermal energy of this quantity of isotope is 8800 Btu/hr. The proposed cask design is a cylindrical geometry of the dimensions given in Fig. V-26. The surface temperature of the cask was determined from the

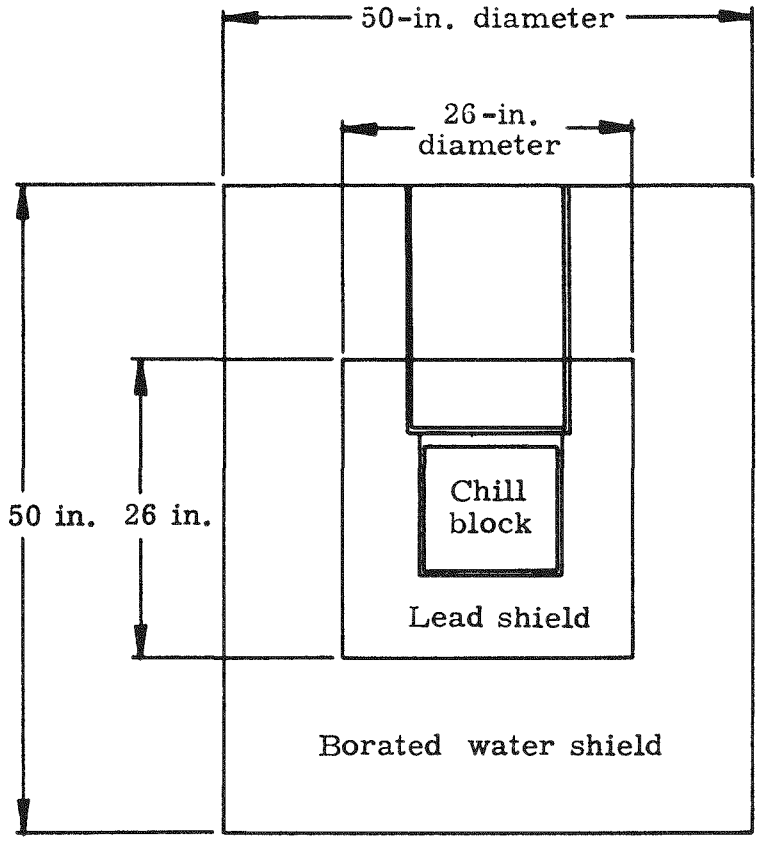

Fig. V-26. Shipping Cask for Irradiated Capsules

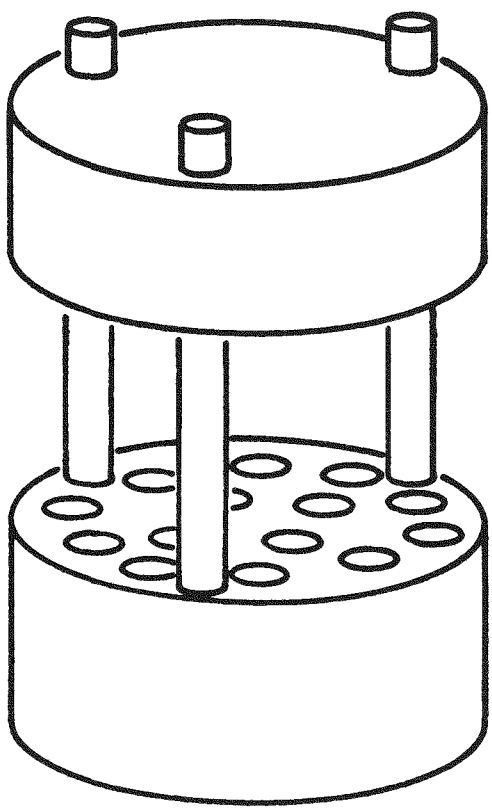

Fig. V-27. Chill Block for Irradiated Capsules

same combined radiation-convection equation employed previously for the capsules. It was assumed that one end of the cask was placed on an insulated surface and that no heat was transferred by conduction. Also, it was assumed that the remainder of the cask surface (68.1 ft^2) was losing heat to an environment at 100° F. A condition of uniform surface and interface temperatures were presumed throughout the analysis. The temperature gradient across the water shield (11 inches thick) was determined by calculating a fin efficiency of the structural members which support the weight of the lead shield. A mathematical expression of fin efficiency for a straight fin of rectangular profile was employed (Ref. V-5) along with a circular fin correction factor (Ref. V-6). The temperature gradient across the shield water was found to be 5° F. Thermal analysis of the lead shield (8.25 inches thick) was accomplished by deriving an expression for heat flow through a cylindrical geometry of uniform thickness (see Appendix V-B). Calculations were based on a uniform surface temperature at both the inner and outer surfaces of the lead shield. Final results of the analysis indicated that the surface temperature of the cask will be 175° F for an ambient temperature of 100° F--or 206° F at an ambient temperature of 140° F. The centerline temperature may vary from 225 to 350° F with the internal cask geometry as shown in Appendix V-B.

TABLE V-3

Film Coefficients

Temperature (°F)	Convection Film Coefficient (Btu/hr-ft^2-°F)	Radiation Film Coefficient (Btu/hr-ft-°F) = 0.20	= 0.35	= 0.50
940	2.41	1.53	2.67	3.82
1000	2.44	1.70	2.98	4.25
1050	2.48	1.85	3.23	4.60
1150	2.54	2.16	3.78	5.40
1200	2.57	2.34	4.10	5.85
1300	2.63	2.72	4.76	6.80

It is currently planned to incorporate the irradiated capsules in a cylindrical metal chill block for purposes of heat transfer during shipment. This chill block will be 9 inches high by 9 inches in diameter; a suggested design is illustrated in Fig. V-27. It is desirable to have the fuel capsules fit loosely in this block, so seizing will not occur as a result of dimensional increases from thermal expansion and/or internal gas pressures. However, for low temperature heat transfer, it is desirable to have maximum physical contact with the chill block. Consequently, the use of a radiation-resistant grease, powdered graphite, or a liquid metal may be required to facilitate heat transfer between the capsules and the chill block, and possibly between the chill block and the lead shield. A radiation-resistant grease which is currently available has been proposed for this purpose. Its use, however, is subject to compatibility with the storage pool water and its ability to withstand the high radiation levels which will be encountered. In the heat transfer analysis of this chill block, it was assumed that the fuel capsules were evenly distributed, thereby permitting a basis for calculation of uniform heat generation throughout the block. The temperature gradient through a stainless steel chill block was then determined to be 50° F (see Appendix V-B). Substituting copper for stainless steel would reduce the temperature gradient from 50 to 3° F; however, this is unnecessary since the centerline temperature is considerably below the melting point of the capsules (MP of aluminum = 1220° F) with a stainless steel chill block. Additional calculations and analyses were conducted on the capsule surface temperature using an aluminum chill block instead of stainless steel in the cask. The results are reported under Subtask 6.5.

A hazards analysis, based on the assumption of accidental loss of the borated water shield, shows that the conduction path (cross-sectional area of 2 ft^2 to support lead shield) is sufficient to limit the temperature rise to 160° F. Thus, the average centerline temperature will rise from 270 to 430° F, which is still safely below the melting point of the aluminum-clad fuel capsules.

Thermal analysis of volatilization process. The surface temperatures of the fuel capsule during the $AlCl_3$ volatilization process were determined for the following furnace conditions:

(1) Argon gas passing over the capsule.

(2) Helium gas passing over the capsule.

(3) A mixture of helium and chlorine gas passing over the capsule (furnace closed).

(4) A mixture of helium and chlorine gas passing over the capsule (furnace open).

In Item 3 the heat of chemical reaction between the aluminum and chlorine raises the thermal energy of the capsule to 1230 Btu/hr. Results for Cases a, b and c are reported in Table V-4.

The furnace configuration for which the fuel capsule surface temperature has been estimated is shown in the following sketch.

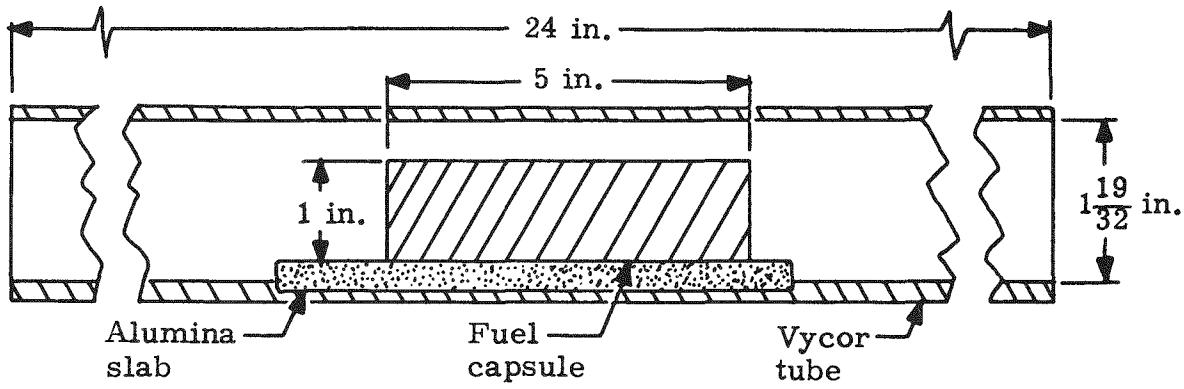

For simplification in analysis, the heat conducted through the alumina slab is neglected and the fuel slug is assumed to be suspended in the center of the Vycor tube. The mathematical model of the furnace in cross section is as shown below.

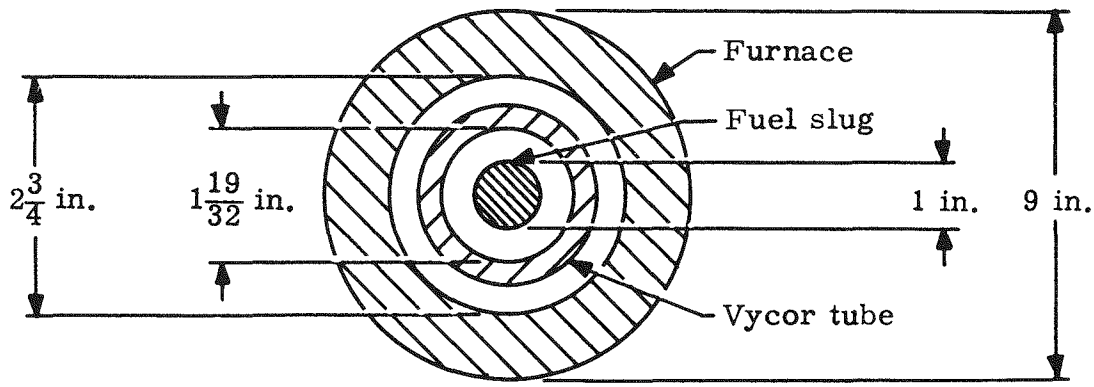

The furnace temperatures attained by the fuel capsule during the aluminum volatilization process were determined for a heat production rate of 615 Btu/hr from the isotope decay and 615 Btu/hr from the heat of chemical reaction, giving a total of 1230 Btu/hr as indicated. The heat of chemical reaction is considered only when chlorine gas is passing over the aluminum capsule.

The primary sources of heat loss which were considered were heat loss through the furnace wall and the heat transferred to the gas by convection. All other heat losses can be related to these two. An iterative technique yields solutions for the four cases, 1 through 4, previously listed. Results of this investigation are reported in Table V-4.

TABLE V-4

Fuel Slug Surface Temperature

	Furnace Closed			Furnace Opened
			(c)	(d)
Gas Flow Rates (ft^3/hr)	(a) Argon Gas (°F)	(b) Helium Gas (°F)	Helium and Chlorine (°F)	Helium and Chlorine (°F)
5	1515	1255	1825	1630
10	1495	1210	1770	1590
15	1485	1145	1700	1525

NOTE: The melting point of aluminum is 1220° F.

From this analysis, it is obvious that an increase in the gas flow and a method of chilling the capsule must be provided once the reaction is initiated.

E. SUBTASK 6.5--IRRADIATION TESTING

The objectives for Subtask 6.5 are as described here:

(1) Develop a Statement of Work.

(2) Establish criteria and program requirements.

(3) Conduct thermal analysis on the capsules under the anticipated environmental condition and different periods of time after removal from the reactor.

(4) Undertake activation analysis to determine radiation hazards involved.

(5) Evaluate neutron flux depression factors of the capsules and establish reactor flux requirements.

1. Irradiation of Americium to Produce Curium

Work has been initiated on arranging an irradiation program in the Materials Testing Reactor or Engineering Test Reactor at Idaho Falls, Idaho. Under this program, capsules containing Americium-241 (as AmO_2) dispersed in an aluminum matrix will be irradiated in a high neutron flux for the purpose of producing Curium-242. The core of each capsule will contain 3.57 grams of Am-241 and 107 grams of aluminum powder. The external dimensions, including clad material, are 1 inch in diameter by 5 inches long for a total of 164 grams.

A program outlining the requirements of this phase has been completed. A trip is planned to the National Reactor Testing Station, Idaho Falls, Idaho, to secure such information as the availability of high neutron flux facilities, possibility of prolonged shutdown periods, approval of shipping container design and proposed test capsules, priority requirements, pre-irradiation integrity tests, etc. Certain data have been generated in preparation for this visit so as to facilitate establishment of criteria and program requirements. The following summarizes the analyses undertaken and the subsequent results.

Thermal analysis. A preliminary thermal analysis was performed to determine temperature levels (core centerline and capsule surface temperatures) of the irradiated capsules under different environmental conditions and periods of time after removal from the reactor. Insufficient data on specific irradiation facilities for these capsules and the manner of positioning precluded a rigorous thermal analysis of the specimens during irradiation. These data will be obtained directly from the National Reactor Testing Station.

Upon completion of the irradiation period, it is planned to cool the capsules in a water "pool" or canal at the reactor site for a period of 30 days. Under the static water conditions which will prevail during this storage period, it was postulated that temperatures may be sufficiently high to cause boiling. Consequently, an analysis was performed which was based on a thermal output of 630 Btu/hr/capsule from the Cm-242 and an additional contribution of 170 Btu/hr/capsule from resi-

due constituents such as fission products. This latter value is an estimate only, based on the best information available at present; also, the decay rate of these fission products, and corresponding decrease in thermal output, has been estimated in this preliminary analysis. A more precise analysis will be conducted at a later date for comparison with the results obtained at this time. Results of this current analysis indicated that the maximum capsule surface temperature occurring in the canal immediately after removal from the reactor was 125° F, with the core centerline temperature being only 14° F above this value. It is thus evident that natural convection of the coolant is sufficient to prevent boiling. A resultant decrease in surface temperature of approximately 15° F will occur after storage in the canal for 30 days. It therefore appears that no deleterious effects will be suffered during this underwater storage period.

Following cool-off, the capsules will be transferred to a shielding cask for shipment to The Martin Company. Upon receipt of the capsules, they will undergo further processing. The possibility of excessive temperatures during this shipment was also investigated. As indicated in Subtask 6.4, it is planned to mount the irradiated capsules in a chill block within the shielding cask to facilitate heat transfer. In this case, an aluminum block was used instead of stainless steel. Based on these environmental conditions, with good thermal contact between capsule and chill block surfaces, it was first assumed that the capsules would be transferred directly from the reactor to the shipping container so that the worst possible case could be analyzed. The subsequent decrease in surface temperature, as a result of radioactive decay, was then determined for a period extending to 30 days after irradiation. This approach was employed to ascertain the feasibility of reducing the cool-off period to less than 30 days. These analyses indicated that immediate containment of the capsules in the cask after irradiation would result in a maximum capsule surface temperature of 317° F, which would decrease to approximately 292° F after 30 days. The aluminum cladding in these capsules has a recrystallization temperature of 550° F and only after prolonged heating at 450 to 500° F will the capsule suffer any significant loss of strength. Disregarding activity levels for the moment, it was concluded from this thermal analysis that the capsules could be shipped almost immediately after removal from the reactor. These results, however, are subject to modification, depending on verification of the thermal characteristics of the fission products and their corresponding decay rate; also, the helium buildup and resultant internal pressure, which has not yet been determined, may have some influence.

Activation analysis. The second major factor governing duration of cool-off time required for the capsules is the radiation common to all neutron-irradiated materials. Therefore, the activity levels of the irradiated capsules were investigated to ascertain any handling problems at the reactor site, and to determine if shipment could be accomplished prior to the estimated 30-day cool-off period. Since the Interstate Commerce Commission specifies the radiation levels on any shielding cask to be 200 mr/hr or less on the cask surface and 10 mr/hr or less at one meter from the cask surface, these values were used in determining the minimum cool-off period necessary.

In addition to gamma radiation, neutron emission from spontaneous fissioning and (α, n) reactions contributes a significant portion of the radiation hazard associated with the capsules and is included in this analysis. Dose rate versus time curves were prepared for points on the cask surface and one meter from the surface. A time period of 0 to 60 days after the irradiation was considered. Radiation levels in this case were determined by "scaling-up" data obtained from a Martin report, MND-P-1972 (Ref. V-2), which covers previous irradiations of 1/4-inch diameter pencils by the Lawrence Radiation Laboratory, Berkeley, California. Due to the "scaling-up" process, the following predicted values may vary somewhat from the actual activity levels, but are sufficiently accurate for this preliminary analysis. Tables V-5 and V-6 list the various activity levels obtained.

TABLE V-5

Activity Levels on Cask Surface

Days After Irradiation	Gamma and Neutron Radiation (mrem/hr)
10	650
15	290
20	130
25	63
30	33

TABLE V-6

Activity Level One Meter From Cask Surface

Days After Irradiation	Gamma and Neutron Radiation (mrem/hr)
10	100
15	43
20	20
25	10
30	5

The above data were based on the following criteria:

(1) The cask contains 14 capsules, with each capsule containing 1.54 grams of Cm-242.

(2) The shipping cask affords 8-1/4 inches of lead and 11 inches of water shielding.

From these data, it appears that the capsules can be shipped at least 25 days after removal from the reactor, and possibly 15 to 20 days after removal, depending on instrument readings of the radiation levels at the time.

Flux depression. The one-inch diameter capsules currently planned for irradiation involve both higher concentrations of Americium-241 and larger overall masses than the 1/4-inch diameter specimens irradiated by the Lawrence Radiation Laboratories (Ref. V-2). Consequently, it was suspected that the flux perturbation and depression caused by Martin's one-inch specimens would be significantly more pronounced than for the 1/4-inch diameter samples. A nuclear analysis was undertaken to evaluate the extent of the flux depression (cell correction factor) encountered when the one-inch diameter capsules are inserted in a reactor. This cell correction factor, coupled with the average effective flux required for the desired conversion, will permit determination of the actual flux which should exist in the irradiation facility prior to insertion of the capsules. It is this flux value which must be specified when requesting irradiation space in the Materials Test Reactor or Engineering Testing Reactor.

For purposes of comparison the 1/4-inch diameter pencils (Ref. V-2) mentioned were investigated along with the one-inch diameter capsules. It was found that the 1/4-inch samples had a flux depression factor of approximately 0.84, while the 1-inch samples had a 0.42 factor. Since the 1/4-inch samples required an unperturbed reactor flux of 4×10^{14} nv to achieve the desired conversion (43% Am-241 to Cm-242) in 84 days of irradiation time (Ref. V-2), it is evident that an unperturbed flux of 8×10^{14} nv (8×10^{14} nv = 4×10^{14} nv x 0.84/0.42) will be required to obtain the same conversion in the same period for the one-inch diameter capsules. Employing another approach, the effective flux required for 43% conversion in the one-inch capsules was calculated to be 4×10^{14} nv. Under these conditions, an unperturbed reactor flux of 9.5×10^{14} nv will be necessary. Consequently, it appears that a reactor flux of 8 to 9 x 10^{14} nv is needed.

APPENDIX V-A

TABLE A-1

Decay Products of Cm-242 and Pu-238

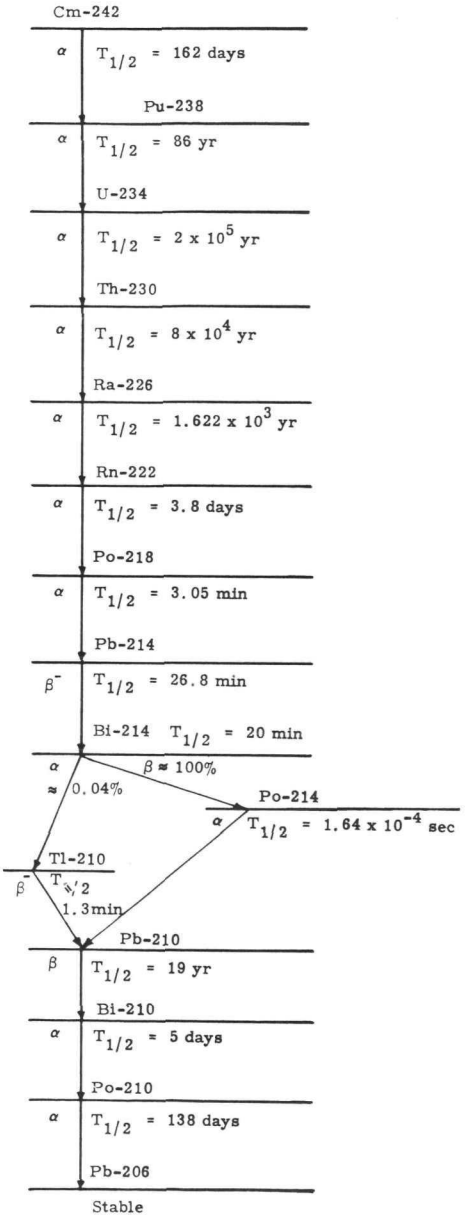

Isotope	Gamma Rays		Neutrons/sec/gm from Spontaneous Fissioning
	Energy (mev)	Fraction of Disintegrations in Which γ-Ray is Produced	
Cm-242	0.044	4.1×10^{-4}	2.013×10^{7}
	0.100	6×10^{-5}	
	0.157	2.7×10^{-5}	
	0.210	2×10^{-7}	
	0.562	1.8×10^{-6}	
	0.605	1.4×10^{-6}	
	0.89	0.9×10^{-7}	
	1.01	10^{-7}	
Pu-238	0.0438	3.8×10^{-4}	4.4×10^{3}
	0.099	8×10^{-5}	
	0.150	1×10^{-5}	
	0.203	4×10^{-8}	
	0.760	5×10^{-7}	
	0.810	$\sim 10^{-7}$	
	0.875	2×10^{-7}	
U-234	0.050	0.283	7.08×10^{-3}
	0.118	0.003	
	0.450	2×10^{-7}	
	0.500	1×10^{-7}	
Th-230	0.068	0.0059	9.6×10^{-4}
	0.110	1×10^{-6}	
	0.142	7×10^{-4}	
	0.184	1.4×10^{-4}	
	0.206	5×10^{-8}	
	0.235	5×10^{-8}	
	0.253	1.78×10^{-4}	
Ra-226	0.184	0.012	
	0.26	7×10^{-5}	
	0.42	2×10^{-6}	
	0.61	2×10^{-6}	
Rn-222	0.51	0.0007	
Po-218	None Listed		
Pb-214	0.241	0.115	
	0.294	0.258	
	0.350	0.450	
Bi-214	0.607	0.658	
	0.766	0.065	
	0.933	0.067	
	1.120	0.206	
	1.238	0.063	
	1.379	0.064	
	1.761	0.258	
	2.198	0.074	
Po-214	None Listed		
Pb-210	0.0465	0.04	
Bi-210	None Listed		
Po-210	0.803	1.8×10^{-5}	

TABLE A-2

Decay Products of Pu-241 and Am-241

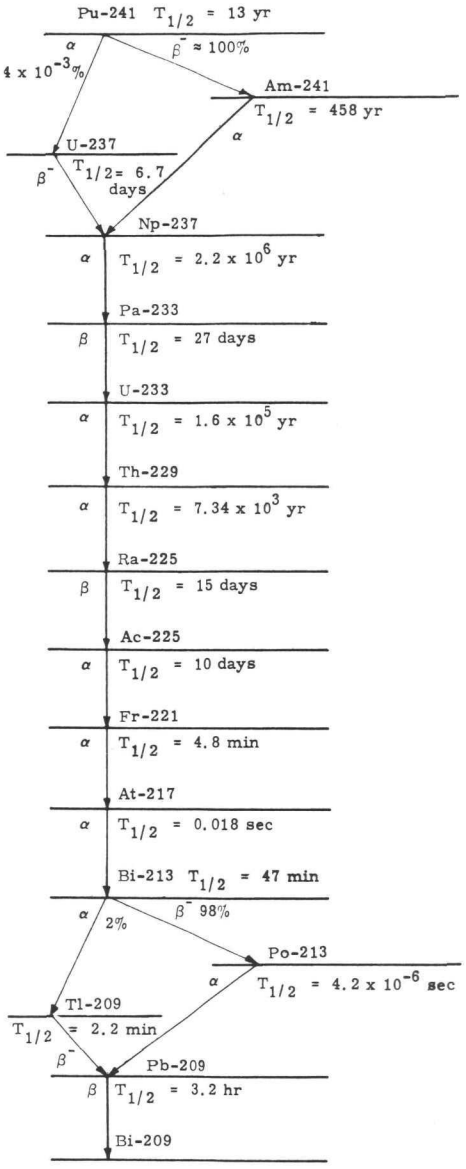

Note: No information on abundance is given in "Table of Isotopes" (Rev. Mod. Phys. 30, 2, Part 2, April 1958) if not listed here.

Isotope	Gamma Rays		Neutrons/sec/gm from Spontaneous Fissioning
	Energy (mev)	Fraction of Disintegrations in Which γ-Ray is Produced	
Pu-241	0.145	2.8 x 10^{-6}	
Am-241	0.027	0.80	
	0.033	0.052	
	0.043	0.11	
	0.056	0.016	
	0.060	0.052	
	0.099	0.000016	
	0.103	0.019	
Np-237	0.029	0.12	
	0.0568		
	0.0869	0.18	
	0.145	0.008	
	0.175	0.001	
	0.200	0.003	
Pa-233	0.016	(see note)	
	0.028		
	0.0401		
	0.0578		
	0.0748		
	0.086		
	0.104		
	0.272		
	0.301		
	0.313	0.80	
	0.341		
	0.376		
	0.400		
	0.417		
	0.476		
U-233	0.0428	0.0005	
	0.0561	0.0001	
	0.099		
Th-229	0.148		
	0.200		
Ra-225	0.040	0.63	
Ac-225	0.0366		
	0.0384		
	0.0628		
	0.0873		
	0.0994		
	0.150		
	0.187		
Fr-221	0.218	0.16	
At-217	None Listed		
Bi-213	0.437		
Tl-209	0.12		
	0.45		
	1.56		
Pb-209	None Listed		

TABLE A-3

Decay Products of Cm-244

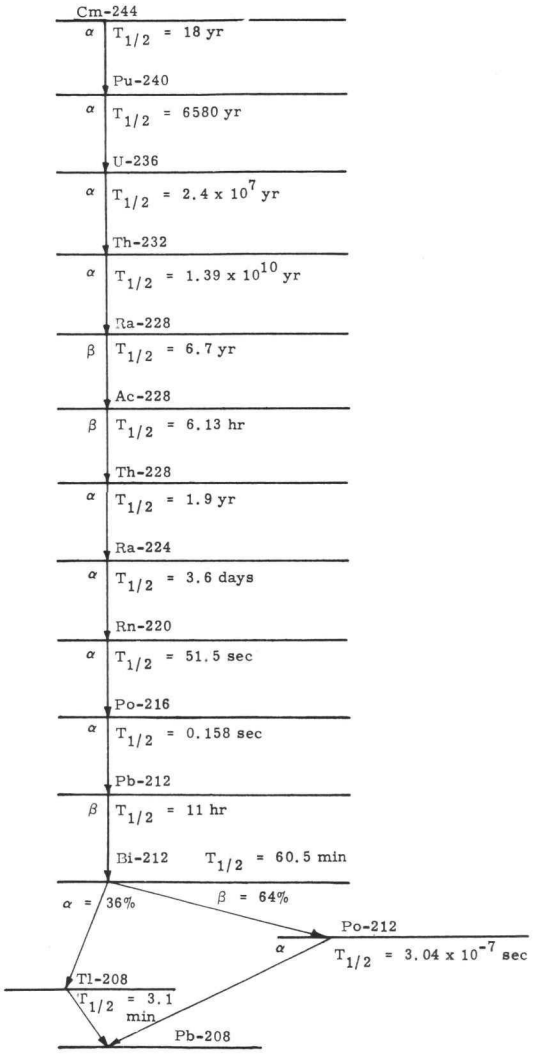

Note: If abundance is not given here, it is not given in "Table of Istopes" (Rev. Mod. Phys. 30, 2, Part 2, April 1958).

Isotope	Gamma Rays	
	Energy (mev)	Fraction of Disintegration in Which γ-Ray is Produced
Cm-244	0.043	0.000021
	0.100	0.000015
	0.150	0.000013
Pu-240	0.045	0.24
U-236	0.050	0.27
Th-232	0.059	0.24
Ra-228	None Listed	
Ac-228	0.0568	(see note)
	0.0978	
	0.179	
	0.184	
	0.232	
	0.336	
	0.410	
	0.458	
	0.907	
	0.965	
	1.035	
	1.095	
	1.59	
	1.64	
Th-228	0.084	0.016
	0.137	0.0026
	0.169	0.0009
	0.205	0.0003
	0.212	0.0027
Ra-224	0.2411	0.037
	0.29	0.00008
	0.41	0.00004
	0.65	0.00009
Rn-220	0.542	0.0004
Po-216	None Listed	
Pb-212	0.115	0.03
	0.1767	
	0.239	0.74
	0.300	0.04
	0.4152	0.0001
Bi-212	0.040	
	0.144	
	0.164	
	0.288	
with α	0.328	
	0.432	
	0.452	
	0.472	
	0.72	0.19
	0.83	0.19
	1.03	0.06
with β	1.34	0.05
	1.61	0.07
	1.81	0.07
	2.20	
Tl-208	0.277	0.036
	0.510	0.090
	0.582	0.288
	0.859	0.054
	2.62	0.36
Po-212	None Listed	

TABLE A-4

Comparison of Isotopes for a 10-Thermal Watt Unit

Isotope	Half Life	Specific Power of Pure Isotope		Amount of Pure Isotope for 10 Thermal Watts		Dose rate at 1 Meter Due to Gamma Radiation (mrem/hr)		Half-Value Thickness of Lead (in.)	Thickness of Lead to Give 10 mrem/hr at 1 meter (in.)
		$\left(\frac{\text{watts}}{\text{curie}}\right)$	$\left(\frac{\text{watts}}{\text{gram}}\right)$	(curies)	(grams)	Per Curie	For 10 Watts		
Sr-90	27.7 y	0.006486	0.921	1542	10.86	64	9.9×10^4	0.45	6.0
Cs-137	33 y	0.003147	0.249	3178	40.16	390	1.24×10^6	0.24	4.1
Ce-144	285 d	0.007400	24.50	1351	0.41	89	1.20×10^5	0.55	7.5
Po-210	138.4 d	0.03146	141.3	318	0.071	0.00453	1.44	0.32	None required
Pu-238	86.4 y	0.0331	0.579	302	17.3	*	*	----	None required
Cm-242	163 d	0.0336	122.2	277	0.082	*	*	----	None required
Cm-244	18 y	0.0348	2.84	287	3.52	*	*	----	None required

*Isotopes Pu-238, Cm-242 and Cm-244 must be investigated for neutrons as well as gamma radiation. Neutrons originate from spontaneous fissions of parent and from (α, n) reactions if fuel form contains light elements. Half-value thickness of water to reduce fast neutron dose rate is about 2.6 inches.

TABLE A-4 (continued)

				Dose Rate from 10-watt Unit at 1 Meter (mrem/hr)	
				Pure Metal	Fuel Form with Light Elements
Pu-238	Spontaneous Fission(neut/sec/gm)	4.391×10^3		0.086	0.086
	(α, n) Reactions(neut/sec/gm)	1.748×10^5		-----	3.438
	Gamma Dose Rate (mr/hr/gm)	0.00669		0.116	0.116
			Total	0.202	3.64
Thickness of Water Shield to Reduce Dose Rate to 10 mrem/hr				None required	None required
Cm-242	Spontaneous Fission(neut/sec/gm)	2.013×10^7		1.88	1.88
	(α, n) Reactions(neut/sec/gm)	3.33×10^7		----	3.10
	Gamma Dose Rate(mr/hr/gm)	20.8		1.70	1.70
			Total	3.58	6.68
Thickness of Water Shield to Reduce Dose Rate to 10 mrem/hr				None required	None required
Cm-244	Spontaneous Fission(neut/sec/gm)	3.87×10^6		15.48	15.48
	(α, n) Reactions(neut/sec/gm)	8.15×10^5		-----	3.26
	Gamma Dose Rate(mr/hr/gm)	0.139		0.49	0.49
			Total	15.97	19.23
Thickness of Water Shield to Reduce Dose Rate to 10 mrem/hr				1.7 in.	2.5 in.

APPENDIX V-B--TASK 6

A. DERIVATION OF HEAT TRANSFER EQUATIONS FOR SHIELDING CASK

1. Lead Shield

An expression has been derived for the heat flow through a cylindrical lead shield of uniform thickness. A uniform surface temperature was assumed at both the inner and outer surfaces of the lead shield. The geometry is shown below with $L_1 = 2r_1$.

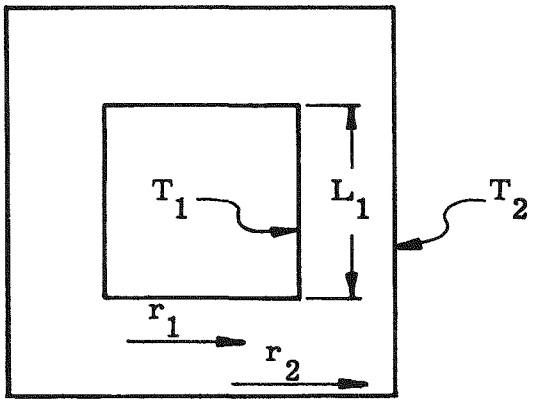

The surface area of a closed cylindrical element of volume at a distance x from the inner surface may be expressed as:

$$A(x) = 2\pi \left[(r_1 + x)(L_1 + 2x) + (r_1 + x)^2\right]$$

Fourier's Third Law may be written in the form:

$$\int_0^{r_2 - r_1} \frac{dx}{A(x)} = \frac{k}{q} \int_{T_2}^{T_1} dT \qquad (1)$$

By the partial fraction method,

$$\frac{1}{A(x)} = \frac{C_1}{r_1 + x} + \frac{C_2}{x + \left(\frac{r_1 + L_1}{3}\right)}$$

$$C_1 = \lim_{x \to -r_1} \left\{ \frac{1}{6\pi \left[x + \left(\frac{r_1 + L_1}{3}\right)\right]} - \frac{C_2 (r_1 + x)}{\left[x + \left(\frac{r_1 + L_1}{3}\right)\right]} \right\} =$$

$$\frac{1}{2\pi (L_1 - 2 r_1)}$$

$$C_2 = \lim_{x \to -\left(\frac{L_1 + r_1}{3}\right)} \left\{ \frac{1}{6\pi (r_1 + x)} - \frac{C_1 \left[x + \left(\frac{r_1 + L_1}{3}\right)\right]}{(r_1 + x)} \right\} =$$

$$\frac{1}{2\pi (L_1 - 2 r_1)}$$

In terms of T_1, the solution of Eq (1) is:

$$\int \frac{dx}{A(x)} = \int_0^{r_2 - r_1} \frac{C_1\, dx}{x + r_1} + \int_0^{r_2 - r_1} \frac{C_2\, dx}{\left[x + \left(\frac{L_1 + r_1}{3}\right)\right]} =$$

$$\frac{\ln \left[\frac{(r_1 + L_1)\, r_2}{(3\, r_2 - 2\, r_1 + L_1)\, r_1}\right]}{2\pi\, (L_1 - 2\, r_1)} . \qquad (2)$$

Equation (2) is the indeterminate form 0/0 for the particular geometry $L_1 = 2\, r_1$. By applying L'Hospital's rule and differentiating the numerator and denominator of Eq (2) separately with respect to L_1 and considering the limit as L_1 approaches $2\, r_1$, we find:

$$\lim_{L_1 \to 2\, r_1} \frac{\frac{d}{dL_1} \left\{\ln \left[\frac{(r_1 + L_1)\, r_2}{(3\, r_2 - 2\, r_1 + L_1)\, r_1}\right]\right\}}{\frac{d}{dL_1} \left[2\pi\, (L_1 - 2\, r_1)\right]} = \frac{r_2 - r_1}{3\, r_1\, r_2} .$$

Substituting in Eq (1) and solving for T_1,

$$T_1 = \frac{q\, (r_2 - r_1)}{6\pi\, k\, r_1\, r_2} + T_2 .$$

2. Chill Block

If the fuel capsules are distributed evenly within the chill block, an assumption of uniform heat generation throughout the block can be used. The temperature at any point in the block may then be determined by a spherical approximation of the cylinder, replacing the cylinder with

a sphere of equal radius or equal surface area. For a sphere of equal radius with a stainless steel chill block,

$$\Delta T = \frac{S(R^2 - r^2)}{6k} = 51^\circ \text{ F for } r = 0$$

and for an equal surface area,

$$\Delta T = 50^\circ \text{ F},$$

where

S = volumetric heat production rate

R = radius of sphere

r = radius at any point in the sphere

k = 12 Btu/hr-ft-° F for a stainless steel.

BIBLIOGRAPHY

1. "Summary Report of Americium Processing to be Performed by The Martin Company," The Martin Company, MND-P-2333, March 1960.

2. "Americium-241 and Curium-242 Fuel Processing Hazards," The Martin Company, MND-P-1972, August 1959.

3. Evans, R. D., "The Atomic Nucleus," p 490, McGraw-Hill Book Company, Incorporated, New York, 1955.

4. Giedt, W. H., "Principles of Engineering Heat Transfer," p 218, Van Nostrand, Incorporated, 1957.

5. Schneider, P. J., "Conduction Heat Transfer," Equations 4 to 11, p 73, Wesley Publishing Company, 1955.

6. Schneider, P. J., "Conduction Heat Transfer," Figures 4 to 11, p 85, Wesley Publishing Company, 1955.